DEVELOPMENT OF RECOMMENDATIONS FOR AIR MIXER AND SAMPLER DESIGN AND COMBINATIONS THEREOF FOR PERFORMANCE TESTING OF HVAC EQUIPMENT

By

HYUNJIN PARK

Bachelor of Science in Mechanical Engineering
Inje University
Gimhae, South Korea
2009

Master of Science in Mechanical Engineering
Inje University
Gimhae, South Korea
2011

Submitted to the Faculty of the
Graduate College of the
Oklahoma State University
in partial fulfillment of
the requirements for
the Degree of
DOCTOR OF PHILOSOPHY
May, 2023

DEVELOPMENT OF RECOMMENDATIONS FOR AIR MIXER AND SAMPLER DESIGN AND COMBINATIONS THEREOF FOR PERFORMANCE TESTING OF HVAC EQUIPMENT

Dissertation Approved:

Dr. Christian K. Bach

Dissertation Adviser

Dr. Craig R. Bradshaw

Dr. Omer San

Dr. Aaron S. Alexander

.

ACKNOWLEDGEMENTS

I would like to express my heartfelt gratitude to my advisor, Dr. Christian Bach, for his unwavering support, invaluable guidance, and exceptional mentorship throughout my research and the writing of this dissertation. His expertise and insights have been instrumental in shaping this work and contributing to my academic growth. I enjoyed all the times we spent discussing my research and various other topics, and will miss our weekly meetings where we talked about everything under the sun. I am deeply appreciative of the valuable feedback and suggestions provided by my committee members, Dr. Craig Bradshaw, Dr. Omer San, and Dr. Aaron Alexander, and the support and constructive criticism provided by my colleagues at the Advanced Technology Research Center (ATRC), which has enriched my experience and contributed to the success of this project.

Furthermore, I am grateful for the financial support provided by the American Society of Heating, Refrigerating, Air-conditioning Engineers (ASHRAE) and the Center for Integrated Building Systems (CIBS), which has enabled me to focus on my research and contribute to the timely completion of this dissertation. I would also like to acknowledge the technical and administrative staff at the Department of Mechanical and Aerospace Engineering at Oklahoma State University for their assistance in various aspects of this research and for providing a conducive environment for learning and growth.

Finally, I want to express my deep appreciation to my family and friends for their unwavering love, support, and understanding throughout my academic journey. Their belief in me has been my source of strength and motivation, and I dedicate this dissertation to them.

Name: HYUNJIN PARK

Date of Degree: May, 2023

Title of Study: DEVELOPMENT OF RECOMMENDATIONS FOR AIR MIXER AND SAMPLER DESIGN AND COMBINATIONS THEREOF FOR PERFORMANCE TESTING OF HVAC EQUIPMENT

Major Field: Mechanical and Aerospace Engineering

Abstract: Advances in equipment performance, and the development of variable speed equipment have led to stricter performance testing of HVAC&R equipment, requiring limited tolerances on capacity and efficiency measurements to 5% of certified ratings. This necessitates the use of third-party performance validation tests by manufacturers. Accurate airside measurement is crucial, and proper air mixing is necessary to minimize airflow nonuniformities before air sampling. However, the available literature and guidelines on air mixing and sampling device design are limited, which can result in discrepancies in measured efficiency beyond the allowable tolerances. To address this issue, this research aims to develop design recommendations for air mixing and sampling devices used in HVAC&R equipment performance testing. The study assessed the mixing effectiveness and pressure drop of three types of air mixers - baseline louvered mixer, orifice-type mixer, and orthogonal pattern louver mixer - under various operating and geometrical conditions. The results showed that all three mixing devices were capable of reducing airflow stratification. However, the orthogonal pattern louver mixer showed the most promising results due to its simple design, and the high mixing performance and low pressure drop in a limited mixing length which can be achieved due to its advantage of creating two-dimensional mixing, which is reliable even if maldistribution profile unknown, contributing to its superior performance compared to the other two mixing devices. Additionally, the investigation of design guidelines for air sampling devices for accurate and reliable performance resulted in design constraints and guidelines for sampling hole size, pitch, sampler material, and other factors. Furthermore, the study explored the effectiveness of combining air mixing and sampling devices to enhance the accuracy of capacity measurements through in-situ testing, focusing on the optimal configuration of the combination. The results suggest that selecting an air mixer with high mixing performance and a sufficient mixing length can contribute to a robust mixer-sampler combination for improved accuracy and precision of capacity and vapor mass balance measurements. Overall, this study provides valuable insights into optimal air mixing and sampling device design and configuration, enhancing bulk air condition accuracy, and improving HVAC equipment capacity measurement accuracy in psychrometric performance testing.

TABLE OF CONTENTS

Chapter Page

Chapter Page

Chapter Page

LIST OF TABLES

LIST OF FIGURES

Figure Page

Figure Page

Figure Page

Figure Page

Figure Page

Figure Page

Figure Page

Figure Page

NOMENCLATURE

2D ·····	Two dimensional
AHRI ·····	Air conditioning, Heating and Refrigeration Institute
ASHRAE ·····	American Society of Heating, Refrigeration and Air Conditioning Engineers
CFD ·····	Computational Fluid Dynamics
CFM ·····	Cubic feet per minute
CFR ·····	Code of Federal Regulation
DB ·····	Dry bulb
DOE ·····	Department of Energy
HVAC&R ·····	Heating, Ventilation, Air Conditioning and Refrigeration
IHX ·····	Internal Heat Exchanger
PID ·····	Proportional-integral-derivative
RH ·····	Relative humidity
RTD ·····	Resistance temperature detector
TC ·····	Thermocouples
ΔP ·····	Pressure drop between up and downstream of air mixing device(s) [inWC or Pa]
Π_P ·····	Euler number, normalized pressure drop
D_h ·····	Hydraulic diameter of the duct in the duct in the test section [inches or m]
$s(\Delta T)$ ·····	Average standard deviation between temperature sample grid points [°F or K]
SP ·····	Static pressure [inWC or Pa]
T ·····	Temperature [°F or K]
v, V ·····	Velocity [ft/s or m/s]
L ·····	Mixing length or overall length; a distance between the inlet of the first mixer and the measurement station in the test section [inches or m]

$\dot{m}$ ·····	Mass flowrate [lbm/hr or kg/s]
n ·····	Number of employed temperature sensors
Q ·····	Volumetric flowrate [CFM or m^3/s]
U ·····	Component velocity in flow direction [ft/s or m/s]

Subscripts/Superscripts

air ·····	Air
av, avg ·····	Average
$cold$ ·····	Cold airstream entering test apparatus
downstream ·····	Downstream of the entire air mixer set
Free-stream, free ·····	Airflow in the test section
hot ·····	Hot airstream entering test apparatus
$in, inlet$ ·····	Inlet of the test apparatus
i ·····	Section of flow in discretized cross-section
low ·····	Lower inlet
m ·····	Mixer element
max ·····	Maximum
$mean$ ·····	Mean
min ·····	Minimum
R ·····	R-chart method
s ·····	Standard deviation
tot ·····	Total
$sampled$ ·····	Air sampled by an air sampler
$test$ ·····	Test section
Up ·····	Upper inlet
Upstream ·····	Upstream of the entire air mixer set
$vapor$ ·····	Water vapor in airflow
x ·····	Confidence interval (e.g., 95% or 99%)

m ····· Mixer element

Greek symbols

α ····· Coverage multiplier

ε ····· Percent mixing effectiveness

ρ ····· Fluid Density [lb_m/ft^3 or kg/m^3]

ω ····· Absolute humidity, humidity ratio [lb_m/lb_m or kg/kg]

CHAPTER I

INTRODUCTION

Advances in equipment performance, as well as the development of variable speed equipment, have increased the capacity specific airflow rate range (e.g., cfm/ton). In parallel, this has decreased the temperature difference across heat exchangers. Under such conditions, psychrometric performance testing of Heating, Ventilating, Air Conditioning, and Refrigeration (HVAC&R) equipment requires more accurate airside measurement of inlet and outlet conditions than in the past. According to published rating standards including AHRI Standards (210/240, 340/360, and 365), and a US federal regulation (10 CFR [DOE, 2017]), tolerances on capacity and efficiency measurements to the certified rating are limited to 5%. To satisfy these standards, manufacturers are required to use third-party performance validation tests. The most reliable approach for accurate airside measurement is minimizing any nonuniformities in the airflow such as temperature, velocity, humidity, and enthalpy prior to air sampling at multiple locations. Well mixed uniform temperature and velocity profiles achieved by the use of air mixing devices prior to the measurement of air conditions can contribute to accurately measuring the capacity of coils. For example, an experimental study dealing with an internal heat exchanger (IHX) has shown that IHX capacity can be affected by up to 15%, depending on using static mixers prior to temperature measurements or not (Musser et al. (2016)).

In summary, differences in the design of the air mixing and sampling apparatus may result in discrepancies in measured efficiency that exceed the allowable performance rating tolerances. In capacity measurements, comparatively small changes in temperature and humidity between air-inlet and outlet of unitary equipment, especially for high-efficiency equipment, is likely to cause a large change in the airside capacity measurement. Figure 1 demonstrates how the measurement error of the temperature difference between the inlet and outlet of a coil affects the uncertainty of capacity measurements. The uncertainty increases linearly with the measurement error of the temperature difference, and this effect is also inversely proportional to the temperature difference between the inlet and outlet. Therefore, accurate airside bulk condition measurement for HVAC&R equipment testing is required to avoid discrepancies between laboratories.

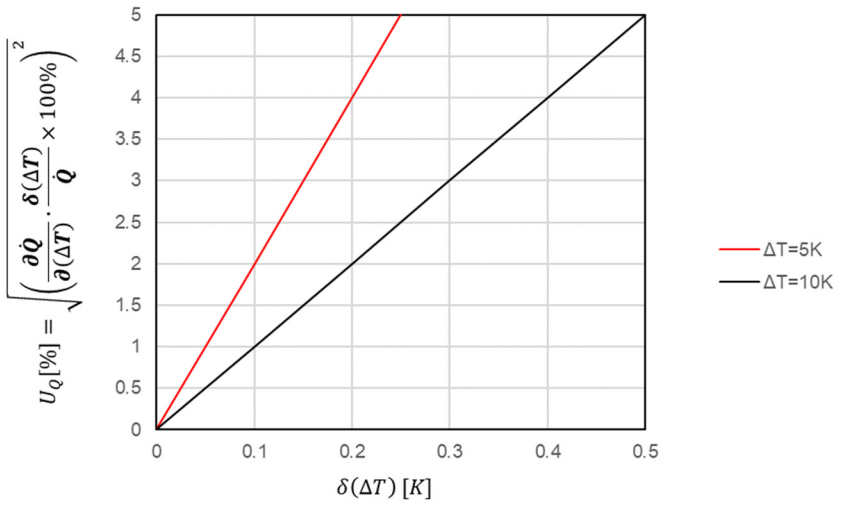

Figure 1 The effect of temperature difference measurement error on the uncertainty of capacity measurement that is typically limited to 5% for HVAC&R measurement purpose

1.1. Motivation

Various shapes of ducts including round, rectangular, and oval are used in air conditioning systems. Traditionally, round ducts have been extensively chosen for the systems due to their advantages such as efficiently conveying moving air with less friction, easy and faster installation, less noise, and cheaper initial cost (Bhatia, 2001). However, due to the fact that round ducts require more

height than rectangular or square ducts, rectangular or square ducts are preferred for many space constrained HVAC&R applications. In addition, not only to be applied to low-pressure systems are these ducts beneficial, but also to have an easy and look-nice connection of fan coil to the main duct. Such advantages have been leading to rectangular and square ducts being more actively adopted to psychrometric performance testing facilities consisting of main components connected using a duct system.

Various efforts to improve measurement accuracy in such facilities have been made, one of which is to eliminate maldistributions in airflow conveyed through duct systems using air mixing devices before measuring the air bulk conditions. Despite the significant impact of uniformity of velocity and temperature in airflow on measurement accuracy, air mixing devices for square ducts commonly used in the HVAC&R industry are not well studied and only limited information on their design and performance is available. Likewise, it is hard to find specific guidelines on the design of air sampling devices although the accuracy in measuring air conditions using such devices is subject to their design parameters, such as sampling hole size, density, spacing, etc.

Considering that the accurate measurement of bulk air conditions in HVAC&R equipment testing significantly depends on how to design air mixing and sampling devices and how to validate their performance, investigation on the performance of air sampling and mixing devices designed for square ducts is necessary to provide guidance for their design.

1.2. Objectives

The objective of this study is to develop the design recommendations of air mixing and sampling apparatus for psychrometric performance testing. The apparatus designed based on the recommendations should provide the accurate measurement of airside capacity of HVAC&R equipment with low pressure drop in a short overall duct length. Therefore, this study specifically aims to

- Provide the design recommendations for air mixing devices reducing nonuniformity in airflow,
- Establish strategies to design air samplers that accurately measure dry and web bulb temperature, and uniform air conditions, and
- Propose methods for evaluating the performance of an air sampler and mixer combination.

1.3. Contribution to Body of Knowledge

An airside measuring apparatus designed based on insufficient guidance may result in discrepancies in measured equipment performance, causing considerable inaccuracy in bulk air conditions measurement, and void testing results for HVAC&R equipment tests. This investigation can contribute to standardizing design guidelines for efficient and effective air mixing and sampling devices which are required for better accuracy in measurements and other practical applications such as economizers, maintaining our industries' credibility.

CHAPTER II

LITERATURE REVIEW

ABSTRACT

With recent advancements in HVAC&R equipment performance and variable speed technology, performance testing has become stricter, requiring limited tolerances on capacity and efficiency measurements to 5% of certified ratings. To meet this tolerances, accurate airside measurement is crucial, and to achieve this, it is essential to minimize airflow nonuniformities before air sampling through proper air mixing. However, differences in design of the air mixing and measuring apparatus due to generous guidelines may result in discrepancies in measured airside capacity that exceed the allowable tolerances, leading to so called “false testing failures”. To maintain our industries’ credibility, it is essential to develop standardized design guidelines for the test apparatus that reduces the probability of such failures. This literature review gives an overview of available and relevant research and standards to provide comprehensive and general information on air mixing and sampling devices and measurement techniques for psychrometric performance testing. Furthermore, this review summarizes the mixing and dynamic performance of representative mixer types, mixer design parameters, sampler design guidance, as well as various testing conditions based on our understanding of experimental results in open literature. A portion of chapter has been published in the Science and Technology for the Built Environment (Park and Bach, 2019).

2.1. Background

Psychrometric performance testing of heating, ventilating, air conditioning, and refrigerating (HVAC&R) equipment requires accurate measurement of air flow rate as well as the inlet and outlet air conditions. Since velocity, temperature, and other properties such as enthalpy and humidity are generally non-uniform at the cross section of air stream in a measuring station, there have been many attempts to accurately measure the average value of such uneven air properties. Separately from measurement applications, non-uniformity of the air in a unitary system is likely to cause various issues, including frozen coils, and inaccurate control of the system (Robinson, 2001).

In order to improve accuracy in measuring average air conditions it is required to remove any non-uniformities from the air flow, including non-uniform temperature distribution of the cross section of the air stream. One of the methods suggested to reduce the non-uniformity in the air stream is employing a mixing process using static mixers. This has been extensively investigated by a study at the National Bureau of Standards (Faison et al., 1967) using round ducts. This forced mixing can be obtained with the use of one or multiple air mixing devices (mixers) which can be installed in a mixing apparatus. The turbulence generated by the mixer(s) allows mixing in the space within the mixing apparatus downstream of the mixer(s).

The open literature shows examples for the design of such mixing devices; ASHRAE Standards 41.1 (2013) and 41.2 (1992) provide some pictures and limited information about the design of mixing devices with some generalized dimension for applications in round ducts. However, other than Faison et al.'s early work, only limited information on the effectiveness is available. In particular, the trend in the HVAC&R industry is to use square ducts for testing, and it is unclear if Faison's results apply to square ducts. Additionally, no standard exists to evaluate the performance of square mixers, resulting in no objective way to compare difference mixer design in terms of mixing effectiveness.

2.2. Measurement of Mixing Performance

This literature review summarizes what is currently available in the open literature, including mixer design, mixing effectiveness, and pressure drop. It also highlights potential issues with grid temperature measurements and includes consideration of a statistical method that can be used to determine the necessary number of RTD temperature sensors.

Quantifying the effectiveness of air flow mixers is of interest for measurement of bulk air conditions as part of equipment performance testing (e.g., AHRI 210/240, AHRI 340/360). Increasing the mixer effectiveness reduces the measurement error caused by uneven air flow temperature, humidity, and velocity. The mixers adopted in ASHRAE Standard 41.1 (2013) and 41.2 (1992) are the top 3 candidate mixers for round ducts described in Faison et al. (1970).

2.2.1. Metrics of Mixing Effectiveness

Mixing performance or mixing effectiveness can be expressed in different ways, based on the intended use of the resulting number. Faison et al. (1966) defines a performance metric;

$$\text{Percent effectiveness} = \frac{max\left(\Delta T_{upstream}\right) - max(\Delta T_{downstream})}{max\left(\Delta T_{upstream}\right)} \cdot 100[\%]$$
$$\left(= \varepsilon = \left(1 - \frac{max(\Delta T_{downstream})}{max\left(\Delta T_{upstream}\right)}\right) \cdot 100[\%]\right), \quad (1)$$

where:

$max\left(\Delta T_{upstream}\right)$	Highest temperature difference between temperature sample grid points prior to (upstream of) air mixer,
$max(\Delta T_{downstream})$	Highest temperature difference between temperature sample grid points after (downstream of) air mixer, and
Percent effectiveness	Dimensionless measure of mixing effectiveness.
ε	Convenience notation introduced here for “Percent effectiveness”.

Faison et al.'s (1966) metric in essence captures the outliers in the sampled points both upstream and downstream of the mixer. This measure is particularly useful if one intends to characterize how well the mixer works under worst case temperature sensor placement – e.g., reduced number of temperature sensors that are placed at the extreme points upstream and downstream of the mixer. Faison et al.'s (1970) report reintroduces equation (1) with slightly different notation and notes that it is much simpler to calculate than the method introduced next but also that it "could be influenced by a single temperature value".

Faison et al. (1970) introduces an additional measure for effectiveness that is based on the average standard deviation of the upstream ($s(\Delta T_{downstream})$) and downstream ($s\left(\Delta T_{upstream}\right)$) measurements, using an updated notation,

$$\varepsilon_s = \left(1 - \frac{s(\Delta T_{downstream})}{s\left(\Delta T_{upstream}\right)}\right) \cdot 100[\%]. \quad (2)$$

Based on the raw data available in Faison et al. (1970), we found that the difference between the two measures is approximately 0 to 10%.

Robinson (2001) chose to use a modified range mixing effectiveness introduced in an earlier publication (Robinson, 2000). His intent was to use the mixing effectiveness primarily for mixing as applicable to unitary equipment (economizer) static mixers, where one of the goals of mixers is to prevent freezing of sections of the coil. He points out that a statistically based mixing effectiveness poorly addresses outliers towards low temperatures, understating how well a mixer helps in preventing coil freezing. Robinson's modified range mixing effectiveness[1] is defined as

$$\varepsilon_R = 1 - \frac{T_{max,downstream} - T_{min,downstream}}{T_{hot,upstream} - T_{cold,upstream}}, \quad (3)$$

[1] Symbols modified for consistency with other equations in this section.

where:

$T_{hot,upstream}$	(average) temperature of hot airstream entering test apparatus,
$T_{cold,upstream}$	(average) temperature of cold airstream entering test apparatus,
$T_{max,downstream}$	maximum temperature downstream of mixing device (individual sensor value), and
$T_{min,downstream}$	minimum temperature downstream of mixing (individual sensor value).

Note that Robinson (2001) chose to use the average air temperature entering the testing apparatus rather than an air temperature measured with a grid directly prior to the mixing apparatus (e.g., mixer and space downstream of mixer allowing mixing process). The disadvantage is that there will be some unaccounted mixing and heat transfer in the components (control dampers, velocity measurement station, straightener grid, and to the ambient through ductwork) prior to reaching the mixer. However, this approach allowed accurate measurement of the inlet air conditions for the uneven hot and cold air flow rates (0-100% cold air ratio) that he was interested in.

Robinson (2001) points out that just relying on a finite number of measurements will not give an accurate value for the confidence we have in the modified range mixing effectiveness ε_R. He therefore proposed to employ the R-chart method described in Montgomery (1997) to determine ε_R with an associated 95% or 99% confidence level. In essence, this adds a multiplier to the second component of equation (3), e.g.

$$\varepsilon_{R,x} = 1 - \alpha_x \cdot \frac{T_{max,downstream} - T_{min,downstream}}{T_{hot,upstream} - T_{cold,upstream}} \tag{4}$$

where x is the confidence interval (e.g., 95% or 99%) and α_x is a coverage multiplier[2] that increases with increasing confidence interval and decreasing number of sensors. Robinson (2001)

[2] Term introduced by the authors.

provides further detail on how α_x is determined. For the effect of this multiplier, see Figure 4.

2.2.2. Additional Requirements for Accurate Bulk or "True Mean" Temperature Measurements

Wile (1947) points out that non-uniformity of flow velocity can lead to substantial measurement error[3]. Such non-uniformity may occur at the exit of modern air handling units, particularly if configured in pull through configuration. Wile conducted a thought-experiment with an assumed flow non-uniformity caused by half the duct being at one velocity while the other half was at 25% of that velocity. With an assumed temperature difference of the two streams of 10°F (5.6°C), a measurement error of 3°F (1.7°C) will occur if the average is solely obtained by sampling the temperature uniformly without considering that flow non-uniformity. To reduce the issue of non-uniform flow velocity, Wile suggested increasing the flow velocity using a Venturi style nozzle with the temperature measurement station located in the throat of the nozzle. This change alone reduced the error in his thought experiment by substantially reducing the flow non-uniformity, leading to a remaining error of 0.13°F (0.07°C) – or approximately 4% of the previously mentioned 3°F (1.7°C) error. Figure 2 shows how Wile included such a Venturi nozzle into his "improved air flow measuring apparatus". Note the application of the now well-known consecutive horizontal/vertical mixer design ahead of the Venturi nozzle to increase mixing and further decrease flow non-uniformity.

[3] Page 518 of his work, starting top right paragraph.

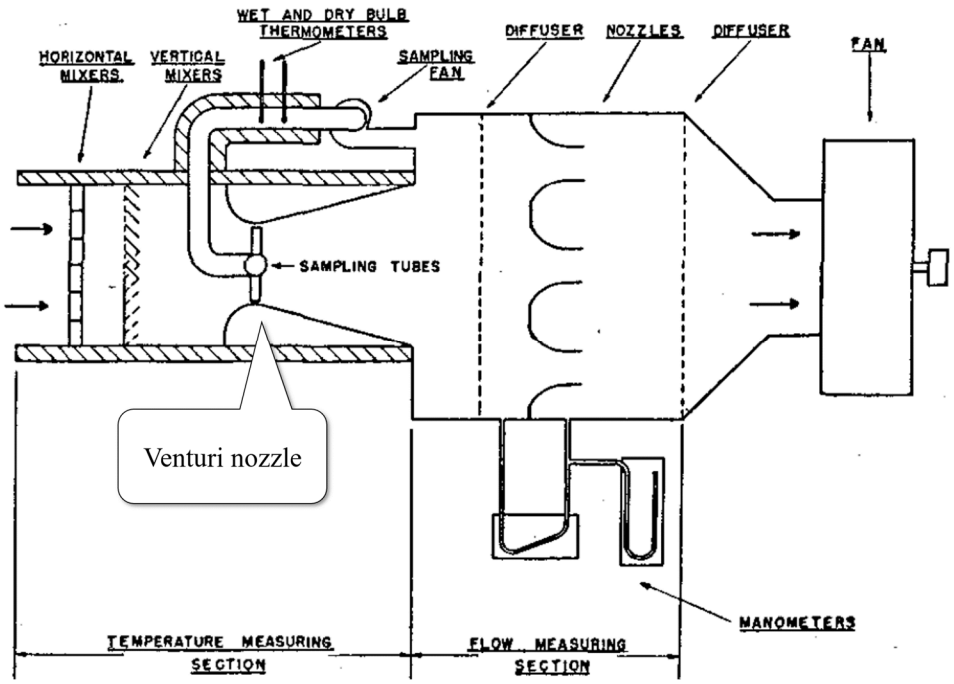

Figure 2 Wile's (1947) 'Improved multiple nozzle air measuring apparatus

Figure 3 shows ASHRAE 33's recommended apparatus for testing coils. Note that an approach similar to what Wile had proposed was chosen, with a smaller cross section area for measuring inlet temperature followed by an expansion with baffle prior to the tested coil. Wile's Venturi nozzle in effect is used once more at point 4 in the ASHRAE 33 apparatus.

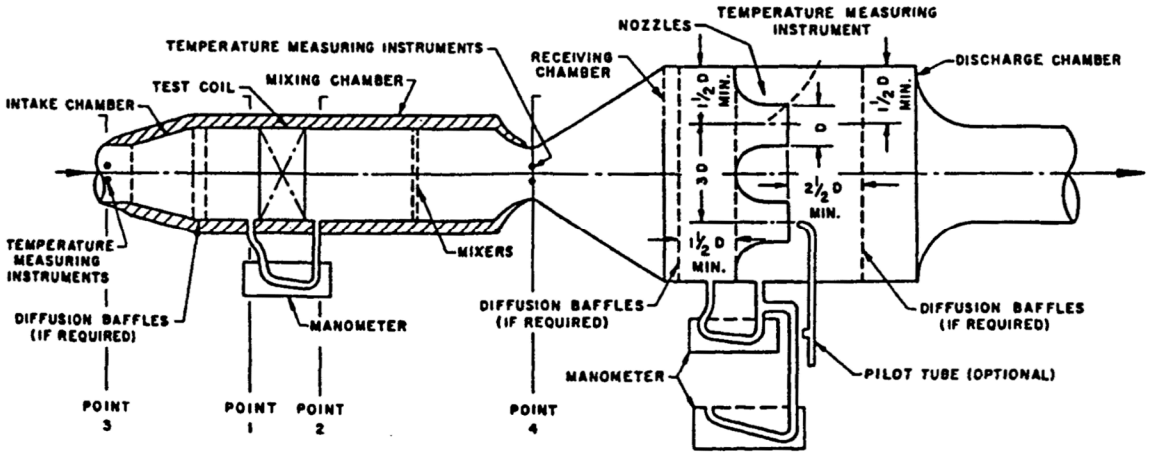

Figure 3 Recommended air flow, air pressure, and air temperature measuring apparatus. Source: ASHRAE 33 (2000)

2.2.3. Risk and Potential Limitations of Temperature Measurement (Thermocouple or RTD) Grids

Wile (1947)'s work contains an anecdote about an experience gained during the calibration of a code tester using a steam heating coil as reference heat input. They employed air sampling trees[4] at the inlet and the outlet of the heating coil. As a check, they also installed 20 thermocouples at the outlet of the coil – that surprisingly showed "considerable variance" relative to the readings of the air sampling tree. This was despite the individual grid points reading very similar values. Additional measurements found inactive steam tubes that were not detected by the grid – highlighting the importance of air mixers.

Wile (1947) also points out a quite obvious limitation of grid-style temperature measurements. To cite his words, a grid with a large number of points "...may be substituted for the sampling tube except that its use is not practical for wet bulb readings." More correctly, the last part of his sentence should read "…except that it is clearly impossible to read wet bulb temperatures with a (dry bulb) temperature measurement grid."

Technology has changed substantially since Wile published his paper in 1947. Dew point meters, which had the first patents filed in 1943 (McIlvaine, 1948), and 1945 (Rieber, 1951) now have sufficient reliability and accuracy. Additionally, they are now available as commercial devices at reasonable cost with high accuracy. Dew point meters in combination with a dedicated, low air volume test air sampling device for humidity sampling combined with a temperature grid may therefore be able to overcome the limitations mentioned by Wile in 1947. The advantage is a

[4] Wile (1947) adopted the term "sampling tube" in his work. However, Figure 7 of his work clearly shows the well-known design that has a main trunk with sampling branches on both sides.

smaller space requirement of the sampling tube arrangement within the air stream when compared to air sampling trees. Potential pitfalls of this low flow rate sampling tube mechanism are pointed out by the Project Monitoring Subcommittee (PMS) of ASHRAE RP-1733 (Kirkwood et al., 2018) are condensation within the sampling tube if the tube is lead through spaces of lower temperature as well as moisture absorption by the tube material.

2.2.4. Determination of Average (Bulk or True Mean) Air Condition

Bulk air conditions prior or after an air mixer can be calculated by mass flow weighted averaging of local conditions. Mathematically, this is multiplying the local value of the variable of interest with the local air mass flow rate, then integrating over the cross section of the flow, and then dividing the result by the total mass flow rate. As an example, for determining the average temperature T_{avg} of a total air mass flow $\dot{m}_{tot}$ in a duct with cross section x by y, a local mass flow $\dot{m}''$ weighted integral of the local temperature T is needed:

$$T_{avg} = \frac{1}{\dot{m}_{tot}} \cdot \int \int \dot{m}'' \cdot T \, dxdy. \tag{5}$$

In practice, the above integral is not possible to solve since all cost-effective experimentation leads to spatial discretization or sampling at individual points. Instead, spatial discretization is used to simplify the measurement by summing up sections i of the flow, e.g.

$$T_{avg} = \frac{1}{\dot{m}_{tot}} \cdot \sum \dot{m}_i T_i = \frac{\sum \dot{m}_i T_i}{\sum \dot{m}_i}. \tag{6}$$

Equations (5) and (6) are identical only if mixing two air streams of known mass flow rate and temperature under adiabatic conditions. However, if we want to determine the flow conditions at the outlet of a heat exchanger, we do not have the luxury of access to airstreams of known temperature and flow rate. Instead, discrete local measurements need to be made by discretizing the flow into sections to estimate the average flow conditions. Flow measurements are often made with pitot tubes that provide a flow velocity v_i, and a simplified approximation version of equation

(6) can be applied, e.g.

$$T_{avg} \approx \frac{\sum v_i T_i}{\sum v_i}. \tag{7}$$

Note that equation (7) no longer addresses changes in density of the air. If large temperature differences between airstreams are chosen, e.g., 50°F (27.8°C) to reduce instrument error, then density difference between the two air streams will be on the order of 9-10% and equation (6) should be used instead.

Temperature grids, such as "sampler-less" RTD grids further simplify Equation (5). They merely provide an averaging of temperatures in the flow without any consideration of the mass flow rate across their "assigned" measured area whatsoever. However, their use and calculation involve the simplest formula in this section, e.g.

$$T_{avg} \approx \frac{\sum T_i}{n}, \tag{8}$$

where n is the number of employed temperature sensors.

For the risks of equation (8), refer to the previously mentioned thought-experiment by Wile (1947), see section 3.2. Equation (8) should only be used if flow velocity is sufficiently uniform.

2.2.5. Effect of Number of Temperature Sensors in Temperature Grid

Robinson (2001) introduces a set of formulas to calculate the range of mixing effectiveness as per equation (3) based on the number of temperature measurements within the duct. His method is based on the R-chart method that is used in process control applications, with his formulas allowing determination of the lower bound confidence interval. The method assumes a normal distribution of the measurements.

Figure 4 shows the range of mixing effectiveness with 95% confidence for a measured mixing effectiveness of 70% based on the formula introduced by Robinson (2001). A typical minimum

requirement in testing standards, e.g., AHRI 210/240 (AHRI, 2008), section 2.5.5 sub b, and ASHRAE 116, Section 7.4.3.4.1 is 9 temperature sensors. The lower 95% confidence bound for a measured effectiveness of 70% is 60% as shown in the figure. Increasing the grid size to 16 sensors increases the lower confidence bound to 66% while 25 sensors further increase the confidence bound to 69%.

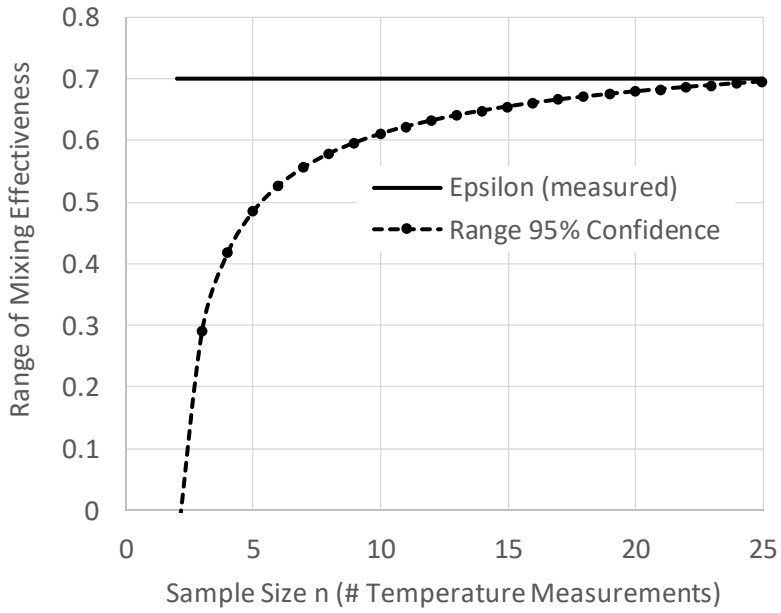

Figure 4 Range of mixing effectiveness for 70% measured mixing effectiveness

On first glance, this suggests that a grid size of 16 (e.g., 4 by 4) or more sensors is required to obtain a lower confidence interval that is sufficiently close to the measured value. However, the range of mixing effectiveness stated in ASHRAE 41.2 (1992), Table 1, is 90 to 99%. Figure 5 shows that the lower 95% confidence interval is 87% for a measured mixing effectiveness of 90% if using 9 temperature sensors. The difference is equivalent to approximately 3% of the measured value, which makes the 3 by 3 temperature grid a good compromise for temperature measurements.

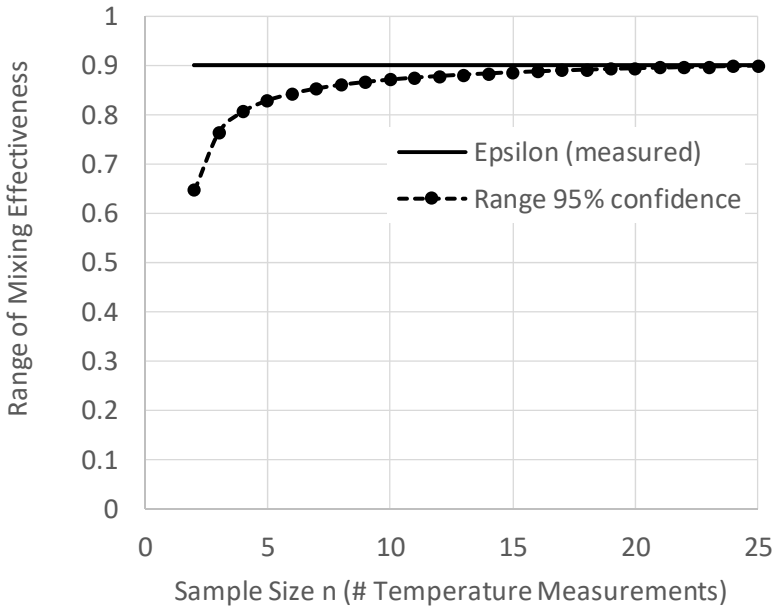

Figure 5 Range of mixing effectiveness for 90% measured mixing effectiveness

2.3. Overview of Mixing Devices

Faison et al. (1970) considered various mixing device candidates. Axial fans and screens were found to be inefficient. Various baffle arrangements (semi-circular, single slats, quartered baffles) were considered but found to be inefficient. Faison et al. (1967) investigated circular baffles as air mixing devices and found 0.33 to 1 ratio of orifice to duct diameter to be effective in reducing temperature differences at the expense of high pressure drop.

One key difference between the mixing devices developed by Faison et al. (1967, 1970) that are still employed in ASHRAE testing standards and modern commercial mixing devices used in air handling units lies in the geometry of the louvers. Rather than abrupt changes in air flow direction (e.g., Figure 6 and 7), airfoil type louvers are employed as shown exemplarily in Figure 8.

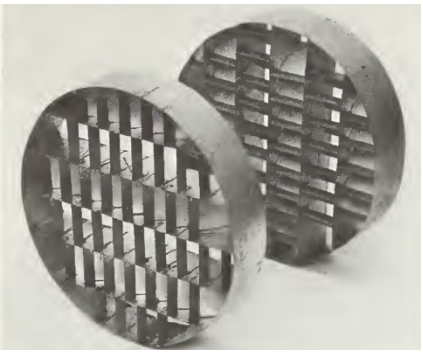

Figure 6 Louvered strip mixing device. Two elements were placed in series, rotated by 90°. Image: Faison et al. (1970)

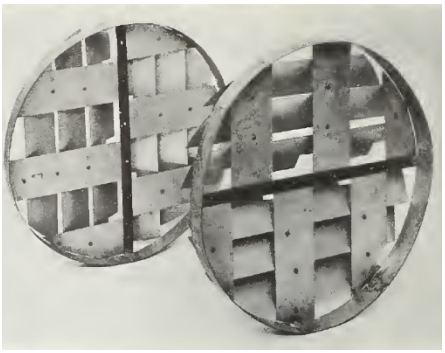

Figure 7 Louver-baffle mixing device. Two elements were placed in series, rotated by 90°. Image: Faison et al. (1970)

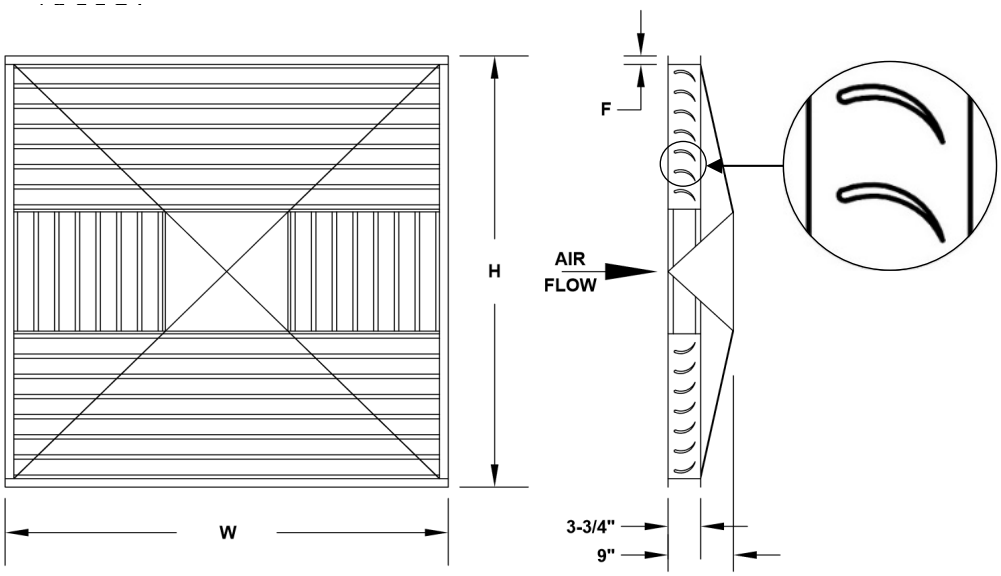

Figure 8 Airfoil horizontal/vertical mixing device. Image: Kees (1998a)

The louver strip device of Figure 6 causes air to flow in opposite direction in small strips, creating blankets of small vortices. In contrast, the commercial device in Figure 8 appears to be aimed at creating large vortices to be more efficient in mixing air from extreme points at the inlet – such as in the manufacturer's intended use as mixer in air handler economizer applications.

A similar approach of creating larger vortices appears to be chosen by one manufacturer for concentric mixers that appear to be a competing product for air handler unit applications. Rather

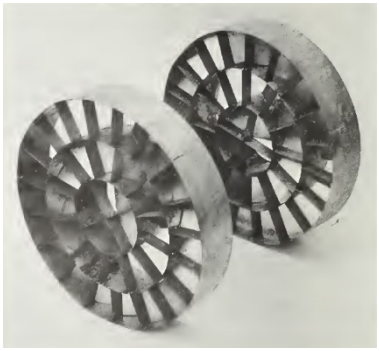

Figure 9 Concentric mixing device. Two elements were placed in series, with direction of mixing elements in opposite direction. Image: Faison et al. (1970)

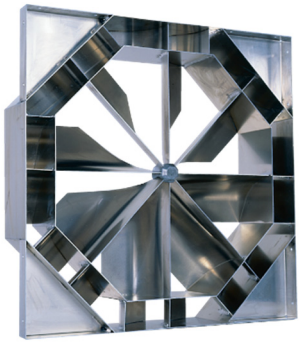

Figure 10 Concentric Static Mixing Device. Image: Blender Products, Inc.

than employing three rings of opposing louvers as shown in Figure 9, only two rings of opposing louvers are employed, as shown in Figure 10. Additionally, the modern commercial device employs an airfoil type louver design to reduce pressure drop at the louver.

Figure 11 shows mixing device include a rectangular array of louver systems invented by Koop (2008). The arrangement of each louver system enables to create vortex flow downstream while air steams passing through each louver system are deflect toward adjacent louver systems. In order to create large vortices more than one various configuration of louver system was suggested as shown in Figure 12.

Table 1 shows the list of patents associated with air mixer design. The majority of the inventions were developed as static mixer having no moving parts and devised to deflect air streams in multiple direction simultaneously, leading to generation of many large and small vortices downstream for an improved mixing process. In addition, some of them are notable for utilizing curved louvers, which presumably helps to achieve smooth transition of the flow direction with lower pressure drop.

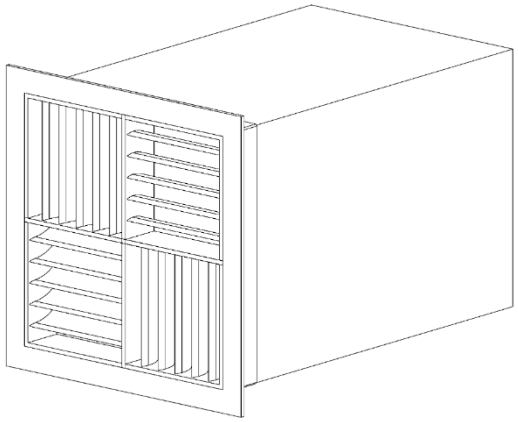

Figure 11 Rectangular array of louver system. Image: redrawn according to Koop (2008)

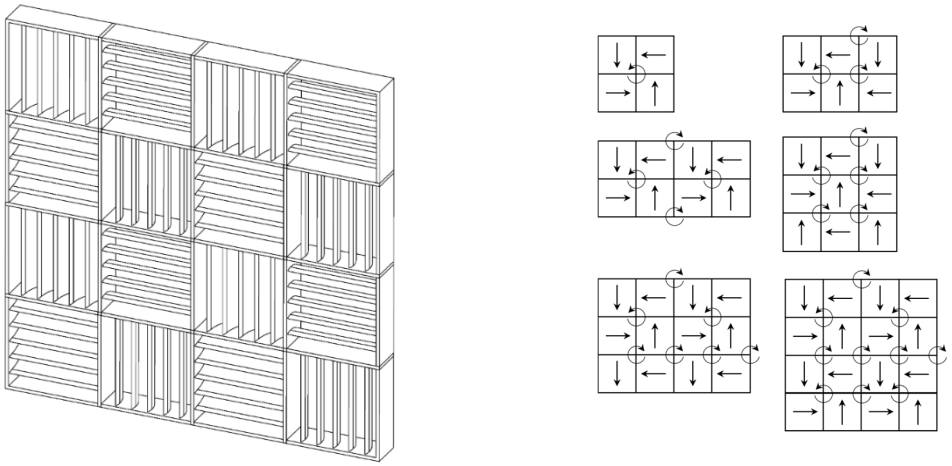

Figure 12 (a) Rectangular louver system and (b) Configurations to generate vortices. Image: redrawn according to Koop (2008)

Table 1 Published patents of air mixing devices

No.	Inventor	Title	Note
1	Edward R. Zieve (1993)	Air Mixer	Combination of vanes in two parallel sets of rectangular regions and pyramid shaped deflector to create an optimal mixing region
2	Hikoroku Sugiura (1998)	Static Mixer	An invention for low pressure loss and high mixing efficiency using a hollow cylinder having a larger diameter than the inlet passage in a mixer body, positioning its opening against inlet port for the impingement of incoming air on its inner side
3	Theodore A. Erickson (1965)	Air Mixer for Air Streams	Utilizing oppositely rotating cyclonic whirls to an air stream to intimately intermix the air
4	Edward N. Koop (2008)	Static Air Mixer	Combination of rectangular array of louver systems to generate vortex flow downstream
5	Keith D. Robinson (2003)	Static Air Mixing Apparatus	Radial vanes in inner enclosure and between inner and outer enclosure with transition member to prolong turbulent mixing of airstreams for better mixing effectiveness
6	Gerold Fleissneer (1992)	Air Mixer Apparatus	Combination of three series-arranged sections of air directing plates to effectively generate vortices

2.4. Effect of Parameters on Mixing Performance using Static Air Mixers

In operation, various parameters contribute to the performance of air mixers in terms of mixing effectiveness and pressure drop. Some of the parameters remarkably influence the performance whereas others have relatively insignificant effects. The extent of the influence depends on the type of mixers as well. In the research conducted by Faison et al. (1966, 1967, and 1970) the effects of relevant variables in utilizing mixers in HVAC&R system measurement applications are well presented, showing how significantly they affect the performance of mixing and pressure drop in the system. In this section, the effects of different parameters for several representative air mixers will be discussed and summarized based on the information from Faison et al.'s experimental

results. All mixing effectiveness data in this chapter were calculated using Equation (2), previously described in section 2.2.1.

2.4.1. Effect of Inlet Air Conditions: Temperature Pattern and Difference, and Total Flowrate

The maldistributed temperature at the cross-section of incoming air flow can have a profile that is often random and unpredictable, making it difficult to define and recreate a representative profile. Hence the need for a comprehensive understanding of simplified representative temperature patterns onto mixing performance, with the goal of identifying the "worst case" temperature profile for a mixer's performance. This approach allows to utilize two well mixed "constant temperature" airstreams for the generation of simplified patterns, which is far easier than generating arbitrary profiles.

Faison et al. (1967, 1970) investigated the variation of mixing effectiveness and pressure drop caused by several types of mixers for different patterns of temperature distribution of inlet airstreams. According to the results of the experiment carried out by Faison et al (1970), it was revealed that increased interface area between air streams having different temperature leads to a more effective mixing process. Additionally, the difference in the air flow ratio of the air streams also has an effect of mixing performance for the same total flow rate. Figures 13(a)-(c) shows that the initial temperature patterns defined by changing configuration of the preconditioned incoming air into circular inlet divided into four quadrants (Faison et al. 1967). It allowed the air streams having different temperatures to experience a change in flow rate, size, and interface area. The results in terms of mixing effectiveness were obtained for an orifice type mixer having three different diameter ratios of 0.33, 0.50, and 0.67 to the duct diameter. The results indicated that the interface area between the cold and warm air contributes to the improvement of the effectiveness. The largest improvement of mixing effectiveness (normalized by the lower value) of 52.9%

occurred for an orifice diameter ratio of 0.67 when the temperature pattern shown in Figure 13(a) was replaced by the one shown in Figure 13(c). The smallest orifice only showed a normalized improvement of 4.3% when changing from the Figure 13(a) to Figure 13(c) pattern. This suggests that increasing orifice diameter ratio increases the sensitivity of the mixing effectiveness to the temperature profile, with a larger interface area leading to a larger mixing effectiveness.

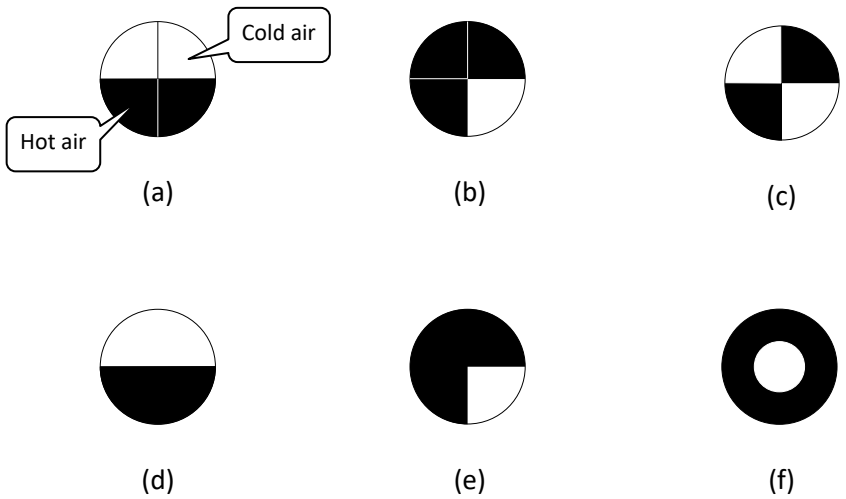

Figure 13 Duct cross section to show temperature patterns of incoming air as used by (Faison et al., 1967 & 1970)

Increasing the ratio of hot air to total flow rate leads to a more effective mixing process. Faison et al. (1967)'s applied different temperature patterns while keeping air velocity constant. This leads to an increase in volumetric flow rate of hot air from 50% to 75% of the total flow rate when changing the temperature pattern from the one shown in Figure 13(a) to the one in Figure 13(b) – which have identical interface area. For this specific temperature profile change, the effectiveness increased by up to 22% for the orifice diameter ratio of 0.67. We attribute this result to the more mass of hot air at a same volumetric flow rate, the more interaction due to lower density caused by higher average temperature of the entire flow. The contribution of interface to better mixing is reconfirmed in another experimental result (Faison et al., 1970). According to the result, the temperature pattern with an inlet concentrically divided in which the same flow rate of hot and cold air enters as shown in Figure 13(f) resulted in the highest mixing performance reaching an effectiveness of 99%. In this case, it is obvious that the inlet pattern leads more interface between

hot and cold air than other inlet patterns shown in Figure 13(d) and (e) which had the effectiveness of 90.2%, and 96.2%, respectively.

The amount of temperature difference in the flow influences the mixing effectiveness since the amount of enthalpy exchange between air particles is affected by their temperature dependent properties. However, it is shown in Faison's experiments (Faison et al., 1967, 1970) that varying the temperature difference of air flow at the inlet from 0.5 to 20.0°F (0.3 to 11.1°C) only has a minor influence on the effectiveness regardless of temperature patterns and mixer types as shown in Figure 14. The maximum change in mixing effectiveness for that range of temperature difference was 1.0 %, except the case for temperature difference in the range from 0.5 to 3°F (0.3 to 1.7°C) showed abnormal effectiveness drop. The authors attributed this behavior to the greater ratio of measurement error to the measured temperature difference for those test conditions.

Faison et al. (1970) found during initial tests that louvered mixer's performance becomes independent of the temperature difference between the two mixed air streams if that temperature difference is larger than 3°F (1.7°C). They suspected instrument error as the culprit for the change of effectiveness for low temperature differences and therefore conducted all other tests at temperature differences of 3°F (1.7°C) or higher.

It was also revealed that the effect of mean velocity at the inlet was insignificant for all cases tested in their experiments whereas pressure drop increased as total flow rate increased while maintaining the same ratio of cold and hot air. According to Faison's results (Faison et al., 1967, 1970), the effectiveness changed less than 5% and 3% for orifice and louver types of mixers, respectively, as shown in Figure 15. In their experiment, the flow rate was varied at 1:6.25 ratio, ranging from 300 to 1,875 CFM (0.14 to 0.89 m^3/s). The result also indicates that the inclusion of baffles in a louvered mixer makes it slightly more sensitive to mean air stream velocity in terms of mixing effectiveness and pressure drop.

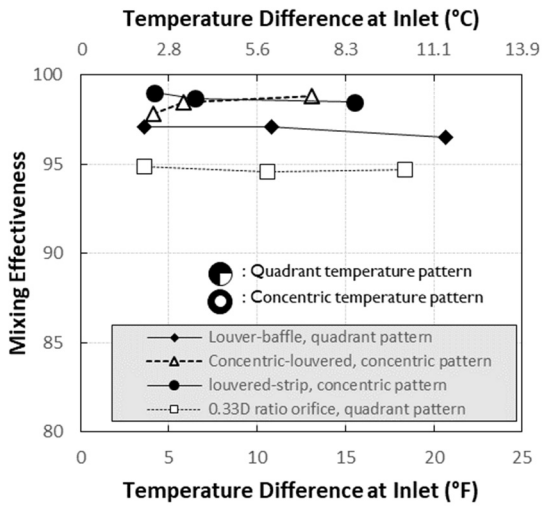

Figure 14 Effect of inlet temperature difference on mixing effectiveness. Data source: Faison et al. (1967 & 1970)

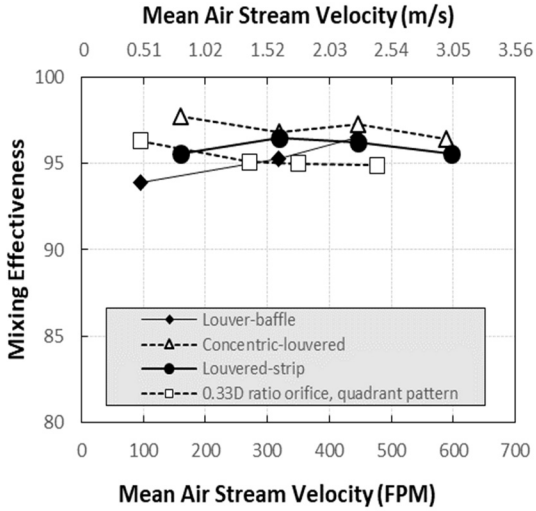

Figure 15 Effect of mean air stream velocity on mixing effectiveness. Data source: Faison et al. (1967 & 1970)

2.4.2. Effects of Air Mixer Design Criteria: Type of Mixers and Louver Angle

Performance testing for several types of air mixers for round ducts, including square-edged (round) orifices, louver strip, louver-baffle, and concentric louver, was conducted by Faison et al. (1967, 1970). Squared-edged orifices' mixing performance was substantially more sensitive to the testing parameters than all tested louver mixers. In addition, the result indicated the overall length and the orifice type mixers' ratio of orifice to duct diameter as the most significant design factors for their mixing effectiveness. In particular, the smaller the diameter ratio, the larger the mixing effectiveness. However, while – for some testing parameters – the smallest diameter ratio orifice showed similar mixing effectiveness to the louvered mixers', it was leading to substantially higher pressure drop. Faison et al. (1967) also tested a combination of orifice type mixers with a target plate. However, the addition of the target plate resulted in no improvement in the mixing performance at the expense of additional increase in pressure drop.

Turbulence-rich flow is required for achieving good mixing effectiveness if duct length is limited but it simultaneously leads to more pressure drop than less turbulent flow. Faison et al. (1970)

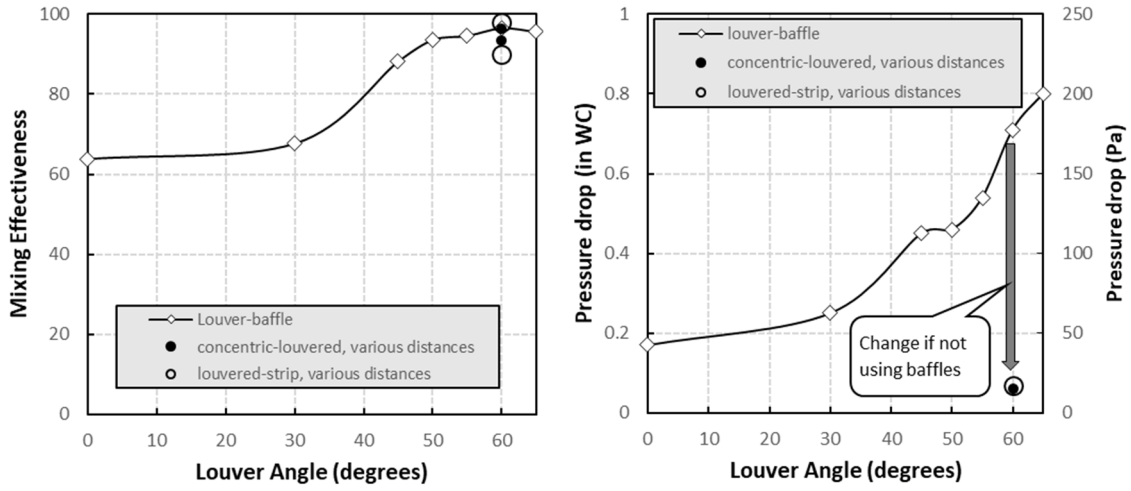

(a) Mixing effectiveness as a function of louver angle

(b) Pressure drop as a function of louver angle

Figure 16 Performance of 24" (0.6096 m) round louver-baffle mixer at 1400 CFM (0.6607 m^3/s) for different louver angles. 0.91 duct diameters spacing between first and second mixing element, 38" (0.9652 m) distance after second mixing element to measurement station. Data source: Faison et al. (1970), Table 3.

investigated different louver angles for two of the three mixer configurations given in ASHRAE 41.2 (1992). Figure 16(a) shows detailed data that they obtained for the louver-baffle configuration of two mixing elements in series. Mixing performance did not improve much past 50° louver angle but pressure drop did increase almost exponentially with angle (Figure 16(b)).

Faison et al. decided to adopt the 60° angle for their other mixer styles that did not include baffles. The baffle-free mixers (concentric-louvered and louvered strip) led to similar mixing performance as the louver-baffle version at roughly one order of magnitude less pressure drop than the louver-baffle version. This is attributed to the results of the more efficient turbulent generation, and it is considered that baffles are substantially less efficient in generating turbulence. At least one commercially available mixing device (Kees, 1998a, 1998b, 2005) employs airfoil type louvers to reduce the losses at the louvers, generating turbulence/eddies more efficiently.

Faison et al. (1970) based their design of having two orthogonal mixing elements in series at a distance as well as the design of the louver-baffle mixer on an earlier work presented by Wile (1947). Wile investigated the use of air mixers as part of the temperature measuring component at the inlet of their code tester design. Wile's work addressed rectangular mixers that interestingly

used louver angles of 45° and 60° as incorporated for round louver-baffled mixers in ASHRAE 41.4. Going back to Figure 16 this corresponds to pressure drop of less than 0.5 inWC (125 Pa) albeit at reduced mixing performance.

Another study investigating rectangular mixers is Robinson (2001). However, Robinson (2001) investigated extremely uneven hot and cold air flow rates. He chose an inlet temperature profile that had a cold air flow stream at the bottom and warm air at the top as a worst-case scenario from previous studies. His result indicates that similar flow rates of the cold and warm airstream lead to the smallest mixing effectiveness, while increasing the difference in the two air flow rates improves mixing effectiveness. The distributions of mixing effectiveness as a function of cold air ratio are not perfectly symmetric in a range from 0 to 1.0; it appears that air density differences may affect the result. In general, mixing effectiveness was shown to increase with increasing distance from the mixer.

2.4.3. Effect of Mixer Spacing and Mixing Length

Multiple air mixers are often utilized in series to achieve improved mixing effectiveness within limited distance, typically with individual mixers rotated by an angle to each other. Such configuration of the mixers allows deflection of air streams in multiple directions; for instance, opposing or perpendicular directions. An increased shearing action at the interface of air streams and turbulence in the flow due to three-dimensionality in their movement leads to the development of more energy transfer, and thus rapid mixing of the air streams.

The distance (e.g., spacing) between a series of mixers is regarded as one of the key variables to control mixing performance. A study that examined the effect of mixer spacing was carried out by Faison et al. (1970) for three of representative air mixer pair types - louvered strip, louver-baffle, and concentric louver. Two identical mixers were installed in series in the test section with the second mixer rotated 90° around the axis of flow direction with respect to the first mixer. The

results of that study are presented in Figure 17; as the distance between mixing elements increases the effectiveness for the louvered-strip mixers increases and then remains constant after reaching a maximum. The case of the louver-baffle and the concentric louvered mixer show different trend: The effectiveness reaches a maximum, and then decreases. It is speculated that, in general, there is a trade-off relation between the first and second mixing process if overall length (e.g., inlet to measurement station) is fixed. The increase in space between mixers increases mixing in between mixers while also dissipating mixing enhancing turbulence. At the same time such an increase in spacing causes a reduction of the space between the second mixer and the measuring station, reducing mixing in that region. Therefore, there may be an optimized distance between the mixers if overall length is fixed. It was also revealed that varying the distance did not influence the static pressure drop caused by the mixers. Therefore, the results suggest that it is important to investigate the optimized distance for the most efficient use of the mixers in a series.

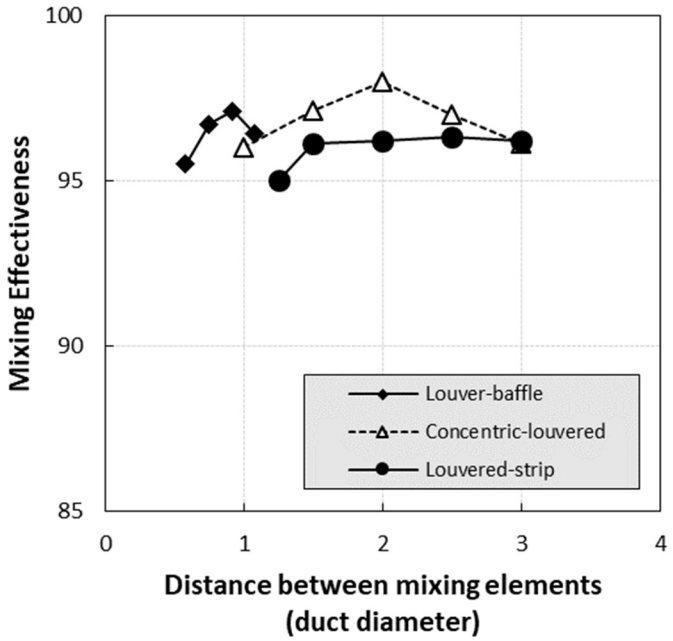

Figure 17 Variation of mixing effectiveness as a function of a distance between mixing elements. Data source: Faison et al. (1970)

The interactions by three-dimensional flow such as large and small vortices, separation, and reattachment occur while the air streams having different thermal properties are passing through

the mixing apparatus, transferring energy between the streams. Such complicated turbulent flow gives rise to significant pressure drop and viscous dissipation, which remains until the flow becomes close to fully developed if sufficient length downstream of the mixer is available.

The above suggests that only when the flow disturbed by the mixers becomes stabilized downstream will it have reached the maximum mixing effectiveness for a specific mixer. At that point, temperature will be very uniform, with the maximum static pressure being regained at the same location. This behavior was proven experimentally by Faison et al. (1966) by measuring the variations of pressure and mixing effectiveness downstream of various mixers. When selecting mixers, it is therefore required to carefully consider the overall length needed for full mixing; if space is limited, then an additional secondary mixer may help to obtain desired mixing effectiveness at the expense of additional pressure drop.

In practice, it is necessary to find a compromise between mixing performance and space limitations in the HVAC industry. A target distance of 1/8 of a duct diameter between consecutive mixers and a downstream mixing distance of no more than 2 duct diameters was suggested as a guideline (Denton et al., 2019).

Figure 18 shows the variation of mixing effectiveness as a function of the distance to the first mixer for several types of mixers employed in pairs (Faison et al., 1970). The rate of an increase in mixing effectiveness shows an exponential behavior with limited rate of return for additional distance. The result indicates that louver-baffle mixers lead to the shortest required distance for the mixing process. This is because the increased flow velocity caused by the baffles flow area reduction is leading to a larger amount of turbulence after the louvers as compared to baffle-free mixers.

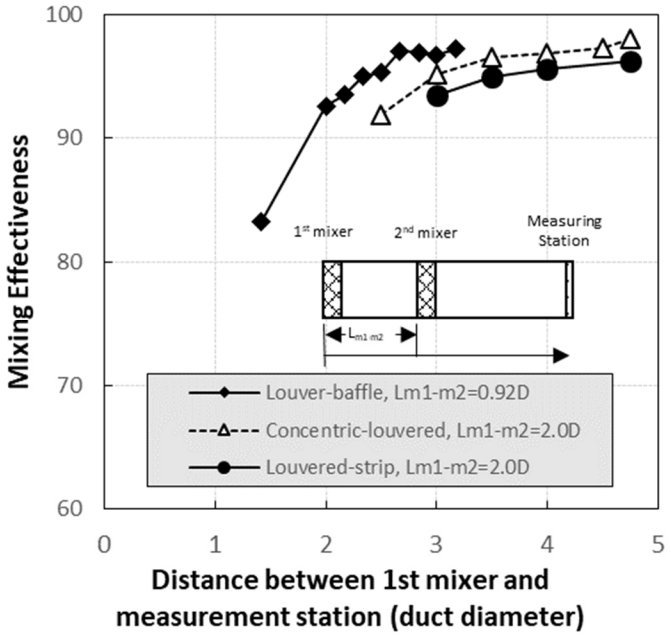

Figure 18 Distribution of mixing effectiveness along downstream. Data source: Faison et al. (1970)

2.5. Overview of Air Samplers

Air samplers, mostly called sampling trees, have been widely used in industry as a means of measuring bulk air conditions by collecting air from numerous points across the flow area and conveying it to a psychrometer where –ideally– its true mean wet and dry bulb temperatures are measured. According to Wile (1947), the most practical way to measure the mean temperature at a cross-sectional area in a duct is to first obtain reasonably uniform velocity pattern using an air mixing device, then average temperatures of the air sampled from many locations of the cross-sectional area using a sampling tree. He also suggested that by installing a sampling tree in the venturi throat, which is shown in Figure 2, it makes it possible not only to sample the air from the uniform air velocity distribution contributing to better accuracy in measuring bulk air conditions, but also help reduce the size required for the air sampling instrumentation.

The air sampled by an air sampler from the measurement section in the duct is conveyed to a psychrometer in which air temperature and humidity are measured with temperature probes in

accordance with ASHRAE Standard 41.1 (2013). In order for accurate measurement of bulk air conditions with air samplers, according to AHRI Standard 210/240 (2017), it is also important, as Wile (1947) also mentioned earlier, to eliminate maldistributed air velocity and temperature before hand, monitoring their distributions with associated devices such as air mixer and thermocouple grid. According to AHRI Standard 210/240 (2017), the maximum allowable temperature difference between individual thermocouples of the grid is limited to 2.0 °F (1.1°C). It is required to maintain the average air temperature at the inlet of the thermocouple grid over time.

The conventional air sampler consists of a trunk with several branch tubes on which multiple sampling holes facing to upstream direction of the air source to draw an air sample are placed as shown in Figure 19. According to AHRI Standard 210/240 (2017), and 10 CFR (US DOE, 2017), the air samplers can be made of stainless steel, plastic, or other durable materials. The standards also propose some guidance of air sampler design as following:

1. >>> Minimum hole density of 6 holes per square foot of area to be sampled
2. Sampler branch tube pitch (spacing) of 6±3 inches
3. Manifold trunk to branch diameter ratio having a minimum of 3:1 ratio
4. Equally distributed sampling holes over the branch (1/2 pitch from the closed end to the nearest hole)
5. Maximum individual hole to branch diameter ratio of 1:2 (1:3 preferred)
6. minimum average velocity of 2.5 ft/s through the sampling holes, determined by evaluating the sum of the open area of the holes as compared to the flow area in the psychrometer <<<

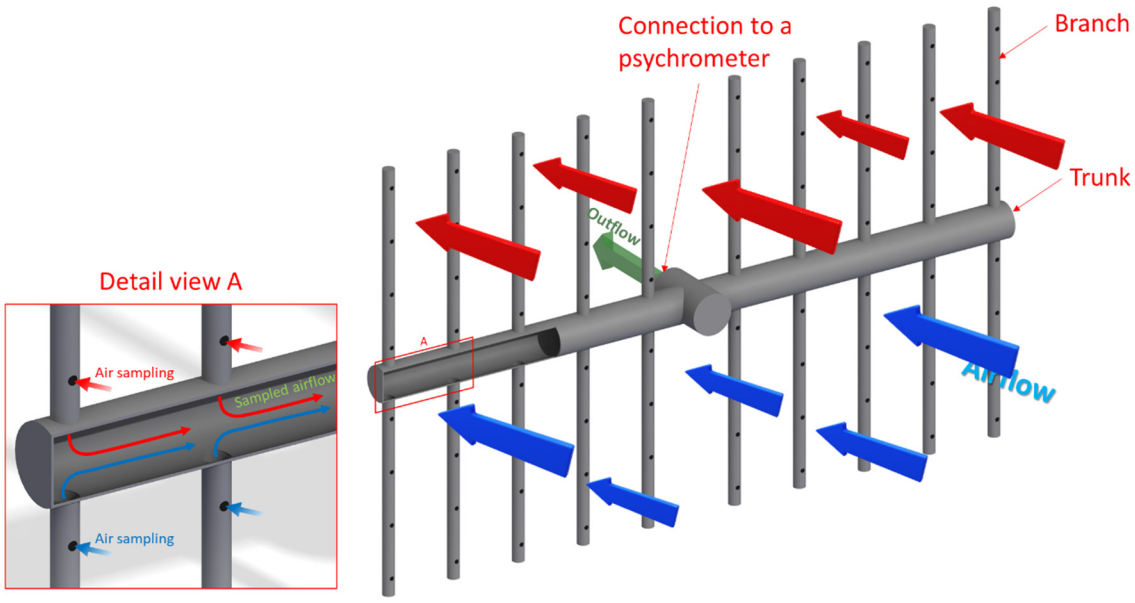

Figure 19 Typical air sampling tree

Most of the standards associated with the air sampler design tend to be somewhat limited. The lack of specific design guidance (e.g., appropriate range of duct size for the minimum hole density rule, maximum flow velocity at the sampling holes) may cause discrepancies in sampler design, risking lack of repeatability of the test results of a unit. Here, ASHRAE TC 8.11 found a research gap for the development of design guidelines for air samplers with better performance. The distribution of air across the sampling holes depends on pressure drop determined by flow velocity at the holes and the dynamic pressure in the free stream.

Therefore, it is required to specifically determine air sampler design allowing it to appropriately flow velocity at sampling holes, ensuring spatially uniform sampling of the air conditions for given duct air flow velocity. In this research, the design recommendations for air samplers will be developed based on observation of the relations between various design parameters obtained from both numerical and experimental testing.

CHAPTER III

AIR MIXER

ABSTRACT

Considering that square ducts are widely utilized for HVAC system performance testing, air mixing devices designed for such ducts were experimentally investigated. The results of these studies can also inform field application of mixers, such as in airside economizer applications of rooftop air conditioning equipment. Three types of air mixing devices were considered; one was a louvered-type mixer designed based on ASHRAE Standard 41.2, and the others were an orifice mixer and an orthogonal pattern louver mixer. With thermally maldistributed airflow, the mixing and flow-dynamic performance of the mixing devices were evaluated for various operating conditions and geometrical conditions. The parameters for the operating conditions include flowrate, flowrate ratio, and overall mixing length while the design parameters tested include mixer spacing and mixer orientation, orifice diameter, orifice-target spacing, louver angle, and louver array size. The results indicate that all mixing devices tested were capable of reducing stratification of the airflow. It was found that the mixing effectiveness, in general, increases as the overall mixing length and/or for dual mixers, spacing, increase. For an overall mixing length of 2.0 duct diameters (D_h), which is the maximum mixing length for industrial use, the mixing effectiveness values of the louvered mixer, orifice mixer, orifice-target mixer, and orthogonal pattern louver mixer were found to be

76.3, 75.1, 69.9%, and 88%, respectively. The pressure drop of the orifice-type mixers was significantly larger than those caused by the louvered mixer types. The findings from the comparison of all the mixer types tested indicate that the orthogonal pattern louver mixer is a promising option due to its simple design, easy fabrication, high mixing performance with low pressure drop, and two-dimensional mixing. Furthermore, it was found that the louvered mixer types are less sensitive to changes in total flowrate and velocity maldistribution of incoming airflow compared to orifice mixer types. This study provides insight into the comprehensive information on the performance and design of air mixing devices available for square ducts. In addition, this study suggests useful guidelines for designing and selecting the best mixer type for industrial use, taking into account factors such as cost-effectiveness, mixing performance, pressure drop, and sensitivity to flow rate and velocity maldistribution. A portion of this chapter has been published in the Applied Thermal Engineering (Park and Bach, 2021).

3.1. Overview

Air mixing devices are widely used in psychrometric performance testing to improve the accuracy of air conditions measurements. Furthermore, such air mixing devices are effectively employed for field applications such as airside economizers of rooftop air conditioning equipment.

Air conditioning systems utilize a variety of duct shapes, such as round, rectangular, and oval. Historically, round ducts have been preferred due to their efficient conveyance of moving air, low friction, easy installation, low noise, and cost-effectiveness (Bhatia, 2001). However, rectangular or square ducts are preferred for many HVAC&R applications due to their ability to fit into tight spaces, as they require less height than round ducts. These ducts are also beneficial for an easy and aesthetically pleasing connection of the fan coil to the main duct.

Rectangular and square ducts have become increasingly popular in psychrometric performance testing facilities that rely on a duct system to connect main components. Efforts have been made to improve measurement accuracy in these facilities, such as the use of air mixing devices to eliminate airflow maldistributions before measuring air bulk conditions. Despite the significant impact of uniform velocity and temperature on airflow measurement accuracy, air mixing devices for square ducts commonly used in the HVAC&R industry are not well-studied, and only limited information on their design and performance is available. They are generally manufactured in relatively simple and static shapes without moving parts for low cost and reliable operation. However, considerable attention is required during their design and configuration to ensure adequate mixing performance. The importance of the design parameters and their effect on the performance of those devices have been extensively discussed in the literature, albeit not for the square ducts.

As shown in the literature review section associated with the performance of air mixing devices, air mixing devices well satisfy their basic purpose. Despite their capability of securing uniformly conditioned airflow with the elimination of nonuniformities being dependent on their design, no studies are available that cover psychrometric HVAC&R performance testing. The guidelines available in the open literature are very limited, as well as, established mainly based on a circular duct, meaning that it is unclear how well they apply to commonly utilized square ductwork. In addition, most of the experimental studies in the literature related to air mixing devices have been performed for relatively long mixing lengths. For example, the experimental results by Faison (Faison et al., 1966, 1967, and 1970) were obtained for the range of overall mixing length from 3.0 to 4.75 duct diameter, which is hard to be applicable for today's industrial purpose due to space limitation: in practice, it is suggested as a guideline in the HVAC industry to target the length of downstream of no more than 2 duct diameters required mixing process according to PMS committee members for ASHRAE research project RP-1733 (Denton et al., 2019). Hence, the investigation on the air mixing devices for application in commonly used squared ductwork was

conducted in this research. Several representative air mixing devices were tested for various geometric and operational parameters, and their mixing performance and static pressure drop were compared to the baseline air mixer, which was designed based on ASHRAE Standards 41.1 (2013) and 41.2 (1992).

3.2. Experimental Apparatus

Figure 20(a) and (b) show a 3D rendering and a simplified schematic of the experimental apparatus for testing air mixer performance, respectively. The inlet is divided into two sections. The air streams supplied to the inlets are differently conditioned in separated psychrometric rooms, allowing to artificially create maldistributed inlet air conditions. The performance of the representative air mixers can be tested under extremely maldistributed airflow conditions with the configuration of the inlet region.

The conditions of each air stream are first measured in the top and bottom inlet measuring stations, which each consists of T-type thermocouple grids (9 TC's each), a relative humidity sensor (accuracy of ±3% FS), and a thermal dispersion airflow meter (accuracy of ±2% of reading of air velocity in FPM). After measuring the two initial conditions of the supplied air streams, they are combined before entering the test section consisting of a square duct with a side length of 18 inches (0.457 m).

In the test section, either a single or a pair of air mixing devices is installed. The maldistributed airflow with different temperature and/or flow velocity experiences a mixing process while passing through the mixing device, then, the conditions of the mixed airflow, such as temperature distribution and static pressure variation downstream, are measured at the measuring station in the test section, which is composed of sixteen T-type thermocouples and four static pressure transducers (0 to 1.0 inWC (0 to 249 Pa), accuracy of ±0.5% Full Scale (FS)). All thermocouples

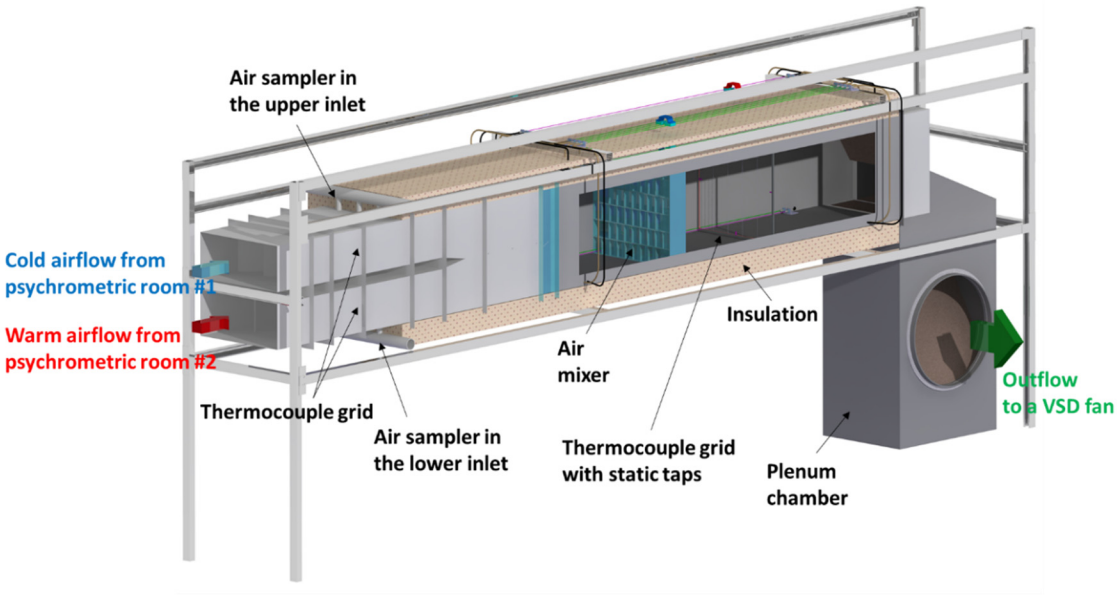

(a) 3D rendering showing the experimental setup.

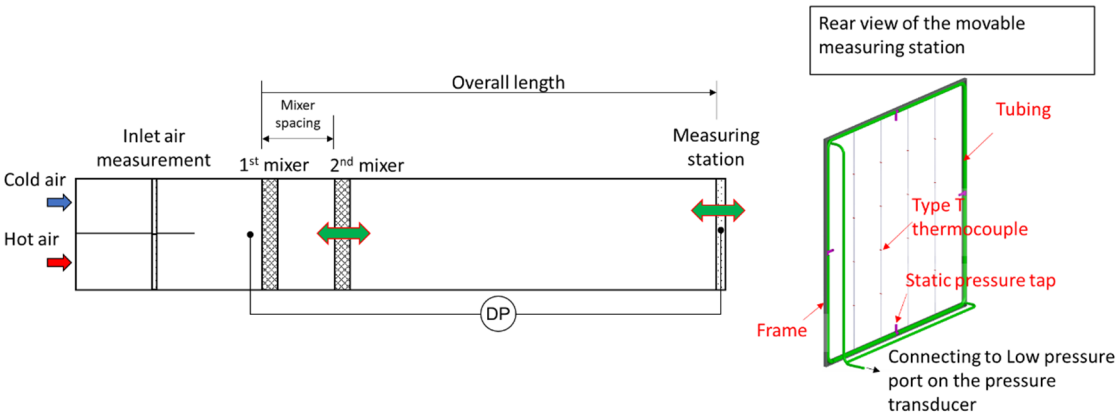

(b) Experimental setup airside overview. 2nd mixer moved by exterior mechanics through cable system.

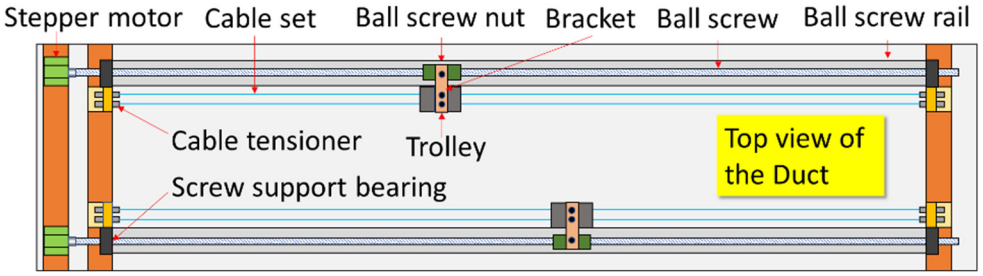

(c) Traversing system mechanics (outside duct) for the 2nd mixer frame and measuring station

Figure 20 Airside overview and traversing system mechanics

employed in testing were calibrated against a resistance temperature detector (accuracy of ±0.1°F (0.06 °C)) in a recirculating chiller (temperature stability of ±0.025°C (0.045°F)), as a result, the overall accuracy of temperature measurement with the calibrated thermocouples and the DAQ system was evaluated to ±0.06°F (±0.033°C). With two independent traversing systems consisting of a synchronized wire mechanism and CNC-controlled linear actuators on the setup (Figure 20(c)), the second mixer and the measuring station in the test section are movable as shown in Figure 20(a). Control logic for the actuators was developed to automate the system operation, leading to accurate independent control of the traversing components.

The test section was entirely insulated 2 in-thick R-10 Styrofoam (50.8 mm thick, 56.8 $m^2 \cdot K/W$) and the insulation thickness was determined based on a heat loss calculation for total flowrate range from 25 to 1,000 CFM (0.012 to 0.472 m^3/s). The result indicated that less than 1°C temperature change between the duct inlet and the duct outlet can be achieved with that insulation thickness if the temperature difference between duct inlet and atmosphere is 11.1°C. Furthermore, a leak test was carried out to improve overall testing accuracy. For that leak test, both inlets of the experimental setup were completely blocked to ensure no airflow through them. Then, the air in the experimental setup was pulled out at the outlet with the use of a fan, measuring air flowrate and pressure in the experimental setup. The fan speed was adjusted until the static pressure in the experimental setup reaches 1.0 inWC (249 Pa). After locating and sealing air leakage points, it was found that the flowrate of the air leakage on the test section was reduced from 70 CFM to 30 CFM (0.033 to 0.014 m^3/s) at the maximum pressure of 1.0 inWC (249 Pa). In other words, the reduction of the air leakage from 5.8% to 2.7% for a static pressure of 1.0 inWC (249 Pa) corresponding to a nominal air flowrate of 1200 CFM (0.566 m^3/s), compared to the fan curve data provided by the manufacturer of the centrifugal fan installed on the experimental setup, was presented, limiting maximum mixing effectiveness uncertainty to 2% for a target mixing effectiveness of 80%.

Figure 21 shows mixer installation in the test section and the candidate air mixing elements tested.

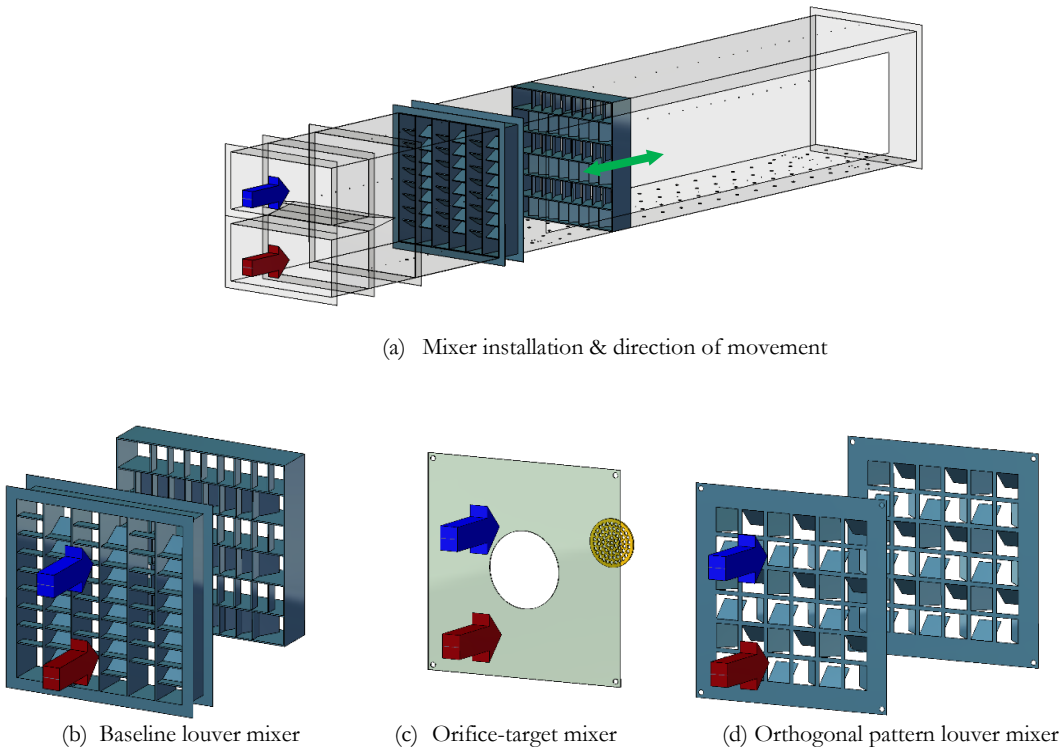

Figure 21 Schematic of mixer installation in the text section, and candidate types of mixers. The red and blue arrows illustrate warm and cold air flow, respectively

As shown in Figure 21(a), each type of mixer is installed in single or series in the test section, which is for the comparison of the characteristics of mixer configuration in terms of mixing performance and pressure drop. Three candidate mixers shown in Figure 21(b), (c), and (d) are baseline louvered (e.g., "cheese grater"), orifice-target mixer, and orthogonal pattern louver mixer, respectively. The baseline louver mixer was specially designed for the square duct, referring to ASHRAE Standards 41.1 (2013) and 41.2 (1992). Note that the second mixer is 90° rotated to the first mixer as shown in Figure 21(b) when employing the baseline mixer in series. This mixer orientation leads to creating air mixing in both vertical and horizontal directions. The orifice-type mixer (Figure 21(c)) is installed solely or with a perforated target plate. The orifice mixer is made of a 6-gauge (4.9 mm) thickness polycarbonate plate, and the size of the orifice hole was chosen to 0.4, 0.5 and 0.6 D_h. The diameter of the target plate is 0.25 D_h, and sixty-seven holes having 0.35 in (8.89 mm) diameter are evenly distributed on the surface of the target plate. The target plate has

an open area ratio of 40.5% of surface area to reduce the additional pressure drops caused by the target plate.

3.3. Experimental Procedure and Data Reduction

3.3.1. Experimental Procedure and Test Plan

The first step of the experimental procedure is to condition the air supply to the two inlets in separate psychrometric rooms. The air temperatures are adjusted to 70°F (21.1°C) and 90°F (32.2°C) within ±0.5°F (±0.3°C), respectively.

To create the flow of the air supplying from the psychrometric room to the experimental setup, a variable speed centrifugal fan connected to the outlet of the experimental setup with a settling chamber is operated at maximum speed. The air damper at each inlet is, then, adjusted to maintain the desired air flowrate with a test operating tolerance of ±10 CFM (±0.005 m^3/s) per inlet with the use of a damper actuator and a PID controller. Independent control of the dampers allows to adjust both total flowrate and flowrate ratio between the inlets to artificially create maldistributed air velocity in the test section.

The measuring station and the second mixer in the test section are positioned with the traversing systems. All sensor signals are monitored and analyzed to show the resulting data, including heat maps at the cross-sections of the inlet and test section, pressure drop values, and mixing effectiveness using the developed data acquisition software. Once all measurands reach a steady state, where the estimated mixing effectiveness and the average temperatures measured using the TC grids at two inlets maintain within the ranges of ±1% and ±0.2°F (±0.1°C), respectively, data recording starts.

The next step is to change the position of the measuring station so that the variation of mixing performance and pressure drop for various total lengths are considered. The same test procedure is

then repeated for different total air flowrates, flowrate ratios between the inlets, and mixer types. Overall, measurements for the present investigation are undertaken with a hydraulic diameter (D_h) of the squared test section of 18 inches, overall length (distance from the first mixer and measuring station) from 1.0 to 3.3 D_h, mixer spacing between a pair of mixers or orifice and target from 0.8 to 2.0 D_h, total flowrate from 100 to 1,000 CFM (0.047 to 0.472 m^3/s) at equal flowrate ratio for both inlets, and flowrate ratio at one inlet to the other from 10 to 90% for a total flowrate of 500 CFM (0.236 m^3/s). The general test plan for all the candidate mixer types is shown in Table 2 for the ranges of the test parameters. Detailed test plan for the orthogonal pattern louver mixers is also shown in Table 3, separately.

3.3.2. Data Reduction

Experimental data is reduced into two metrics for each data point, mixing effectiveness and dimensionless friction factor. Mixing effectiveness can be defined by several metrics, such as temperature range-based metrics (Faison et al., 1966 and Robinson, 2000 and 2001) or statistics-based metrics (Faison et al., 1967 and 1970), depending on the anticipated use of the results which were presented in detail in the literature review. In this research, a measure of mixing effectiveness that is based on the average standard deviation of the upstream and downstream temperature distributions (Faison et al., 1967 and 1970) was chosen as it was deemed most appropriate for heat exchanger and equipment performance measurements. That metric is defined as

$$\varepsilon = \left(1 - \frac{s(\Delta T_{downstream})}{s(\Delta T_{upstream})}\right), \tag{9}$$

where:

$s(\Delta T_{upstream})$	Average standard deviation between temperature sample grid points prior to (upstream of) the first air mixer,
$s(\Delta T_{downstream})$	Average standard deviation between temperature sample grid points after (downstream of) the second air mixer, and
ε	Percent mixing effectiveness.

Table 2 Mixer test plan

#	Mixer Spacing*, D_h	Overall Length*, D_h	Temp. @ upper inlet, °F (°C)	Flowrate @ upper inlet, CFM (m^3/s)	Temp. @ lower inlet, °F (°C)	Flowrate @ lower inlet, CFM (m^3/s)	Total Flowrate, CFM (m^3/s)	Note
1	0.6	1.0	70 (21.1)	250 (0.118)	90 (32.2)	250 (0.118)	500 (0.236)	• Effect of mixer spacing on the effectiveness and pressure drop • Effect of overall length on mixing effectiveness
2		1.5						
3		2.0						
4		2.5						
5		3.0						
6		3.3						
7	1.0	1.5						
8		2.0						
9		2.5						
10		3.0						
11		3.3						
12	1.5	2.0						
13		2.5						
14		3.0						
15		3.3						
16	2.0	2.5						
17		3.0						
18		3.3						
19	1.5	2.0	70 (21.1)	50 (0.024)	90 (32.2)	50 (0.024)	100 (0.047)	• Effect of total flowrate on the effectiveness and pressure drop • 10:1 total flowrate ratio with the consideration of the comment of one of the PMS members
20				125 (0.059)		125 (0.059)	250 (0.118)	
21				250 (0.118)		250 (0.118)	500 (0.236)	
22				375 (0.177)		375 (0.177)	750 (0.354)	
23				500 (0.236)		500 (0.236)	1000 (0.472)	
24	1.5	2.0	70 (21.1)	50 (0.024)	90 (32.2)	450 (0.212)	500 (0.236)	• Effect of flowrate ratio on the effectiveness • The flowrate ratio at the upper inlet ranges from 10 to 90% of total flowrate.
25				150 (0.071)		350 (0.165)		
26				250 (0.118)		250 (0.118)		
27				350 (0.165)		150 (0.071)		
28				450 (0.212)		50 (0.024)		

* The definitions of mixer spacing and overall length are illustrated in Figure 2 (a).

Table 3 Detailed test plan for the orthogonal pattern louver mixer

No. of Mixers	Mixer Orientation*	Mixing Length (D_h)	Mixer Spacing (D_h)	Air Temp @ upper inlet (F)	Air Temp @ lower inlet (F)	Total Air Flowrate (CFM)**	Flowrate Ratio between Upper and Lower Inlets***	Louver Angles (°)	Louver Array Size
Single	CCW	1.0 1.5 2.0 2.5 3.0 3.3	N/A	70	90	100 250 500 750 100	1:9 3:7 5:5 7:3 9:1	30 40 50 60 70	6 x 6 4 x 4 2 x 2
Dual	CCW-CCW CCW-CW		0.6 1.0 1.5 2.0			100 250 500 750 100	1:9 3:7 5:5 7:3 9:1		

* The orthogonal pattern louver mixer features multiple sets of louvers, with each set consisting of four louvers arranged in a square shape on the mixer and bent orthogonally in either a clockwise (CW) or counterclockwise (CCW) direction. When using dual mixers, the louvers on both mixers can be bent in the same direction (CCW-CCW) or in opposite directions (CCW-CW). Figure 3 illustrates the arrangement of louvers on the orthogonal pattern louver mixer.

** For a single mixer, the total air flowrate varied at a mixing length of 2.0 D_h, and a flowrate ratio between the inlets of 0.5.

** For dual mixers, the total flowrate varied at a mixing at a mixing length of 2.0 D_h, a mixer spacing of 1.5 D_h, and a flowrate ratio between the inlets of 0.5.

*** For a single mixer, the flowrate ratio of upper inlet to lower inlet varied at a mixing length of 2.0 D_h, and a total flowrate of 500 CFM.

*** For dual mixers, the flowrate ratio of upper inlet to lower inlet varied at a mixing at a mixing length of 2.0 D_h, a mixer spacing of 1.5 D_h, and a total flowrate of 500 CFM.

The advantage of employing this metric is that it prevents a single temperature value outlier from dictating the overall result, which can happen with temperature range-based metrics.

The flow-dynamic characteristic of the airflow passing through mixing elements is evaluated using pressure drop ΔP between the inlet of mixer and measurement station, expressed in terms of Euler number, the relationship between a local pressure drop caused by a restriction and the kinetic energy per volume of the flow,

$$\Pi_P = \frac{\Delta P}{\rho V^2}, \tag{10}$$

where, ρ is the air density and V is the average flow velocity in the test section.

3.4. Discussion of Results

3.4.1. Temperature Distribution in Airflow due to Mixing Process

The characteristics of the mixing process for different mixing devices were investigated by monitoring the variation of temperature distribution in the airflow where enthalpy exchange between the air streams occurs after passing through the devices. The results showed that not only does mixing performance depend on the types of mixing devices, but also their configuration and/or orientation. The spatially-resolved data at different locations with respect to the downstream region was measured using a thermocouple grid consisting of evenly distributed sixteen thermocouples that moves along the duct in order to visualize how the mixing process develops downstream.

Figure 22 shows the variation of the temperature distribution downstream when no mixer is employed in the test section. The air streams conditioned at different temperatures of 90°F (32.2 °C) and 70°F (21.1 °C) and supplied to the upper and lower inlet respectively are combined after being stabilized with the flow straightener. While they flow downstream in the test section, inherent mixing at the interface between the two main streams becomes noticeable.

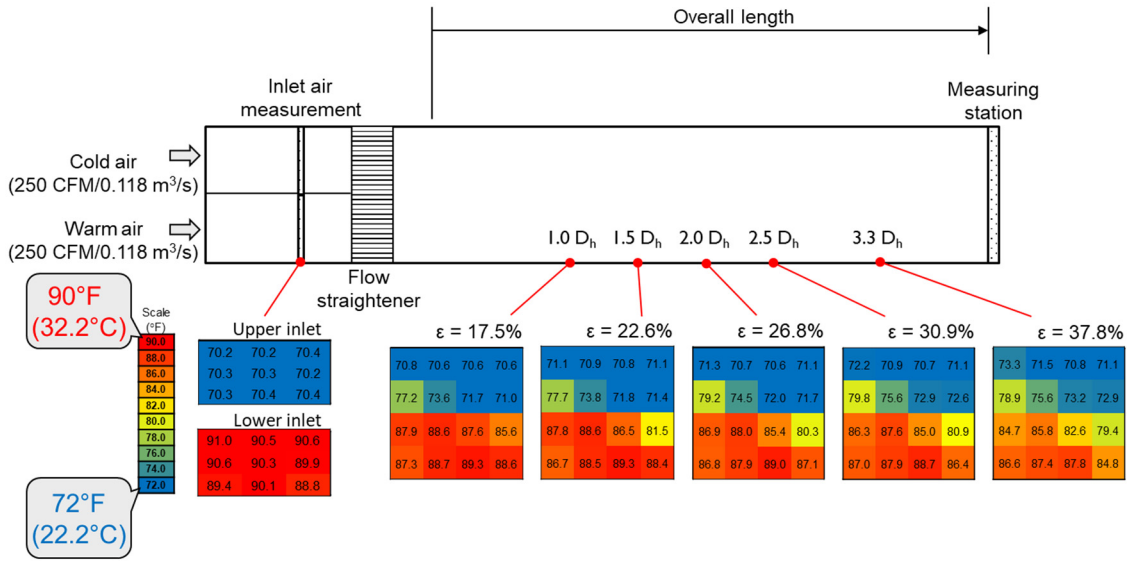

Figure 22 Temperature distribution for inherent mixing in airflow

The temperature distribution illustrates an air mixing pattern where cold air occupying the upper flow region gradually penetrates the lower flow region where warm air flows from right end of the interface, while the warm air moves up to the cold airflow region from the opposite side of the interface. This asymmetric mixing pattern might be caused by nonuniform pressure distributions in each flow region and/or geometric issues on the duct design; however, this result clearly shows that it is not possible to achieve the performance required for any practical purpose with inherent mixing caused by flow diffusion, especially if upstream turbulence, such as in this test section or if an inlet duct is utilized, is held at minimum.

Figure 23 illustrates air mixing with a pair of baseline mixers installed in series. Note that the louvers on the first baseline mixer are tilted in up and down directions repetitively, while those on the second mixer are oriented horizontally as shown in Figure 21(b). The results show that a significant enhancement in mixing performance can be achieved compared to the no-mixer case. To be specific, the temperature distribution of the airflow leaving from the mixer set indicates that three-dimensional complexity in the air streams is generated due to the mixers, resulting in very active and effective turbulent mixing. Such mixing contributes to rapid enthalpy exchange and

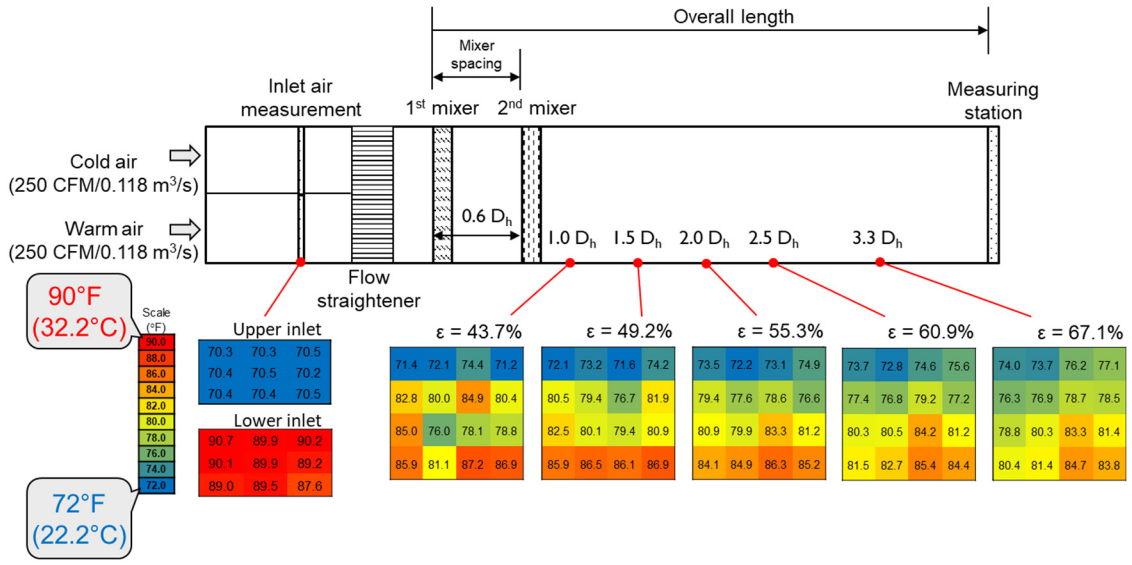

Figure 23 Temperature distribution for the mixing process caused by dual louvered baseline mixers with the second mixer rotated 90 degrees relative to the first mixer.

elimination of nonuniformity in the airflow, and thus, it makes it possible to shorten the mixing length required for desired mixing performance.

As shown in Figure 24 and 25, the baseline air mixer can be employed as a single mixer as well. However, the orientation of it causes different results in terms of mixing pattern and effectiveness. In Figure 24, the louver of the single mixer is oriented deflecting air streams in horizontal direction. As a result, the initial temperature distribution after the mixer is comparable to the no-mixer case. In addition, the characteristic of mixing propagation throughout the cross-section of the airflow is similar to the no-mixer case, resulting in relatively low mixing effectiveness compared to the dual baseline mixer case. In contrast, Figure 25 shows a completely different result. The pattern of mixing at the shortest mixing length is somewhat similar to the no-mixer case, but it develops much faster. In other words, a single baseline mixer oriented to deflect air streams in vertical direction is, in general, capable of reducing flow nonuniformity much quicker than a dual baseline mixer – if (and only if) the orientation of the temperature maldistribution is also vertical. This implies that taking into account the nature of nonuniformity of the airflow (if known) greatly contributes to maximizing mixing performance for a set type of mixer as it allows to adjust mixer orientation

accordingly.

Orifice-type mixers show completely different mixing patterns compared to the louvered baseline mixer as shown in Figure 26 and 27. In general, orifice-type mixers have a much higher mixing performance than the baseline mixer. The temperature nonuniformity is mainly observed at the center of a cross-section of airflow at the overall length of 1.0 D_h. The variation of temperature

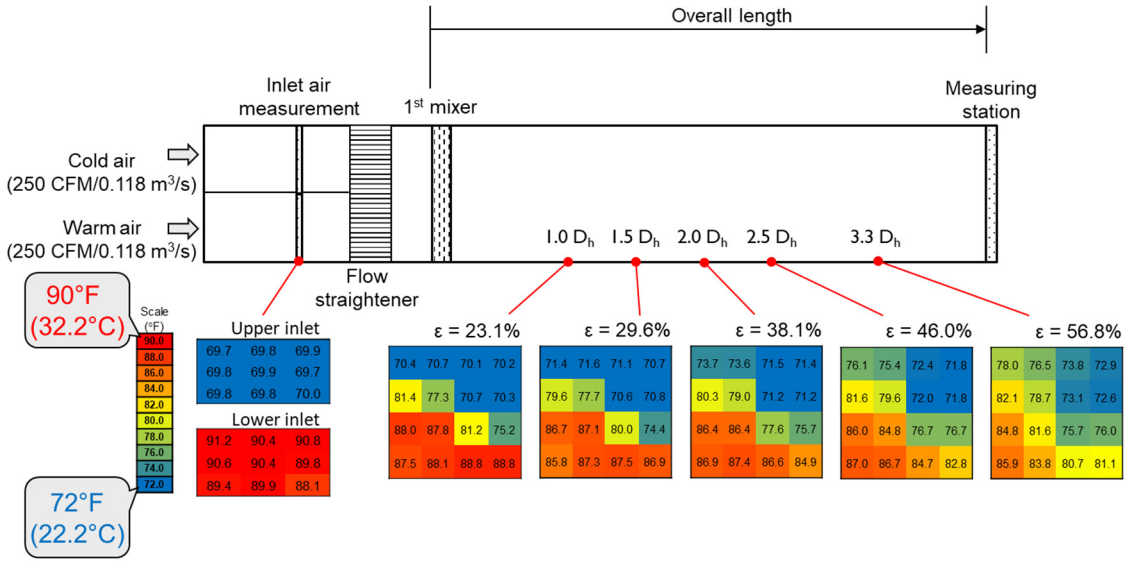

Figure 24 Temperature distribution for mixing process caused by a single baseline mixer with louvers in horizontal orientation

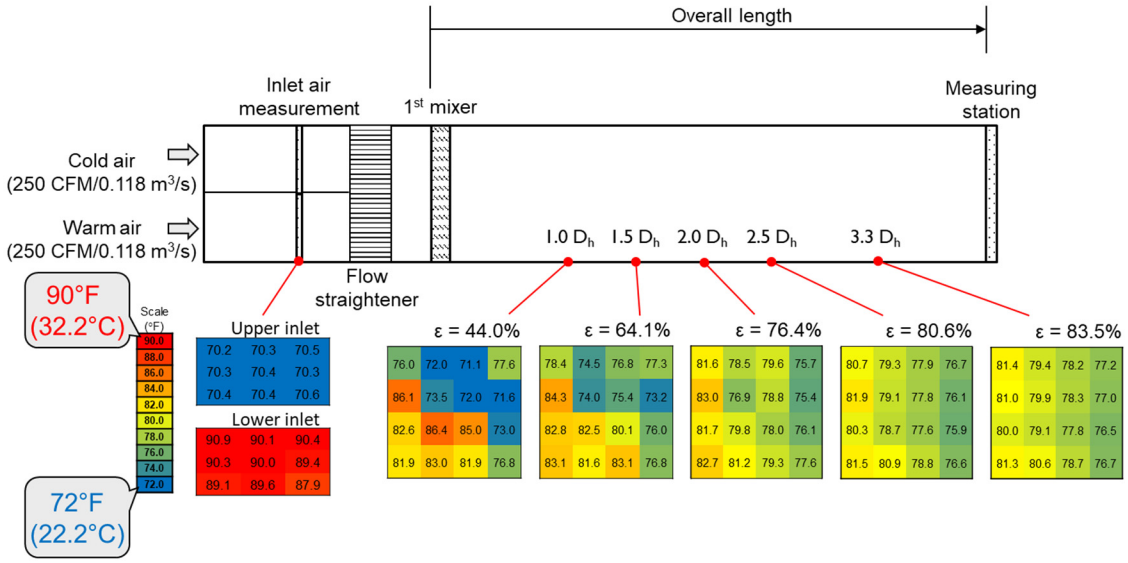

Figure 25 Temperature distribution for mixing process caused by a single baseline mixer with louvers in vertical orientation

distributions along the duct shows that this nonuniformity quickly disappears, reaching the mixing effectiveness of 89.7% at 3.3 D_h from the mixer inlet.

This rapid elimination of temperature nonuniformity in the core region may be attributed to the fact that sudden contraction of airflow due to the orifice increases air velocity, increasing turbulence-based interaction between the molecules after the orifice and resulting in more active enthalpy transfer. However, just because the orifice-type mixers eliminate temperature maldistribution

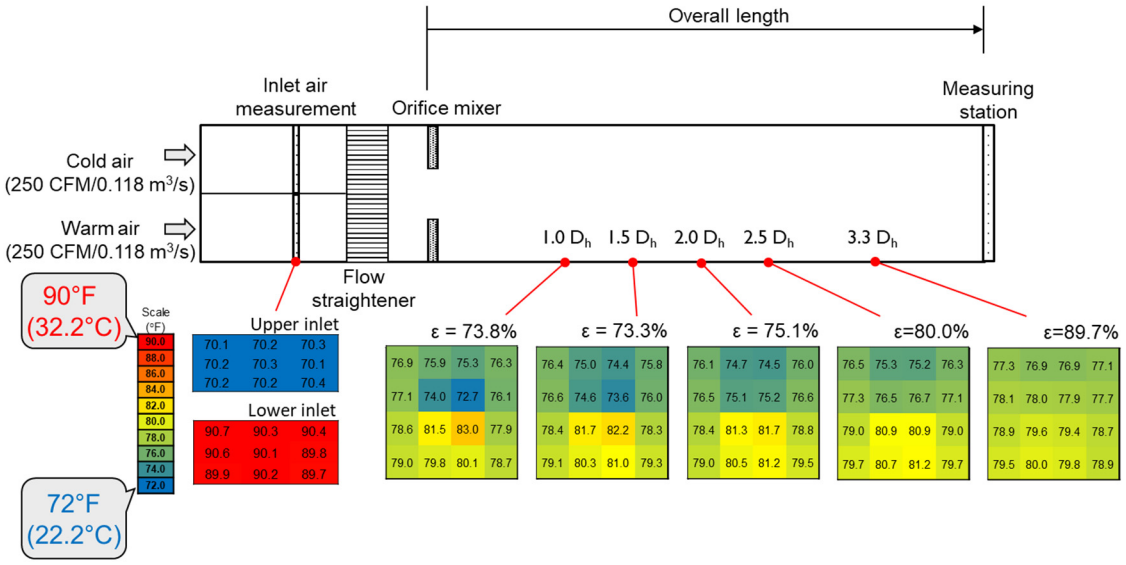

Figure 26 Temperature distribution for mixing process caused by an orifice mixer with 0.4 D_h orifice hole diameter

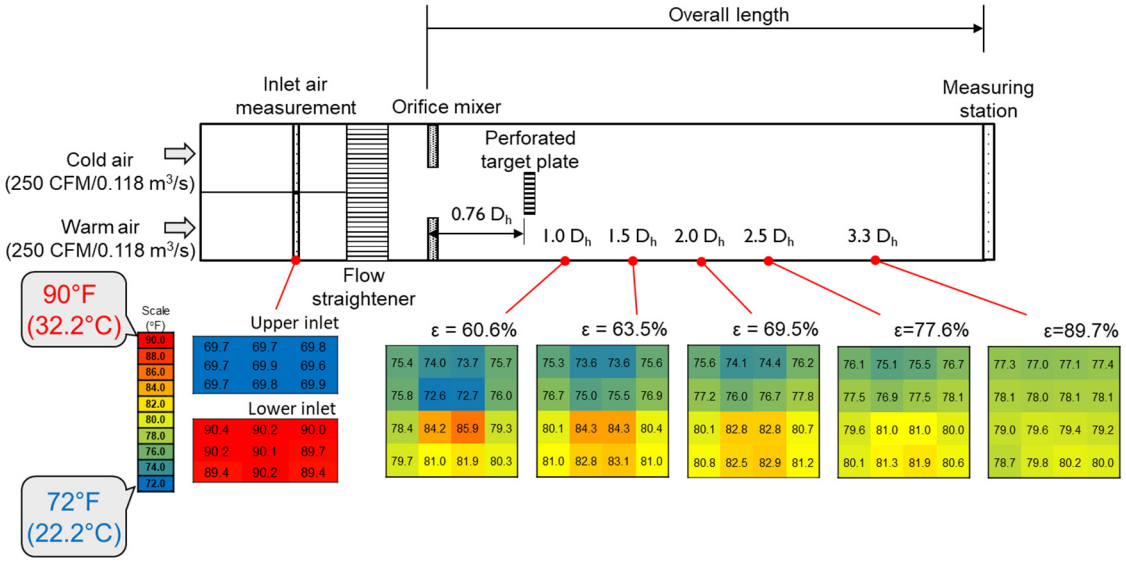

Figure 27 Temperature distribution for mixing process caused by an orifice-target combination mixer with 0.4 D_h orifice hole diameter

quickly does not mean that velocity uniformity is achieved at the same time. According to Ahmed (Ahmed et al. 2019), the air stream passing through the orifice-type mixer is significantly accelerated, forming “jet flow”, and flow recirculation is formed in the region near the jet flow. Air recirculating into the lower velocity areas outside the jet flow entrains air from downstream of the duct that has more uniform conditions. Differences in velocity are not captured by the experimental mixing performance metric, and the results of the orifice-type mixers, therefore, have to be interpreted with caution.

It was also found that the addition of a perforated target plate to the orifice mixer did not affect mixing performance much as shown in Figure 27. The jet flow formed while passing through the orifice strikes the target, then diverges. However, this jet impingement causes a little disturbance in the main jet stream rather than creating large or many small vortices which can help enhance mixing. Due to the disturbance in the jet stream and wake region behind the target, the temperature maldistribution in the airflow is maintained longer, however, the result shows that the maldistribution is reduced at a similar level to the no-baffle case if the overall mixing length exceeds 3.0 D_h.

While the baseline louver mixer causing only one-dimensional mixing in horizontal or vertical direction should be used in dual manner to achieve high mixing performance, it seems that the orthogonal pattern louver mixer has sufficient mixing performance since this mixer type can obtain two-dimensional mixing with the geometrically unique design of its louvers. In Figure 28, the temperature distribution shows rapid and effective mixing process even though this mixer type was used as single unit.

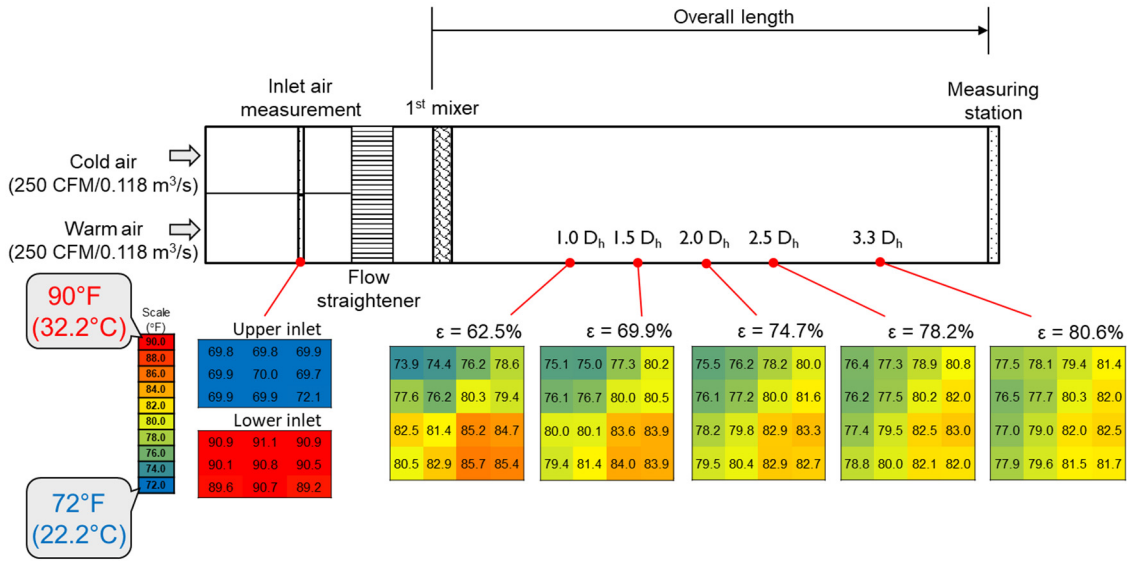

Figure 28 Temperature distribution for mixing process caused by a single orthogonal pattern louver mixer with 6 by 6 louvers and a louver angle of 60°

3.4.2. Effect of Overall Length on the Mixing and Flow Performance

3.4.2.1. Baseline louvered mixer

The mixing and flow-dynamic performance for the baseline louvered mixer were investigated in terms of the variation of mixing effectiveness and pressure drop for different overall mixing lengths and the results are shown in Figure 29, respectively. Note that in the test section is 500 CFM (0.236 m^3/s) and the flowrate ratio of cold airflow to the total flowrate is 0.5. As a result of the testing, it was found as shown in Figure 29(a) that, in general, the longer overall length for mixing, the higher mixing performance, with the mixing effectiveness ranging from 43.5 to 80.1% for the given test conditions depending on the spacing between the mixers. For short mixer spacing in a range from 0.6 to 1.0 D_h, the result shows a linear increase in effectiveness while the trend of the increase seems to gradually turn into nonlinear as the mixer spacing increases up to 1.5 D_h. For the largest spacing of 2.0 D_h, a slight effectiveness drop is observed as the overall length increases from 2.5 to 3.0, it, however, rebounds and reaches the maximum effectiveness value for the given testing conditions. It is also found from Figure 29(a) that an increase in mixer spacing generally contributes to the enhancement of mixing effectiveness in overall even though the relation between the

increment of the spacing and the effectiveness seems not to be linear.

The pressure drop between up and downstream with respect to the set of mixers also increases as increasing the overall mixing length and mixer spacing, respectively. However, this increment in the pressure drop is negligibly small ranging from 0.013-0.019 inWC (3.11-4.73 Pa). Therefore, it can be concluded that the baseline louvered mixer has an advantage in terms of flow-dynamic performance, making it a good choice for applications that require low-pressure drop.

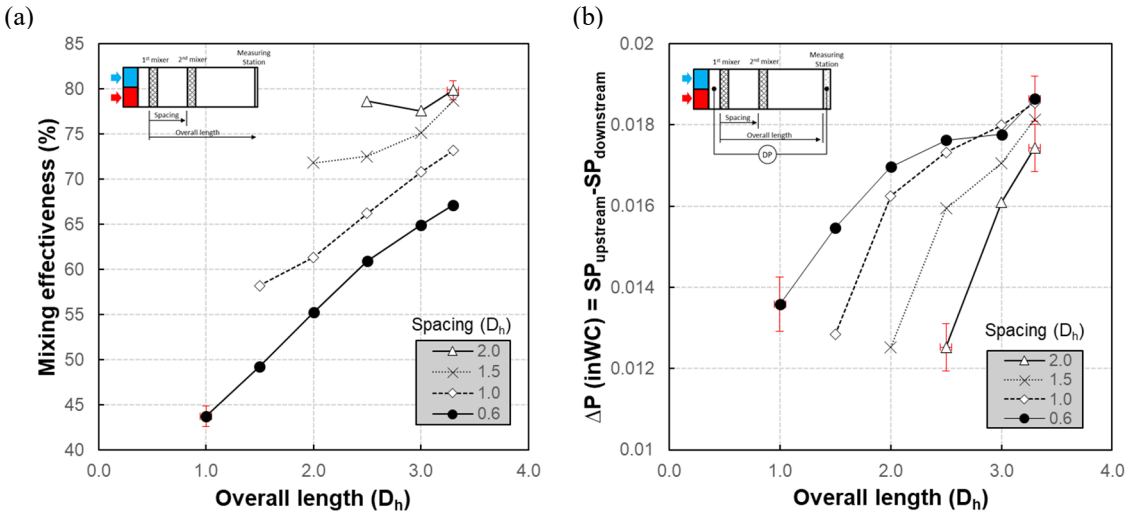

Figure 29 Variations of (a) mixing effectiveness and (b) pressure drop as a function of overall length for dual baseline mixers with mixer spacings of 0.6, 1.0, 1.5, and 2.0 D_h at a total flowrate of 500 CFM (0.236 m^3/s) and a flowrate ratio of cold air to warm air of 0.5

3.4.2.2. Orifice-type mixer

In Figure 30, the mixing and flow-dynamic performance of orifice mixers are present as a function of overall mixing length. For the testing, three orifice diameters of 0.4, 0.5, and 0.6 D_h were chosen, and the total flowrate and flowrate ratio of cold air at the inlet were 500 CFM (0.236 m^3/s), and 0.5, respectively. The result shows a monotonous increase in mixing effectiveness as the overall length given for mixing process increases. In addition, it is found that the smaller orifice diameter helps enhance the mixing effectiveness; mixing effectiveness for the orifice mixer with a hole diameter of 0.4 D_h ranges from 73.8 to 89.7% while the effectiveness for the orifice with the largest hole diameter of 0.6 D_h is evaluated to the effectiveness of 50.5-78.1%.

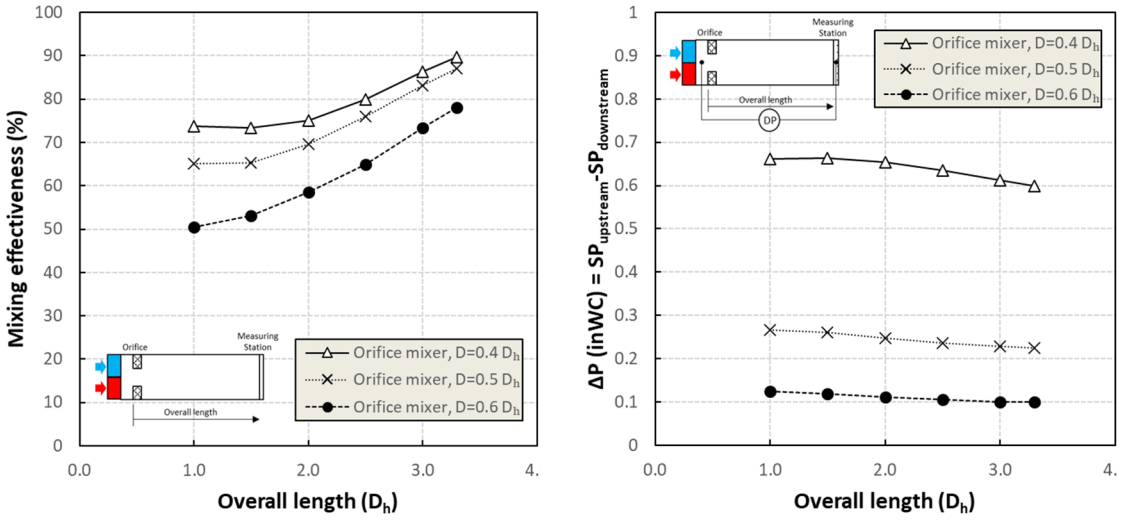

Figure 30 Variations of (a) mixing effectiveness and (b) pressure drop as a function of overall length for an orifice mixer with orifice hole diameters of 0.4, 0.5, and 0.6 D_h at a total flowrate of 500 CFM (0.236 m^3/s) and a flowrate ratio of cold air to warm air of 0.5

The pressure drop caused by the orifice mixers is significantly larger than the baseline louvered mixer. The result showed a monotonous decrease in pressure drop as increasing overall length, which is observed similarly from all the orifice diameters tested as shown in Figure 30(b). Furthermore, it seems that decreasing the orifice diameter results in an almost exponential increase in pressure drop. Considering that pressure drop due to instrumentation for bulk air condition measurement is generally limited to 0.25 inWC (62.3 Pa) for industrial use, the use of orifices with hole diameters smaller than 0.4 D_h may not be acceptable. However, if the pressure drop up to 0.25 inWC (62.3 Pa) is acceptable, orifice-type mixers with relatively large hole diameters including 0.5 and 0.6 D_h could be a better option due to the ease with which orifice-type mixers can be designed and manufactured – compared to much more complex louvered-type mixers.

Figure 31 shows the variation of mixing performance for the orifice-target combination mixer. It was found that placing an additional target plate behind the orifice mixer as a flow distributor is not helpful for the enhancement of mixing performance. Also, the result shows that the spacing between the orifice and the target does not influence the mixing performance.

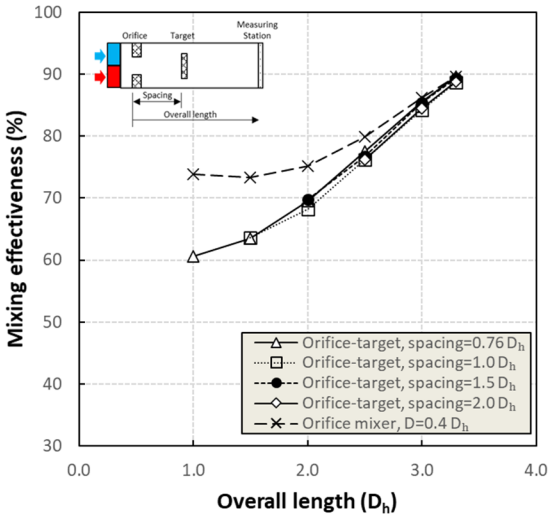

Figure 31 Variation of mixing effectiveness as a function of overall length with combination of an orifice mixer with an orifice hole diameter of 0.4 D_h and a perforated target plate (orifice-target combination) for spacing between orifice and target of 0.76, 1.0, 1.5, and 2.0 D_h at a total flowrate of 500 CFM (0.236 m^3/s) and a flowrate ratio of cold air to warm air of 0.5

3.4.2.3. Orthogonal pattern louver mixer

3.4.2.3.1. Effect of mixer orientation and spacing for dual mixers

Figure 32(a) and (b) show the orthogonal pattern louver mixer tested and how the air flow changes when it passes through the mixer. The louver pattern applied to this mixer type can create vortex flow. The small vortices created downstream due to multiple duplicated louver patterns on this mixer lead to complex mixing in both horizontal and vertical directions. Figure 32(c) shows the flow pattern of vortices at the view from downstream, also, indicates that this mixer type can be employed in a single or more due to complex downstream flow mixing air streams in both horizontal and vertical directions. For the case of using this mixer type in dual, the orientation of the first and second mixer which can create vortices in the same or opposite rotational directions may affect flow behavior downstream. Therefore, the effect of mixer orientation for dual orthogonal pattern louver mixers on the mixing performance and flow-dynamic performance was investigated and the result is shown in Figure 33. In this figure, CW and CCW indicate rotational directions of vortices in clockwise and counterclockwise, respectively.

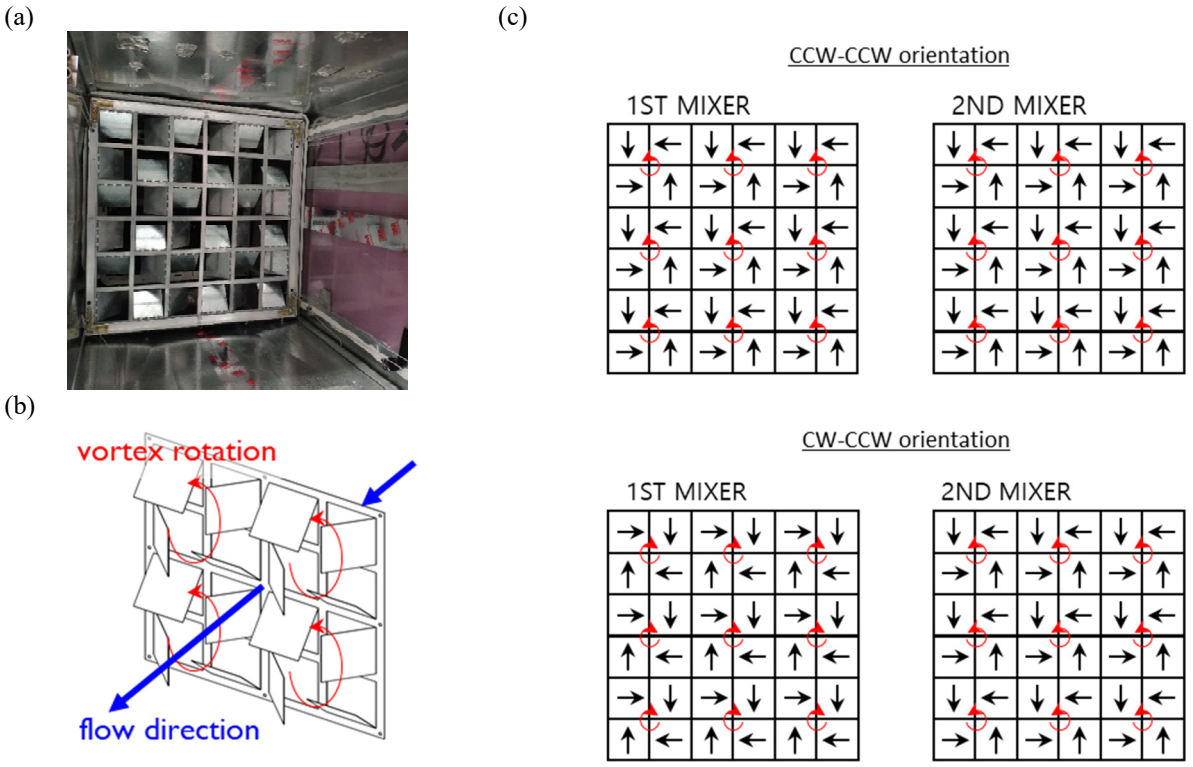

Figure 32 Orthogonal pattern louver mixer installed in the test section: (a) Geometry of the mixer, (b) Flow behavior downstream of the mixer, and (c) Mixer orientations causing vortices in the same (CCW-CCW) or opposite (CW-CCW) directions.

The result shows that in general, the longer mixing length, the better mixing performance, however, the impact of mixing length on pressure drop is negligible. It was clearly found in these figures that when dual orthogonal pattern louver mixers are installed in series, both mixers should be installed in the same orientation allowing to create vortices rotating in the same direction downstream of each mixer for much better mixing performance. This is attributed to that the combination of mixers in the same orientation enhances the momentum with respect to the mixing direction, while in the combination of mixers rotating air in different directions, the rotational inertia of the vortices is weakened by the louvers of the second mixer arranged in the reverse direction. On the contrary, the result indicates that the difference in the orientation of dual orthogonal pattern louver mixers causes only minor influence on pressure drop due to the mixers. Figure 33 also shows the effect of mixer spacing on the mixing performance when the mixers are employed in dual. Interestingly, it was found that the mixing performance according to the variation in the mixer spacing shows

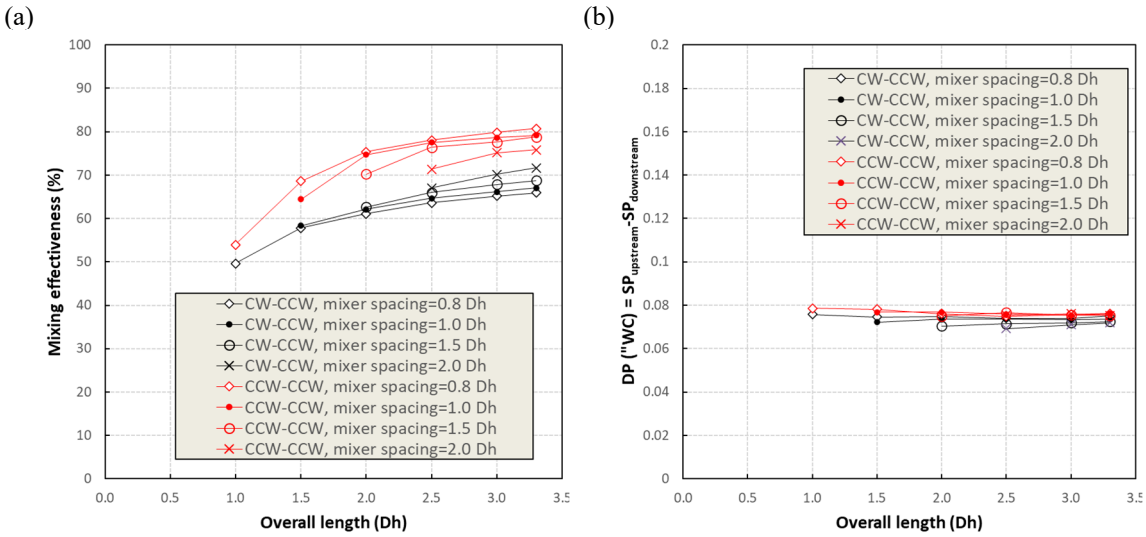

Figure 33 Variations of (a) mixing effectiveness and (b) pressure drop as a function of overall length for dual orthogonal pattern louver mixers with two different orientations: CW-CCW and CCW-CCW, at a total flowrate of 500 CFM (0.236 m^3/s), and a flowrate ratio of cold air to warm air of 0.5

contradictory results for two mixer orientations, CW-CCW, and CCW-CCW, tested for the investigation. For dual mixers with louvers bended identically, the closer the two mixers are to each other, the higher the mixing performance. In contrast, for dual mixers creating vortices in opposite directions, one mixer does not help the mixing that the other mixer generates. For this reason, in this case, the closer the two mixers are, the more disturbed each mixing is, resulting in a decrease in mixing performance.

3.4.2.3.2. Comparison of characteristics of single and dual mixers

In Figure 34 and 35, the performance of dual orthogonal pattern louver mixers was compared to that of a single mixer for louver angle of 30° and 60°, respectively. As shown in both figures, the orthogonal pattern louver mixers have better mixing performance when they are employed in dual compared to a single mixer. The change in mixing effectiveness caused by the number of mixers employed for the testing ranges from 2 to 10%. The addition of an orthogonal pattern louver mixer improving mixing performance contrasts with the baseline louver mixer which was found to not always perform better when used in pairs. This is because when using dual orthogonal pattern

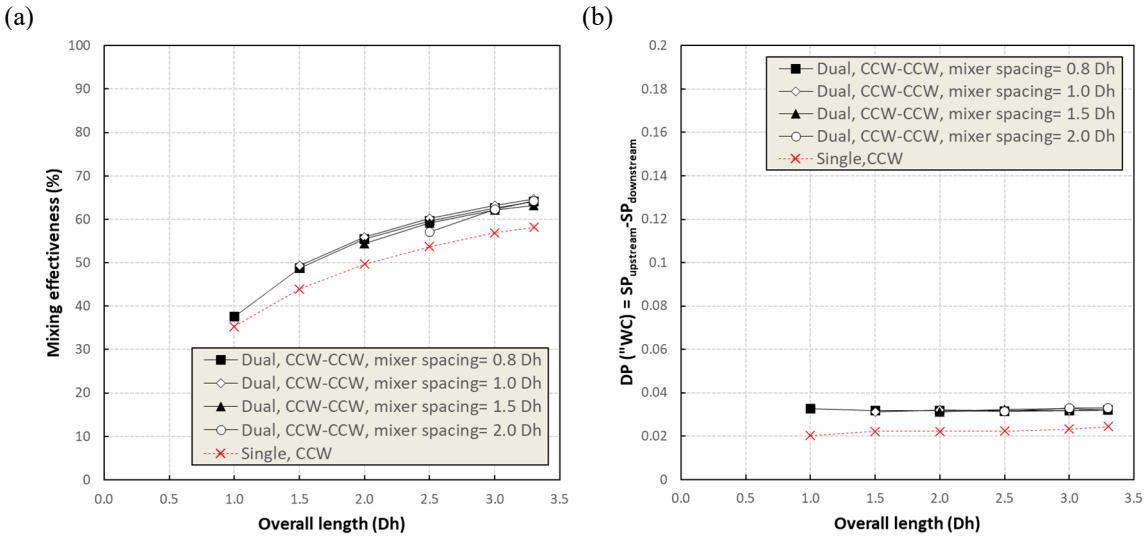

Figure 34 Comparison of the performance of a dual and single orthogonal mixer with a louver angle of 30°, as a function of overall length at a total flowrate of 500 CFM (0.236 m^3/s) and a flowrate ratio of cold air to warm air of 0.5: (a) Mixing effectiveness and (b) Pressure drop

louver mixers, both mixers work identically, creating two-dimensional mixing in the same pattern and direction, unlike the baseline louver mixer, which creates one-dimensional mixing. However, the increase in pressure drop due to the addition of the mixer appears to be significant, especially with steeper louver angles, as shown in Figures 34(b) and 35(b). Based on these results, the mixing performance of this mixer used in a single form may be slightly lower than that of dual mixers,

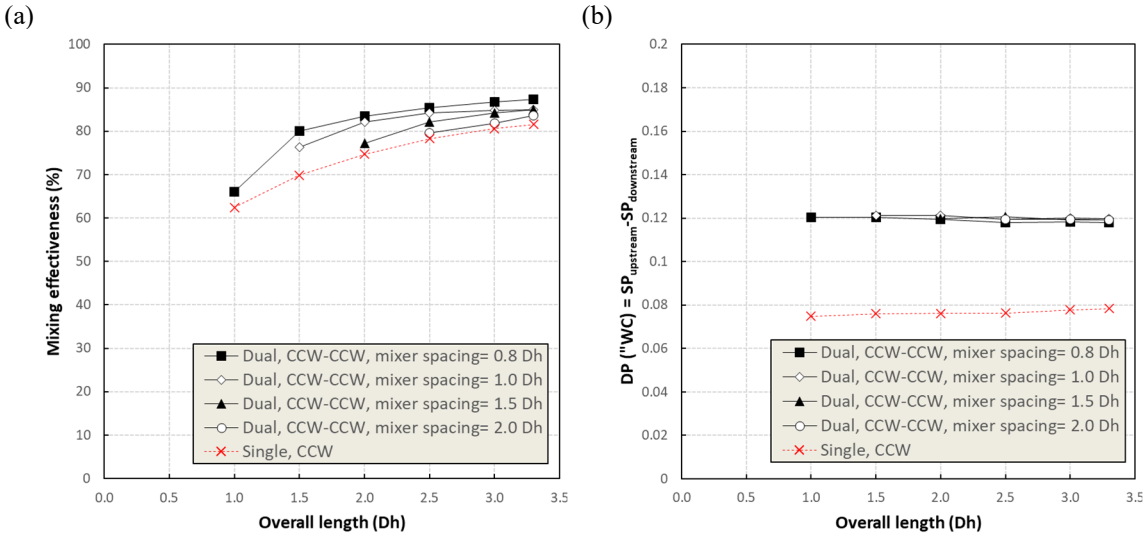

Figure 35 Comparison of the performance of a dual and single orthogonal mixer with a louver angle of 60°, as a function of overall length at a total flowrate of 500 CFM (0.236 m^3/s) and a flowrate ratio of cold air to warm air of 0.5: (a) Mixing effectiveness and (b) Pressure drop

however, it may be worth with the consideration of much less pressure drop, cost, and limited space for use.

3.4.2.3.3. Investigation on louver mixer design parameter

So far, it was investigated how to install air mixing devices, for example, their location, orientation, and mixing spacing, influences mixing effectiveness and pressure drop. As shown in Figure 36 (a) and (b), it was revealed that louver angles also significantly contribute to mixing process caused by the mixers. This means that, in addition to the determination on their installation, it is also important to find the right mixer design parameters such as the angle and array size of the louvers for the best mixing with acceptable pressure drop based on the geometric characteristics of the orthogonal pattern louver mixers. In this research, the investigation on the effects of louver angle and array size was also carried out and the results are shown in Figure 36 and 37, respectively. In Figure 36, the mixing effectiveness generally increases with an increase in a louver angle. However, it can be clearly seen that the increment becomes reduced when the louver angle increases from 60° to 70° (Figure 36(a)). On the other hand, pressure drop increases exponentially with louver angle as shown in Figure 36(b). This trend is observed for all the overall mixing lengths ranging

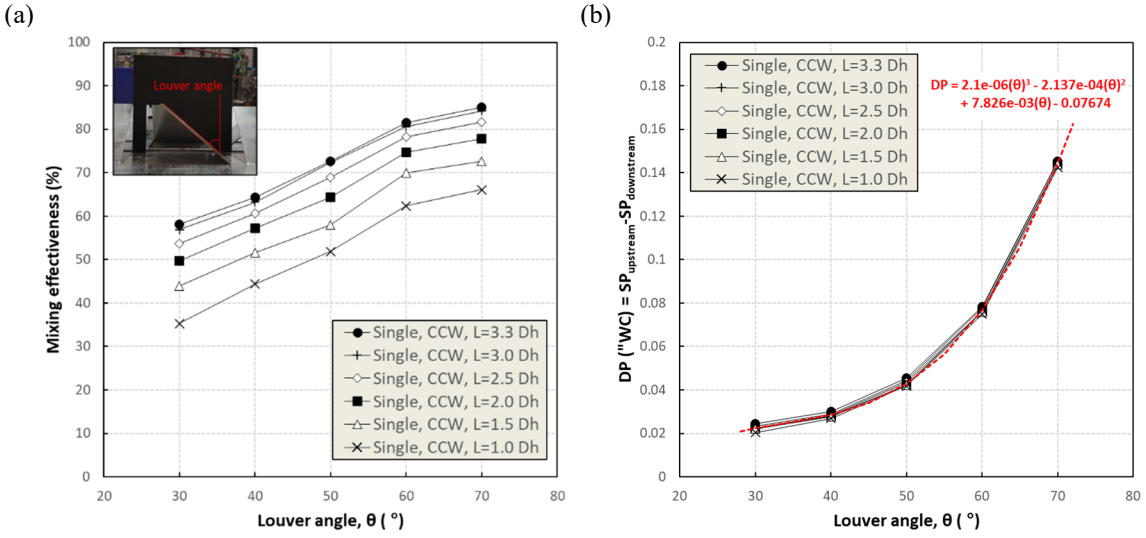

Figure 36 Effect of louver angle of the orthogonal pattern louver mixer on (a) mixing effectiveness, and (b) pressure drop for a range of overall mixing lengths from 1.0 to 3.0 D_h at a total flowrate of 500 CFM (0.236 m^3/s) and a flowrate ratio of cold air to warm air of 0.5.

from 1.0 to 3.3 D_h, and it is quite similar to the findings from Faison's study for the effect of louver angles on mixing performance for the baseline louver mixer in a circular duct shown in Figure 16. Likewise of the angle of the louvers, the size of louver array has a significant impact on the performance of the mixer. In Figure 37, several orthogonal pattern louver mixers having 2 by 2, 4 by 4, and 6 by 6 louvers are compared to one another. The result shows that when the size of louver array decreases from 6 by 6 to 4 by 4, the mixing effectiveness increases, and it is accompanied with negligibly small increment in pressure drop. The findings suggest that larger louvers resulting from a smaller size of louver array applied to the same-sized mixer frame can facilitate more rapid deflection and longer movement of airflow in the cross-sectional direction of the duct, potentially leading to faster mixing. Despite the general feature of the louver size, it can be seen in Figure 37 that optimization of the sizes of louver and louver array are required. As the louver array size reduced from 4 by 4 to 2 by 2, it was found that although pressure drop significantly increased, mixing effectiveness decreased. As the overall mixing length increases, however, the difference in mixing effectiveness between the two louver array sizes gradually decreases, finally, leading to a cross-over point at an overall mixing length of 3.0 D_h.

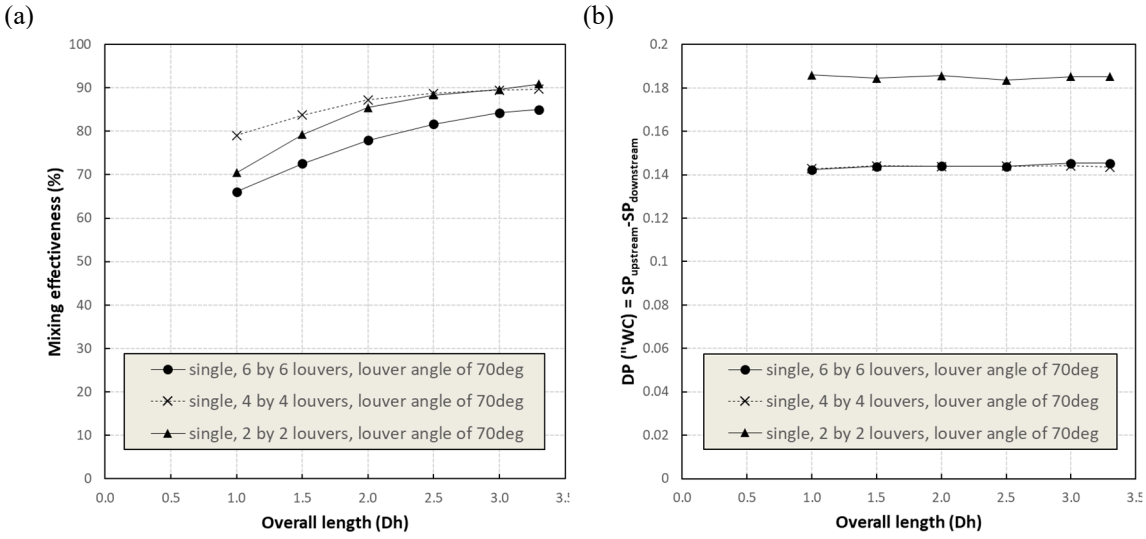

Figure 37 Comparison of louver arrays of the orthogonal pattern louver mixer for overall mixing length ranging from 1.0 to 3.0 D_h at a total flowrate of 500 CFM (0.236 m^3/s) and a flowrate ratio of cold air to warm air of 0.5; (a) Mixing effectiveness, and (b) Pressure drop

3.4.3. Comparison of Mixer Types

The variations of mixing effectiveness and pressure drop for various types of mixers are compared as shown in Figure 38. All the testing for data presented in the figure was performed under conditions given as the total flowrate of 500 CFM (0.236 m^3/s) and the flowrate ratio of cold airflow to the total flowrate of 0.5 since identical flowrate ratio between the inlets allows to evaluate the performance of mixer with minimized inherent mixing effect. The dual orthogonal pattern louver mixers were tested with mixer spacing of 0.8 D_h.

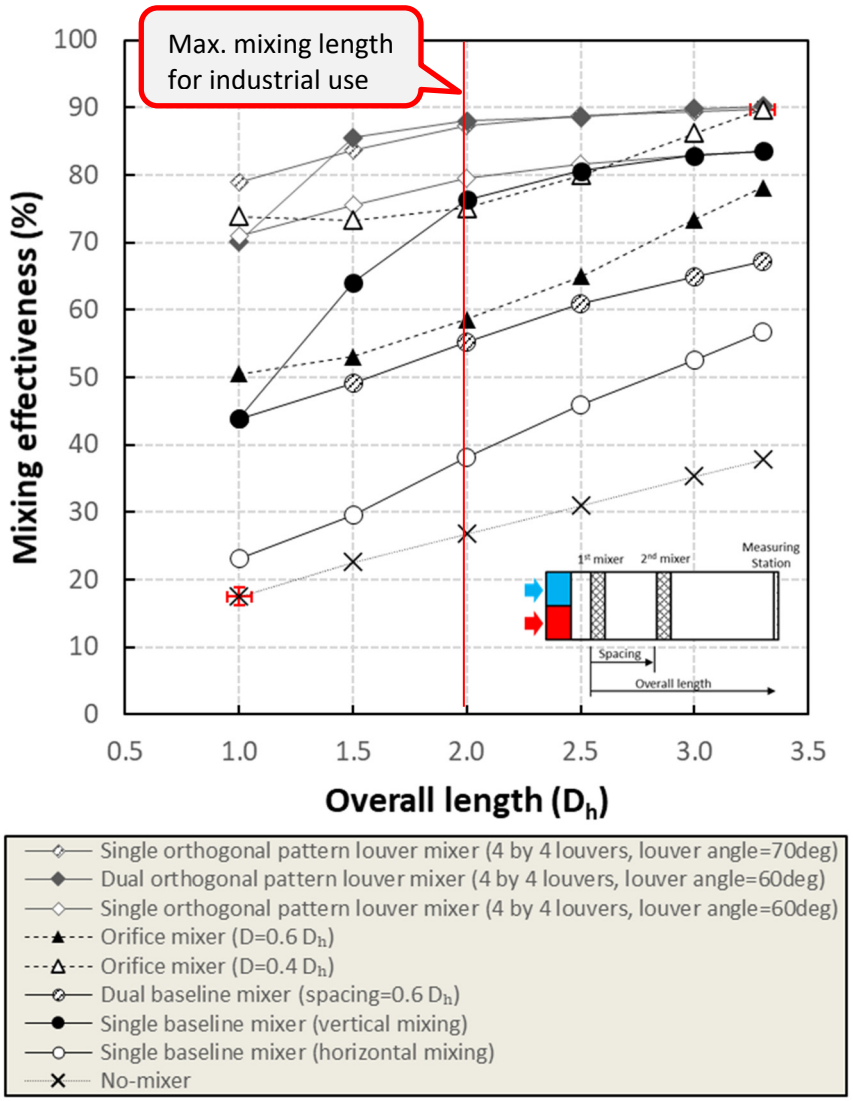

Figure 38 mixing effectiveness for various mixer types tested at a total flowrate of 500 CFM (0.236 m^3/s) and a flowrate ratio of cold air to warm air of 0.5 at a total flowrate of 500 CFM (0.236 m^3/s) and a flowrate ratio of cold air to warm air of 0.5.

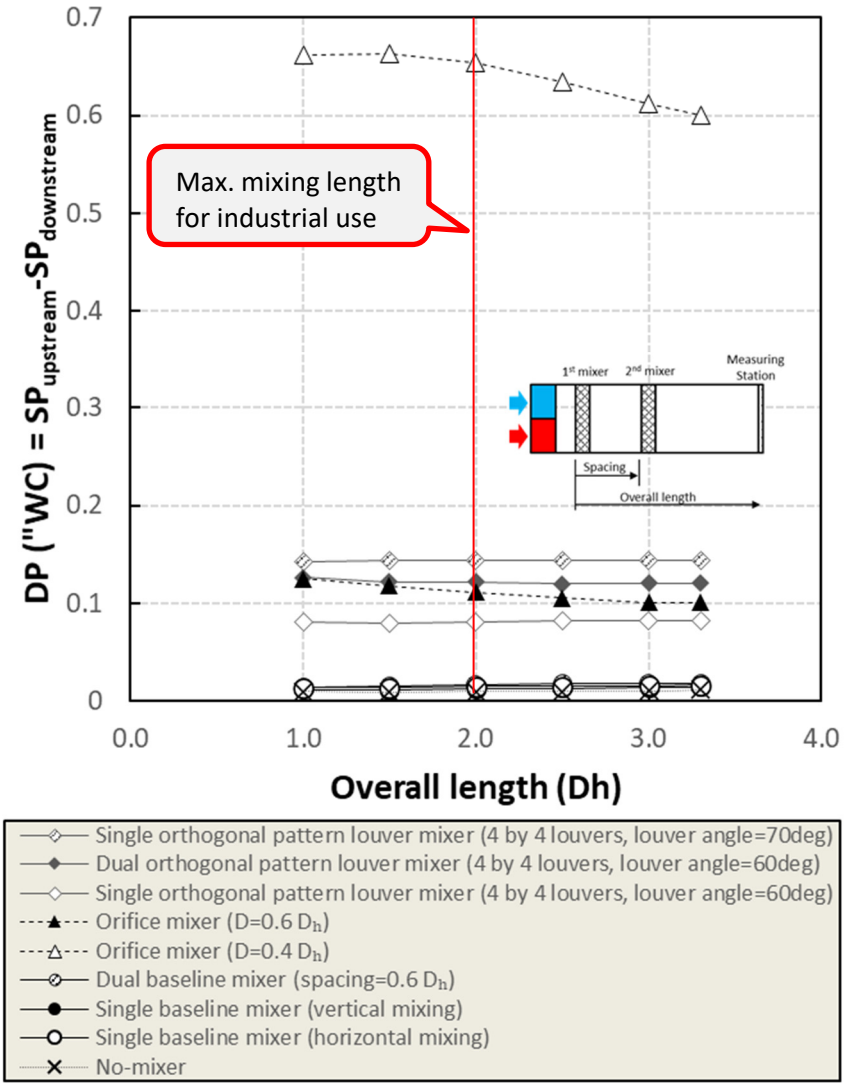

Figure 39 Pressure drops for various mixer types tested at a total flowrate of 500 CFM (0.236 m^3/s) and a flowrate ratio of cold air to warm air of 0.5

The result shows that, in general, mixing effectiveness gradually increases with increasing overall length for all mixer types tested. It is also clearly shown that the existence of mixing elements effectively helps mix the maldistributed airflow compared to inherent mixing without a mixer. The single baseline mixer oriented to deflect airflow in horizontal direction has better mixing performance than other mixer types for the overall length of 2.0 D_h which is largely regarded as the maximum mixing length for industrial use. However, orifice-type mixers show a steeper increase in mixing effectiveness. This is attributed to the sudden contraction and expansion that the flow goes through while passing through the orifice-type mixers; air mixing gradually increases as the

drastic pressure drop caused by the orifice mixer is recovered downstream as shown in Figure 39. According to Faison (Faison et al. (1966)), mixing is approximately complete at the plane where maximum static pressure regain was first observed. Based on this result, it appears that orifice-type mixers require a much longer overall length for mixing to achieve maximum mixing performance, and therefore, may not be an appropriate choice as air mixing devices for the industry use due to space limitations and high-pressure drop.

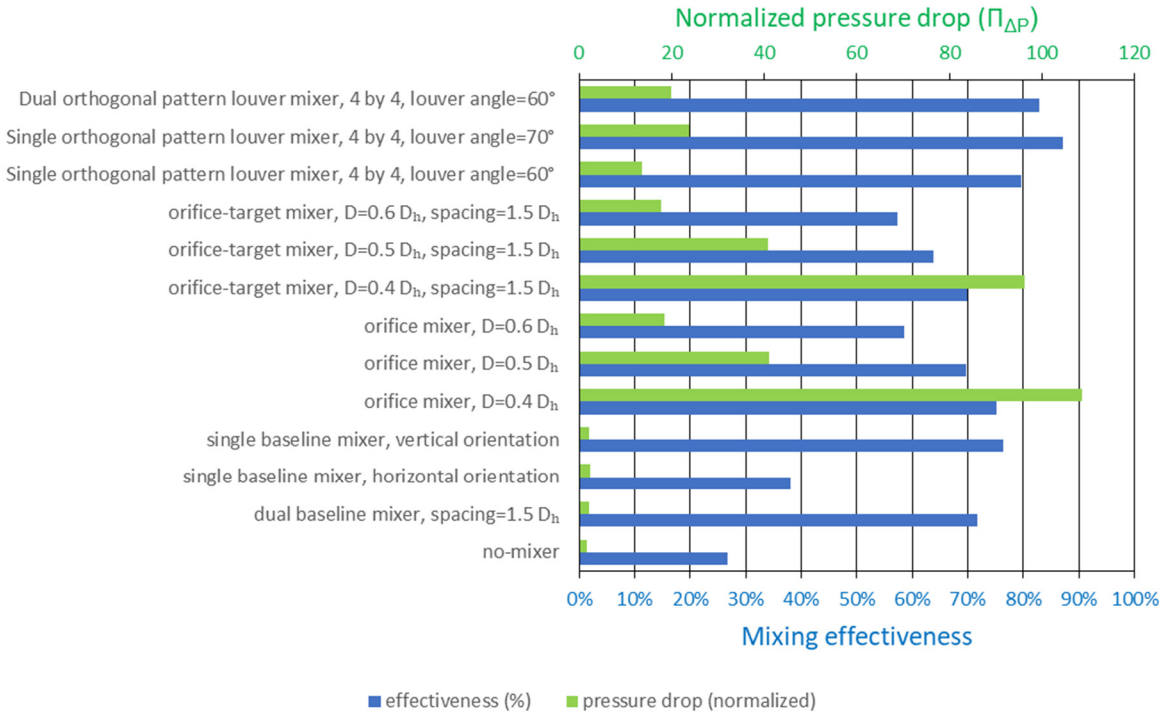

Figure 40 Comparison of mixer types in terms of mixing effectiveness and normalized pressure drop for a total flowrate of 500 CFM (0.236 m^3/s) and a flowrate ratio of cold air to warm air of 0.5 at a fixed overall mixing length of 2.0 D_h.

Figure 40 shows the comparison of all mixer types tested in terms of mixing effectiveness and pressure drop normalized using Eq. (10). This comparison was made for the testing conditions of an overall length of 2.0 D_h, a total flowrate of 500 CFM (0.236 m^3/s), a flow velocity of 2.25 FPM (0.011 m/s), and a flowrate ratio of cold air to the total flowrate of 0.5. As shown in the figure, inherent mixing without a mixing element shows the effectiveness of 26.8% with the smallest

pressure drop. The effectiveness of a dual baseline mixer with a spacing of 1.5 D_h has 71.7%. An interesting result is that a single baseline mixer deflecting the airflow in vertical direction shows better mixing performance than dual baseline mixers while the single mixer deflecting airflow in horizontal direction does improve air mixing much over the no-mixer baseline. This result indicates that the mixing performance significantly depends on the direction of air deflection caused by the louvered baseline mixer. Note that the air condition is artificially maldistributed vertically with the inlet configuration divided into top and bottom. This means that a single baseline mixer deflecting air streams to the same direction of maldistribution provides good mixing performance whereas air mixing in orthogonal direction to the maldistribution is ineffective. Hence, dual baseline mixers can have lower performance than a single baseline mixer since the second mixer is not effective due to its orientation orthogonal to the maldistribution. The air deflection depending on the orientation of louvered baseline mixers is illustrated in Figure 41.

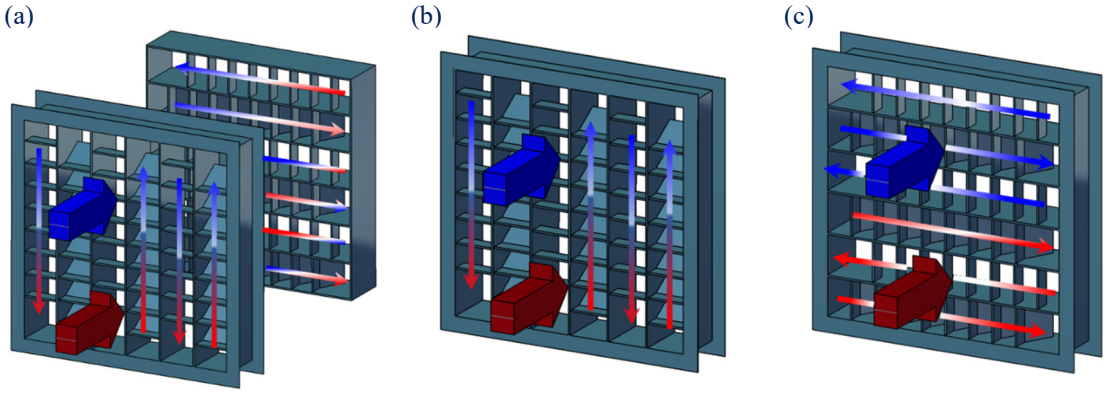

Figure 41 Deflection of vertically maldistributed air streams while passing through three different mixer designs: (a) Dual louvered baseline mixers, (b) Single louvered baseline mixer with louvers oriented vertically, and (c) Single louvered baseline mixer with louvers oriented horizontally.

Orifice and orifice-target combination generally showed similar or better mixing performance compared to the baseline mixer, however, this was at the expense of high-pressure drop as shown in Figure 40. Note also that this does not capture issues with extremely nonuniform flow velocity caused by orifices. Based on the results, it was concluded that orifice-type mixers are not recommended due to high-pressure drop.

Overall, the result shows that the baseline louvered mixers have acceptable mixing performance at the lowest pressure drop. Considering that each of this mixer type creates one-dimensional mixing due to its geometric design, however, it generally requires to be dual used to create effective mixing in both horizontal and vertical directions. On the other hands, if approximate maldistribution in the airflow is known, a single baseline mixer may work for the purpose at a lower cost and lower pressure drop. Also, the ease with which orifice-type mixers are designed and fabricated can provide validity for the use of such mixers as an alternative for any application where relatively high-pressure drop, but not exceed 0.25 inWC (62.3 Pa), is allowable. The result of mixer type comparison shows the orthogonal pattern louver mixer has the best mixing performance with acceptable pressure drop for industry use. The mixing effectiveness of the dual orthogonal pattern louver mixers with a louver angle of 60° is only 0.8% different from that of the single orthogonal pattern louver mixer with a louver angle of 70°. This result implies that a strategy for a cost-effective design of orthogonal pattern louver mixers can be established with the consideration of louver angle, pressure drop, and space limit.

3.4.4. Effect of Total Flowrate and Flowrate Ratio

The effect of total flowrate on mixing performance depends on the type of mixers as shown in Figure 42. The dual orthogonal pattern louver mixers were tested with spacing of 1.5 D_h. The result shows that mixer types with better mixing performance show more consistent performance over the entire total flowrate range. For example, if a mixer effectively deflects the air streams in the maldistributed direction just as the cases of dual baseline mixer and single baseline mixer deflecting the air stream vertically, the change in total flowrate does not influence the effectiveness much except at very low total flowrate. This idea is also proven with the orthogonal pattern louver mixers. The results indicates that the orthogonal pattern louver mixers which showed the highest mixing performance compared to other mixer types tested were found to be least affected by the change in the total flowrate.

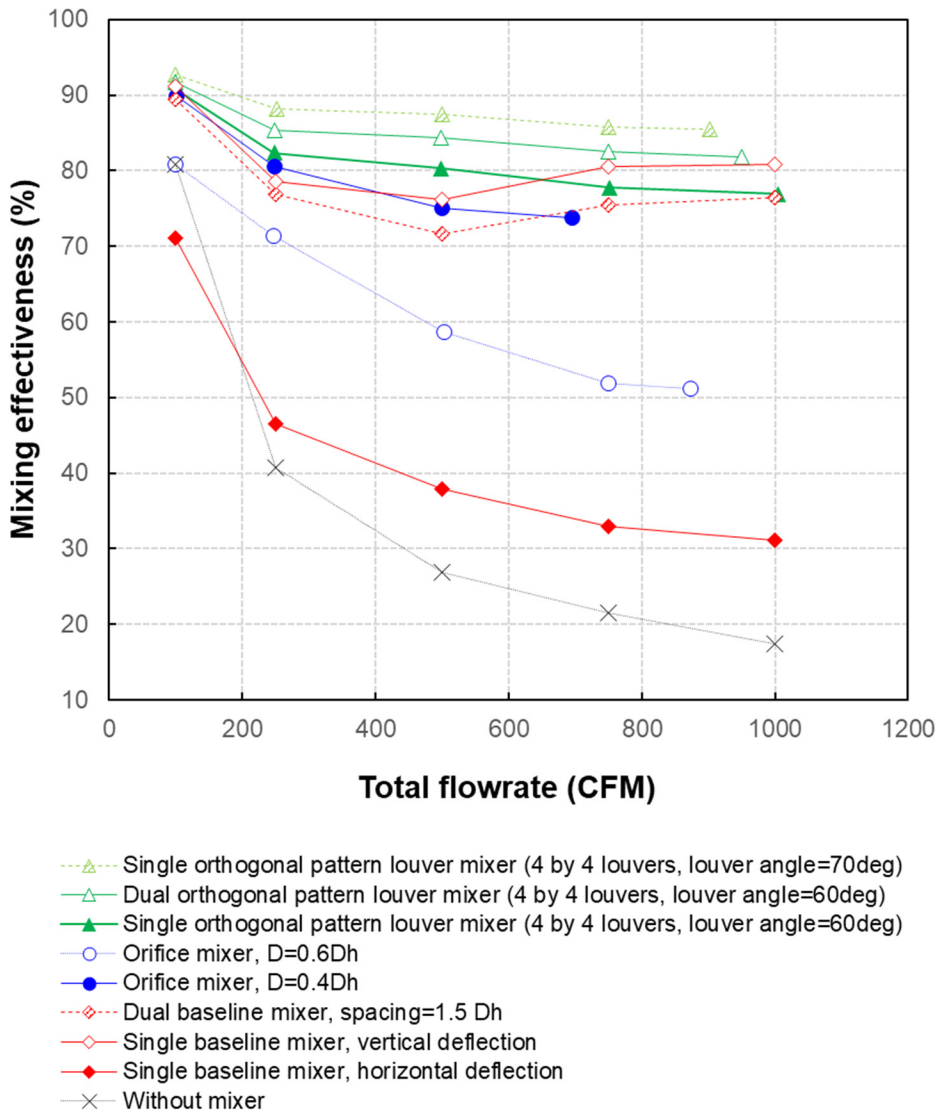

Figure 42 Effect of total flowrate on mixing effectiveness for various mixer types with a flowrate ratio of cold air to warm air of 0.5 at an overall length of 2.0 D_h.

In contrast, other cases such as orifice mixers, and the single baseline mixer deflecting the air streams horizontally showed that the mixing performance was significantly affected by the total flowrate. For the dual baseline mixers and the single baseline mixer oriented for the direction of temperature maldistribution in airflow, the effectiveness showed a fairly flat behavior on the plot except at the lowest total flowrate case. This means that these mixer types may be appropriate to be used as air mixing devices, showing stable performance over the entire flowrate range.

For most types of mixers tested, mixing performance was lowest if the flowrate ratio between warm

and cold air was identical as shown in Figure 43. If the flowrate in one side increased, the mixing performance also increased. This is attributed to less initial nonuniformity of the overall airflow due to the dominant one of the two airstreams, resulting in less required mixing for a temperature equilibrium. The result also shows that louver-type mixers creating effective mixing for both thermal and flow-dynamic uniformities tend to be less affected by the flowrate ratio.

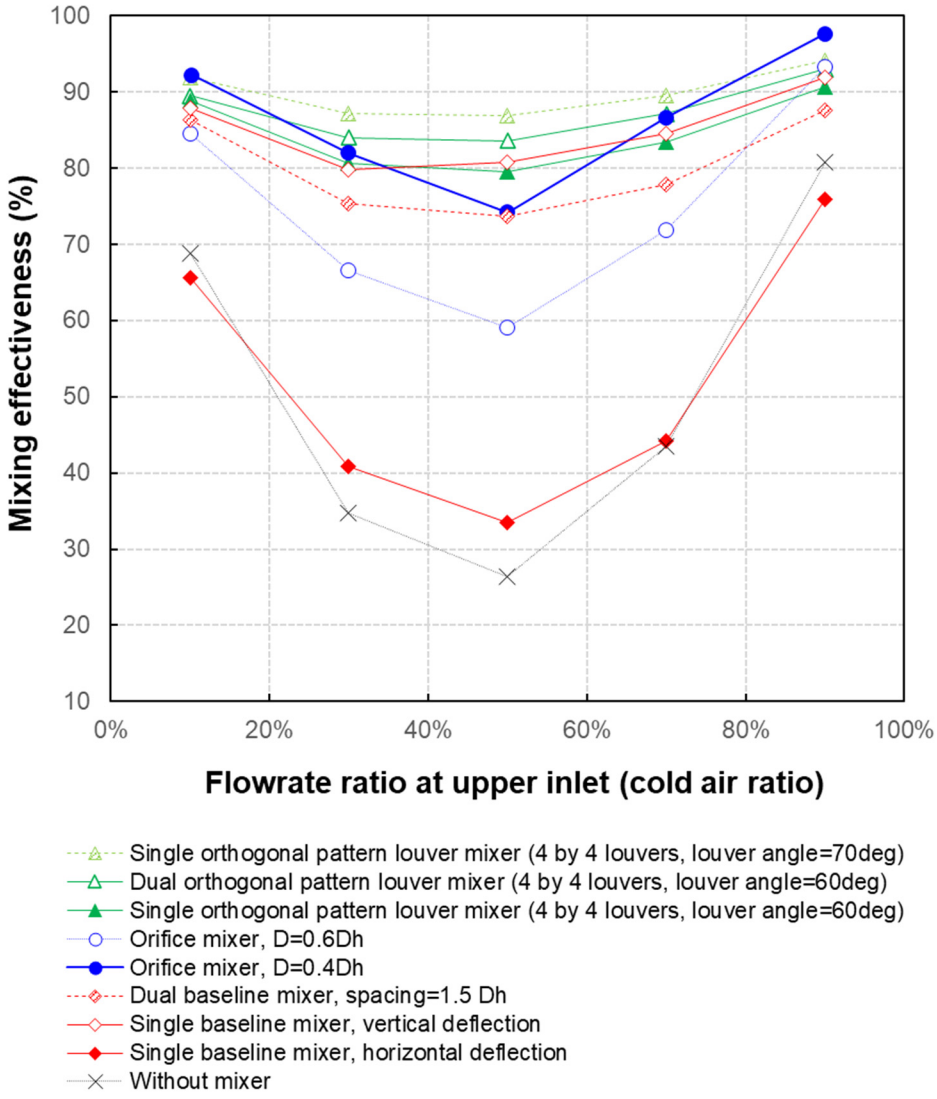

Figure 43 Effect of flowrate ratio between cold air and warm air on mixing effectiveness for various mixer types at a total flowrate ratio of 500 CFM (0.236 m^3/s) at an overall length of 2.0 D_h

3.5. Conclusions

In this research, the performance of various mixing devices designed for a square duct was investigated. The types of mixers included louvered mixers designed based on ASHRAE Standard 41.2, orifice-type mixers, and orthogonal pattern louver mixers. Outcomes of interest were mixing effectiveness and static pressure drop. Tests were conducted considering both geometrical and operational parameters such as mixer types, orientation, orifice diameter, spacing between mixer series, louver angle, louver array size, overall mixing length, total flowrate, and flowrate ratio between cold and warm air.

As shown in Table 4, the mixer types tested were compared to each other. The experimental results showed that, in general, mixing gradually develops downstream, meaning that a longer overall mixing length results in better mixing performance for all types of mixers tested. For the range of overall mixing length, 1.0-2.0 D_h, which is preferred by the HVAC industry, orthogonal pattern louver mixers were found to be outstanding compared to the other mixer types. The maximum mixing effectiveness with this mixer type for an overall mixing length of 2.0 D_h was 88%, followed by 75.1% and 71.8% mixing effectiveness for orifice-type mixers and dual baseline louvered mixers, respectively. The orifice-type mixer showed a rapid increase in mixing effectiveness downstream with static pressure being regained over the baseline louvered mixers. However, the fact that the static pressure recovery initiates after passing through the orifice mixer requires a long distance to reach the maximum mixing performance, and the large pressure drop renders them unacceptable for measurement applications, despite their good mixing performance. Therefore, orifice-type mixers, including the orifice-target combination, are generally not recommended due to high-pressure drops. In contrast, the louver mixers, including the baseline mixer and the orthogonal pattern louver mixer, showed that they have an advantage of causing very small pressure drops, as shown in Table 4.

Based on the experimental results, it was discovered that the mixing performance of the baseline mixer, designed to deflect air streams in either horizontal or vertical directions, significantly relies on the maldistribution of airflow. In other words, the mixers may not be effective if louvers are oriented orthogonal to the maldistribution. The key takeaway from the comparison of all the mixer types is that the ASHRAE Standard 41.2 mixer design can still be a good option for mixing flow in the direction of the louvers with the lowest pressure drop, especially when it is appropriately oriented with respect to the maldistribution. However, considering the complicated design and manufacturing difficulties of such mixers, the orifice-type mixers could be an option when relatively large pressure drops are acceptable. A good alternative that covers both the baseline louvered mixer's and orifice-type mixers' advantages is the orthogonal pattern louver mixer. This mixer type has a simple shape that is easily fabricated, high mixing performance with an acceptable pressure drop, and causes two-dimensional mixing, so it can work effectively when solely used in a limited mixing length, regardless of the direction of air maldistribution.

Additionally, it was found that the mixing performance for all the candidate mixers was significantly influenced by the total flowrate and flowrate ratio between warm and cold air. As the total flowrate is adjusted, the maximum changes in mixing effectiveness for the vertical single baseline louvered mixer, orifice mixer with a 0.6 D_h-hole, and the single orthogonal pattern louver mixer with louver angles of 70° were found to be 14.9%, 19.6%, and 7.1%, respectively. For the range of flowrate ratios tested, the variations in their mixing effectiveness were also found to be in the same order, indicating that the mixing performance of the orthogonal pattern louver mixer is significantly less sensitive to flowrate and velocity maldistribution than those of other mixer types. Thus, they are more appropriate for testing conditions that are unpredictable and/or vary in a wide range. Based on the observation from the mixer testing and comparison with other mixer types, the orthogonal pattern louver mixer may be the best option for general use.

Based on the experimental testing results, design guidelines for the orthogonal louver mixer as the

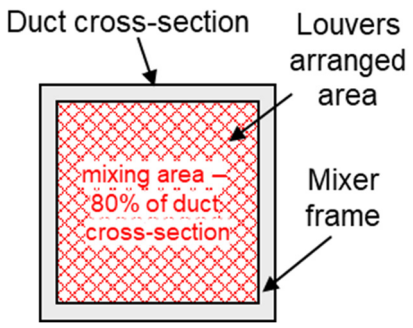

(a) Required mixing area

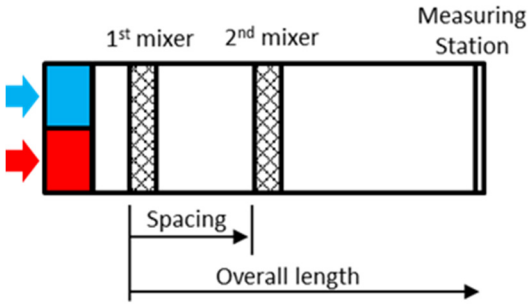

(b) Mixing length (overall length) and mixer spacing (spacing)

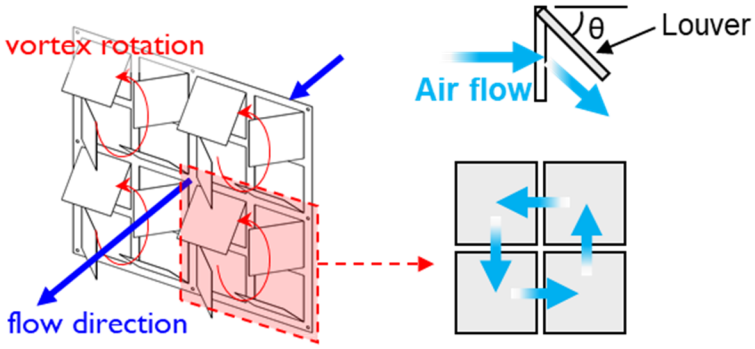

(c) Louver pattern and angle

Figure 44 Schematic of the orthogonal pattern louver mixer design

most promising mixer type were established as following:

- 80 percent of duct cross-section for mixing zone required (Figure 44 (a)).
- A louver pattern in which four louvers are arranged in square shape to switch the direction of the air orthogonally in a clockwise or counterclockwise direction (Figure 44(c)).
- Identical louver pattern across all louver sets (Figure 44(c)).
- 4 by 4 louver array size preferred (Figure 44(c)).

- No more than 60° of louver angle recommended (Figure 44 (c)).
- A mixing length of 2.0 D_h required for more than 80% mixing effectiveness (Figure 44(b)).
- Dual mixers:
  - Identical louver pattern between the mixers required.
  - Less than 1.0 D_h mixer spacing recommended.
  - A mixing length of 1.5 D_h required for 80% mixing effectiveness.

Table 4 Comparison of mixer types

	Dual Baseline Louver Mixers: spacing= 0.6-1.5 D_h	Single Baseline Louver Mixer		Orifice Mixer			Orifice-target Mixer: spacing=0.6-1.5 D_h		Orthogonal Pattern Louver Mixer		
		vertical	horizontal	$D_{orifice}$= 0.4 D_h	$D_{orifice}$= 0.5 D_h	$D_{orifice}$= 0.6 D_h	$D_{orifice}$= 0.4 D_h	$D_{orifice}$= 0.6 D_h	single, louver angle=60°	single, louver angle=70°	dual, louver angle=60°
Mixing effectiveness for overall length range of 1.0-2.0D[1] [%]	43.7-71.8	44-76.3	23.1-38.1	73.8-75.1	65.1-69.6	50.5-58.6	60.5-69.9	45.8-57.4	71.0-79.6	79.0-87.2	70.1-88.0
Pressure drop for overall length range of 1.0-2.0D (normalized)[1] [-]	2.3-2.1	1.9-2.0	2.3-2.5	109.8-108.6	44.1-41.2	20.8-18.5	100.1-96.2	20.0-17.7	13.3-13.5	20.3-21.0	23.7-23.9
Change in mixing effectiveness for range of flowrate tested[2] [%]	17.8	14.9	39.9	34.31	27.8	19.6	-	-	13.69	7.1	9.86
Change in mixing effectiveness for velocity maldistribution tested[3] [%]	14	12.1	42.4	32.8	26.1	23.5	-	-	11.14	7.2	9.41
Min. mixing length required for effectiveness of 70%[4] [D_h]	2.0	2.0	-	1.0	2.0	3.0	2.0	3.0	1.0	1.0	1.0
Min. mixing length required for effectiveness of 80%[4] [D_h]	3.5	2.5	-	2.5	3.0	3.5	3.0	3.5	2.0	1.0	1.5

1. No velocity maldistribution with a total flowrate of 500 CFM and a flowrate ratio of 0.5 were applied.
2. The flowrate ratio at inlets was fixed at 0.5 while the total flowrate was adjusted in a range from 100 to 1000 CFM.
3. The total flowrate at inlets was fixed at 500 CFM while the flowrate ratio was adjusted in a range from 0.1 to 0.9.
4. Spacing for the dual louvered mixers, dual orthogonal pattern louver mixers, and the orifice-target mixer was 1.5D_h.

CHAPTER IV

AIR SAMPLER

ABSTRACT

This study focused on developing design recommendations for air sampling devices that are accurate and reliable for psychrometric performance testing. Although the dependence of air sampler performance on design parameters is significant, limited guidelines are available for designing these devices, resulting in discrepancies in measured results between different testing facilities. The study investigated the accuracy dependence on design parameters using numerical and experimental approaches and discussed various attempts to compensate for these discrepancies. Computational fluid dynamics (CFD) analysis was used to investigate the characteristics of airflow and energy transfer inside the air sampler and create several representative operational conditions. An experimental study was conducted to validate the results of the numerical study. The investigation considered various design parameters and operating conditions, and the findings suggest that adjusting the sampling hole size and spacing can significantly improve the uniformity of air influx across the sampling holes. The study recommends the use of aluminum and PVC as sampler materials. Based on the results, the study established design constraints and guidelines for air sampling devices, including a recommended sampling hole diameter to sampler branch diameter ratio and the use of biased sampling holes.

4.1. Overview

Air samplers are widely utilized in psychrometric performance testing to uniformly sample air across a test section for the measurement of dry and wet bulb temperature determining the bulk air conditions such as humidity, temperature, and dew point. The dependence of how effectively the apparatus can sample the air for the measurement of accurate bulk air condition on design parameters is likely to be significant. Nonetheless, due to limited guidelines available for the design of required air temperature/humidity sampling devices, in many cases, the design of the devices tends to rely on each manufacturer's empirical data and know-how, which may cause discrepancies in measured results between different testing facilities, called "false testing failures". Therefore, it needs to standardize the design guidelines for the accurate and creditable performance of air sampling devices, which can contribute to for HVAC&R industry.

Inaccuracy in measuring air bulk conditions is mainly caused by nonuniformly sampled air from the sampling holes. The sampling holes can be designed to be uniformly distributed at a cross-sectional area of the main airflow. It is, however, likely for the amount of air sampled at each sampling hole to be different due to the pressure gradient formed along the flow path where the sampled air streams are combined and mixed together in the sampler branch. In order to compensate for the discrepancy in the amount of air influx at the sampling holes, manufacturers may apply various methods such as variably sized sampling holes and increasing or decreasing hole pitches. However, all these attempts have not been based on any standardized rule due to the lack of guidance in relevant regulations.

The development of design guidelines for air sampling devices requires thorough investigation on the characteristic of heat transfer and flow inside air sampler. Based on the investigation, it may be possible to determine the performance and characteristics of the air sampling devices for design parameters including:

- Dimension and spacing for sampling holes,
- Dimensional ratio between sampler branch and trunk, and
- Various operational conditions defined from velocity and temperature distribution in the airflow.

Investigating the characteristics of airflow and energy transfer inside the air sampler and creating several representative operational conditions are experimentally challenging. In order to resolve these difficulties, computational fluid dynamics (CFD) analysis was used in this study. The ease with which geometrical and operational conditions change on CFD allows performing parametric study for a number of cases, saving time and cost. Based on the results from the numerical study an experimental study was also carried out for the representative testing cases for the purpose of validation. Based on the qualitative validated CFD model and the experimental results, finally, design recommendations and guidelines for air sampling devices were established.

4.2. Numerical Study

4.2.1. Methodology

The domain of the numerical analysis was determined based on the baseline air sampler designed to meet 10 CRF (DOE, 2017) criteria, and thus, it has four branches with five sampling holes on each branch, and its geometry and further details are described in Figure 45 and Table 5, respectively. For the numerical simulation, a CFD package, Ansys Fluent 2020 R2 (Ansys® Academic Research Mechanical and CFD), was chosen to predict the behavior of airflow and energy transfer for the given boundary conditions. The simulation domain for the analysis was simplified to a single branch of the baseline air sampler in an 18 inches x 18 inches square duct as shown in Figure 46. The grid system consists of approximately 4,500,000 cells including polyhedral cells in the mainstream region and eight layered prism cells near the walls. In order to

accurately capture the boundary layer near wall, predicting the behavior of airflow due to the viscous effect, the k-ω SST turbulence model was chosen for the analysis.

Table 5 Dimensions and the 10 CFR criteria (DOE, 2017) applied to the baseline sampler design

Baseline sampler dimensions designed based on DOE standards

Duct Size (inch x inch)	Branch Diameter d_1 (inch)	Trunk Diameter d_2 (inch)	Sampling Hole Diameter, d_3 (inch)	Number of Branches	Number of Holes per Branch	Max. Total Flowrate (CFM)
18x18	1.05	3.5	3/8	4	5	1000

10 CFR Dimensional Criteria

	Criteria	Designed	Units	Reference/Comments
Minimum distance of any part of sample tree to floor	2	2	inch	10 CFR 2017, section 2.5
Minimum coverage of inlet air	75	60.5	%	10 CFR 2017, section 2.11 - this appears to apply only to outdoor unit!
Sampling hole position, facing upstream direction	-	satisfied	-	-
Minimum sampling hole density	6	8.89	per square foot sampled area	10 CFR 2017, section 2.14.1
Sampler branch tube pitch	3-9	3.5	inch	
Manifold to branch diameter ratio, minimum	3	3.3	-	
Hole spacing equally distributed over branches	-	satisfied	-	
Hole to branch diameter, preferred	1/3	1/3	-	
Hole to branch diameter, max	1/2	1/3	-	
Minimum average velocity through holes	2.5	3.7	ft/s	

For the variety of possible testing conditions, three temperature profiles in linear, inverse linear, and parabolic shape were also chosen for the thermal boundary condition at the inlet, and temperatures for all the profiles were distributed in a range from 70 to 90°F (21.1 to 32.2°C) as shown in Figure 47. Six representative velocity profiles for inlet flowrate of 1,000 CFM (0.472 m^3/s) at duct inlet were also considered for the inlet boundary conditions and they include linear, inverse linear, constant, parabolic, inverse parabolic, and random velocity profiles as shown in Figure 48 and 49. Note that Position (in), the variable on the vertical axis in Figure 47 and Figure 48, is defined with respect to the y-axis of the coordinate system shown in Figure 46(a). The velocity and temperature boundary conditions were created using the user defined functions (UDFs) built in the CFD package.

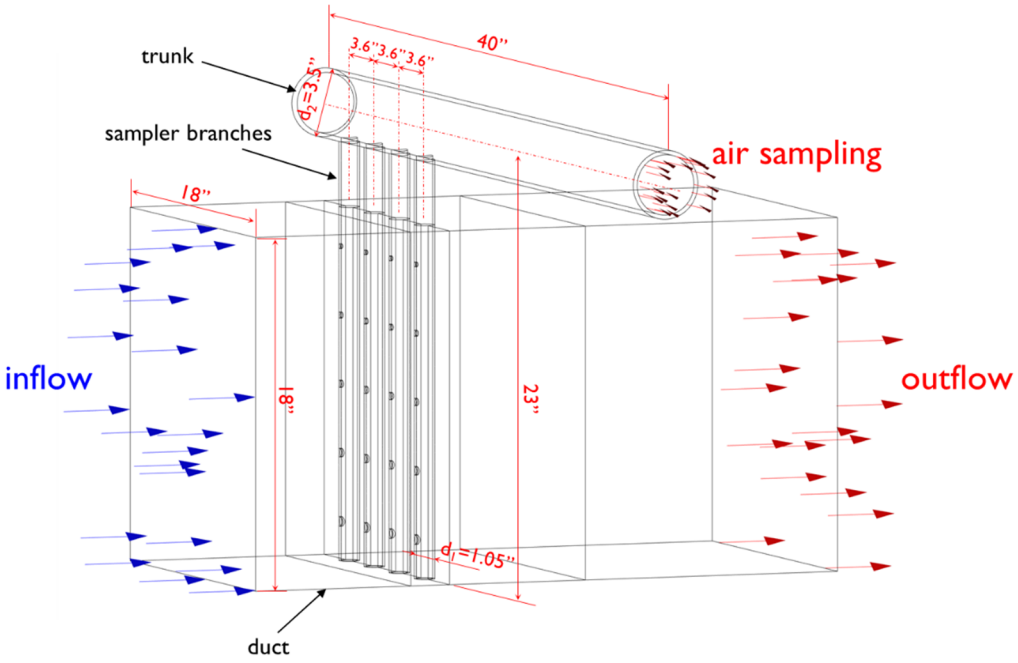

Figure 45 Geometry of the baseline air sampler device, used as the reference point for comparison with other air sampler designs.

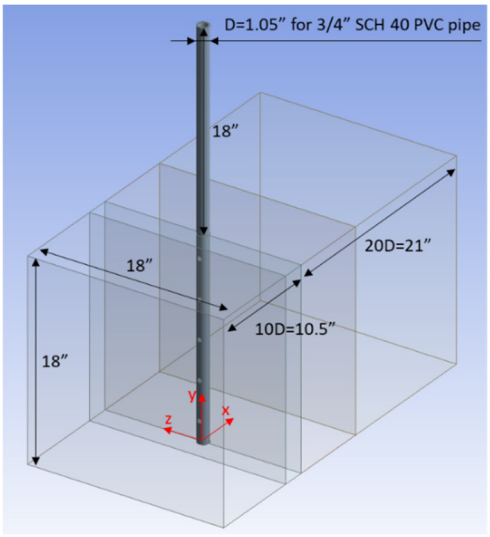

(a) Geometry with dimensions

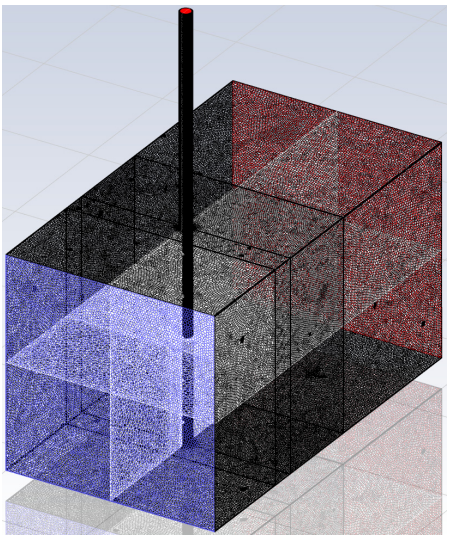

(b) Overview of grid system

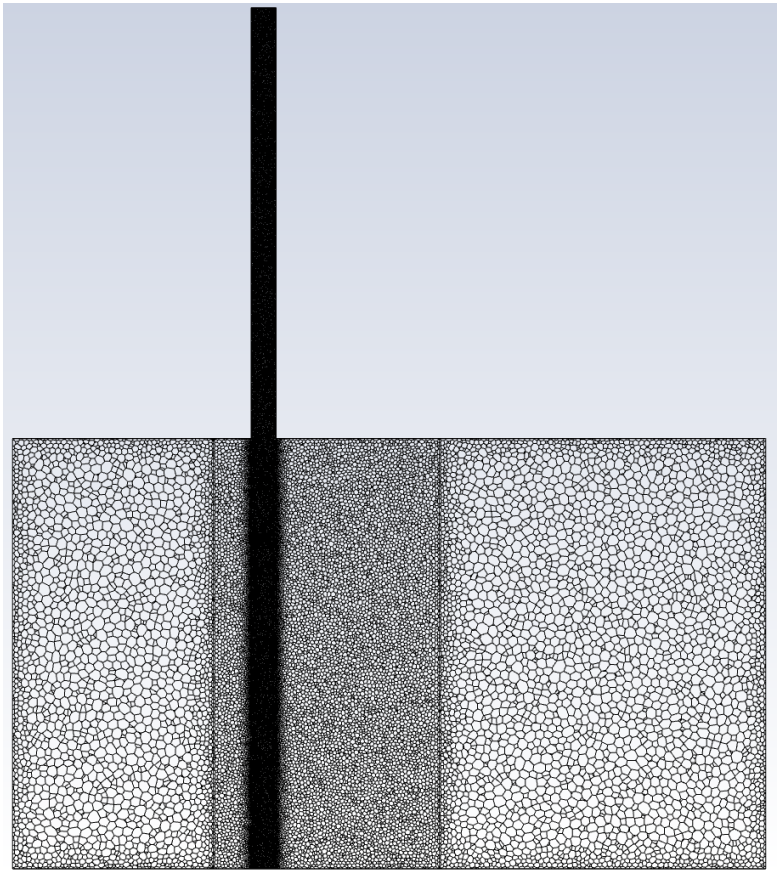

(c) Detail (lengthwise cross-section) of meash system, inlet is at left

Figure 46 Geometry and mesh detail for sampler branch simulation

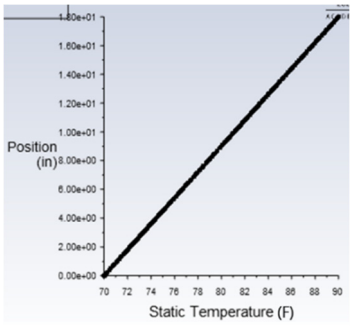

(a) Linear

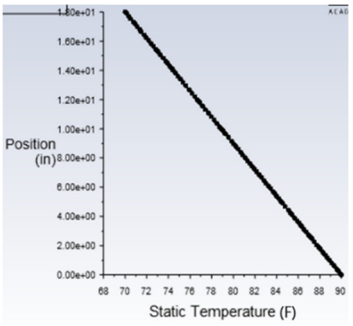

(b) Inverse linear

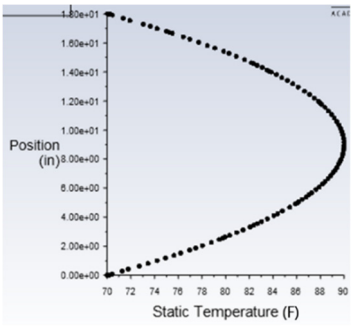

(c) Parabolic

Figure 47 Inlet temperature profiles

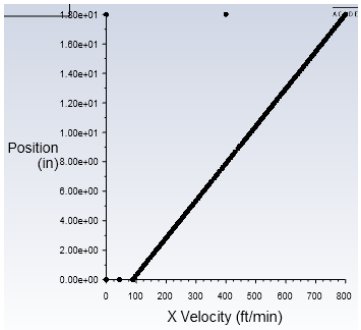

(a) Linear

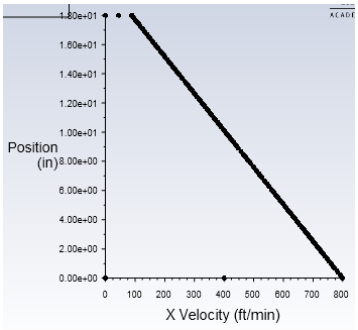

(b) Inverse linear

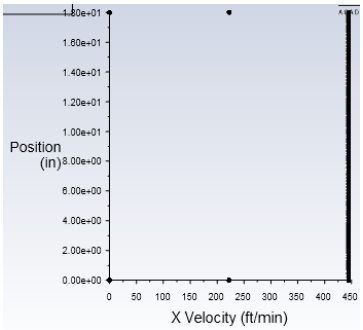

(c) Uniform

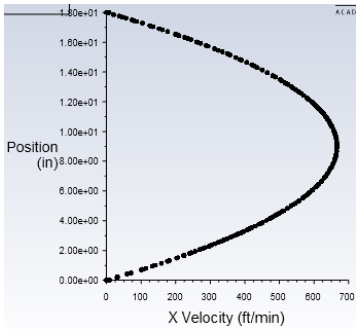

(d) Parabolic

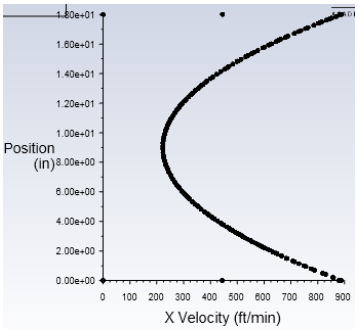

(e) Inverse parabolic

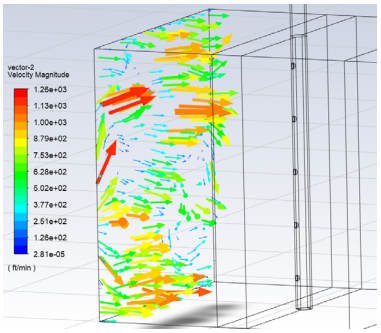

(f) Random

Figure 48 Inlet velocity profiles

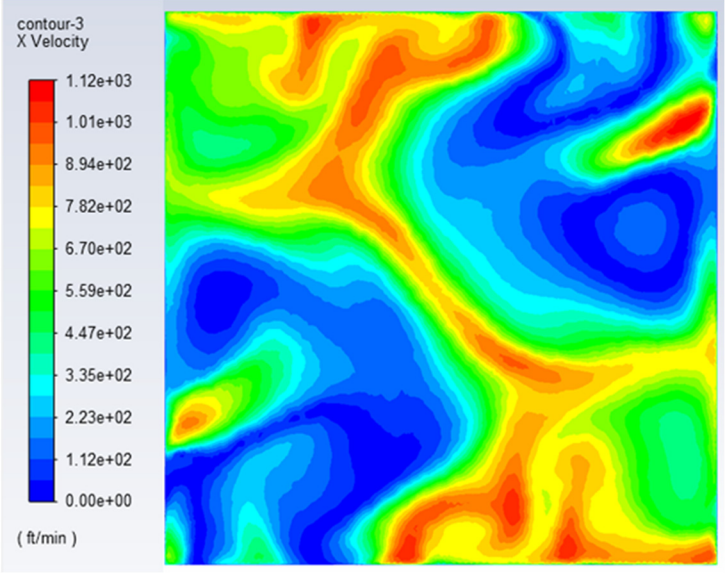

Figure 49 Contour of velocity distribution for the random velocity profile inlet boundary condition

4.2.2. Discussion of Results

4.2.2.1. Flow field in the baseline sampler

The streamlines of the airflow in the sampler branch were captured at a cross-section in the sampler branch as shown in Figure 50 and they were analyzed to understand flow characteristics which can be used to improve sampler design for better distribution of mass influx and measurement accuracy of bulk temperature of the airflow. The flow behavior in a branch of the air sampler was predicted for the six velocity profile cases as shown in Figure 51. The baseline sampler design, the diameter of 0.375 inch (9.525 mm) and spacing of 3.5 inches (88.9 mm) for five sampling holes equally distributed on the sampler branch, was adopted for the simulation.

The streamlines illustrate that air influx at each sampling hole is significantly influenced by airflow distribution approaching the sampler. This obviously shows that the air enters all sampling holes, or no air sampling occurs at some holes due to backflow, depending on the shape of the velocity profile of airflow in front of the air sampler. Even for the constant velocity profile of airflow, the amount of air influx is not uniform for all the sampling holes. Based on this result, it becomes clear

that the well-defined design guidelines for air sampler must be established based on the investigation on the flow patterns in the sampling devices so that uniform air influx at the sampling holes can be made leading to an increase in accuracy in measuring bulk air conditions.

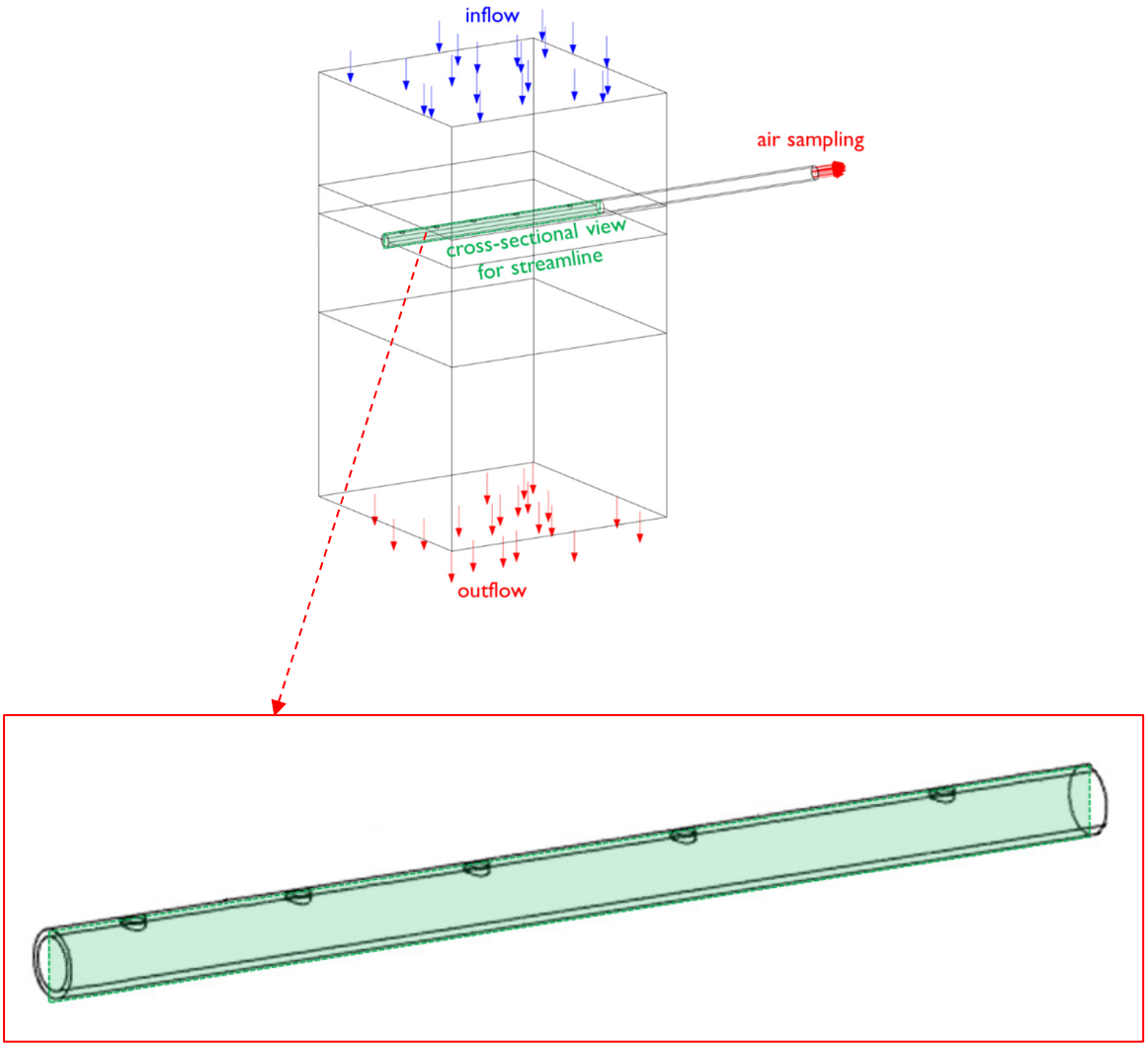

Figure 50 Cross-sectional view of the air sampler branch tube, used to capture streamlines of airflow inside.

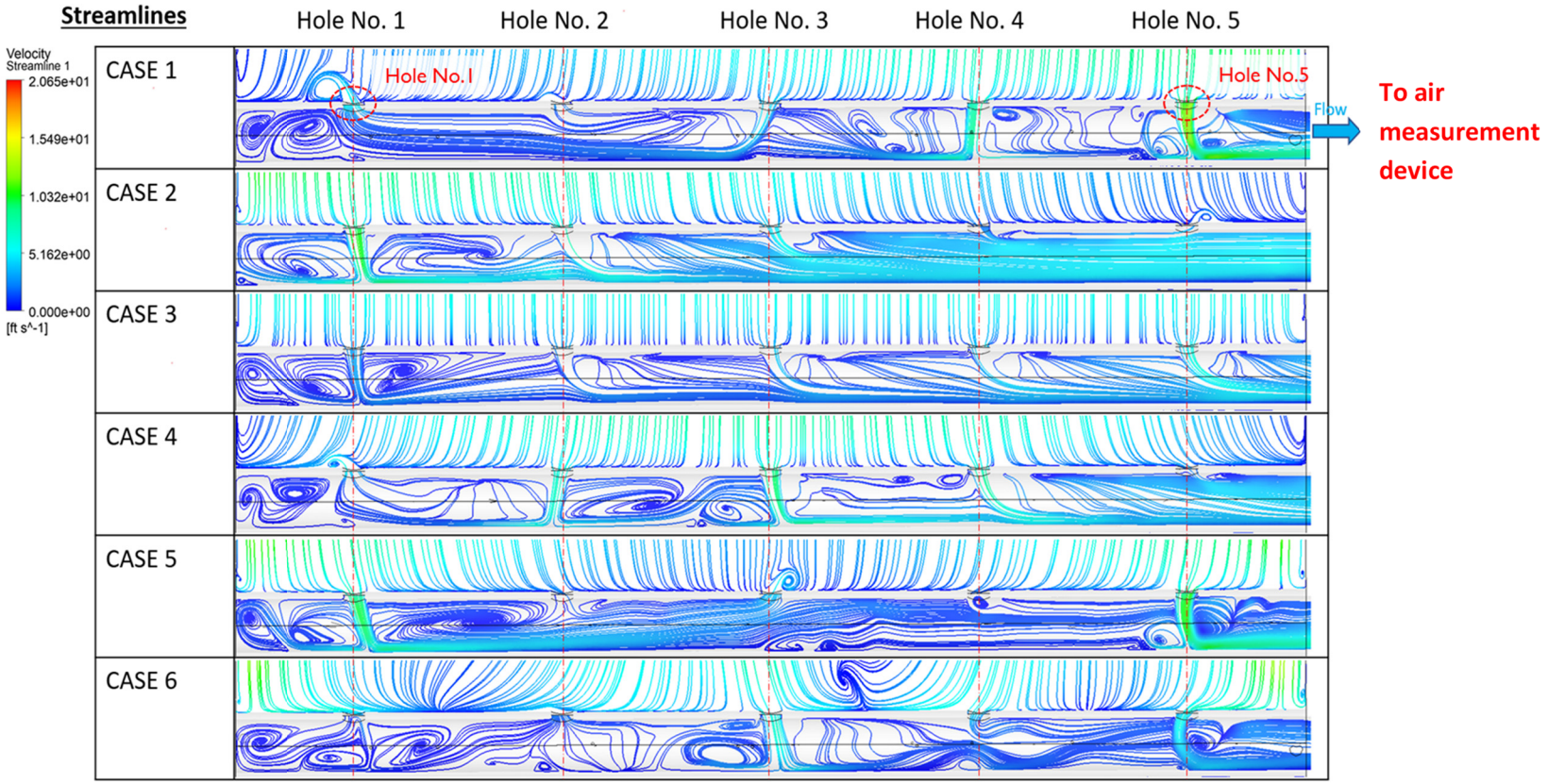

Figure 51 Streamlines captured on the view shown in Figure 47 for the six cases studied: (1) linear velocity profile, (2) inverse linear velocity profile, (3) constant velocity profile, (4) parabolic velocity profile, (5) inverse parabolic velocity profile, and (6) "random" velocity profile.

4.2.2.2. Measurement accuracy and free-stream flowrate

An air sampler was investigated numerically in terms of its accuracy of measuring mass-weighted mean temperature under various test conditions. In this section, the effect of free-stream flowrate in the duct on the air sampler accuracy is investigated for several combinations of flowrates at the duct inlet and the sampler branch outlet, as well as, two types of sampling hole sizes. The diameters of the sampling holes on the sampler were constant at 3/8 inch (9.525 mm). In addition to the constant sampling hole size, the variable sampling hole size in which the sampling hole diameter decreases from 1/2 to 1/4 inch (12.7 to 6.35 mm) with a decrement of 1/16 inch (1.588 mm) toward the outlet of the sampler branch was tested. The test was first conducted for several combinations of free-stream and air sampling flowrate shown in Table 6, and three velocity profiles including constant, linear, and inverse linear velocity profile were employed. The result of the test is illustrated in Figure 52.

Table 6 Testing flow velocity combinations between free-stream and sampled air

Case	Flowrate @inlet [CFM]	Flowrate @sample [CFM]	$\dot{m}$ @sample [kg/s]	Vel @hole [ft/s]	Hole D. [in]	No. of holes	Spacing [in]
high-high	1,000	1.611	9.312E-04	7	3/8	5	3.5
high-low	1,000	0.575	3.326E-04	2.5	3/8	5	3.5
low-high	100	1.611	9.312E-04	7	3/8	5	3.5
low-low	100	0.575	3.326E-04	2.5	3/8	5	3.5

The accuracy of measuring the mean temperature was determined as the ratio of the maximum temperature difference at the duct inlet (this temperature difference is defined as the difference of the mean temperature to the maximum or minimum temperature at duct inlet) to the temperature difference between the mean temperature at duct inlet and the sampled air temperature. Therefore, as this ratio of temperature differences is closer to zero, it means the mean temperature of the air sampled by the air sampler is closer to the bulk temperature of the free stream. Based on the result shown in Figure 52, it seems hard to find a general rule in choosing a best flowrate combination for different free-stream conditions. In other words, the accuracy of the air sampler in measuring a

mean temperature significantly depends on the flow distribution across the free stream in a duct. Therefore, it can be concluded that it is almost impossible to define a design rule for simply shaped air samplers that can consistently be applied to all possible flow maldistributions. Assuming that, as stated in ASHRAE 41.1 (2013), the nonuniformity of air velocity is eliminated beforehand using associated apparatus, it seems appropriate to achieve specific design guidelines for sampler design for a representative velocity distribution, constant velocity profile case employed in this investigation.

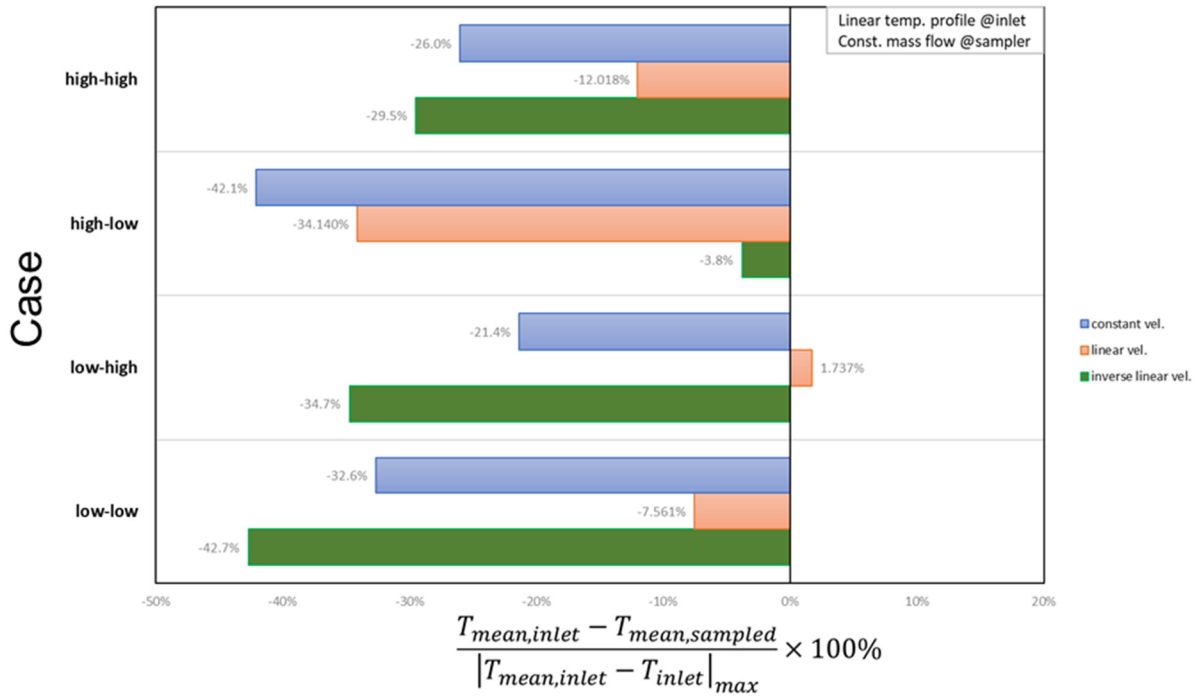

Figure 52 Effect of flowrate combination between free-stream and sampled air for different velocity profiles approaching to the air sampler

Figure 53 shows how the free-stream velocity determined by air flowrate in the duct influences the sampler performance of measuring the bulk temperature of the free-stream as the flowrate of sampled air maintains constant at 0.6 CFM. The air flowrate at the duct inlet was adjusted in the range from 100 to 1,000 CFM. In general, an increase in the free-stream velocity which flows toward the sampling holes on the air sampler leads to a decrease in the accuracy of measuring the mean temperature of the sampled air. At a constant free-stream velocity, the higher the ratio of

sampled air volume to free stream velocity, the better the average temperature measurement is. The same trend is observed in both constant and variable sampling hole size case.

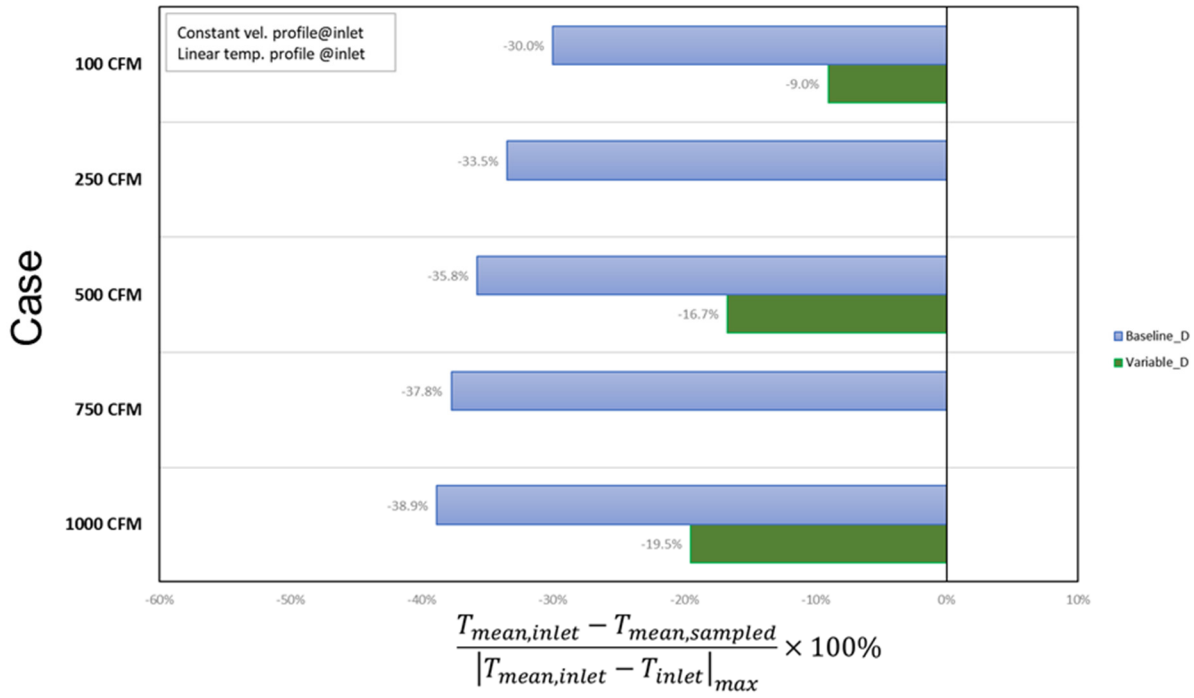

Figure 53 Effect of free-stream velocity on the measurement of bulk temperature of air sampled.

4.2.2.3. Effect of sampler material

As stated in AHRI Standard 210/240 (2017), and 10 CFR Criteria (US DOE, 2017), plastic, stainless steel, or other durable materials can be chosen as air sampler material. However, it may also require considering the fact that conduction and/or radiation heat transfer across the sampler structure depends on the materials when designing air samplers since there is no specific information on how significant the thermal effects acting on the mean temperature of the sampled air may be or not. Therefore, the effects of thermal conduction and radiation heat transfer on the mean temperature of the air sampled by the air samplers were evaluated for several materials that are mostly used for air sampler design.

4.2.2.3.1. Effect of conduction heat transfer on sampler measurement accuracy

The effect of conduction heat transfer on the mean temperature of sampled air was investigated for various conditions. Three materials including PVC, aluminum, and stainless steel were chosen for the test, as well as, adiabatic thermal boundary condition on the sampler wall was tested for the purpose of comparison. The accuracy of measuring the mean temperature of free stream for each sampler material was evaluated, and the results were compared to each other. Several types of sampling hole sizes on the air sampler branch including the small diameter of 1/4 inch, baseline diameter of 3/8 inch, and variable diameters ranging from 1/4 to 1/2 inch were employed in the test. Sampling holes on the sampler branch were equally distributed along it with 3.5 inches spacing or the variable spacing that the spacing between the holes gradually increases toward the branch outlet in a range of 1.4 to 4.5 inches was applied to the air sampler.

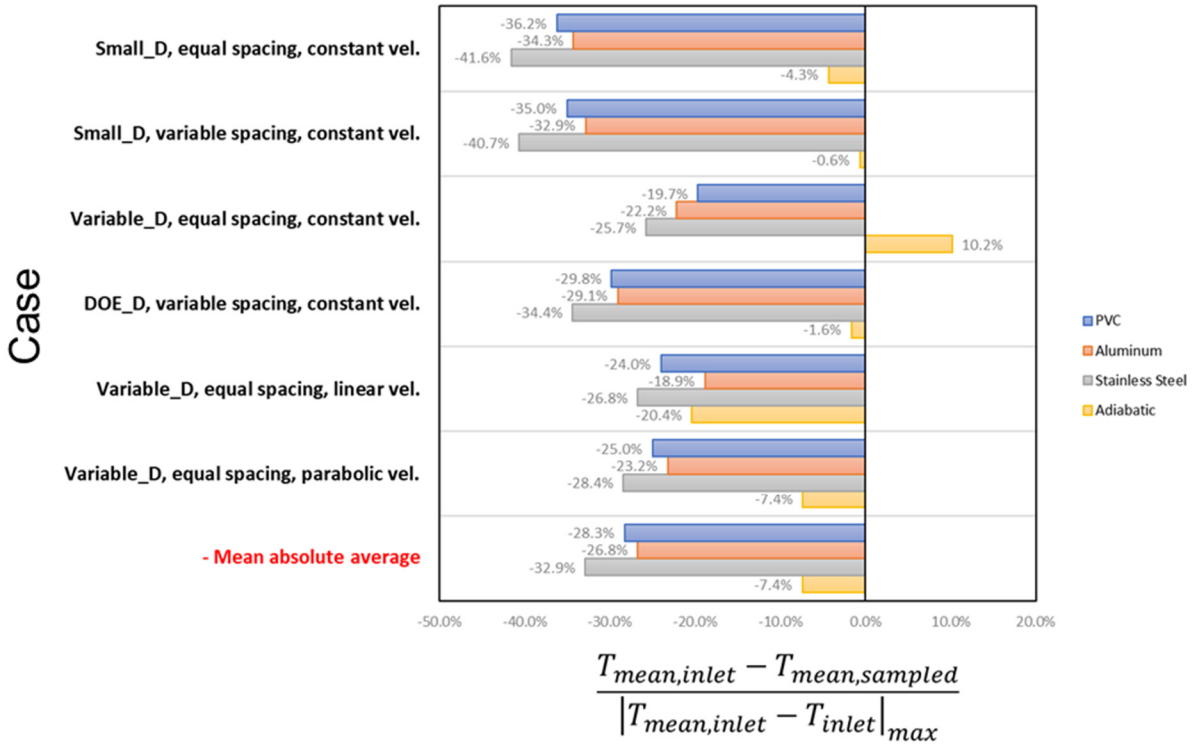

Figure 54 CFD simulation result of sampler material comparison in terms of the air sampler performance

As shown in Figure 54, the differences in the accuracy of mean temperature measurement due to different air sampler materials showed similar results for most test conditions. To be specific, the air sampler tested under the adiabatic wall condition showed the highest accuracy for most tested cases. In addition, the result showed that an air sampler made of aluminum material can have better accuracy than PVC and stainless steel, indicating that thermal conductivity of the sampler material does not have a linear effect onto accuracy; aluminum has higher thermal conductivity than PVC and stainless steel, however, the adiabatic thermal boundary case has zero thermal conductivity. As an extreme case, infinite conductivity will lead to temperature averaging due to conduction along the air sampler. A potential concern with metal air samplers would be thermal mass that could lead to a slow response. Except for the adiabatic sampler, which is generally difficult to produce practically, both PVC and aluminum seem to be suitable materials for the air sampler, but which one performs better can be determined depending on the design of the sampling hole and the conditions of the upstream airflow.

4.2.2.3.2. Effect of radiation heat transfer on sampler measurement accuracy

In order to investigate the radiation heat transfer effect in the simulation domain, the surface-to-surface radiation model was applied to the solver. The emissivity on the duct wall was set to 0.28 for galvanized steel, while the emissivity for both air sampler inner and outer wall made of aluminum was adjusted to 0.1, 0.5, and 0.95 in order. The black body temperature at the duct outlet was set to the mean temperature of the airflow at the duct inlet as an approximation to near isothermal conditions in psychrometric rooms, and its emissivity was set to 0.28. The air sampler employed for the testing had the baseline hole diameter of 3/8 inch with variable spacing described in the previous section. Air flowrate at the duct inlet was set to 1000 CFM with a constant velocity profile and the temperature profile employed for the testing was in the linear or parabolic shape.

The comparison of radiation heat transfer effects for different emissivity values is presented in

Figure 55. This result shows that the change in the mean temperature measurement accuracy caused by radiation heat transfer ranged from 1.6% to 3.2% compared to the case with no radiation effect, depending on the temperature profile in the duct flow. Therefore, based on these findings, it can be concluded that the effect of radiation heat transfer on the accuracy of mean temperature measurement is not significant enough to influence the temperature distribution of the air stream flowing inside the air sampler or the bulk temperature of the air stream leaving the air sampler.

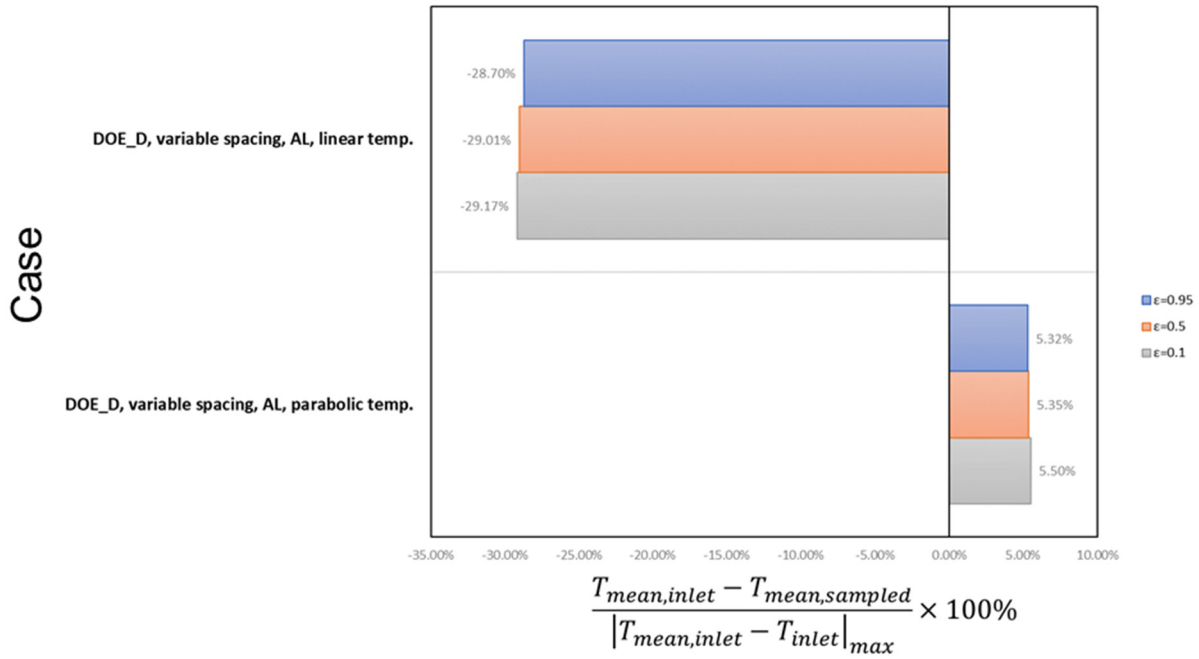

Figure 55 Effect of radiation heat transfer on the mean temperature of sampled air

4.2.2.4. Effects of sampling hole spacing, orientation, and size

The equal sampling hole spacing on the baseline sampler design was compared to the variable sampling hole spacing to investigate a change in the accuracy of mass-weighted mean temperature at the sampler outlet. Figure 56 shows how the sampling holes were distributed for the variable sampling hole spacing case. The location of each hole was determined based on a calculation that allows for each hole to have the same coverage in terms of flowrate using the flowrate distribution obtained from the result of the equal hole spacing case. From the test result, we found that variable spacing contributes to uniform flowrates across the holes; the range of $Q(x_i)/\Delta x_i$ reduced from 0.41-

0.75 (CFM/in) to 0.43-0.59 (CFM/in). As shown in Figure 57, the result indicates that an air sampler with sampling holes distributed by variable spacing has higher accuracy in measuring mean temperature, however, it seems that the effect of sampling hole spacing on the accuracy is significant in general.

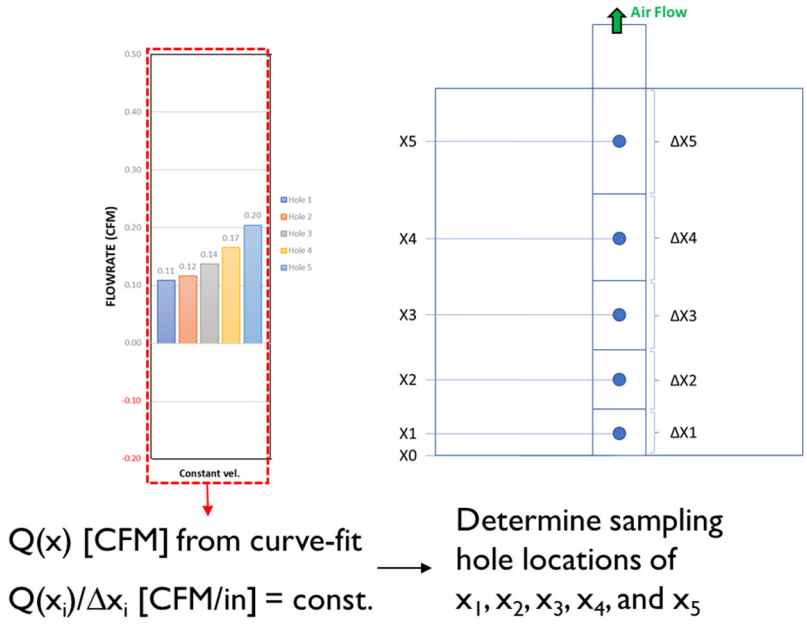

Figure 56 Variable pitch of sampling holes for the same flowrate coverage per each hole

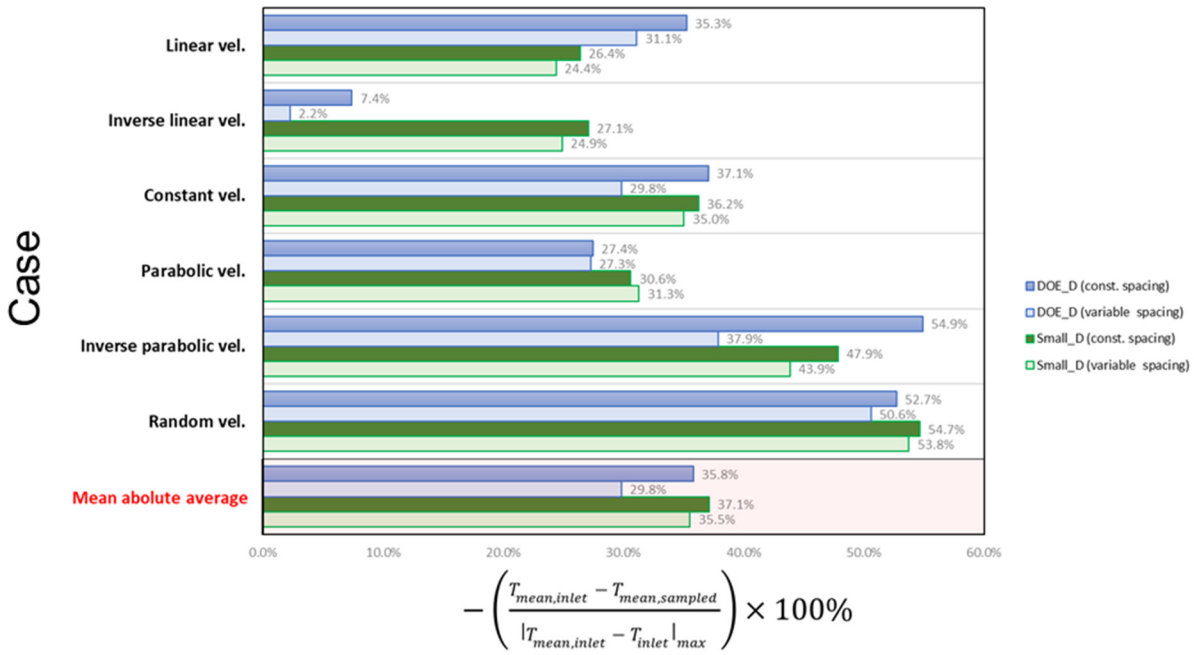

Figure 57 Comparison of sampling hole spacing types in terms of the air sampler performance

In the conventional use of air sampling devices, they are always arranged to allow the sampling holes to face toward the direction of the free-stream air flowing in. Although such a way can be intuitively considered as the best to uniformly sample the air, it is unclear how to arrange the air sampling holes in the free stream approaching them influences the uniformity in sampling the air. Therefore, in this research, what influence on the uniformity of air sampling can be made by the sampling hole orientation were investigated by varying the angle between the directions of sampling holes facing normal and free stream.

Figure 58 shows top views of a single air sampler branch placed in the duct. As shown in the figure, the angle between the directions of sampling hole facing to and free stream flowing from was set to 0, 90 and 180°. The measurements of the mean temperature accuracy for the different sampling hole orientations were compared in Figure 59.

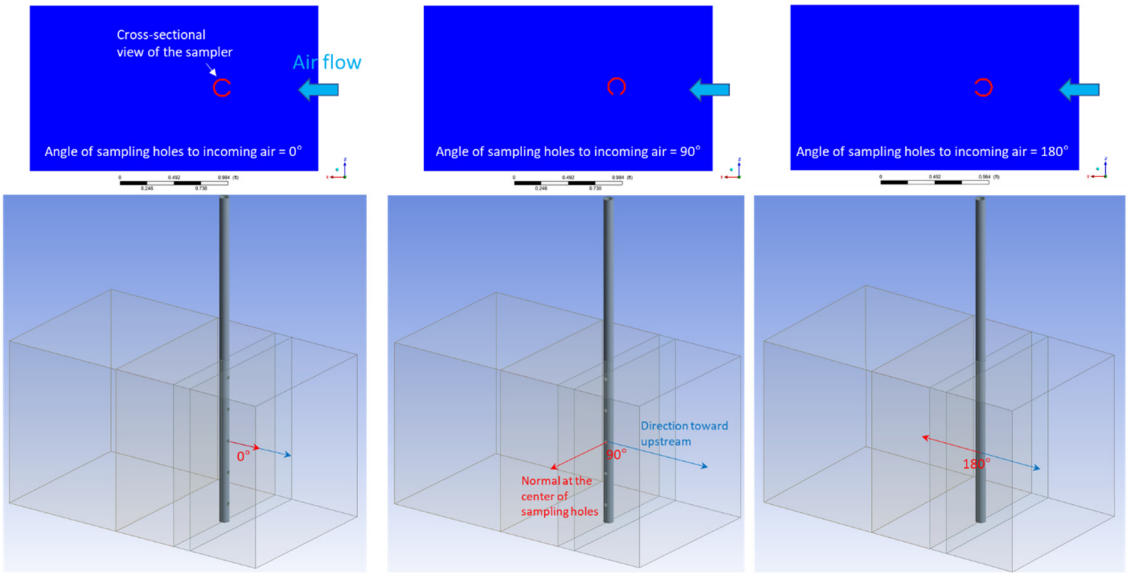

Figure 58 The angle between the normal direction of air sampling holes and the upstream direction: 0 deg. (left), 90 deg. (middle), and 180 deg. (right)

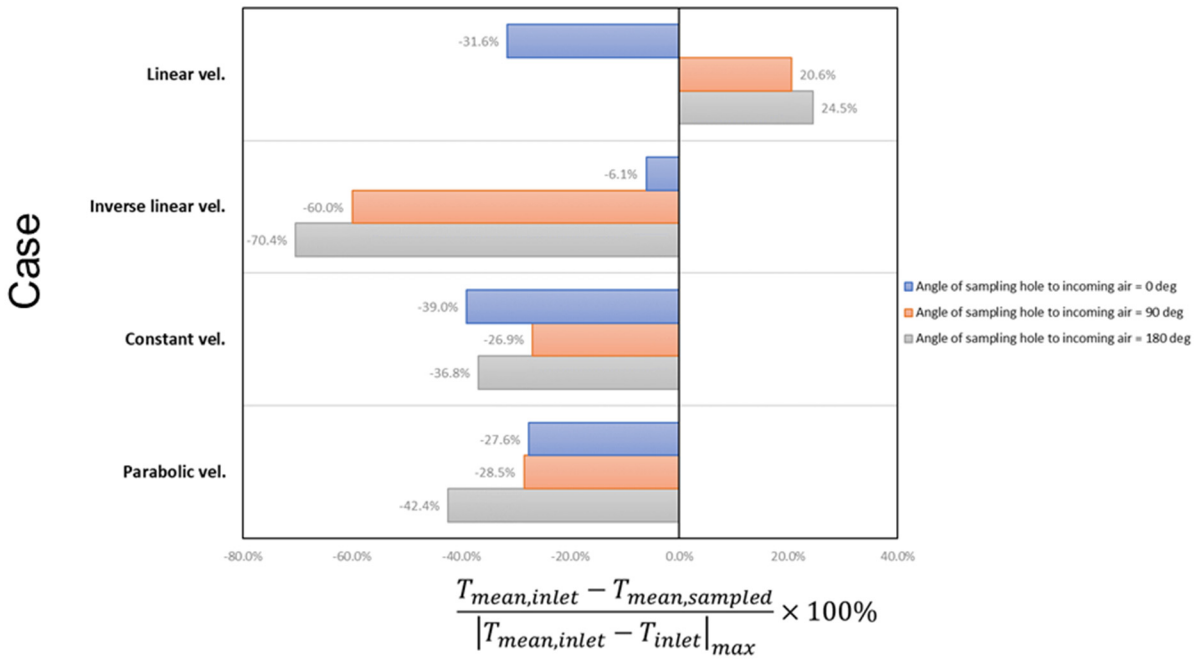

Figure 59 Comparison of sampling hole orientation in terms of the air sampler performance

The result of the testing shows that the mean temperature of the sampled air depends on sampling hole orientation, however, it seems impossible to generalize the best rule on how to orient sampling holes with respect to the airflow direction. This is due to the fact that the best orientation of sampling holes for uniform air sampling across them significantly depends on the velocity profile of airflow approaching to the sampler.

The effect of sampling hole diameter on the accuracy of bulk air temperature was also investigated. Compared to the baseline sampling hole diameter of 0.375 inch (9.525 mm), the hole size was adjusted to be larger (0.5 inch, 12.7 mm) or smaller (0.25 inch, 6.35 mm). Variable hole size (0.25 to 0.5 inch, 6.35 to 12.7 mm) on a sampler branch was also tested. In the Figure 60 and 61, the results indicate that a sampler branch with variable sampling hole size, in general, has the best accuracy in measuring mass-weighted mean temperature of the inlet airflow for all velocity profiles tested.

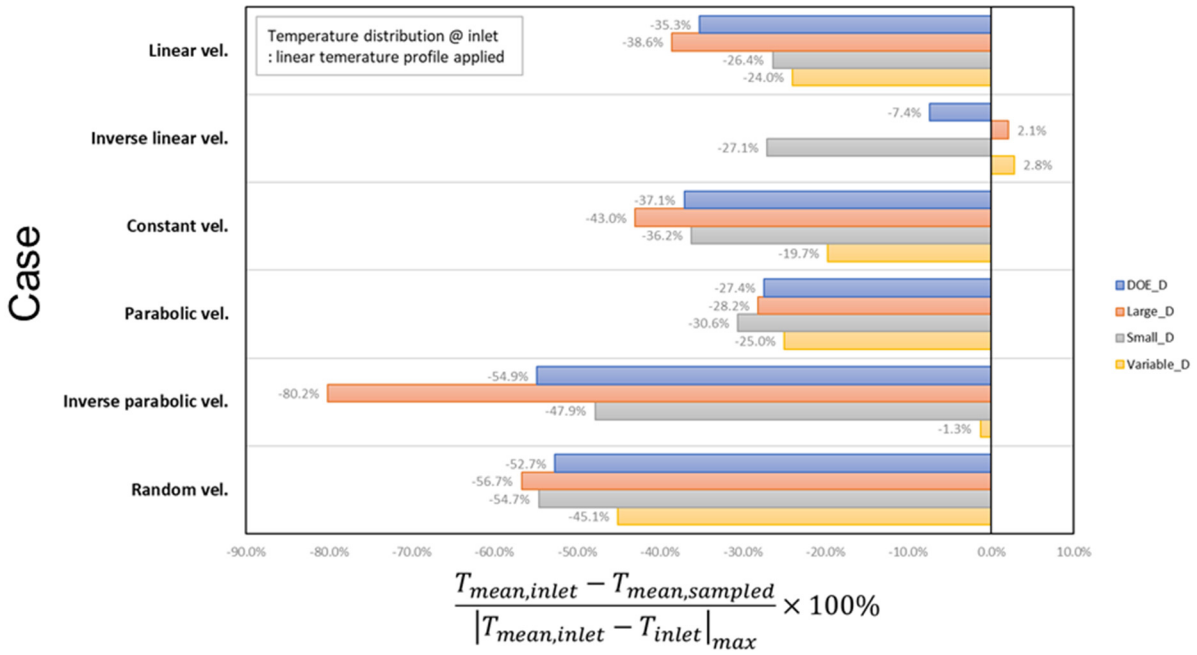

Figure 60 Effect of sampling hole size on the mean temperature of sampled air for velocity profiles

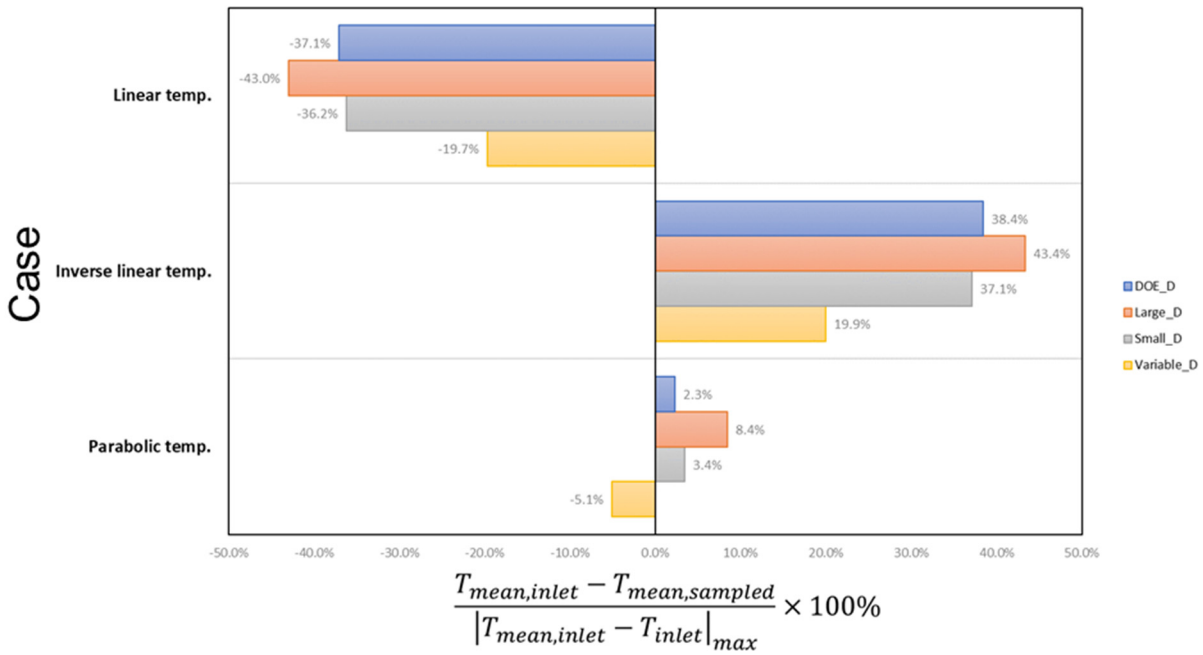

Figure 61 Effect of sampling hole size on the mean temperature of sampled air for different temperature profiles

For the variable hole diameter case, the size of sampling hole gradually decreases along the direction of sampler branch leading to the sampler trunk. Air entering the sampling hole, located far away from the outlet of the branch, will go through a relatively greater pressure drop as it travels along the inside of the branch. Therefore, gradually reducing the size of the sampling hole toward the branch outlet allows to compensate the larger pressure drop at farther sampling holes, and thus, the maldistributed air influx across the sampling holes can be offset, leading to more uniform air sampling. The result also shows that in general, the measurement accuracy gets better as the hole size decreases, which is, however, dependent on the distribution of airflow in the mainstream.

4.2.2.5. Optimization of sampling hole size

In order to optimize the sampling hole size for given conditions of free-stream flowing to an air sampler branch, the distribution of mean air velocities at the sampling holes was quantitively investigated for the free-stream flowrate of 1000 and 100 CFM (0.472 and 0.047 m^3/s), corresponding to flow velocity of 7.41 and 0.74 FPS (2.26 and 0.23 m/s), respectively. The diameters of the sampling holes were 1/8, 1/4, 3/8, and 1/2 inch (3.175, 6.35, 9.525, and 12.7 mm), and they were equally distributed along the branch. As shown in Figure 62, the branch, in general, samples air more uniformly across the sampling holes on it as the size of the holes decreases. This trend is found consistently regardless of a change in free-stream velocity and mean velocity of air passing through the sampling holes.

Figures 63, 64, and 65 show the results of testing the performance of an air sampler for different sampling hole diameters. The domain consists of a square duct having a side length of 18 inches, and a sampler branch having a diameter D of 1.05 inches. Also, free-stream conditions at duct inlet are defined to be a constant velocity profile of 7.41 ft/s (2.26 m/s) for 1000 CFM (0.472 m^3/s), and a linear temperature profile ranging from 70°F to 90°F (21.1°C to 32.2°C). Figure 63 shows how mean temperature measurement accuracy varies as increasing a ratio of sampling hole diameter, d,

to branch diameter, D. As shown in the figure, all the data series have minimum deviation from the true inlet temperature in a range of d/D = 0.238-0.357 depending on different dimensionless air velocities at sampling holes.

Considering better accuracy in measuring a mean temperature of sampled air, Figure 64 clearly shows that d/D should be determined in a range of 0.238-0.357. Although a crossover point between the datasets of d/D = 0.238 and 0.357 around $V_{sampled,av}$/ $V_{free\text{-}stream}$ = 3.0 is presented in Figure 64, it is clearly shown in Figure 65 that d/D = 0.238 is the best in terms of pressure drop. If the dimensionless mean velocity at the sampling holes is approximately lower than 3.0 and a normalized pressure drop less than 20, equivalent to 0.5 inWC in this test, is acceptable, d/D = 0.357 can be a better choice for a sampler design in terms of accuracy.

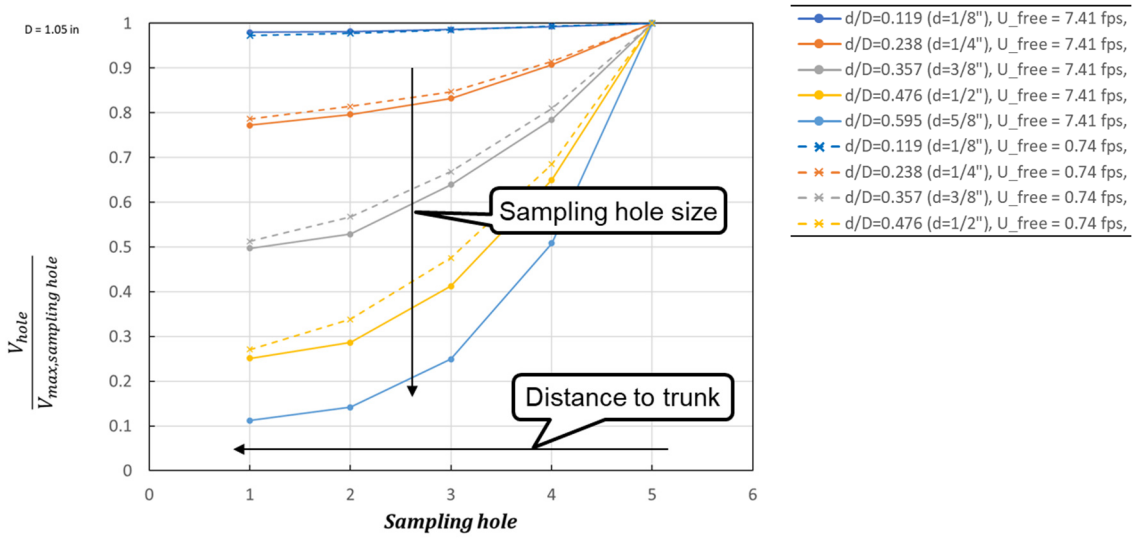

D: outer diameter of the branch
d: sampling hole diameter
U_{free}: velocity of freestream approaching the branch

$$V_{av,sampling\ hole} = \frac{\dot{m}_{total,sampling}}{\rho_{air} A_{total,sampling}}$$

$$A_{total,sampling} = N_{sampling\ hole}\left(\frac{\pi d^2}{4}\right)$$

* U_free = 7.41 fps for the air flowrate of 1000 CFM at the duct inlet
* U_free = 0.74 fps for the air flowrate of 100 CFM at the duct inlet

Figure 62 Velocity distributions at the sampling holes for different sampling hole diameters at free-stream velocity of 0.74 and 7.41 fps.

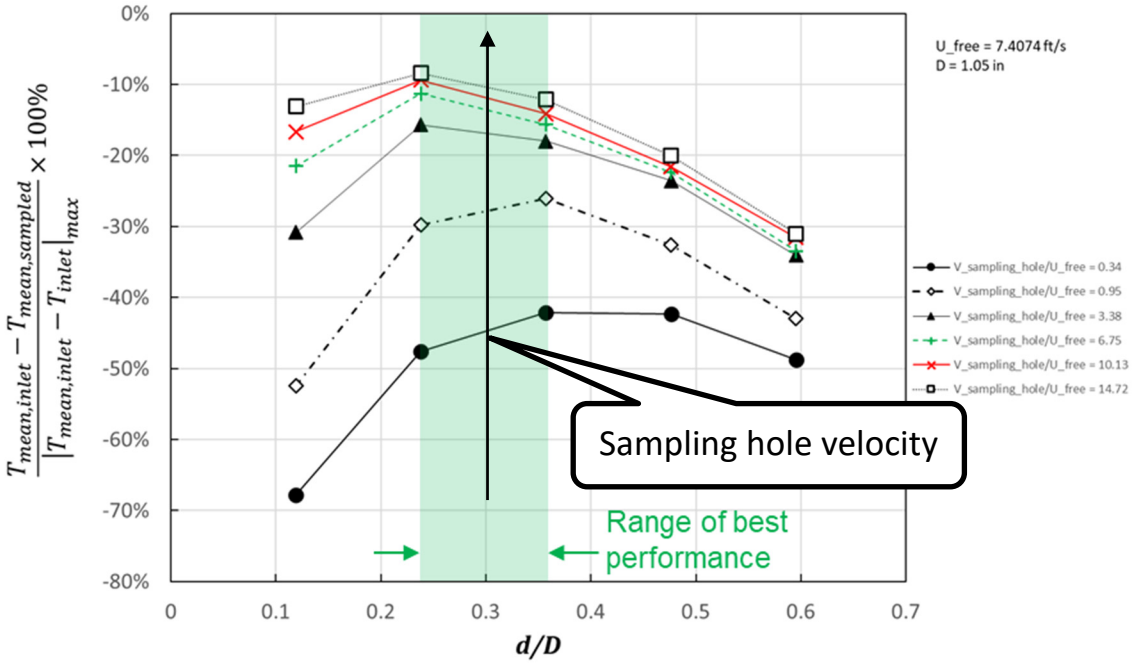

Figure 63 Variation of accuracy in measuring the mean air temperature for different sampling hole diameters under free stream flowrate of 1000 CFM (0.472 m^3/s) in an 18"x18" duct

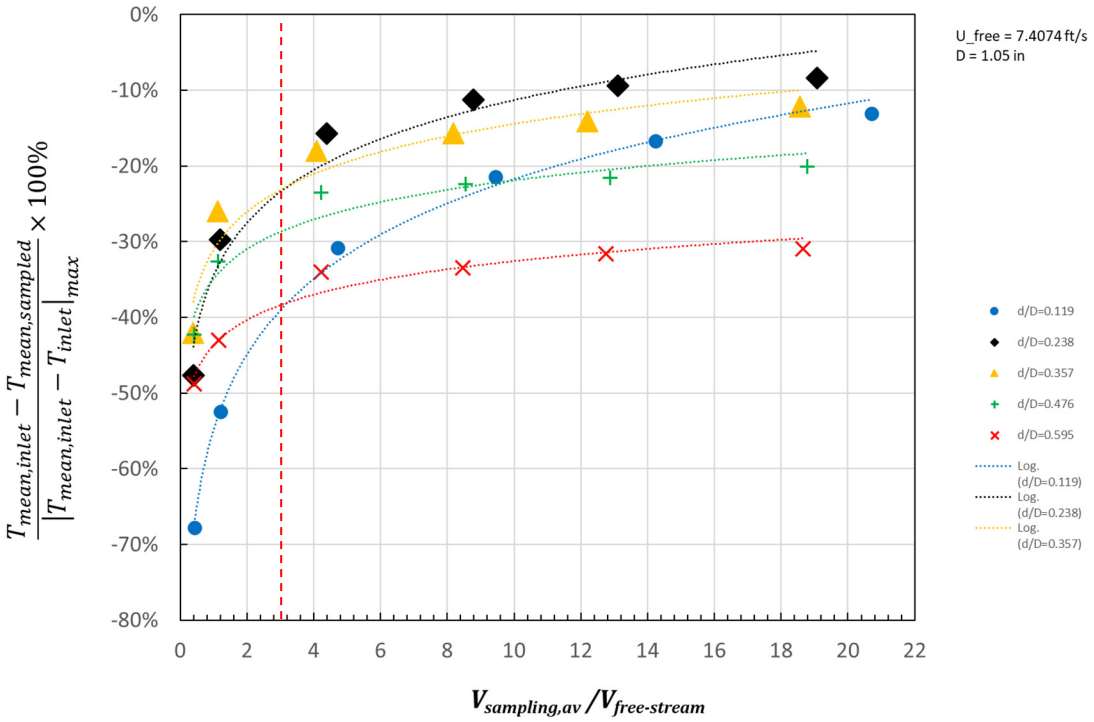

Figure 64 Variation of accuracy in measuring the mean air temperature for different average air velocities passing through the sampling holes under free stream flowrate of 1000 CFM (0.472 m^3/s) in an 18"x18" duct

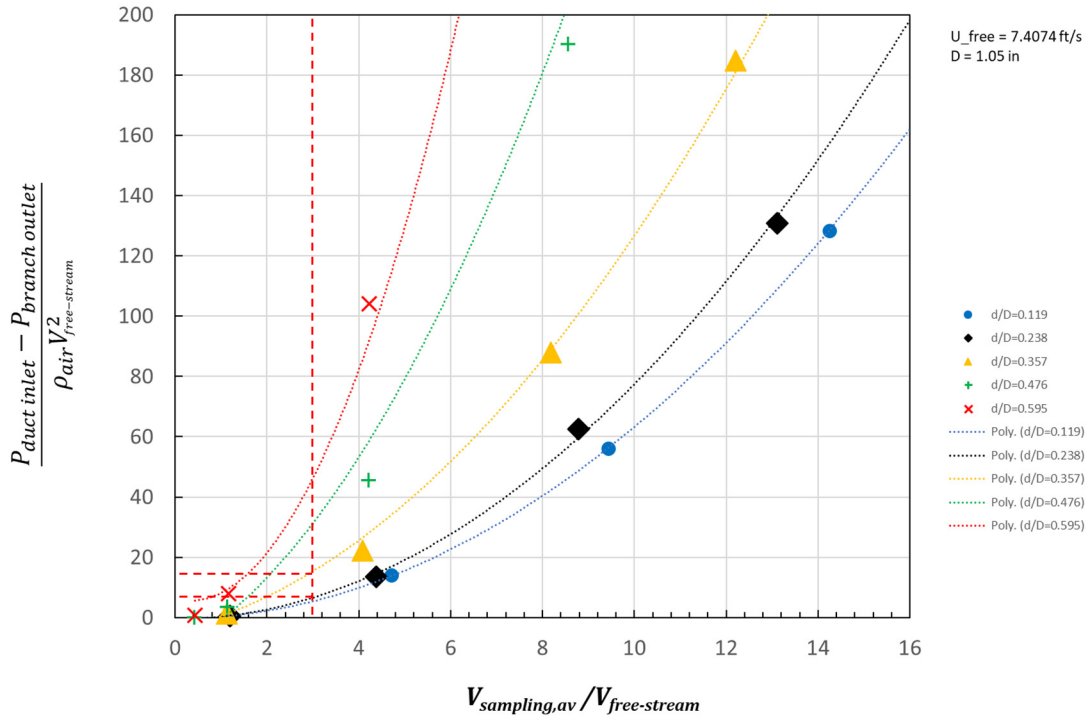

Figure 65 Pressure drop between the duct inlet and the sampler outlet for different average air velocities at the sampling holes when free stream in an 18"x18" duct flows at 1000 CFM (0.472 m^3/s)

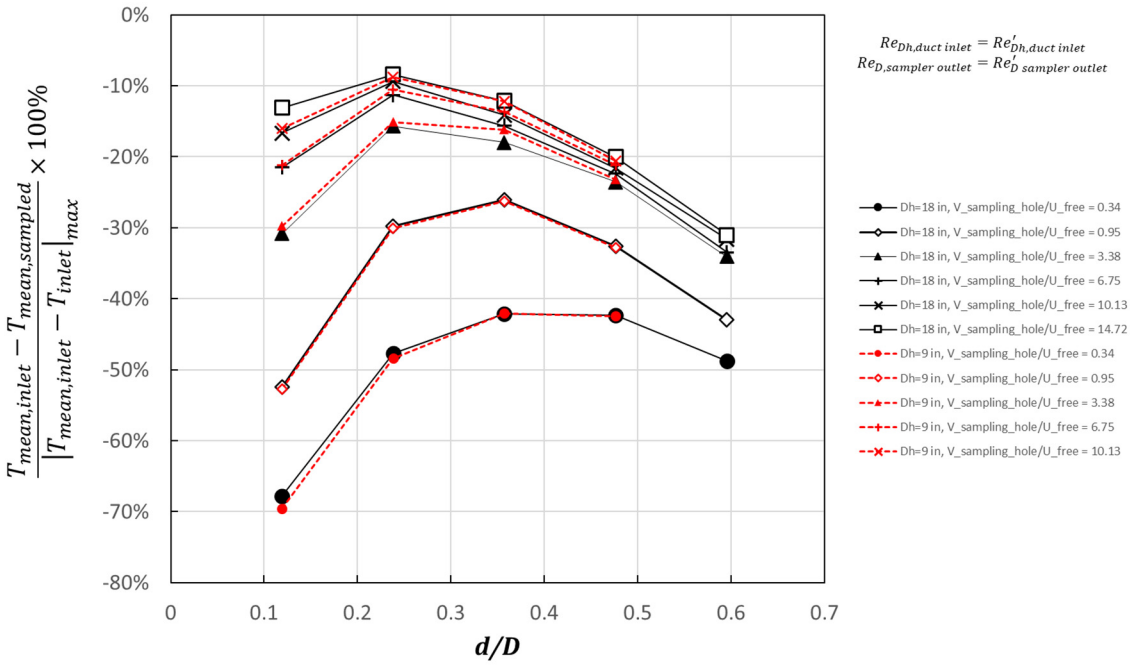

Figure 66 Validation of flow similarity for differently sized simulation domain

The similarity of airflow in the simulation domain was validated. For this test, the size of simulation domain reduced to half of the baseline domain so that the domain was composed of 9 inches x 9 inches duct and a sampler branch having a diameter, D, of 0.525 inch, and the simulation result was compared to that obtained from the baseline domain. The free-stream condition at duct inlet was defined to constant velocity profile and the free-stream velocity was determined based on the Reynolds number applied to the baseline case. The flowrate at the outlet of the sampler branch was also determined in the same manner. As shown in Figure 66, the results obtained from scaled down domain are, in general, in a good agreement to those from the baseline domain.

4.2.2.6. Sampling hole density

The determination of the optimal sampling hole density for uniform air sampling was investigated in this study. For the boundary condition of air at the duct inlet a user-defined function was utilized to generate a step-change temperature profile as illustrated in Figure 67. The number of sampling holes varied from 3 to 8 and the holes were equally spaced according to the number of holes, as outlined in Table 7. The diameter of the sampling holes remained constant at 3/8 inch or was varied linearly from the branch outlet side to the other end of the branch. The sizes and locations of the holes are shown in Table 8 and Figure 68, respectively.

The results obtained under various airflow conditions are presented in Figure 69. In general, variable hole diameters across the sampling holes led to more uniform air sampling over a constant hole diameter. It was also found that increasing the number of sampling holes does not necessarily improve the accuracy of measuring the bulk temperature of the airflow. In fact, it was observed that as the number of sampling holes increased, the increase in air influx at the sampling holes closer to the trunk (where the branch outlet is connected) was much larger than that at the sampling holes farther away from it due to pressure drop distribution. This led to a greater discrepancy between the temperature of the sampled air and the mean temperature of the airflow at the inlet.

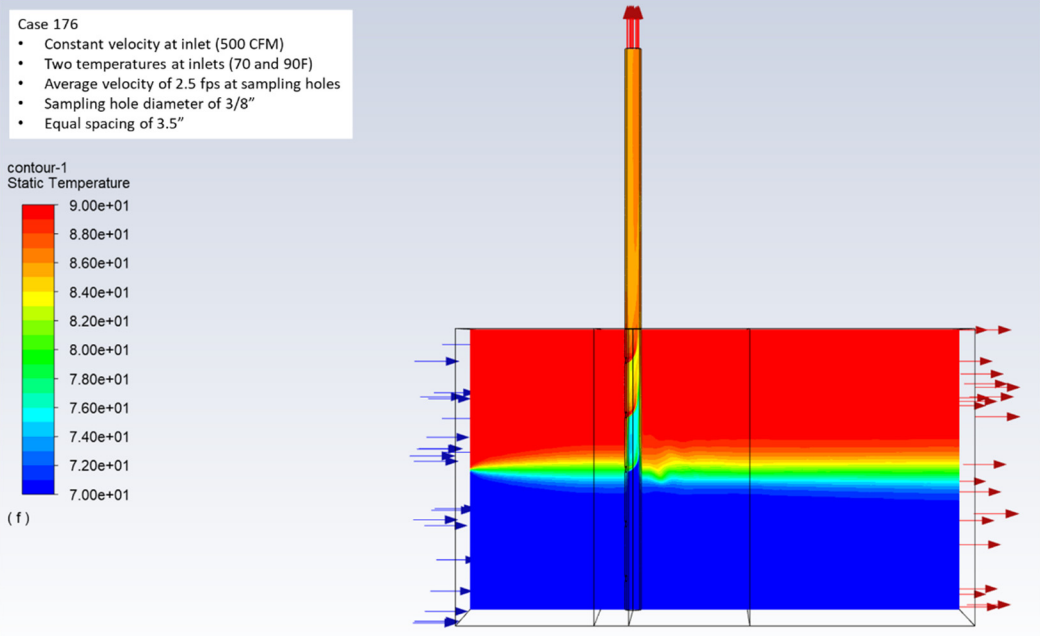

Figure 67 Baseline boundary conditions and temperature distribution in the domain

Table 7 Sampling hole configuration for a 3/8-Inch constant hole diameter: Number and spacing of sampling holes

No. of Sampling Holes	Spacing (inch)
3	7
4	4.67
5	3.5
6	2.8
7	2.33
8	2

Table 8 Sampling hole configuration for variable hole diameters: Number and size of sampling holes

No. of Sampling Holes	Variable Sampling Hole Diameter (inch)							
	hole 1	hole 2	hole 3	hole 4	hole 5	hole 6	hole 7	hole 8
3	1/2	3/8	1/4	-				
4	1/2	0.417	0.333	1/4	-			
5	1/2	0.438	3/8	0.313	1/4	-		
6	1/2	0.45	0.4	0.35	0.3	1/4	-	
7	1/2	0.458	0.417	3/8	0.333	0.292	1/4	-
8	1/2	0.464	0.429	0.393	0.357	0.321	0.286	1/4

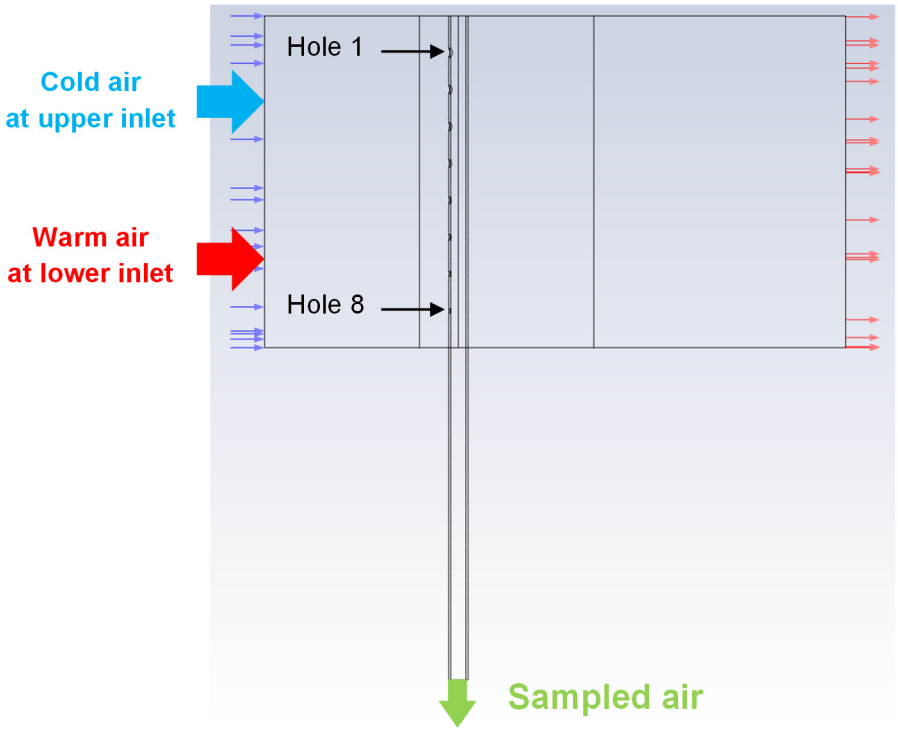

Figure 68 Sampling hole locations on the sampler branch for variable sampling hole sizes

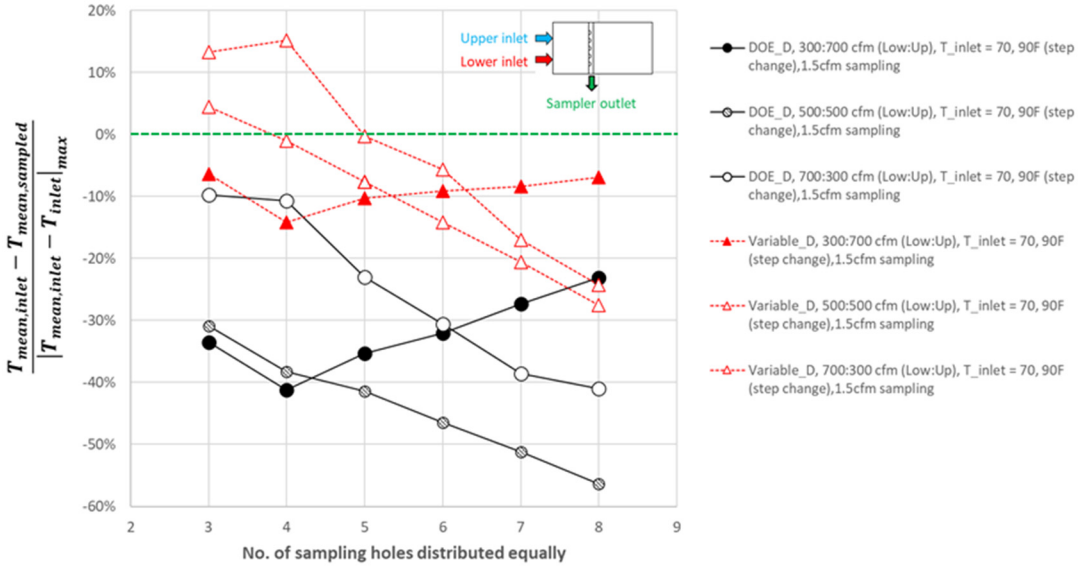

Figure 69 Effect of sampling hole density equally distributed on the accuracy of bulk temperature measurement.

When there is a wide distribution of temperature nonuniformity across the airflow, it may be more effective to increase the number of sampling holes to achieve a more accurate measurement of the bulk temperature. This is because a larger number of holes will allow for a more comprehensive sampling of the airflow, which can help compensate for the nonuniformity. However, it's important to note that increasing the number of sampling holes does not always guarantee better accuracy, as the location and spacing of the holes also play a crucial role in determining the effectiveness of the sampling method.

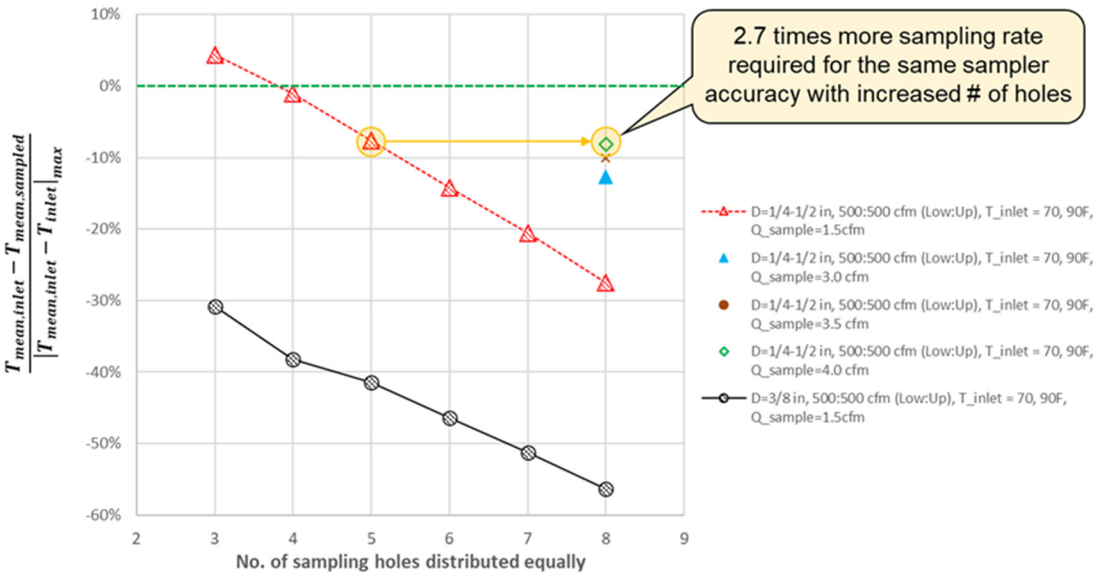

Figure 70 Effect of sampling hole density on mean temperature accuracy

Increasing the number of sampling holes also increases the required air sampling rate to maintain the same sampler accuracy as shown in Figure 70. In this test, it was decided to use five sampling holes on the baseline sampler, as the number of sampling holes required to meet the 10 CFR criteria, which mandates a minimum of six holes per square foot of sampled area, ranged from four to fifteen for the testing setup used in this study. As increasing the number of variable sampling holes from five to eight, the required flowrate for air sampling increases by a factor of 2.7 to maintain the same sampling accuracy. Therefore, while the determination of the number of sampling holes should generally follow the guidelines outlined in 10 CFR regulations (DOE, 2017), increasing the number

of sampling holes can be a helpful strategy in cases where there is significant nonuniformity in the airflow. This approach involves balancing the increase in sampling holes with a corresponding increase in sampling rate, and can lead to more accurate measurements of the air properties.

Figure 71 illustrates the distribution of air influx across the sampling holes. It is evident from the figure that as the hole density increases, the air influx becomes more uniform. The mass flow-weighted average temperatures of air at the sampling holes were calculated using Equation (6) for five, seven, and eight sampling holes on the sampler branch. These average temperatures were compared to the average temperatures measured at the sampler branch outlet, and the results are presented in Table 9. The variation of mass flow-weighted average temperature at the sampling holes reveals that for the highest sampling hole density, the average temperature of the air entering the sampling holes was closest to the average temperature at the inlet of the duct. However, the average temperature at the sampler outlet was higher than that at the sampling holes. In this CFD study, conduction and radiation heat transfer on the sampler surface was also taken into account. Therefore, the sampled air undergoes heat transfer on the sampler's inner wall, where energy interaction with duct flow occurs through the sampler wall thickness, resulting in an increased temperature of the sampled air at the sampler outlet. Figure 70 shows that having fewer sampling holes than the number required by the 10 CFR criteria may result in better sampler accuracy. However, estimating the amount of heat loss or gain that the sampled air experiences due to contact with the sampler's inner wall is challenging. Therefore, to achieve the expected sampler accuracy, it is recommended to increase the number of sampling holes to achieve more even air sampling across the holes while minimizing heat transfer through the sampler material.

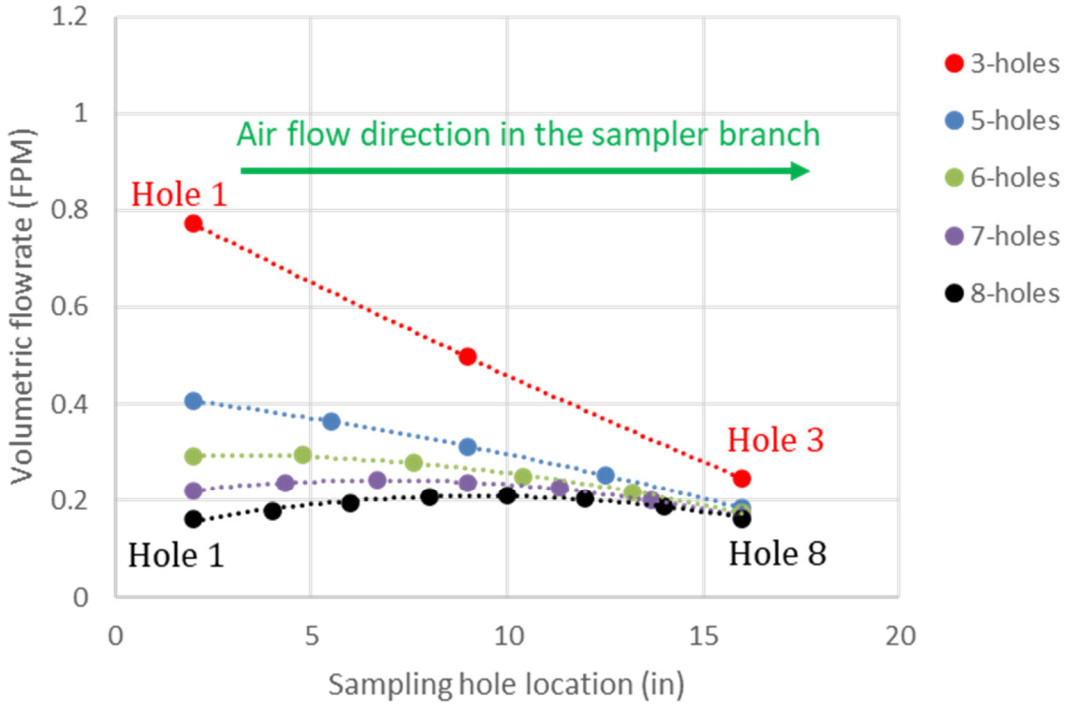

Figure 71 Effect of sampling hole density on the distribution of air influx across the sampling holes for variable sampling hole diameter, D=1/2-1/4 in, and uniform velocity distribution in the duct at a total flowrate of 1,000 CFM

Table 9 Comparison of the average temperatures between sampling holes and sampler outlet for different numbers of sampling holes

Temp (F)	5-holes	7-holes	8-holes
$T_{mean,in}$	80.0	80	80.0
$T_{av,\ sampling\ hole}$	77.5	79.0	79.9
$T_{av,\ sampler\ outlet}$	80.8	82.1	82.8

4.3. Experimental Study

4.3.1. Experimental Setup for Air Sampling Devices

Experimental tests were conducted on air sampling devices to validate the CFD results qualitatively. The experimental setup was modified from the mixer testing setup and is illustrated

(a)

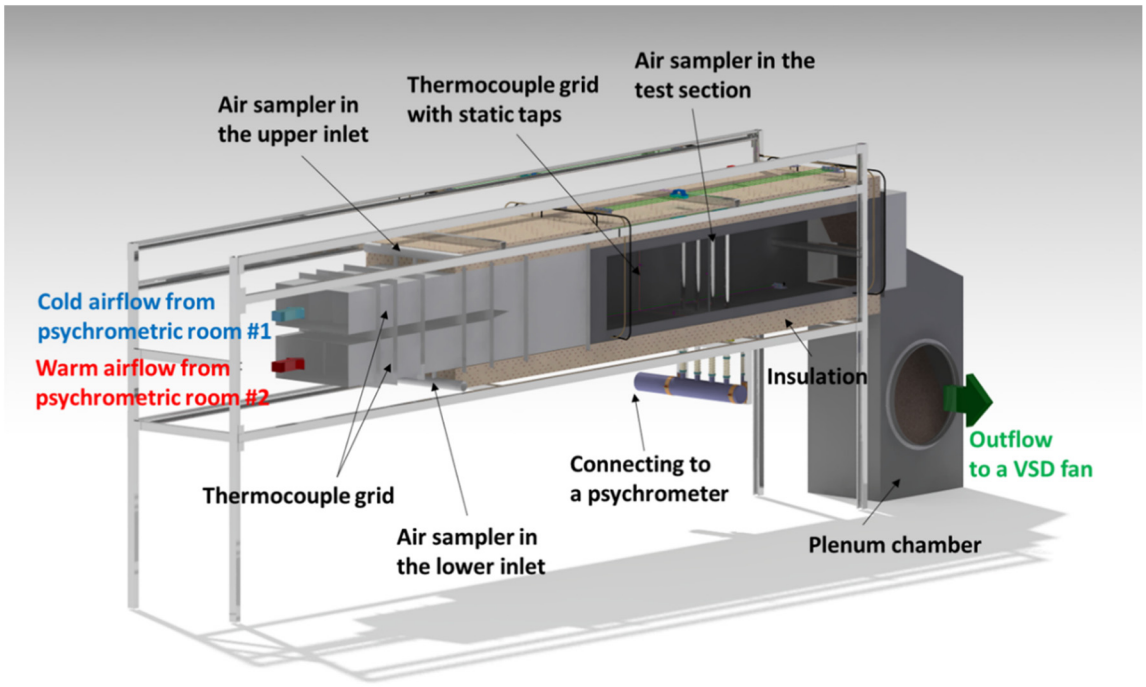

(b)

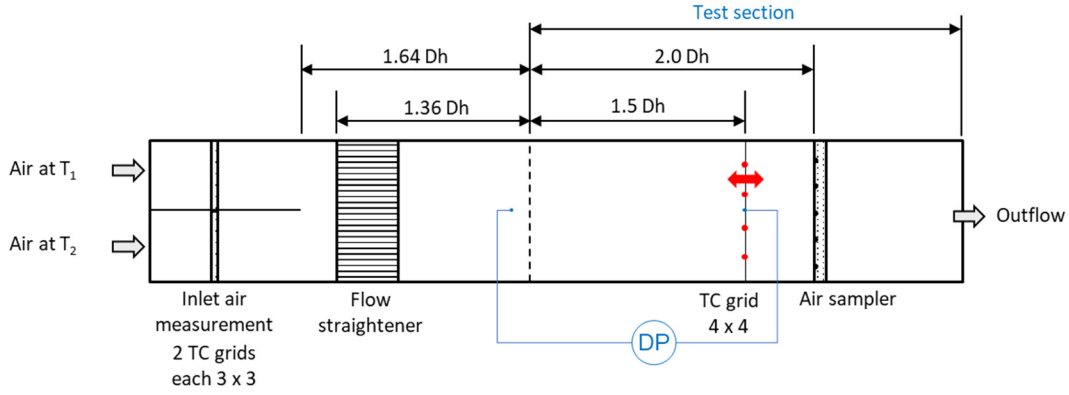

Figure 72 Experimental setup for air sampling devices: (a) 3D CAD model and (b) Schematic diagram.

in Figure 72. Like the mixer testing, two inlets were used to supply air from two psychrometric rooms with different temperatures. Two thermocouple grids, each consisting of 3 by 3 thermocouples for each inlet, were employed to measure the mean temperature of the inlet air. A flow straightener was placed after the inlet region to prevent the inherent mixing of airflow before

(a)

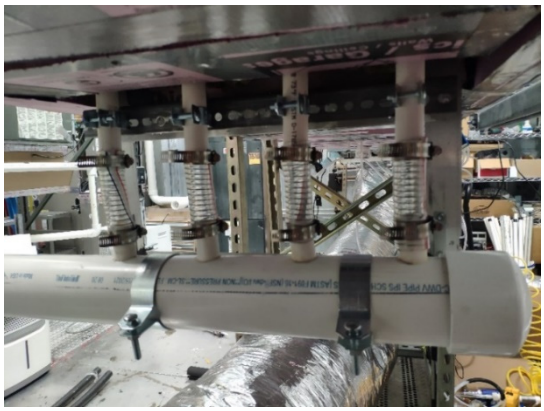

(b)

(c)

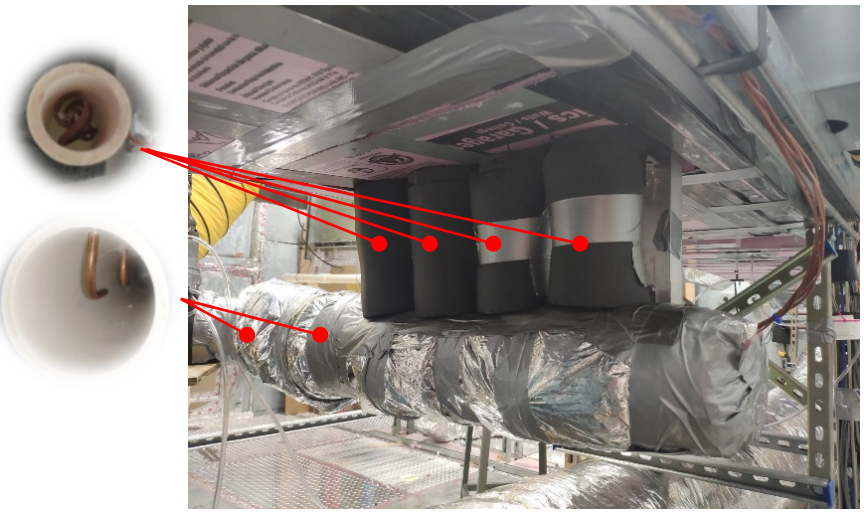

(d)

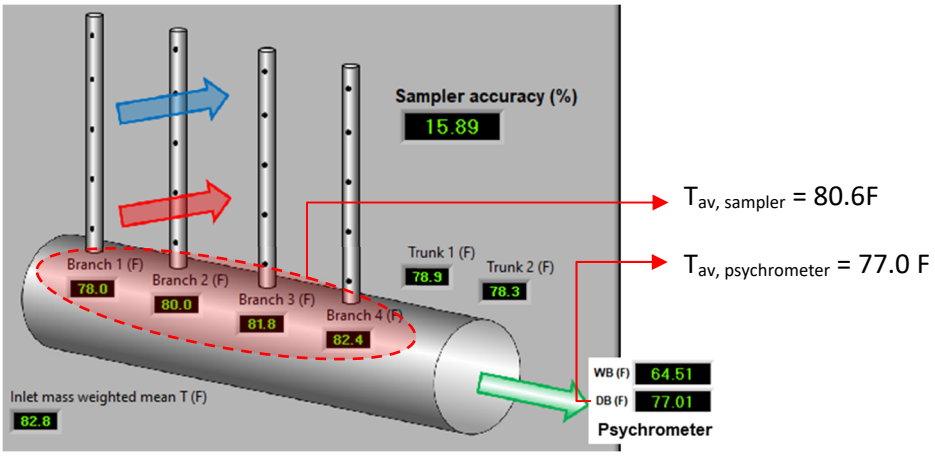

Figure 73 Instrumentation for air sampling device: (a) Branch-replaceable sampler, (b) Sampler installation, (c) Thermocouple locations, and (d) Temperature variation in the sampling device.

entering the test section. In the test section, all mixing devices were removed, and the 4 by 4 thermocouple grid and the air sampler were placed at distances of 1.5 D_h and 2.0 D_h, respectively, from the original location of the air mixing devices, considering the maximum mixing length in case any air mixing devices were used.

Figure 73 depicts the air sampling devices used. The branch tubes of the air sampler were designed to be replaceable for testing various types of air sampling tubes. The branch tubes of the sampler, made of 1-inch PVC pipes, pass through the ductwork where the mainstream flows, and their outlets exposed to the outside of the ductwork are connected to the trunk, a 3-inch PVC pipe, using flex hose, allowing for easy replacement with another type of candidate branch tubes, as shown in Figure 73(a) and (b). To monitor the temperature variation of the sampled air, multiple temperature sensors were installed in the air sampler, and the locations of the sensor installation are indicated in Figure 73(c). The addition of sensors and adequately thick insulation on the part of the air sampler exposed to the environment allowed for accurate estimation of the performance of sampler branch designs with negligible environmental effect such as heat gains or losses. The dry bulb temperature of the sampled air measured in the psychrometers showed fairly difference to the average temperature on the 6 by 6 thermocouples grid installed prior to the sampler as shown in Figure 73(d) due to heat loss while the sampled air travels along the sampler inside despite thick insulation (two insulation layers consisting of 3/8 inch-thick DPDM with a thermal conductivity of 0.25 W/m·K, and insulated polyester flexible duct with R value of 6.0). Therefore, rating the sampler performance in measuring the bulk temperature was done by comparing the sampled air temperature at the sampler branch outlet to the mass flow weighted mean temperature of the air at the inlet of the test section.

The branch tubes of the sampling device were designed while considering various geometric parameters, such as sampling hole size, pitch, and sampler material. The shapes and dimensions of the potential sampler branch tubes are shown in Figure 74(a). 3/8 inch pipes with the outer diameter

(a)

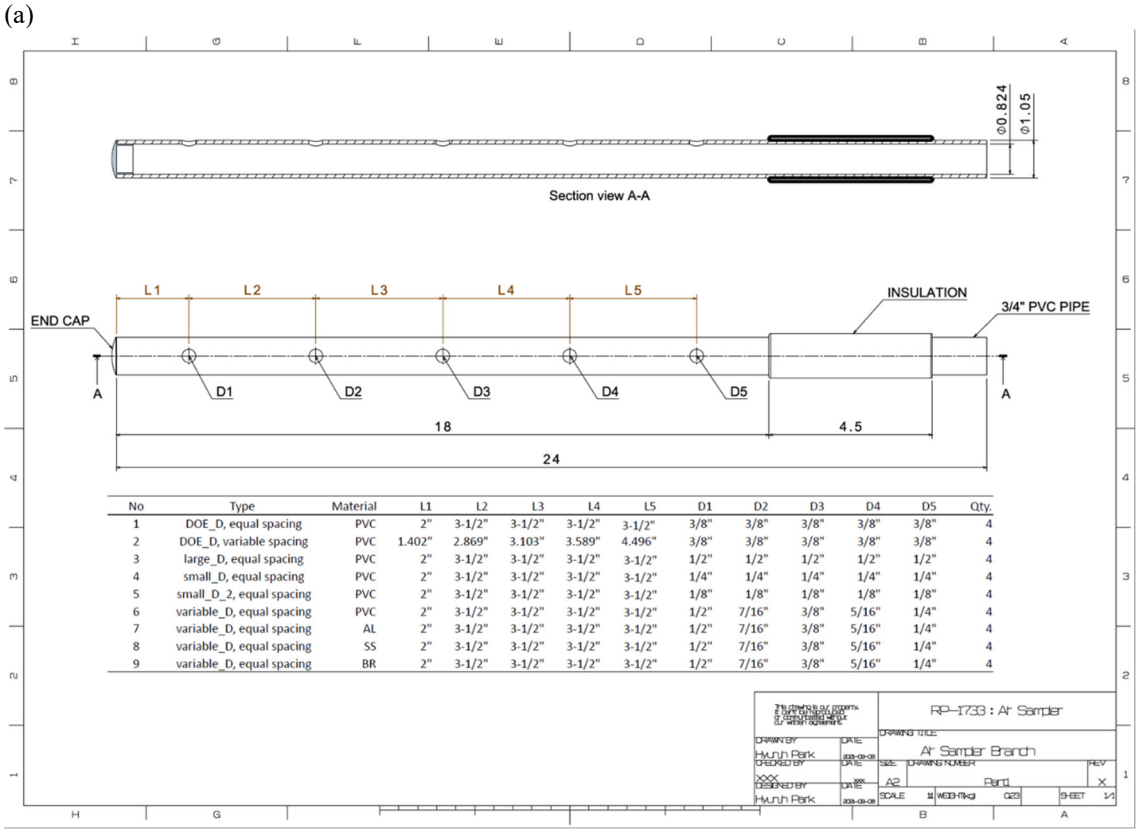

No	Type	Material	L1	L2	L3	L4	L5	D1	D2	D3	D4	D5	Qty.
1	DOE_D, equal spacing	PVC	2"	3-1/2"	3-1/2"	3-1/2"	3-1/2"	3/8"	3/8"	3/8"	3/8"	3/8"	4
2	DOE_D, variable spacing	PVC	1.402"	2.869"	3.103"	3.589"	4.496"	3/8"	3/8"	3/8"	3/8"	3/8"	4
3	large_D, equal spacing	PVC	2"	3-1/2"	3-1/2"	3-1/2"	3-1/2"	1/2"	1/2"	1/2"	1/2"	1/2"	4
4	small_D, equal spacing	PVC	2"	3-1/2"	3-1/2"	3-1/2"	3-1/2"	1/4"	1/4"	1/4"	1/4"	1/4"	4
5	small_D_2, equal spacing	PVC	2"	3-1/2"	3-1/2"	3-1/2"	3-1/2"	1/8"	1/8"	1/8"	1/8"	1/8"	4
6	variable_D, equal spacing	PVC	2"	3-1/2"	3-1/2"	3-1/2"	3-1/2"	1/2"	7/16"	3/8"	5/16"	1/4"	4
7	variable_D, equal spacing	AL	2"	3-1/2"	3-1/2"	3-1/2"	3-1/2"	1/2"	7/16"	3/8"	5/16"	1/4"	4
8	variable_D, equal spacing	SS	2"	3-1/2"	3-1/2"	3-1/2"	3-1/2"	1/2"	7/16"	3/8"	5/16"	1/4"	4
9	variable_D, equal spacing	BR	2"	3-1/2"	3-1/2"	3-1/2"	3-1/2"	1/2"	7/16"	3/8"	5/16"	1/4"	4

(b)

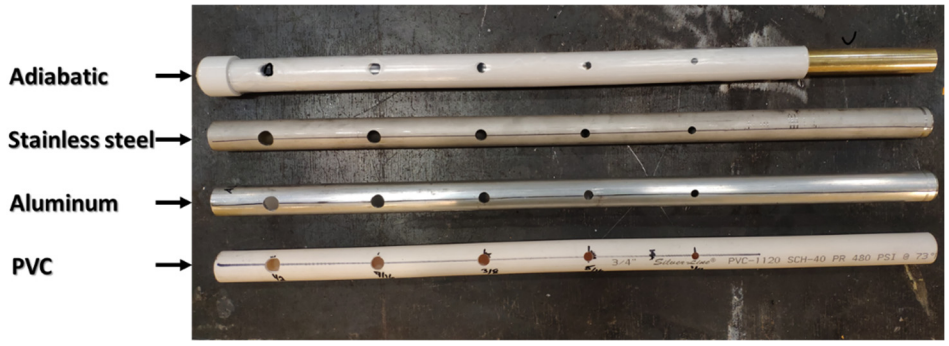

Figure 74 Candidate sampler branch tubes: (a) Drawing for various sampling hole sizes, pitches, and materials to be tested, and (b) Branches fabricated in accordance with the design.

of 1.05 inches (26.67 mm) and the inner diameter of 0.804 inch (20.42 mm) were chosen for sampler branch design. A sampling hole size of 3/8 inch (9.525 mm) was chosen as the baseline, based on DOE 10 CFR criteria (DOE, 2017). For testing purposes, larger and smaller hole sizes of 1/2 and 1/4 inch (12.7 and 6.35 mm), respectively, were selected, along with a variable hole size ranging from 1/2 to 1/4 inch. Both constant and variable spacing were considered for the sampling

hole pitch. To determine how conduction and radiation heat transfer through different sampler materials influence the mean temperature of sampled air, PVC (thermal conductivity of 0.147 W/m·K), stainless steel (thermal conductivity of 14.924 W/m·K), aluminum (thermal conductivity of 202.4 W/m·K), and adiabatic tubes were employed. The candidate sampler branch tubes that were fabricated are shown in Figure 74(b). Adiabatic sampler branch tubes were made of brass tubes wrapped with 0.08-inch-thick (2.0 mm) aerogel insulation tape (thermal conductivity of 0.04 W/m·K) and 0.045-inch-thick (1.1 mm) heat shrink tubing.

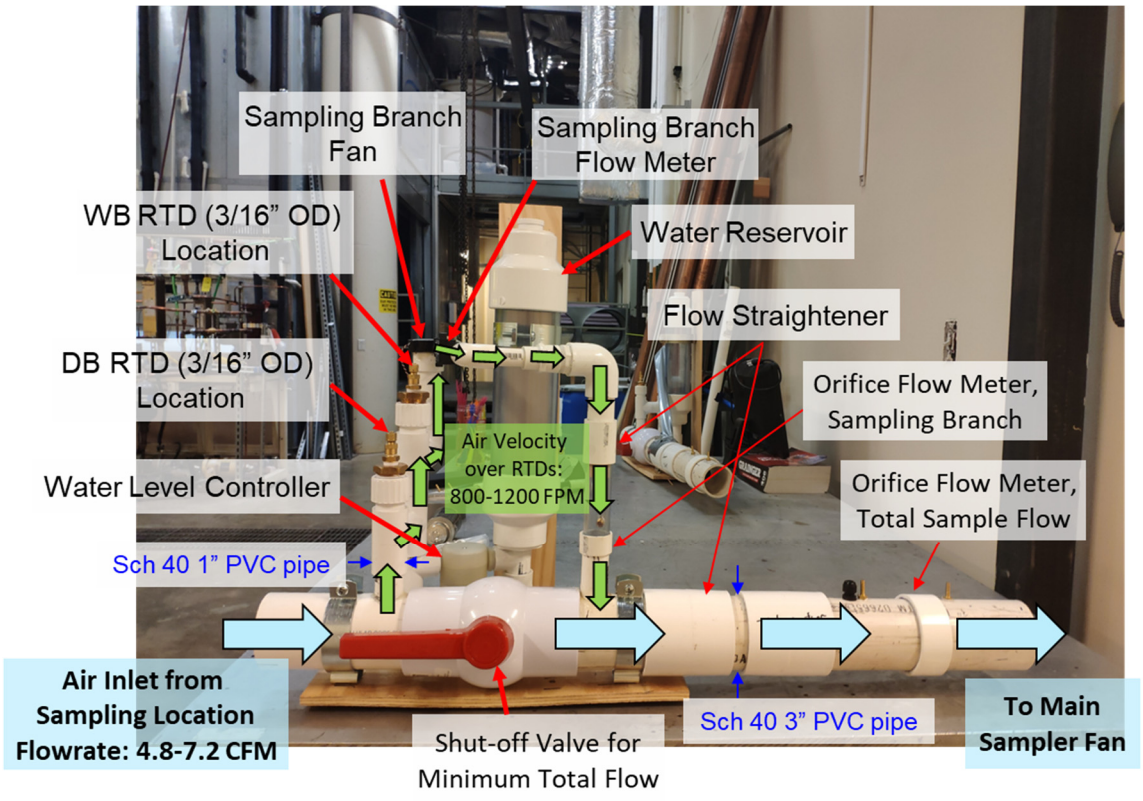

Figure 75 Progress and system overview of bypass psychrometer

The process of establishing the experimental set-up for air sampler testing involved developing a psychrometer based on a bypass design. This type of psychrometer enables coverage of a wide range of sampled air flow rates to identify the optimal air velocity at the sampling holes for achieving good accuracy with the air sampler. The psychrometer designed for this purpose is shown in Figure 75.

The airflow from the air sampler is first adjusted by the variable speed drive fan (VSD fan), and its flow rate is measured using an orifice flow meter installed inside the flow passage. Then, a part of the air stream is bypassed to the sampling branch of the psychrometer using the sampling branch fan. The flow rate of the bypassed air is adjusted by the shut-off valve installed on the main flow pipe to ensure reasonable accuracy in measuring wet bulb temperature on the RTD sensor. According to 10 CFR (DOE, 2017) criteria, the minimum velocity of air blowing across the temperature sensors is 1,000±200 ft/min (5.08±1.02 m/s). The adjustment of bypass flow in the psychrometer enables the minimum velocity requirement for wet bulb temperature measurement to be met.

4.3.2. Data Reduction

The mass flow-weighted method for determining the average (bulk or true mean) air condition, as introduced in the literature review and expressed in equation (6), was adapted to measure the mean temperature of the airflow at the inlet. This mean temperature was then used to evaluate normalized sampler bias in measuring the average temperature of the airflow. The formulations for determining the inlet mean temperature and rating the sampler accuracy are presented below:

$$T_{mean,\,inlet} = \frac{(T\rho\dot{V})_{in,low}+(T\rho\dot{V})_{in,up}}{(\rho\dot{V})_{in,low}+(\rho\dot{V})_{in,up}}, \tag{10}$$

$$Normalized\ Sampler\ Bias = \frac{T_{mean,\,inlet} - T_{sampled}}{\left|T_{mean,\,inlet} - T_{inlet}\right|_{max}} \tag{11}$$

where:

T_{in}	Inlet temperature, average temperature measured by thermocouple grid installed in each inlet
ρ	Density of moist air determined by T_{in}, absolute pressure, and humidity ratio
$\dot{V}$	Volumetric flowrate measured using a thermal dispersion airflow meter
$T_{sampled}$	Average of temperatures measured using thermocouples installed in the sampler branch outlets OR average of 4 x 4 TC grid if indicated in figure legend

It should be noted that the closer the sampler accuracy rating is to 0, the higher the measurement accuracy of the sampler.

4.3.3. Discussion of Results

Experimental air sampler testing was carried out to validate the results of the numerical study. The comparison between the experimental results and the CFD results for the effect of sampling hole type on the sampler performance is shown in Figure 76 and 77.

(a)

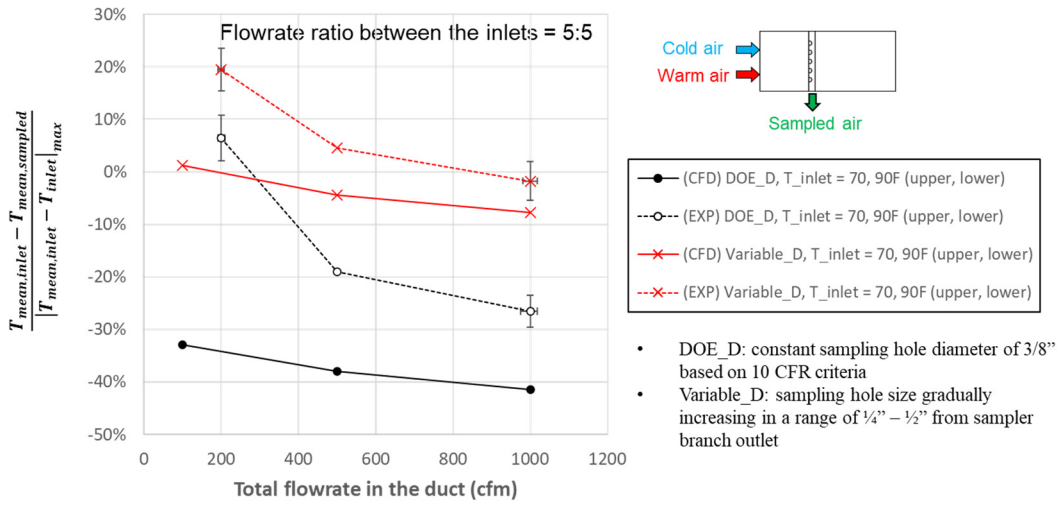

(b)

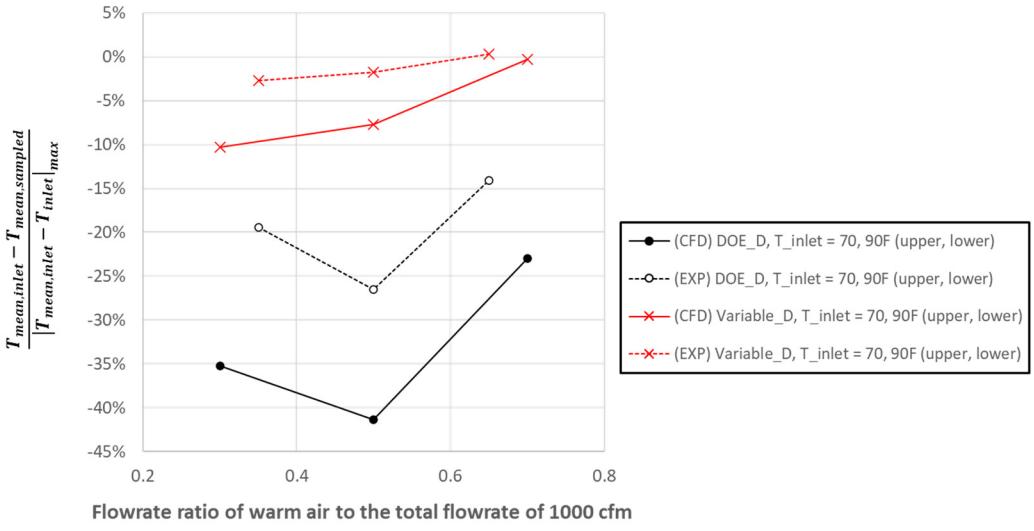

Figure 76 Comparison of the experimental results to CFD: Effect of sampling hole type on the sampler performance for (a) different total flowrate and (b) flowrate ratio at the duct inlet

The experimental results demonstrate a similar trend compared to the CFD results. Overall, both results show that an air sampler with a variable sampling hole size has better performance in accurately measuring the average air temperature, as shown in Figure 76(a). Moreover, both results indicate that sampler accuracy depends on the velocity of the airflow approaching the sampler. Therefore, it is essential to account for the sampling rate accordingly. The results also suggest that variable sampling hole size is beneficial for unknown velocity maldistribution since it allows the sampler performance to be less affected by velocity nonuniformity, as shown in Figure 76(b).

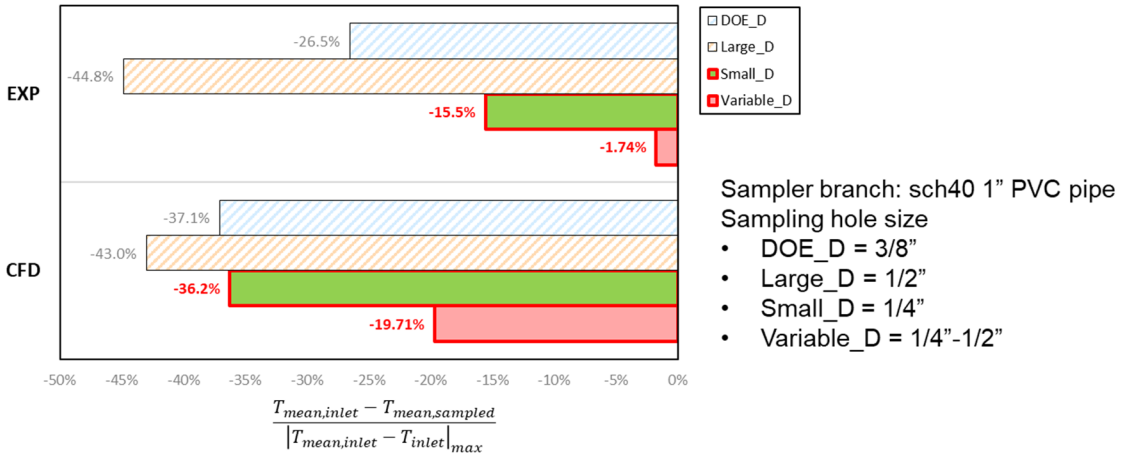

Figure 77 Comparison of the experimental results to CFD: Effect of sampling hole size on the sampler performance

Figure 77 presents the comparison between experimental and CFD results for all the sampling hole sizes tested under the same testing condition. The flowrate ratio between the duct inlets was set to be identical for a combined total flowrate of 1,000 CFM (0.472 m^3/s corresponding to a flow velocity of 444.4 FPM (2.26 m/s)). The temperatures at the upper and lower inlet of the ductwork were 70°F and 90°F (21.1 and 32.2°C), respectively. The only difference between the CFD boundary condition and the experimental setting was the sampling rate. In the experiment, the sampling rate was adjusted to achieve an average sampling rate of 1.5 CFM (0.042 m^3/s) per branch tube, while in CFD, the sampling rate varied based on the sampling hole size due to the boundary condition at the branch tube outlet being set to ambient pressure of 0 PSIG (0 kPa). Thus, the sampling rate depended on the pressure drop caused by different sampling hole sizes. As the

sampling hole size decreases, the pressure gradient within the sampler increases, which reduces the air sampling rate. Therefore, according to CFD results, as the sampling hole size decreases, the sampler's accuracy decreases significantly due to the reduced sampling rate compared to the experimental results obtained at a fixed sampling rate.

The results from both the experiment and CFD indicate that the variable sampling hole size is the most preferable, followed by the small sampling hole size, as it allows for more uniform air intake through the sampling holes by reducing the pressure gradient along the sampler branch tube.

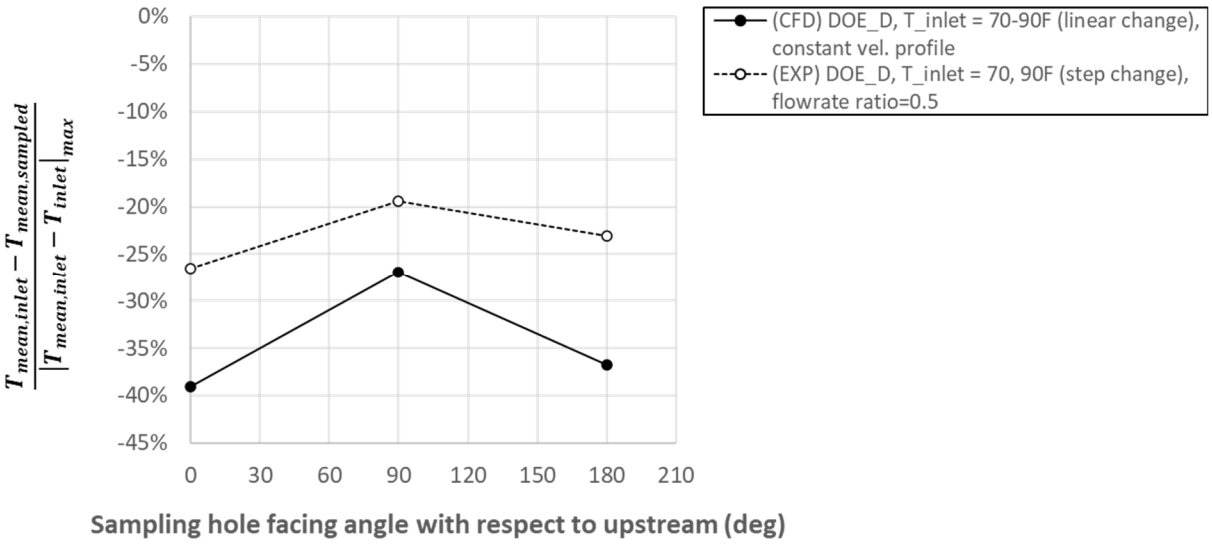

Figure 78 Comparison of the experimental results to CFD: Effect of sampling hole facing angle on the sampler performance

Figure 78 shows the effect of sampling hole facing angle on the sampler performance. Sampling hole facing angles to upstream flow are illustrated in Figure 58. The experimental result showed a trend that is consistent with the characteristic trend of the CFD result that indicates better accuracy with sampling hole facing perpendicular to the upstream without the influence of upstream stagnation and downstream wake.

The effect of sampler material on sampler performance was also observed experimentally, and the result was compared to the CFD result as shown in Figure 79. The experimental result was found

to be somewhat different from the CFD result. Specifically, stainless steel was found to perform slightly better than aluminum as an air sampler material for a flowrate ratio of 0.5 in CFD simulations, which differed from the experimental result. However, this possible discrepancy could be attributed to measurement uncertainty resulting from relatively large fluctuations in temperature measurement and flowrate control. Nonetheless, both the experimental and CFD results suggest that PVC pipe samplers outperform metallic sampler branch tubes.

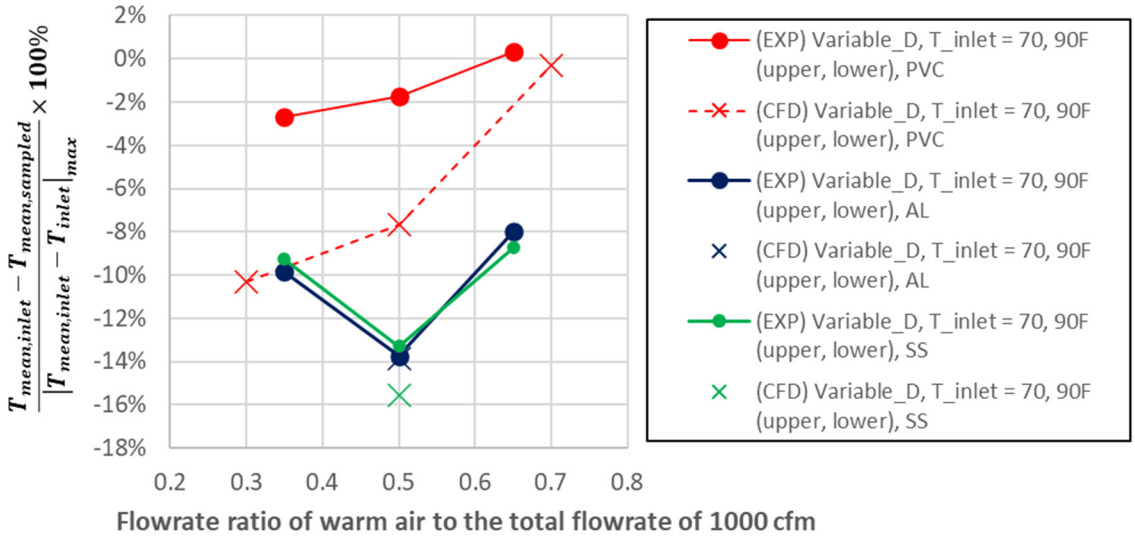

Figure 79 Comparison of the experimental results to CFD: Effect of sampler materials on sampler performance

Overall, the experimental results showed a trend similar to that of the CFD results. Despite the difference in magnitude, it can be concluded that the CFD model was qualitatively validated by comparing its results to the experimental results. This is because both the experimental and CFD results agree well in terms of their characteristic features. Possible causes for the discrepancy in magnitude include:

1. The CFD assumed perfectly uniform inlet velocity and temperature distribution, which may not have been the case in the experiment.

2. The CFD model assumed adiabatic wall boundary conditions and no thermal interaction

between the inlets. In contrast, heat loss occurred in the experiment, which could affect the temperature distributions in the inlet region.

3. Measurement errors may have occurred, and these errors from various measurement devices could have contributed to a large change in the final parameter.

4. The CFD geometry was a simplified version of the testing setup, resulting in differences in flow channel shape, sampler design, sampler orientation, and dimensional precision.

5. Additionally, the metric used to rate sampler performance is significantly sensitive to even small temperature differences.

The investigation also looked into the effectiveness of using an air mixer on the performance of an air sampler. The testing was conducted under specific conditions, including upper and lower inlet temperatures of 70°F and 90°F (21.1 and 32.2°C), a total flow rate of 1,000 CFM (0.472 m^3/s), and a sampling rate per branch tube of 1.5 CFM (0.0007 m^3/s). A single orthogonal pattern louver mixer with a 4 by 4 louver array and a louver angle of 60° was employed for the testing. Various flow rate ratios between the inlets were used, ranging from 0.35 to 0.65, to adjust the velocity nonuniformity upstream of the sampler. The difference between the average temperatures at the inlet and in the test section was measured. The 4 by 4 TC grid and the air sampler were both used to measure the average temperature in the test section for comparison purposes, the result is shown in Figure 80.

As the results show, without an air mixer in the test section, the performance of the air sampler varies greatly depending on upstream conditions, while the average temperature measured by the TC grid remains relatively consistent. However, with the use of an air mixer, the accuracy of measuring the true mean temperature based on the inlet mean temperature and the consistency of measurement accuracy are significantly improved. Therefore, the test results indicate that the use

of an air mixer contributes to maintaining the performance of the air sampler consistently, even with changes in upstream conditions. Figure 81 illustrates the temperature distributions prior to the sampler with and without an air mixer. The figure clearly shows that the air mixer works to reduce nonuniformities in airflow, resulting in more accurate bulk temperature measurement, and the air sampler performance is less affected by upstream conditions. Additionally, the results suggest that the use of a TC grid may be better than an air sampler in measuring the average dry bulb temperature of airflow in psychrometric testing in terms of measurement accuracy and consistency.

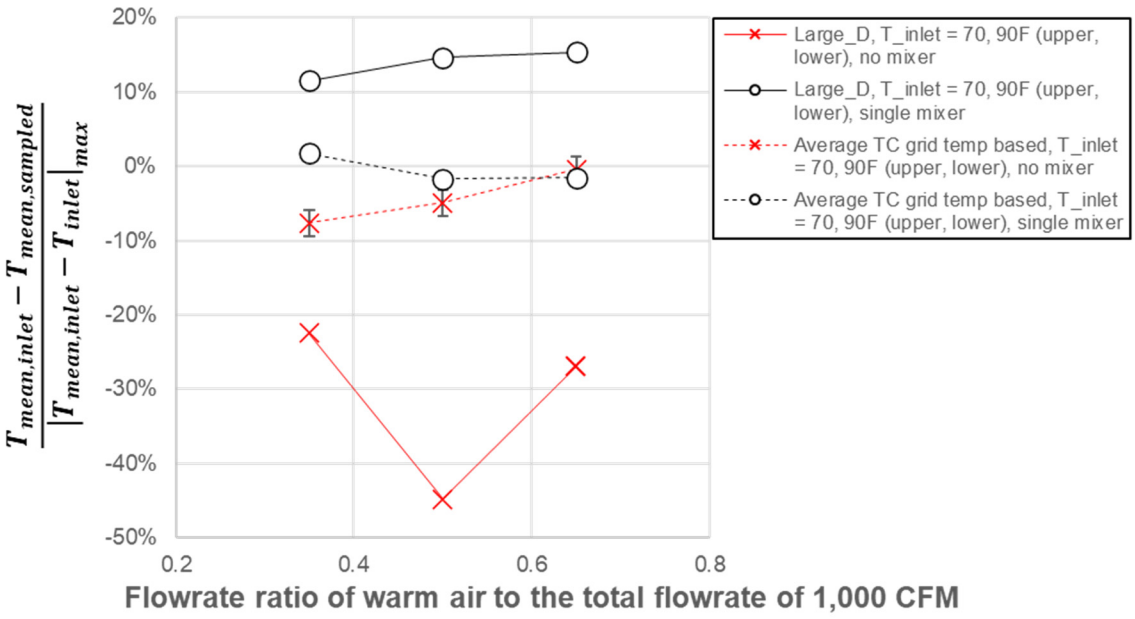

Figure 80 Effect of air mixer use on sampler performance

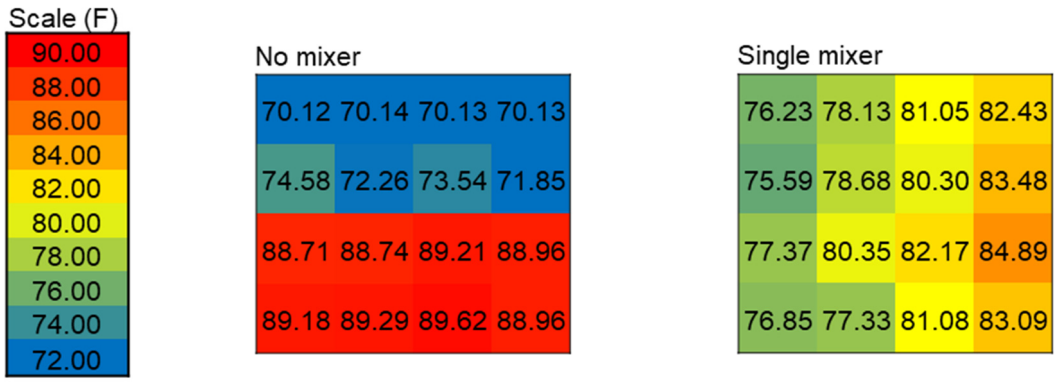

Figure 81 Temperature distribution prior to the air sampler

4.4. Conclusions

An investigation was carried out to assess the performance of air sampling devices using both numerical and experimental approaches. The study aimed to evaluate the impact of representative design parameters on the accuracy of the air sampler under various testing conditions. The design parameters considered in the study included sampling hole type, pitch, orientation, size, density, and sampler material, while the baseline sampler design was established based on the 10 CFR Criteria (DOE, 2017). Regarding the operating conditions, various shapes of velocity and temperature profiles for the upstream airflow were selected and used as the inlet boundary conditions in the CFD study. Similarly, maldistributed temperature and velocity conditions were created and utilized in the experimental testing.

The CFD study on air sampling devices investigated the influence of geometrical parameters on their performance in terms of pressure distribution of airflow in the branch of an air sampler and the accuracy of mass-weighted mean temperature at its outlet. The results showed that, depending on the pressure distribution formed inside air sampler branches, the mass of air influx could not be uniform between the sampling holes, which could lead to reverse flow in extreme cases. Such pressure maldistribution could be relieved by adjusting the sampling hole size. Gradually reducing the size of the sampling hole from the outlet to the opposite end plugged could adjust the amount of pressure drop caused when external air passes through the sampling hole and reduce the deviation of pressure dispersed according to the airflow direction in the sampling hole. Sampling hole spacing can also influence the uniformity of air influx across sampling holes. Variable hole spacing, in general, helps to sample air more uniformly across the holes, but the improvement is not significant. In the investigation of the effect of conduction heat transfer through the sampler wall, aluminum and PVC were found to be helpful in obtaining a mean temperature of sampled air closer to the bulk temperature of free stream, compared to other stainless steel, but which one between aluminum and PVC performs better can be determined depending on the design of the

sampling hole and the condition of the upstream airflow. Other sampler design variables were also investigated, and the findings are briefly summarized as follows:

- Adjusting the sampling hole size to gradually decrease from the sampler branch outlet is required to compensate for the discrepancy in pressure drop between sampling holes.
- A ratio of sampling hole diameter to sampler branch diameter (d/D) of 0.238-0.357 is recommended for equal-sized sampling holes.
- Adjusting the sampling hole spacing according to the velocity profile of free stream approaching the sampler can help to sample air uniformly across the holes if the flow pattern of the air stream outside the sampler is known.
- Aluminum and PVC are recommended as the sampler material.
- The effect of radiation heat transfer on the mean temperature of sampled air was found from the result of testing at total flowrate of 1000 CFM to be negligibly small.
- No general rule that works for all velocity distributions employed in the test was found on how to place sampling holes with respect to the direction of free stream. However, when the velocity maldistribution was minimized using an air mixer, sampling holes oriented orthogonal to the duct flow direction significantly improved sampler accuracy.
- More sampling holes do not guarantee more accurate measurement of bulk air condition. Sampling holes biased toward the sampler branch outlet could be helpful in sampling air uniformly from a cross-section of a duct.

To validate the results of a numerical study on air sampler performance, an experimental study was conducted simultaneously. In order to maintain consistency in the testing conditions, additional cases were chosen that could be tested both numerically and experimentally. While there was a

significant difference in the magnitude of sampler accuracy between the experimental and CFD results, both exhibited similar trends in terms of characteristic features. This led to the conclusion that the CFD results were qualitatively validated.

The investigation also examined whether the use of an air mixer could improve air sampler performance under specific conditions. Testing was conducted with and without an air mixer, using various flow rate ratios between the inlets to control the velocity nonuniformity upstream of the sampler. The results showed that the use of an air mixer significantly improves measurement accuracy and consistent performance of an air sampler, indicating that an air sampler should be utilized with an air mixing device. Furthermore, utilizing a TC grid can contribute to improved sampler accuracy. However, it is crucial to acknowledge that the measurement uncertainty associated with thermocouples may result in substantial inaccuracies when determining the bulk temperature of airflow. This is particularly true if the maximum temperature difference at the inlet is minimal, necessitating the use of more precise temperature sensors, such as RTDs, or using thermocouples with high accuracy cold-junctions.

Based on both the CFD and experimental testing results, the guidelines for air sampler design were developed as shown in Table 10.

Table 10 Guidelines for air sampler design

Design Parameter	Design Recommendation	Note
Sample branch dia., D_B	$\leq 0.06\ D_h$	$Re_{D\_B} < 3x10^5$: to maintain laminar boundary layer up to the separation point
Sampling hole dia., d	$0.24D_B - 0.48D_B$	Linearly decreasing "d" toward branch outlet
Trunk dia., D_T	$\geq 3D_B$	Referred to 10 CFR 2017, section 2.14.1
Sampling hole density along branch	≥ 5 holes/D_h	
Branch tube pitch, P	$0.125\ D_h \leq P \leq 0.25\ D_h$	
Average velocity at sampling holes	$\geq 1.0\ V_{free\text{-}stream}$	
Sampling hole facing angle to upstream	90°	A nearly uniform velocity distribution of free-stream required
Min. distance of sampler from the wall	$0.1\ D_h$	
Thermal conductivity of sampler material	≤ 0.19 W/m-K of PVC	Minimal heat transfer through sampler wall required

CHAPTER V

IN-SITU TEST

ABSTRACT

This study aimed to investigate the effectiveness of combining air mixing and sampling devices to enhance the accuracy of capacity measurements through in-situ testing. The study carefully selected air mixing and sampling devices based on the testing results of each component. The results showed that an air mixer can significantly improve the accuracy and consistency of sampler-based measurements for heating capacity and vapor mass balance, especially in the presence of unpredictably maldistributed upstream airflow. The study also focused on the optimal configuration of the combination, with a specific emphasis on the impact of flow velocity on measurement accuracy. The effect of temperature and velocity nonuniformities in flow distribution was investigated and found that the dependence of measurement accuracy on thermal and flow-dynamic nonuniformities can be insignificant as long as an air mixer with good mixing performance is utilized in airflow that is fast enough. The results suggest that selecting an air mixer with high mixing performance and optimizing the mixing length can contribute to a robust mixer-sampler combination for improved accuracy and precision of capacity and vapor mass balance measurements. Overall, this study provides valuable insights into the optimal configuration of air mixing and sampling devices to enhance the accuracy of capacity measurements.

5.1. Overview

Air mixing and sampling devices are essential for ensuring accurate measurement of bulk air conditions in psychrometric performance testing. The impact of design parameters and testing conditions on the performance of air mixing and sampling devices was discussed in the preceding sections. It was discovered that the utilization of air mixing devices can considerably enhance the accuracy and consistency of air sampling devices in the measurement of bulk air conditions, particularly in the presence of unpredictably maldistributed upstream airflow. However, despite the benefits of combining air mixing and sampling devices, there are no specific guidelines on how to properly use them. Thus, this study aims to investigate the effectiveness of this combination in enhancing the accuracy of capacity measurements and how to configure it for optimal performance through in-situ testing.

The performance of the combination was assessed by measuring the enthalpy change resulting from heating elements placed prior to the test section. The heating pattern across the airflow and the flow rate ratio between the duct inlets were manipulated to control maldistributed airflow in temperature and velocity, which can lead to inherently inaccurate measurement of heating capacity. By conducting in-situ testing, the study aimed to optimize the mixing and sampling combinations against various scenarios of maldistributed flow conditions.

This study aimed to optimize the mixing and sampling combinations against various scenarios of maldistributed flow conditions. Overall, the results of this study provide valuable insights into the impact of design parameters and testing conditions on the performance of air mixing and sampling devices, as well as the effectiveness of combining these devices in enhancing the accuracy of capacity measurements. By optimizing the mixing and sampling combinations through in-situ testing, the accuracy and consistency of air mixing and sampling devices can be improved, leading to more reliable measurements of bulk air conditions.

5.2. Experimental Setup

The testing setup for in-situ testing was manipulated from the existing setup for the mixer and sampler testing referring to the configurations and plenums as specified in ASHRAE 37 (2009). Figures 82 and 83 depict the overall shape and schematic of the in-situ testing setup, respectively. Unlike air mixer and sampling tests, the air supplied to both inlets was conditioned to the same temperature and humidity as shown in Figure 82.

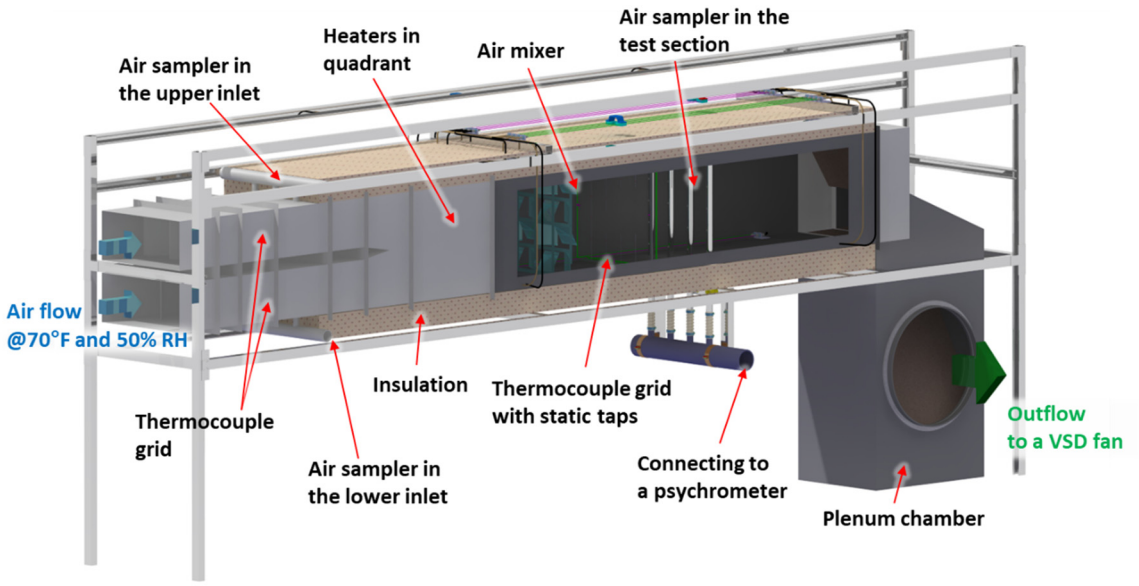

Figure 82 3D model of the mixer and sampler testing setup for in-situ testing.

As illustrated in Figure 83, a heating source consisting of four electric heaters (1.5 kW each) was installed prior to the test section. These heaters were mounted in a frame dividing the flow section into quadrants, enabling the creation of a thermally maldistributed airflow through independent control of the heaters. This manipulation allowed the temperature pattern across the airflow entering the test section to be varied in different ways including diagonal and low half heating pattern, as shown in Figure 84. For heater operation, a safety circuit was designed with electric relays and an airflow sensor to prevent any potential malfunctions. The power consumption of each heater is measured using a power meter unit, and the data is acquired using real-time image processing with a webcam and LabVIEW VISION.

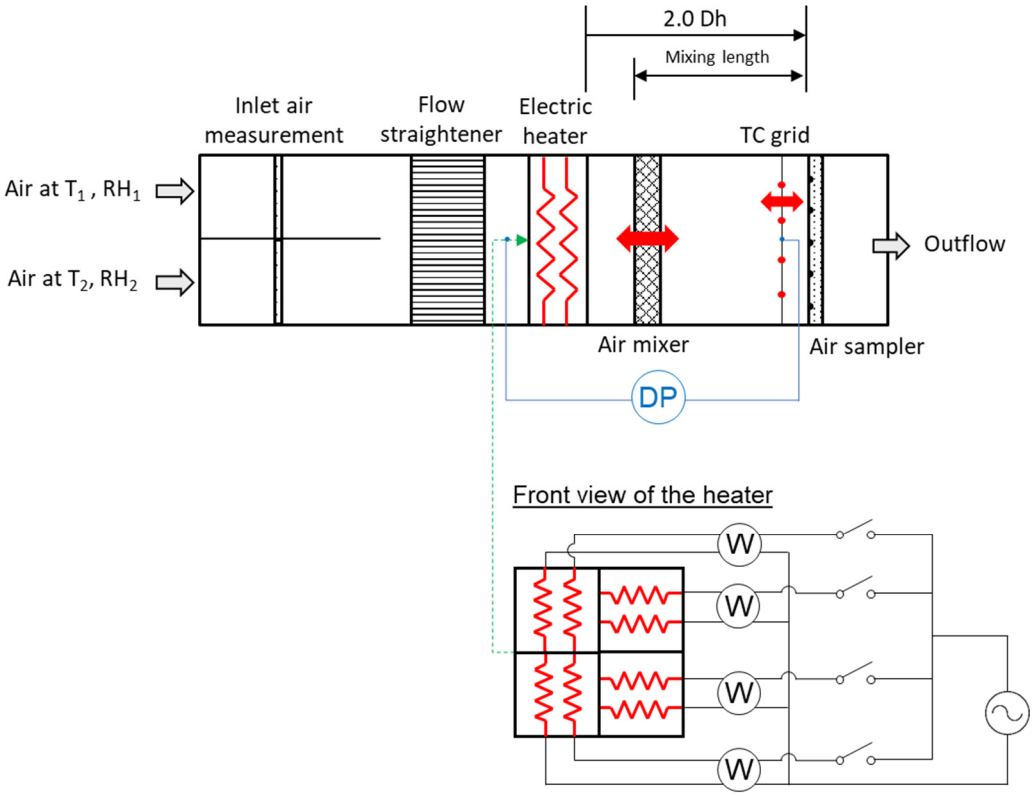

Figure 83 Schematic of in-situ testing setup

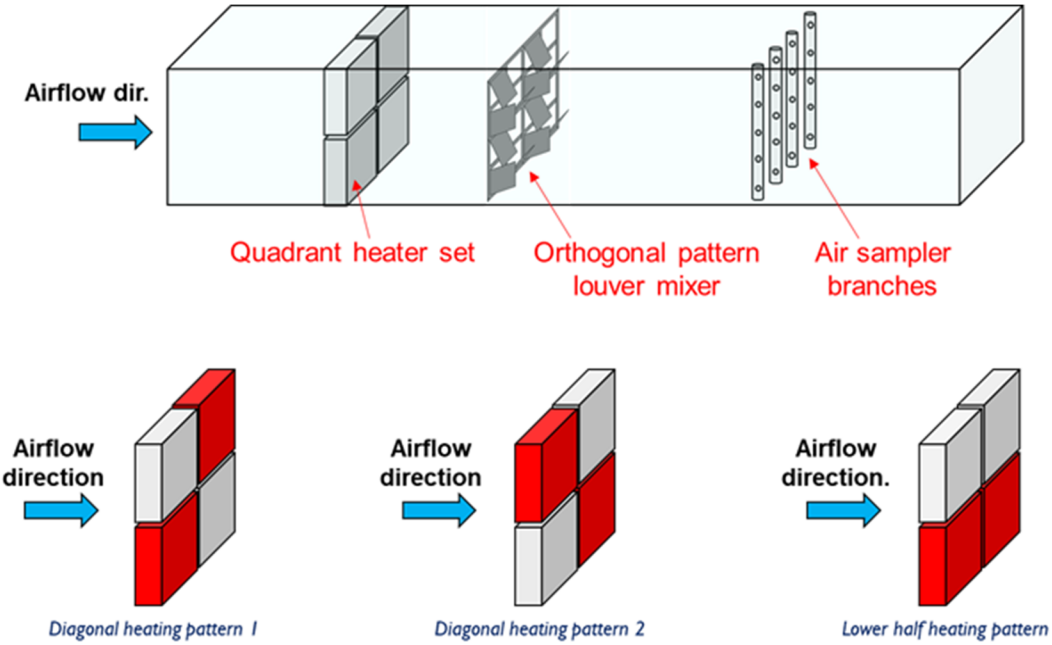

Figure 84 Heater operation: Heating patterns

In the test section, an air sampler was installed 2.0 D_h away from the outlet of the heaters. This distance was chosen to meet the industry's requirement for the maximum allowable length of air mixing and sampling instrumentation in compact-sized facilities with limited space. An air mixer, located between the heaters and the air sampler, was mounted on a movable frame with a traversing system, enabling the monitoring of the temperature distribution on a thermocouple grid. This allows to maximize the mixing effect on the airflow, reducing non-uniformity in the airflow as much as possible before air sampling. The TC grid was also utilized to capture the temperature distribution of the mixed airflow prior to the air sampler.

The air mixer and sampler chosen for in-situ testing were carefully selected based on their testing results. First, the orthogonal pattern louver mixer was chosen as the mixer type for testing since it showed much higher mixing performance with acceptable pressure drop compared to other mixer types tested, as shown in Figure 40. The ease of designing and fabricating this mixer type was also taken into consideration. A louver angle of 60° was chosen for the mixer, as the results showed that changing the louver angle has a significant impact on the mixer performance, and a louver angle steeper than 60° may result in a significant pressure drop despite relatively small improvement in mixing performance, as shown in Figure 36. Additionally, a 4 by 4 louver array size for a single orthogonal pattern louver mixer was chosen due to its good mixing performance, consistency of mixing performance, and low pressure drop, as seen in Figure 37.

For the air sampler employed in the testing, a variable sampling hole with hole sizes ranging from 1/4 inch to 1/2 inch was chosen. This selection was based on the results shown in Figure 77, which demonstrate that both experimental and CFD results for different sampling hole sizes indicate that gradually increasing the sampling hole size from the sampler branch tube outlet can lead to more uniform air influx across the holes. This is due to the contribution of variable sampling holes compensating for pressure drop in the airflow along the branch tube. The sampling hole facing angle of the selected sampler was determined to be perpendicular to the upstream flow based on

the testing results shown in Figure 78. Finally, considering that PVC performed best as a sampler material in both CFD and experimental tests, as shown in Figure 79, the air sampler used for in-situ testing was made of PVC pipe.

Figure 85 shows the orthogonal pattern louver mixer and the four electric heaters installed in and prior to the test section, respectively.

(a) (b)

Figure 85 Experimental setup for in-situ testing: (a) Single orthogonal pattern louver mixer with 4 by 4 louver array and 60° louver angles, and (b) Four electric heaters installed in quadrants.

5.3. Data Reduction and Test Plan

The performance of the air mixer and sampler combination was evaluated by assessing the accuracy of capacity and vapor mass balance measurements. The metrics below were used to determine the ratings:

$$Capacity\ Measurement\ Accuracy =$$

$$\frac{(Enthalpy\ flow_{test,\ sampled}[kW] - Enthalpy\ flow_{inlet}[kW]) - Heater\ power[kW]}{Heater\ power\ [kW]} \cdot 100\% \quad (12)$$

where,

$$Enthalpy\ flow[kW] = Air\ enthalpy[kJ/kg] \cdot \dot{m}_{air}[kg/s]$$

$$Air\ enthalpy\ [kJ/kg] = f(T_{DB}, \omega)$$

$$Vapor\ Mass\ Balance =$$

$$\frac{Vapor\ mass_{test,sampled}\ [lb/min] - Vapor\ mass_{inlet}[lb/min]}{Vapor\ mass_{inlet}\ [lb/min]} \cdot 100\% \quad (13)$$

where,

$$Vapor\ Mass\ [lb/min] = \rho_{vapor}[lb/ft^3] \cdot \dot{V}[CFM]$$

$$\rho_{vapor}[lb/ft^3] = \left(\frac{0.0022 \cdot p_{vapor}[N/m^2]}{T_{DB}[K]}\right) \cdot 0.06243\ \left[\frac{lb/ft^3}{kg/m^3}\right]$$

For capacity measurement, the airside enthalpy gain was compared to the heater power consumption. The airside enthalpies gained by heating with the electric heaters were defined as the difference in airside capacity between the inlet and the test section. This difference was then compared to the heater power consumption, which was measured using power meter units. This comparison was represented by Equation (12).

The balance of vapor mass in the airflow was determined using Equation (13). The vapor density was estimated using the sampler-based psychrometric quantities. By multiplying the density with the volumetric flow rate of the airflow, the mass flow rate of vapor could be estimated. By comparing the mass flow rates of vapor between the inlet and the test section, the vapor mass balance could be evaluated.

The testing conditions for the in-situ testing are presented in Table 11. The airflow at the inlets was

conditioned identically at a temperature and relative humidity of 70°F and 50%, respectively. To investigate the performance of the air mixer and sampler combination, the testing was conducted under various conditions by adjusting the airflow distribution across the airflow with different inlet flowrate ratios. Independent control of the electric heaters allowed for adjusting the non-uniform temperature distribution in the airflow. The effect of mixing length on measurement accuracy was also investigated by adjusting the mixing length from 0.5 to 2.0 D_h. Finally, the effectiveness of using the air mixer in improving the accuracy of sampler-based capacity and vapor mass balance measurement was observed.

Table 11 Experimental testing conditions for the in-situ testing

#	Air Condition @upper inlet	Flowrate @ upper inlet	Air Condition @lower inlet	Flowrate, Total	Heating Pattern	Nominal Capacity of Heating Source	Mixer Type	Overall Mixing Length
1	70°F DB, 50% RH	315 CFM	70°F DB, 50% RH	900 CFM	Diagonal 1	1 ton	Single orthogonal louver Louver: 4x4, 60deg	2.0 D_h
2		450 CFM						
3		585 CFM						
4		450 CFM			Diagonal 1			
5		450 CFM			Diagonal 2			
6		450 CFM			Low			
7		450 CFM			Diagonal 1			1.25 D_h
8								1.0 D_h
9								0.75 D_h
10								0.5 D_h
11	70°F DB, 50% RH	175 CFM	70°F DB, 50% RH	500 CFM	Diagonal 1	1 ton	Single orthogonal louver Louver: 4x4, 60deg	2.0 D_h
12		250 CFM						
13		325 CFM						
14		250 CFM			Diagonal 1			
15		250 CFM			Diagonal 2			
16		250 CFM			Low			
17	70°F DB, 50% RH	125 CFM	70°F DB, 50% RH	250 CFM	Diagonal 1	1 ton	Single orthogonal louver Louver: 4x4, 60deg	2.0 D_h
18		250 CFM		500 CFM				
19		375 CFM		750 CFM				
20		450 CFM		900 CFM				
21	70°F DB, 50% RH	125 CFM	70°F DB, 50% RH	250 CFM	Diagonal 1	1 ton	No mixer	-
22		250 CFM		500 CFM				
23		375 CFM		750 CFM				
24		450 CFM		900 CFM				
25	70°F DB, 50% RH	250 CFM	70°F DB, 50% RH	500 CFM	Diagonal 1	1 ton	No mixer	-
26					Diagonal 2			
27					Low			

5.4. Discussion of Results

The in-situ testing was performed under various operational conditions, including changes in total flowrate, nonuniform flow distribution, and mixing length. The results of these tests provided not only a general understanding of the effectiveness of using air mixing and sampling devices to improve the measurement accuracy of bulk air conditions, but also valuable insights for designing psychrometric performance testing setups that are less vulnerable to variations and unpredictability in airflow conditions. By carefully selecting the mixing length and an air mixer with high performance and minimal sensitivity of effectiveness to total flowrate, the robustness of the setup can be increased, ultimately improving the accuracy and precision of capacity and vapor mass balance measurements. These findings are significant for industries and research fields that require precise psychrometric measurements.

5.4.1. Effect of Total Flowrate

Figure 86 presents the results of capacity and vapor mass balance measurements for different total flow rates with and without the single orthogonal pattern louver mixer. The flowrate ratio between the inlets was set to be identical, resulting in uniform flow distribution prior to the test section. The dry bulb temperature and relative humidity of the air at the inlets were conditioned to be 70°F and approximately 45%, respectively. The supplied air was heated in the diagonal heating pattern 1, as illustrated in Figure 84, and the heating capacity measured by the power meters was approximately 3.3 kW, corresponding to approximately 1 ton. The air sampling rate was adjusted to 6 CFM (0.003 m^3/s) to achieve 1.5 CFM (0.0007 m^3/s) sampling rate per sampler branch tube. This allowed the velocity of sampled air flowing through the wet bulb RTD to be maintained between from 800 to 1200 ft/min (4.06 to 6.1 m/s) which is the range of the required air velocity across wet bulb temperature sensor, as specified in 10 CFR Criteria (DOE, 2017). The mixing length, which is the distance between the mixer inlet and the air sampler branch tubes, was set to 2.0 D_h.

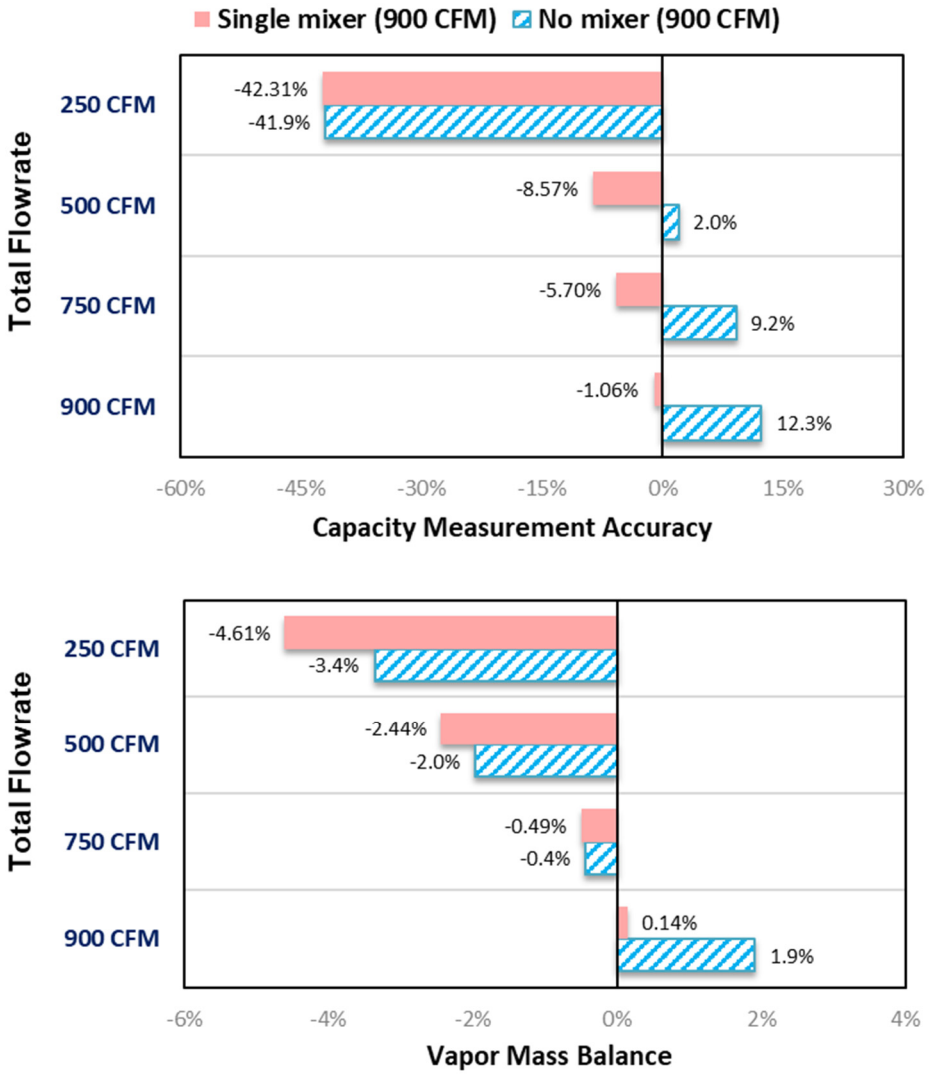

Figure 86 In-situ testing result: Effect of total flowrate on capacity measurement accuracy (top) and vapor mass balance (bottom)

The results indicate that the use of an air mixer can enhance the accuracy of measuring both heating capacity and vapor mass balance in general. Moreover, it was observed that the accuracy of both measurements is largely influenced by the total flow rate, as the measurement accuracy improves with an increase in total flow rate. However, the testing of the mixer in Figure 42 on page 63 revealed a contrary result, where the mixing effectiveness decreases as the total flow rate increases. This suggests that while an active mixing process can aid in accurate measurement for capacity and vapor mass balance, the impact of flow velocity on measurement accuracy is more significant, as higher airflow results in less heat loss experienced by the airflow to the duct as it travels from the

duct inlet to the test section. Additionally, the vapor mass balance was measured within 5% for all test cases. This is likely due to the nearly identical relative humidity of the airflow supplied to the inlet. Since there was almost no non-uniformity in the vapor mass within the airflow, the results may not be as significant in understanding the vapor mass balance under different conditions.

5.4.2. Effect of Nonuniform Flow Distribution

In psychrometric performance testing, the airflow passing through a coil can possess thermal and flow nonuniformities that depend on the coil type and tube circuitry patterns. It is typically impossible to predict how the airflow will be thermally and/or flow-dynamically maldistributed. In this in-situ testing, temperature and velocity maldistributions in the airflow were artificially created under control by operating heating sources in designated patterns and adjusting the flowrate ratio of airflow between the top and bottom inlets.

The dependence of measurement accuracy for capacity and vapor mass balance on thermal nonuniformity in airflow was investigated, and the results are shown in Figure 87. During the testing, the flowrate ratio between the inlets remained identical to obtain flow-dynamically uniform flow distribution. Meanwhile, the electric heaters were controlled to create different thermal maldistributions in the airflow, as illustrated in Figure 84. The temperature and relative humidity at the inlets were 70°F (21.1°C) and 45%, respectively. The total heating capacity was adjusted to be about 3.3 kW (equivalent to approximately 1 ton), measured using power meters. The mixing length between the mixer and the sampler was 2.0 D_h. The testing was performed for two different total flowrates of 500 and 900 CFM (0.236 and 0.425 m^3/s). The results illustrated in Figure 87 show that a change in temperature nonuniformity in airflow does not have a significant impact on the measurement accuracy for both heating capacity and vapor mass balance when using a mixer with sufficiently fast airflow, as evidenced by the results for the single mixer use in the airflow of 900 CFM (0.425 m^3/s). In other words, using a good mixer in sufficiently fast airflow consistently

improves the accuracy in measuring capacity and vapor mass balance, regardless of how the airflow is maldistributed. The result for vapor mass balance indicates that the near independence for heat loss in the fast airflow allows for more accurate measurement of mass balance as well.

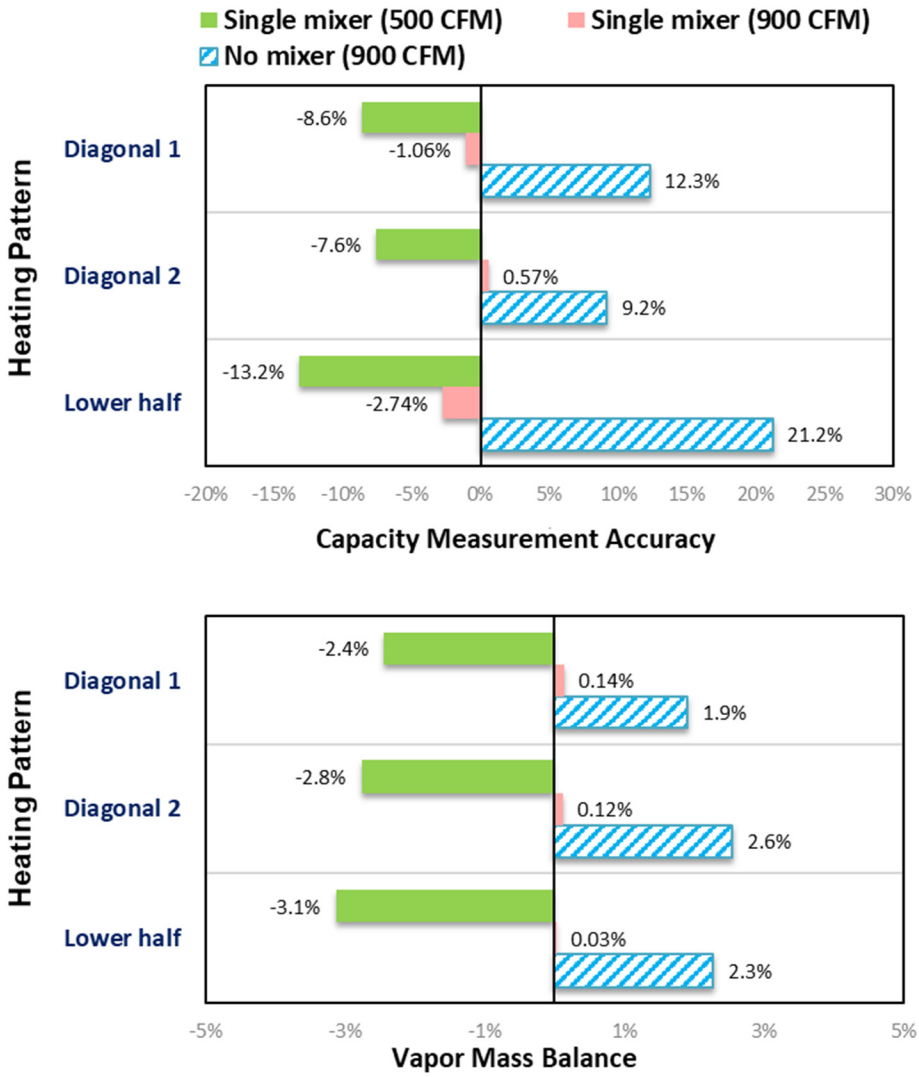

Figure 87 In-situ testing result: Effect of temperature nonuniformity on capacity measurement accuracy (top) and vapor mass balance (bottom)

The impact of velocity nonuniformity on the accuracy of capacity and vapor mass balance measurements is presented in Figure 88. The airflow was deliberately maldistributed by adjusting the flowrate ratio between the top and bottom inlet, with total flow rates of 500 and 900 CFM (0.236 and 0.425 m^3/s). The Diagonal heating pattern 1 from Figure 84 was selected as the standard

testing condition for consistency. The other testing conditions, including the inlet air conditions, heating capacity, air sampling rate, and mixing length, remained the same as those applied to the testing case set for the effect of temperature nonuniformity.

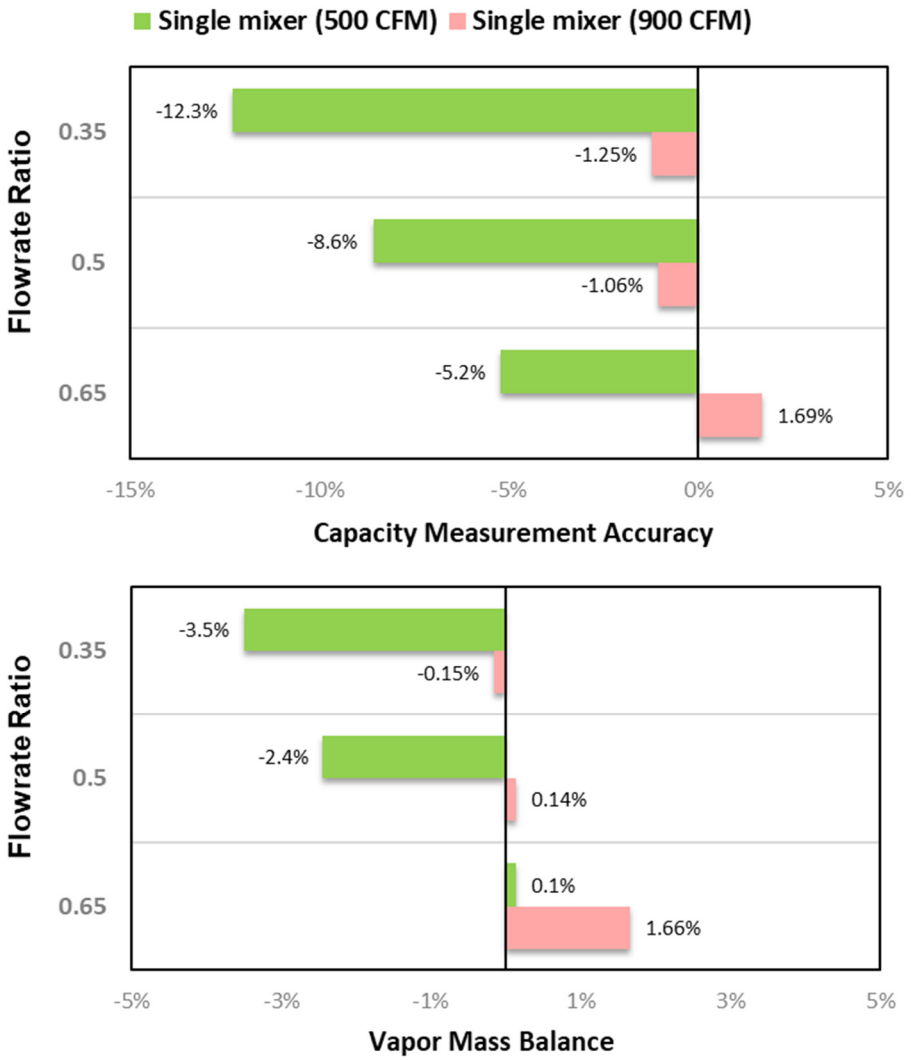

Figure 88 In-situ testing result: Effect of velocity nonuniformity on capacity measurement accuracy (top) and vapor mass balance (bottom)

The results indicate that the use of a mixer with a sufficiently fast flow rate can effectively reduce velocity nonuniformity, resulting in better accuracy of capacity measurement. This result once again shows that the airflow velocity for a total flowrate of 500 CFM (0.236 m^3/s) is not enough for this testing setup with an air mixer to achieve acceptable vapor mass balance and capacity

measurement accuracy, due to large accuracy variation caused by changes in flow conditions.

5.4.3. Effect of Mixing Length

The study investigated the minimum mixing length required to achieve consistent accuracy in capacity and vapor mass balance measurement. The effect of mixing length on measurement accuracy is presented in Figure 89. During testing, the mixing length was adjusted within a range of 0.5 to 2.0 D_h for two different total flow rates of 500 and 900 CFM (0.236 and 0.425 m^3/s). Other testing conditions, including a flow rate ratio of 0.5, an inlet condition of 70°F (21.1°C) and RH 45%, heating capacity of 1 ton (3.3 kW) for the diagonal heating pattern 1, and a sampling rate of 6 CFM (0.003 m^3/s), remained consistent with the testing conditions applied to other testing cases introduced in previous sections.

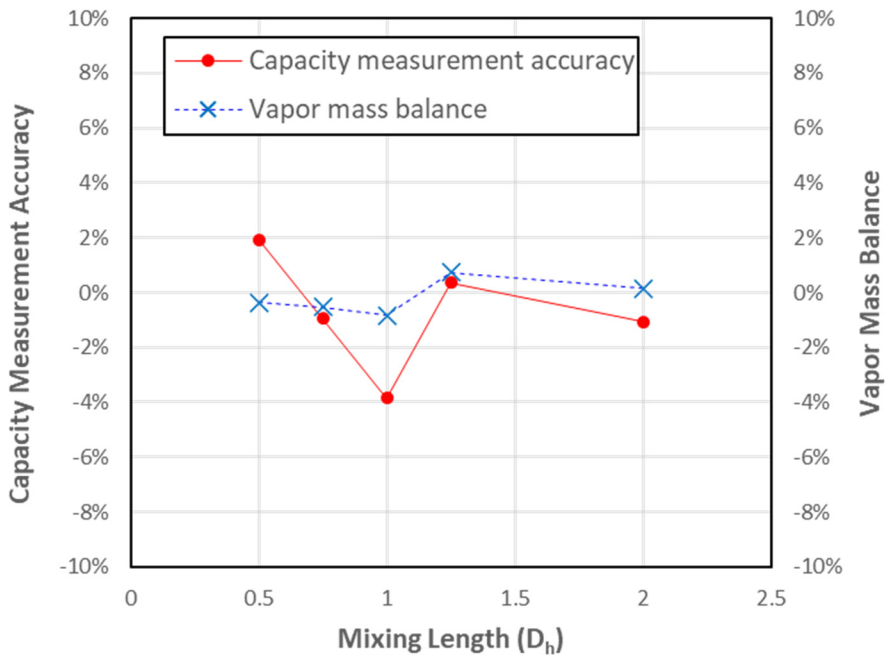

Figure 89 In-situ testing result: Effect of mixing length on capacity measurement accuracy and vapor mass balance.

The results show that in general, an air mixer with good mixing performance does not significantly affect accuracy in sampler-based capacity measurement if heat loss to the duct is minimized with sufficiently fast airflow. Additionally, the results suggest that a mixing length larger than 1.25 D_h

can minimize changes in measurement accuracy for both capacity and vapor mass.

5.5. Conclusions

Air mixing and sampling devices are essential for ensuring the accurate measurement of bulk air conditions in psychrometric performance testing. This study aimed to investigate the effectiveness of combining air mixing and sampling devices to enhance capacity measurements' accuracy and configuration them for optimal performance through in-situ testing.

The air mixing and sampling devices to be used in combination were carefully selected based on the testing results of each component. The study found that the use of an air mixer can significantly improve the accuracy and consistency of sampler-based measurements for heating capacity and vapor mass balance, particularly in the presence of unpredictably maldistributed upstream airflow. The accuracy of the measurements is mainly influenced by the total flow rate, with the impact of flow velocity on measurement accuracy being more significant. Higher airflow reduces heat loss, resulting in more accurate and consistent sampler-based measurements. However, it is important to note that faster air velocity can reduce mixing effectiveness, as determined from mixer testing. Therefore, the study concludes that selecting an air mixer with good mixing performance should be the foremost consideration since such mixers' performance was found to be less affected by changes in the incoming airflow velocity, as demonstrated in the mixer testing.

The study also investigated the effect of temperature and velocity nonuniformities in flow distribution and found that the dependence of measurement accuracy for capacity and vapor mass balance on thermal and flow-dynamic nonuniformities in airflow can be insignificant as long as the air velocity is fast enough (e.g. $V_{free\text{-}stream} \geq 750$ CFM for $D_h = 18$ inches; $Re_{Dh} \geq 50000$). By carefully selecting an air mixer with high performance and minimal variation for changes in total flow rate and sufficient the mixing length ($\geq 1.25\ D_h$), the setup's robustness can be increased, ultimately improving the accuracy and precision of capacity and vapor mass balance measurements.

CHAPTER VI

CONCLUSIONS AND FUTURE WORK

6.1.Summary and Conclusions

The aim of this research is to optimize the design of air mixing and sampling devices by investigating their performance and identifying the challenges associated with obtaining accurate measurements despite airflow maldistribution. Accurate measurement of bulk air conditions is crucial for psychrometric performance testing and HVAC equipment; however, measurement discrepancies may arise from varying designs of air sampling and mixing devices due to limited literature and guidelines. Consequently, manufacturers are advised to consider third-party performance validation tests. To address this issue, various types of air mixing and sampling devices were reviewed, and the factors influencing their performance were discussed. The study found that current air mixing and sampling devices have limitations in their design, and there is potential for improvement through design changes. Thus, the primary objective of this study is to investigate the impact of design parameters and testing conditions on the performance of air mixing and sampling devices and provide insights into their design guidelines for optimization. The goal is to achieve precise measurements and consistent accuracy in psychrometric performance testing while considering the importance of correctly configuring these devices, ultimately leading to optimal HVAC equipment performance.

An investigation was conducted on the design of air sampling devices to determine the impact of various geometrical and operational conditions on their performance, specifically in terms of mixing effectiveness and pressure drop. The candidate mixers were designed for square ducts, commonly used in HVAC system performance testing. This research examined three types of air mixing devices: a louvered-type mixer based on ASHRAE Standard 41.2, an orifice mixer, and an orthogonal pattern louver mixer. The study assessed the mixing and flow-dynamic performance of these devices under a range of operating and geometrical conditions. Tested operating conditions included flow rate, flow rate ratio, and overall mixing length, while the design parameters tested encompassed mixer spacing and orientation, orifice diameter, orifice-target spacing, louver angle, and louver array size. The results indicated that all mixing devices were capable of reducing airflow stratification. In general, the mixing effectiveness of the devices increased as the overall mixing length and/or spacing for dual mixers increased. For an overall mixing length of 2.0 D_h, the maximum mixing length for industrial applications, the mixing effectiveness values for the louvered mixer, orifice mixer, orifice-target mixer, and orthogonal pattern louver mixer were 76.3%, 75.1%, 69.9%, and 88%, respectively. The baseline louvered mixer demonstrated good mixing performance and the lowest pressure drop compared to other mixer types. It was revealed that this mixer type's performance is significantly influenced by airflow maldistribution patterns caused by one-dimensional mixing with the louver shape's geometrical characteristics. To address this issue, this mixer type should be used in pairs, rotated 90 degrees from each other, enabling two-dimensional mixing and reducing unexpected airflow maldistribution. However, for applications with limited instrumentation space, this mixer configuration, with dual mixers placed in series, may not be suitable. The study also found that orifice mixer types are unsuitable as air mixing devices due to a significantly large pressure drop and velocity maldistribution caused by jet flow, despite acceptable mixing performance. In contrast, the orthogonal pattern louver mixer emerged as the most promising option because of its simple design, easy fabrication, high mixing performance with low pressure drop, and two-dimensional mixing. The study indicated that

louvered mixer types are less affected by alterations in total flow rate and incoming airflow velocity maldistribution compared to orifice mixer types. Consequently, the study provides an extensive analysis of air mixing devices' performance and design for square ducts. The design recommendations suggested in this research can assist in designing and selecting the optimal mixer type for industrial applications, taking into account factors such as cost-effectiveness, mixing performance, pressure drop, and sensitivity to flow rate and velocity maldistribution.

The study also explored the impact of design parameters on air sampling devices using both numerical and experimental methods, offering design recommendations to ensure accuracy and reliability. Key findings emphasized that adjusting sampling hole size and spacing can significantly improve air influx uniformity across the sampling holes. Aluminum and PVC were recommended as sampler materials due to their superior performance in obtaining a mean temperature of sampled air closer to the free-stream bulk temperature compared to other materials like stainless steel. Variable sampling hole sizes were found advantageous in reducing pressure gradients along sampler branch tubes, resulting in more uniform air sampling across the holes. The study also suggested a recommended ratio of 0.238-0.357 for sampling hole diameter to sampler branch diameter for equal-sized holes, ensuring optimal performance. Modifying sampling hole spacing based on the free-stream velocity profile can help achieve more uniform air sampling if the air stream flow pattern outside the sampler is known. Radiation heat transfer had a minor impact on the mean temperature of sampled air, suggesting other factors are more critical for sampler performance. Additionally, more sampling holes allows for more uniform air sampling across the sampling holes, but do not necessarily ensure more accurate measurements of bulk air conditions due to heat loss or gain through the sampler wall. Variable sampling holes where sampling hole size gradually decreases towards the sampler branch outlet could be beneficial for uniform air sampling across the sampling holes. The experimental study conducted for validation purposes revealed a significant difference in sampler accuracy between experimental and CFD results.

However, both displayed similar trends in characteristic features, leading to the conclusion that the CFD results were qualitatively validated. The investigation also explored the use of an air mixer to enhance air sampler performance under specific conditions. Results indicated that employing an air mixer significantly improves measurement accuracy and consistent performance of an air sampler, suggesting that air samplers should be used with air mixing devices. Moreover, the study proposed that the use of a TC grid can contribute to ensuring sampler accuracy.

An in-situ test was conducted to recommend standardization for configuring air mixing and sampling device combinations to enhance capacity measurement accuracy in psychrometric performance testing. In this study, air mixing and sampling devices were meticulously selected based on each component's testing results to ensure optimal performance. The research found that using an air mixer significantly improves the accuracy and consistency of sampler-based measurements for capacity and vapor mass balance, particularly in cases of unpredictably maldistributed airflow. The study also concentrated on the optimal configuration of the mixer-sampler combination. It was determined that measurement accuracy is significantly influenced by changes in total flow rate, even with uniform velocity distribution across the flow field and identical flow rate ratios between airstreams supplied to top and bottom inlets. This was attributed to higher air velocity reducing heat loss, resulting in more accurate and consistent sampler-based measurements. Therefore, the study concludes that selecting an air mixer with excellent mixing performance should be the primary consideration since such mixers' performance is found to be less affected by changes in incoming airflow conditions. In other words, these mixers can be effectively used in fast airflow for minimized heat loss and less reduction in mixing performance, resulting in consistently accurate capacity measurements of HVAC&R equipment regardless of variable upstream conditions. This conclusion is also supported by the in-situ testing discovery that the dependence of measurement accuracy for capacity and vapor mass balance on changes in thermal and flow-dynamic nonuniformities can be insignificant if the air velocity is fast enough.

Consequently, although air sampler performance varies due to inconsistent uniformity of air sampling across the sampling holes with upstream conditions, the robustness of sampler-based capacity measurements for HVAC&R equipment can be increased by carefully selecting a high-performance air mixer and ensuring sufficient mixing length.

In conclusion, this study offers valuable insights into design parameters and testing conditions' impact on air mixing and sampling devices' performance and the effectiveness of combining these devices to enhance capacity measurement accuracy. Based on the testing results' analysis, this study proposes general guidance on designing optimal air mixing and sampling devices. By optimizing mixer and sampler combinations through in-situ testing, the results demonstrated that the accuracy and consistency of air mixing and sampling devices can be improved, leading to more reliable measurements of bulk air conditions.

6.2. Future Work

Building on the conclusions of this research, several avenues could be explored to advance the understanding and optimization of air mixing and sampling devices. One potential direction is to investigate their performance in non-square ducts, such as rectangular or circular ones, to determine the applicability of the results to a wider range of HVAC&R systems. Additionally, developing and testing novel air mixing devices that improve upon the strengths of the orthogonal pattern louver mixer while addressing its limitations could lead to higher mixing performance and lower pressure drop.

Another promising approach includes employing machine learning techniques, such as optimization algorithms or surrogate modeling, to optimize air mixing and sampling devices' design by exploring a larger design space with more complex geometries and configurations. Conducting experiments in real-world HVAC&R systems and environments would yield valuable insights into

the influence of factors such as dust accumulation, moisture, and varying operating conditions on device performance, ensuring their effectiveness under real-world conditions.

A valuable extension of this research involves examining the performance of air mixing and sampling devices in various duct sizes and configurations, which could determine whether the observed trends and findings hold true across a broader range of scenarios. This extension would provide a comprehensive understanding of the devices' performance, enhancing their applicability in diverse HVAC&R systems and other applications with varying duct sizes.

Long-term performance and durability are crucial considerations. Future research could investigate how different materials and designs of air mixing and sampling devices withstand long-term use, wear, and corrosion, and assess the impact of these factors on performance over time. Based on the insights from this study and future research, developing a comprehensive design guideline and standard would provide HVAC&R manufacturers and designers with a clear and concise reference for designing and selecting optimal air mixing and sampling devices.

Lastly, exploring the applicability of this research's findings to other applications beyond HVAC&R systems, such as industrial processes and environmental monitoring, where accurate air mixing and sampling is crucial, could have a broader impact on multiple industries and contribute to more accurate and reliable air measurements in various settings.

REFERENCES

Ahmed, M., Park, H., Bach, C.K., and San, O. 2020. Numerical Investigation of Air Mixer for HVAC Testing Applications (ASHRAE RP-1733). *Science and Technology for the Built Environment* 26(9):1252-1273

AHRI. 2008. ANSI/AHRI Standard 210/240 with Addendum 1 (formerly ARI Standard 210/240), 2008 Standard for Performance Rating of Unitary Air-Conditioning & Air-Source Heat Pump Equipment. Arlington: AHRI.

AHRI. 2009. ANSI/AHRI Standard 365 (I-P), 2009 Standard for Performance Rating of Commercial and Industrial Unitary Air-Conditioning Condensing Units. Arlington: AHRI.

AHRI. 2015. ANSI/AHRI Standard 340/360 (I-P), 2015 Standard for Performance Rating of Commercial and Industrial Unitary Air-conditioning and Heat Pump Equipment. Arlington: AHRI.

ANSI/ASHRAE. 2000. Standard 33-2000, Method of Testing Forced Air Cooling and Heating Coils. Atlanta: ASHRAE.

Ansys® Academic Research Mechanical and CFD, Release 2020 R2, Ansys, Inc.

ASHRAE. 1992. Standard 41.2-1987 (RA 92), Standard Methods for Laboratory Airflow Measurement. Atlanta: ASHRAE.

ASHRAE. 2013. Standard 41.1-2013, Standard Method for Temperature Measurement. Atlanta: ASHRAE.

ASHRAE (2009). Standard 37-2009 -- Methods of Testing for Rating Electrically Driven Unitary Air-Conditioning and Heat Pump Equipment (ANSI Approved). Atlanta: ASHRAE

ASHRAE. 2017. 1733-TRP, Develop Design Criteria for Psychrometric Air Sampler and Mixer Apparatus for Use in ASHRAE Test Standards. Request-for-Proposal (RFP). Atlanta: ASHRAE.

Bhatia, A. 2001. HVAC-how to size and design ducts. Course No: M06-032, Continuing Education and Development, Inc.

Blender Product, Inc. Series IV Air Blender static mixer. https://www.blenderproducts.com. Accessed 11/19/2019.

Denton, D., Kirkwood, A.C., and Cheesman, S. 2019. RP1733- Request to review the draft of a review article. Email communication with PMS members, March 03 to 7, 2019.

Erickson, T.A. 1965. Air Mixer for Air Streams. US Patent 3180245, filed March 12, 1965.

Faison, T.K., Davis, J.C., and Achenbach, P.R. 1966. A test apparatus for the study of forced air-mixing devices. *Journal of Research of the National Bureau of Standards - C. Engineering and Instrumentation.* 70c (1):25–31.

Faison T.K., Davis, J.C., and Achenbach, P.R. 1967. Performance of square-edged orifices and orifice-target combinations as air mixers. *Building Science Series* 12. US Department of Commerce– NIST, USA.

Faison T.K., Davis, J.C., and Achenbach, P.R. 1970. Performance of louvered devices as air mixers. *Building Science Series* 27. US Department of Commerce – NIST, USA.

Fleissneer, G. 1992. Air mixer apparatus. US Patent 5150535, filed October 1, 1990.

Sugiura, H. 1998. Static mixer. US Patent 5779361, filed May 12, 1997.

Kees, Inc. 1998a. Air Mixxer model MX and MXP. https://www.kees.com. Accessed 11/19/2019.

Kees, Inc. 1998b. Panel Mixxer in plenum section model PMP. https://www.kees.com.

Kees, Inc. 2005. Air Mixxer box model TM. https://www.kees.com. Accessed 11/19/2019.

Kirkwood, C., Denton, D., Cheesman, S., and Stone, C. 2018. RP1733 - #2 - November Update and Discussion. Email communication with PMS members, November 12 to 13, 2018.

Koop, E.N. 2008. Static air mixer. US Patent US2008/0153409A1, filed December 21, 2008.

McIlvaine, O.T. 1948. Dew point detector. US Patent 2435895, filed June 24, 1943.

Montgomery, D.C. 1997. Introduction to Statistical Quality Control. 3rd Ed. Appendix VI, for constructing variables control charts. ed. New York: John Wiley & Sons, Inc.

Musser, A., Hrnjak, P., and Elbel, S. 2016. Internal Heat Exchanger Performance Quantification and Comparison Testing Methods Including Exploration of the Effects of Location of Measurements and Oil in Circulation. Proceeding of 16th International Refrigeration and Air Conditioning Conference, July 11, 2016, West Lafayette, IN, USA

Park, H., and Bach, C.K. 2019. A Literature Review of Air Mixing Devices for Psychrometric Performance Measurement Applications (ASHRAE RP-1733). *Science and Technology for the Built Environment* 26(2):1-25

Park, H., and Bach, C.K. 2021. Performance Characterization of Air Mixing Devices for Square Ducts. *Applied Thermal Engineering* 199(25):117495

Rieber, F. 1951. Dew point meter. US Patent 2542944, filed April 20, 1945.

Robinson, K.D. 2000. Rating air-mixing equipment. *ASHRAE Journal* 42(2):63–70.

Robinson, K.D. 2001. A test apparatus and method to rate the mixing performance of air mixers. *ASHRAE Transactions* 107:136-142.

Robinson, K.D. 2003. Static air mixing apparatus. US Patent US6,595,848B1, filed July 3, 2002.

US DOE. 2017. 10 CFR Ch. II (1–1–17 Edition). Subchapter D — Energy Conservation - Appendix M to Subpart B of Part 430—Uniform Test Method for Measuring the Energy Consumption of Central Air Conditioners and Heat Pumps. Subsections 2.14.1 and 1.14.2. Code of Federal Regulations. US Department of Energy.

Wile, D.D. 1947. Air flow measurement in the laboratory. *Refrigerating Engineering – Journal of ASRE* 53(6):515-521.

Zieve, E.R. 1994. Air mixer. US Patent 5,364,305A, filed June 14, 1993.

APPENDICES

Appendix A: List of Conference Paper and Journal Publication

1. Conference Papers
   i. Y. Hossain, R. Maulik, **H. Park**, M. Ahmed, C. K. Bach, and O. San, "Improvement of unitary equipment and heat exchanger testing methods (ASHRAE RP1733/43)", Proceedings of the ASHRAE Annual Conference, Kansas City, USA, June 22-26, 2019
   ii. **H. Park**, C. Bach, and O. San, "An Update on the Evaluation of Air Mixer Performance (RP-1733)", Proceedings of the ASHRAE 2020 Virtual Conference, June 29-July 2, 2020

2. Journal Papers
   i. **H. Park**, and C. K. Bach, "A Literature Review of Air Mixing Devices for Psychrometric Performance Measurement Applications (ASHRAE RP-1733)", Science and Technology for the Build Environment, vol. 26(6), pp. 778-789, 2020
   ii. M. Ahmed, **H. Park**, C. K. Bach, and O. San, "Numerical Investigation of Air Mixer for HVAC Testing Application (ASHRAE RP-1733)", Science and Technology for the Build Environment, vol. 26(9), pp. 1252-1273, 2020
   iii. **H. Park**, and C.K. Bach, "Performance Characterization of Air Mixing Devices for Square Ducts", Applied Thermal Engineering, vol. 199(25), pp. 117495, 2021

3. Papers unpublished or under revision
   i. **H. Park**, and C.K. Bach, "Orthogonal Pattern Louver Mixer for Two-Dimensional Air Mixing in HVAC Applications: Performance and Design Optimization", Applied Thermal Engineering, unpublished manuscript submitted for publication, 2023
   ii. **H. Park**, and C.K. Bach, "Numerical Investigation of the Effects of Design Parameters on the Performance of an Air Sampling Device used for HVAC Equipment Testing", Manuscript in preparation, 2023
   iii. **H. Park**, and C.K. Bach, "In-Situ Assessment and Optimization of Air Mixing and Sampling Devices for Enhanced HVAC Performance Testing: A Comprehensive Study", Manuscript in preparation, 2023

Appendix B: Photographs of Experimental Instrumentation

Figure 90 shows the experimental setup used for testing air mixing and sampling devices. The setup consists of a test section, inlet section, and instrumentation for control and data analysis. The test section includes the devices being tested and measures temperature, pressure, and flow rate. The inlet section regulates the incoming air for accuracy and reproducibility. This setup provides a platform for device testing, informing design and optimization for improved performance.

(a)

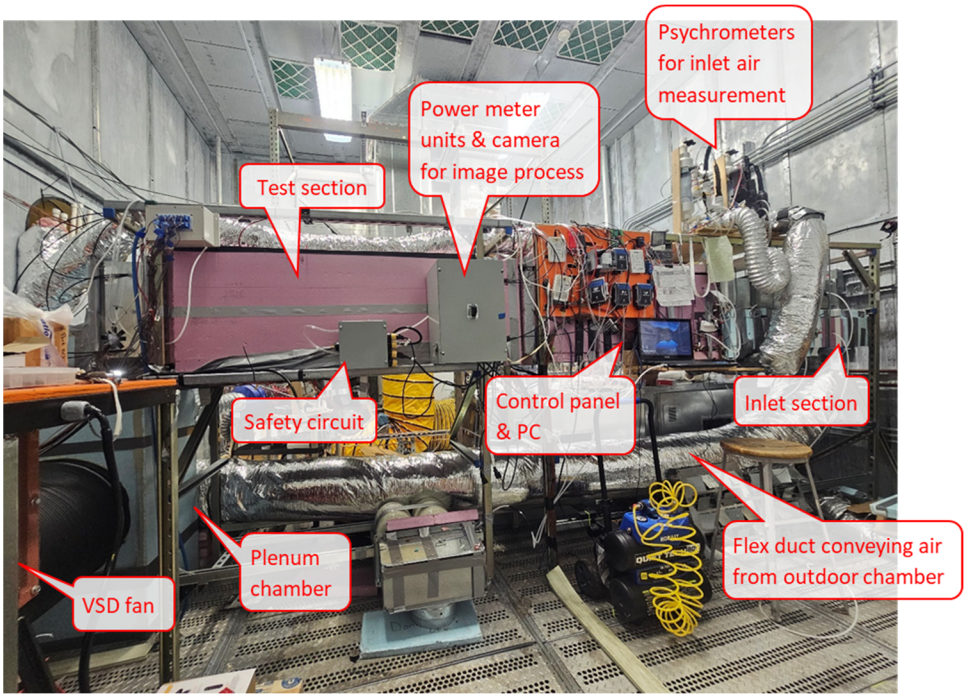

(b)

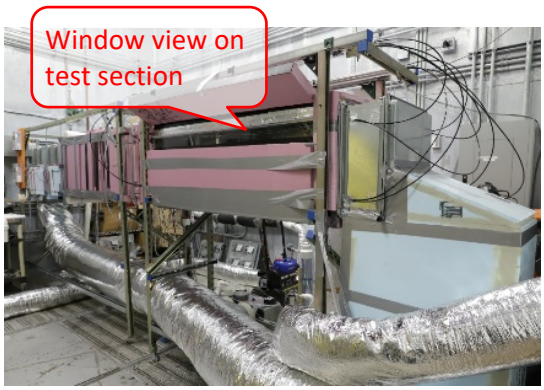

(c)

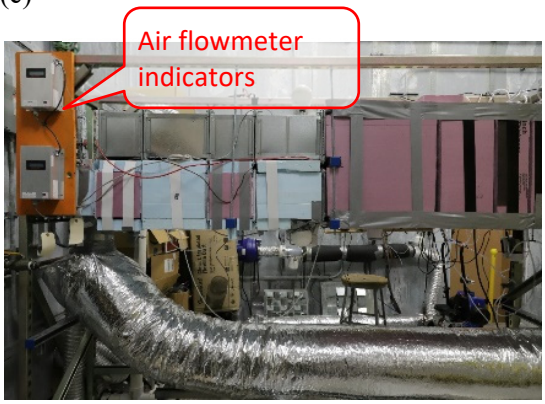

Figure 90 Overall experimental setup: (a) Front view of the setup, (b) Test section, and (c) Inlet section.

Figure 91 displays the mixer types employed for the mixer testing. These mixers were evaluated for their performance in terms of mixing effectiveness and pressure drop, and to facilitate the design and fabrication of new air mixing devices.

(a)

(d)

(b)

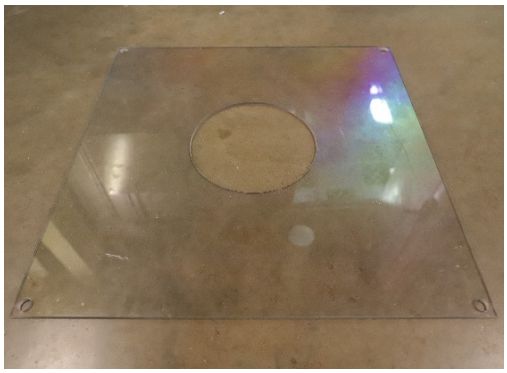

(e)

(c)

(f)

Figure 91 Air mixer types tested: (a) Baseline louvered mixer, (b) Orifice mixer, (c) Perforated target plate for orifice-target mixer, (d) Orthogonal pattern louver mixer with 6 by 6, (e) 4 by 4, and (f) 2 by 2 louver arrays.

Figure 92(a) shows the instrumentation for in-situ testing including the safety circuit and heating capacity indicators. The figure shows the safety circuit and power meter units used for controlling the heater and measuring the heating capacity during in-situ testing of air mixing and sampling devices. The safety circuit provides protection against electrical hazards, while the power meter

(a)

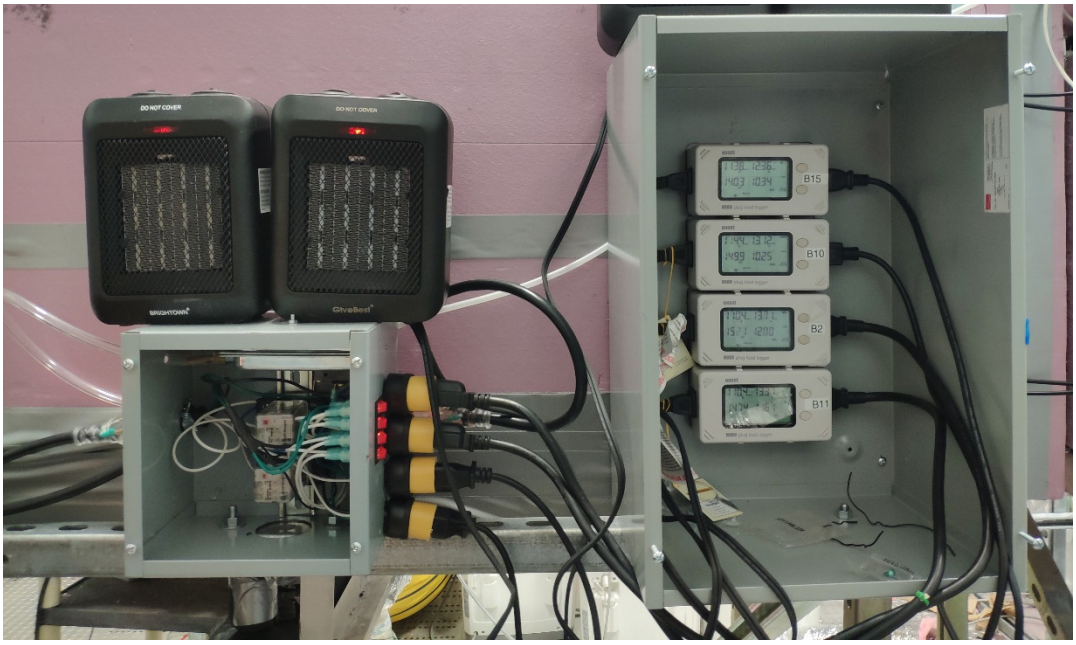

(b)

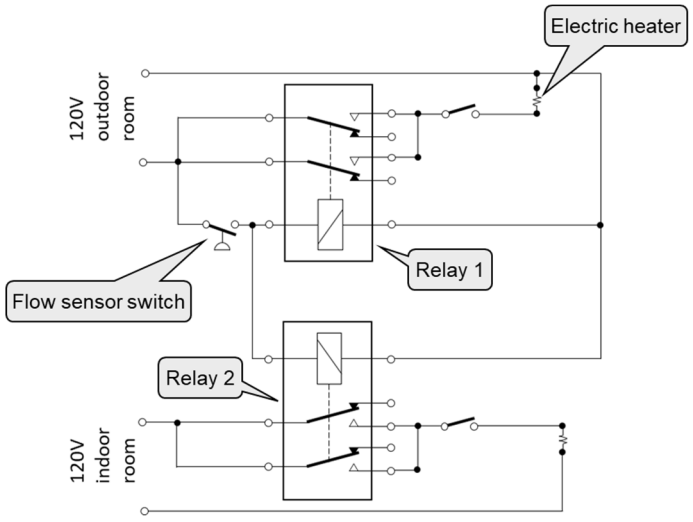

(c)

Figure 92 Instrumentation for in-situ testing of the combination of air mixing and sampling devices. (a) Safety circuit and power meter units for heater control and measurement of heating capacity, (b) Wiring diagram for the safety circuit, and (c) Monitoring the heating capacity using a webcam for data acquisition with LabVIEW VISION.

units measure the power consumption of the heater, which is used to calculate the heating capacity. In Figure 92(b), the wiring diagram illustrates the connections between various components of the safety circuit, including the power source, flow switch, and relay. Figure 92(c) shows the use of a webcam for data acquisition during in-situ testing of air mixing and sampling devices. The webcam captures images of the heater during operation, which are processed using LabVIEW VISION software to measure the heating capacity. The instrumentation provides a reliable and accurate method for measuring the heating capacity of air mixing and sampling devices during in-situ testing, which can inform the design and optimization of these devices for improved performance.

Figure 93 shows the software programmed using LabVIEW for system control, data acquisition, and data analysis. Figure 93(a) shows the front panel of the main host VI. This main host VI communicates with the target VI on the NI PXI Chassis and the client VI on a remote on-site PC,

(a)

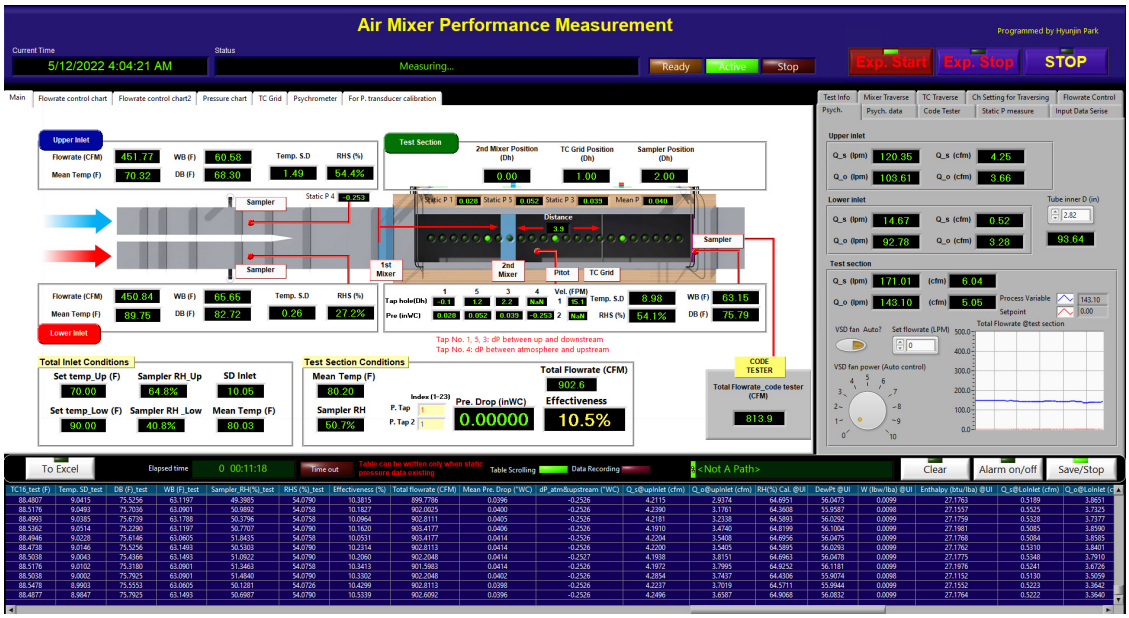

(b)

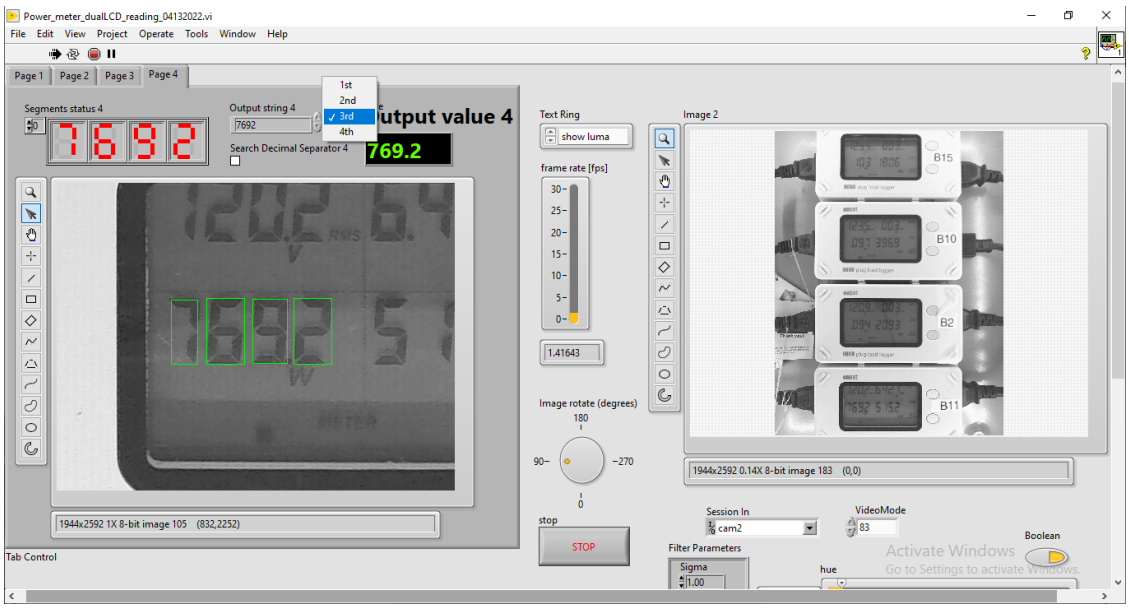

Figure 93 Instrumentation software programmed using LabVIEW for system control, data acquisition, and data analysis. (a) Main host VI communicating with the target VI on NI PXI Chassis and the client VI on a remote on-site PC. (b) Client VI on the on-site PC for image processing of acquired data and TCP communication with the host VI.

allowing for remote monitoring and control of the system. Figure 93(b) shows the client VI used for image processing of acquired data and TCP communication with the main host VI. The client VI uses LabVIEW VISION software for image processing and TCP communication protocols to communicate with the main host VI. The software provides a reliable and flexible platform for system control, data acquisition, and data analysis during air mixer, sampler, and in-situ testing.

Appendix C: Drawings of the Air Mixer Designs

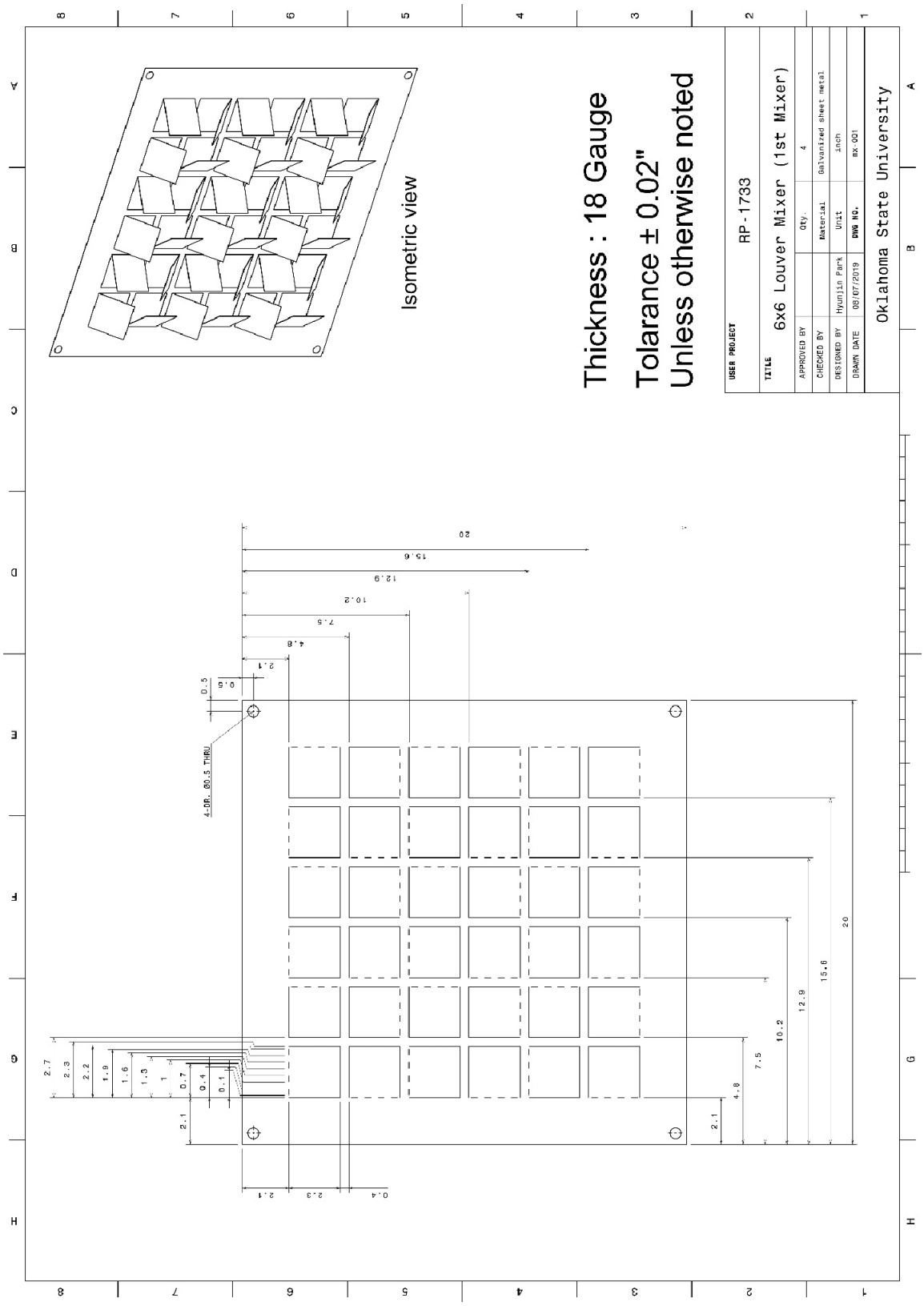

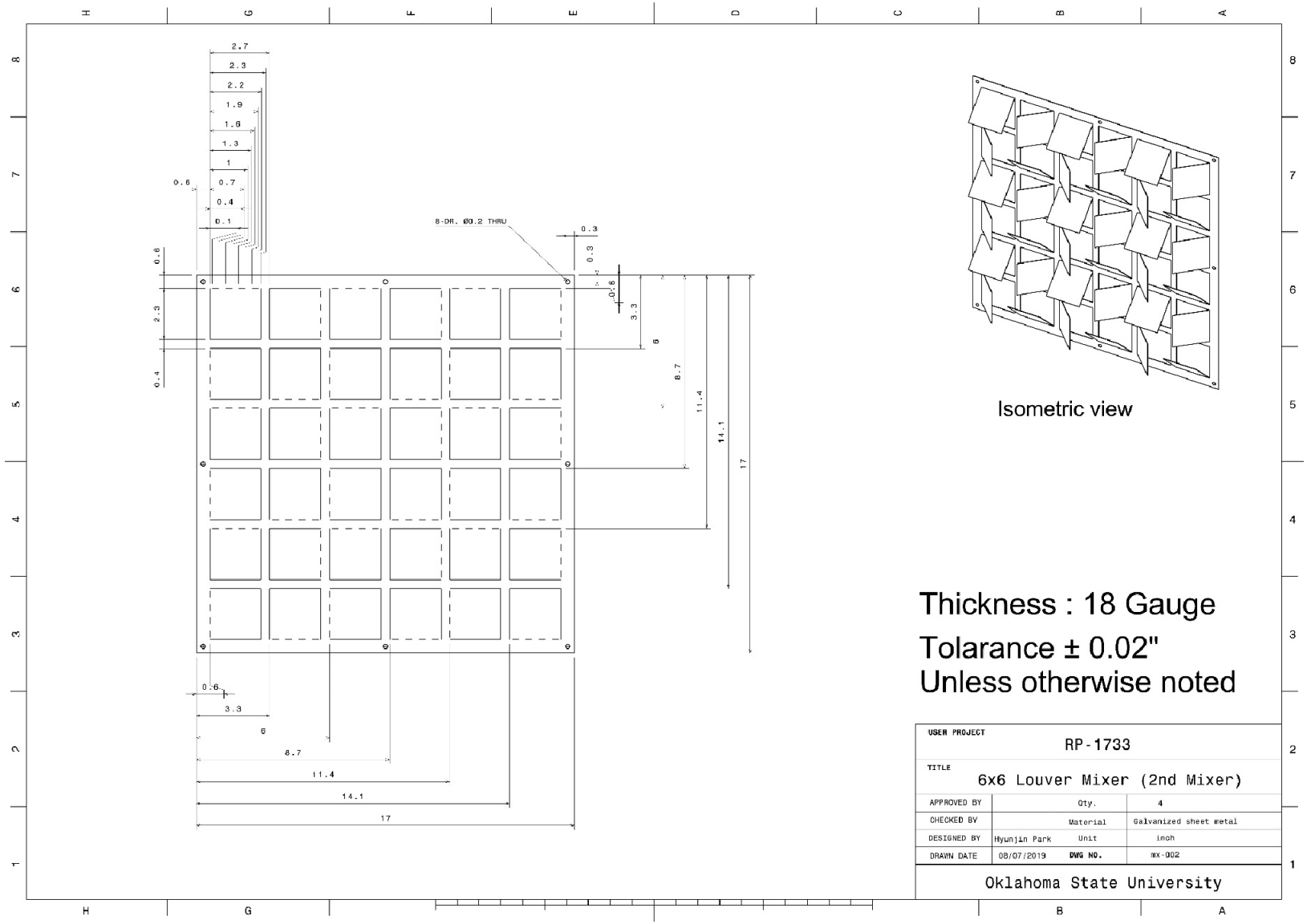
8-DR. ØØ.2 THRU
Isometric view
Thickness : 18 Gauge
Tolarance ± 0.02"
Unless otherwise noted
USER PROJECT
RP-1733
TITLE
6x6 Louver Mixer (2nd Mixer)
APPROVED BY
CHECKED BY
DESIGNED BY
Hyunjin Park
DRAWN DATE
08/07/2019
Qty.
4
Material
Galvanized sheet metal
Unit
inch
DWG NO.
mx-002
Oklahoma State University

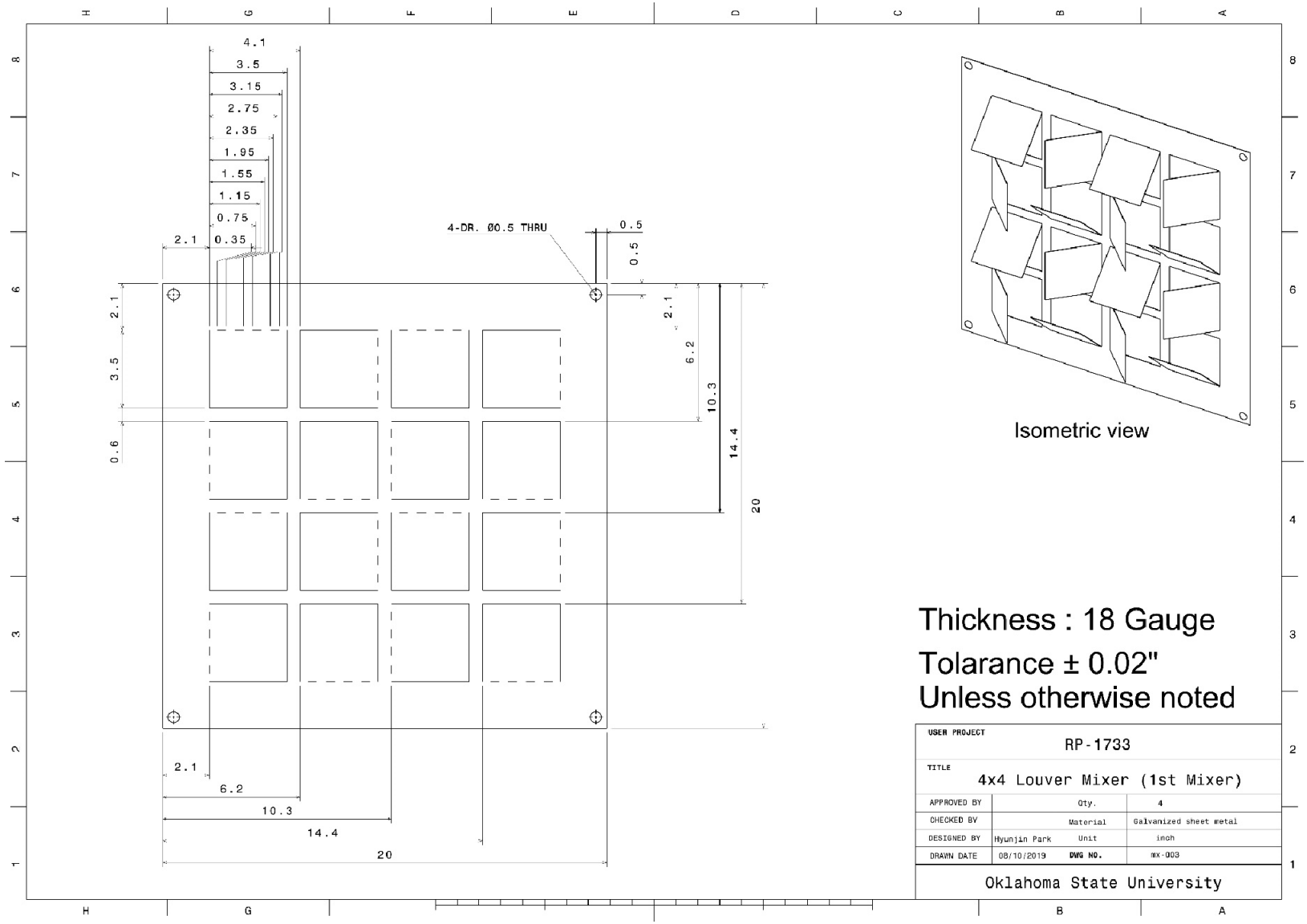
4.1
3.5
3.15
2.75
2.35
1.95
1.55
1.15
0.75
0.35
2.1
4-DR. Ø0.5 THRU
0.5
0.5
2.1
3.5
2.1
0.6
6.2
10.3
14.4
20
2.1
6.2
10.3
14.4
20
Isometric view
Thickness : 18 Gauge
Tolarance ± 0.02"
Unless otherwise noted
USER PROJECT
RP-1733
TITLE
4x4 Louver Mixer (1st Mixer)
APPROVED BY
CHECKED BY
DESIGNED BY
Hyunjin Park
DRAWN DATE
08/10/2019
Qty.
4
Material
Galvanized sheet metal
Unit
inch
DWG NO.
mx-003
Oklahoma State University

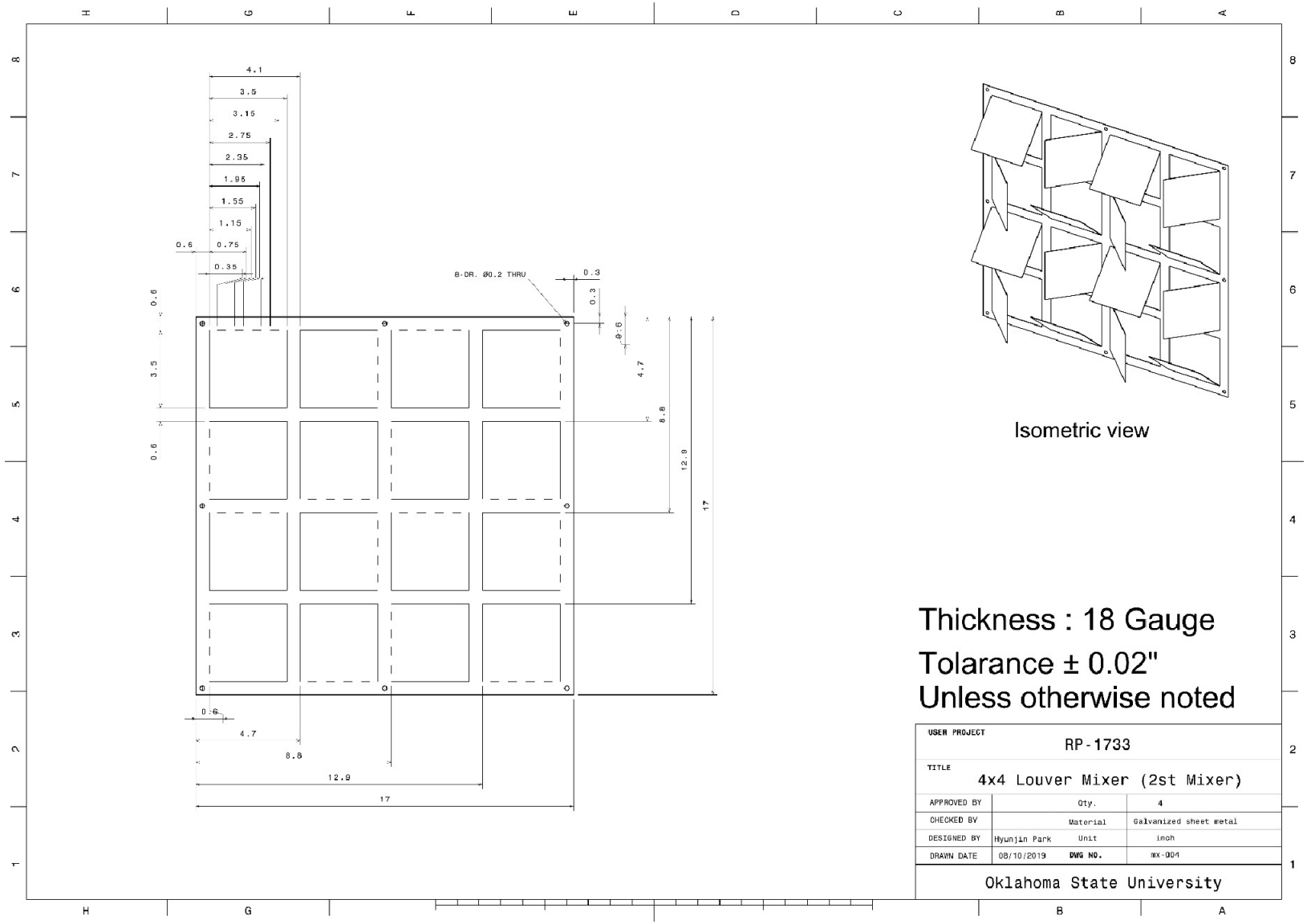

Isometric view

Thickness : 18 Gauge

Tolarance ± 0.02"
Unless otherwise noted

USER PROJECT	RP-1733		
TITLE	4x4 Louver Mixer (2st Mixer)		
APPROVED BY		Qty.	4
CHECKED BY		Material	Galvanized sheet metal
DESIGNED BY	Hyunjin Park	Unit	inch
DRAWN DATE	08/10/2019	DWG NO.	mx-004

Oklahoma State University

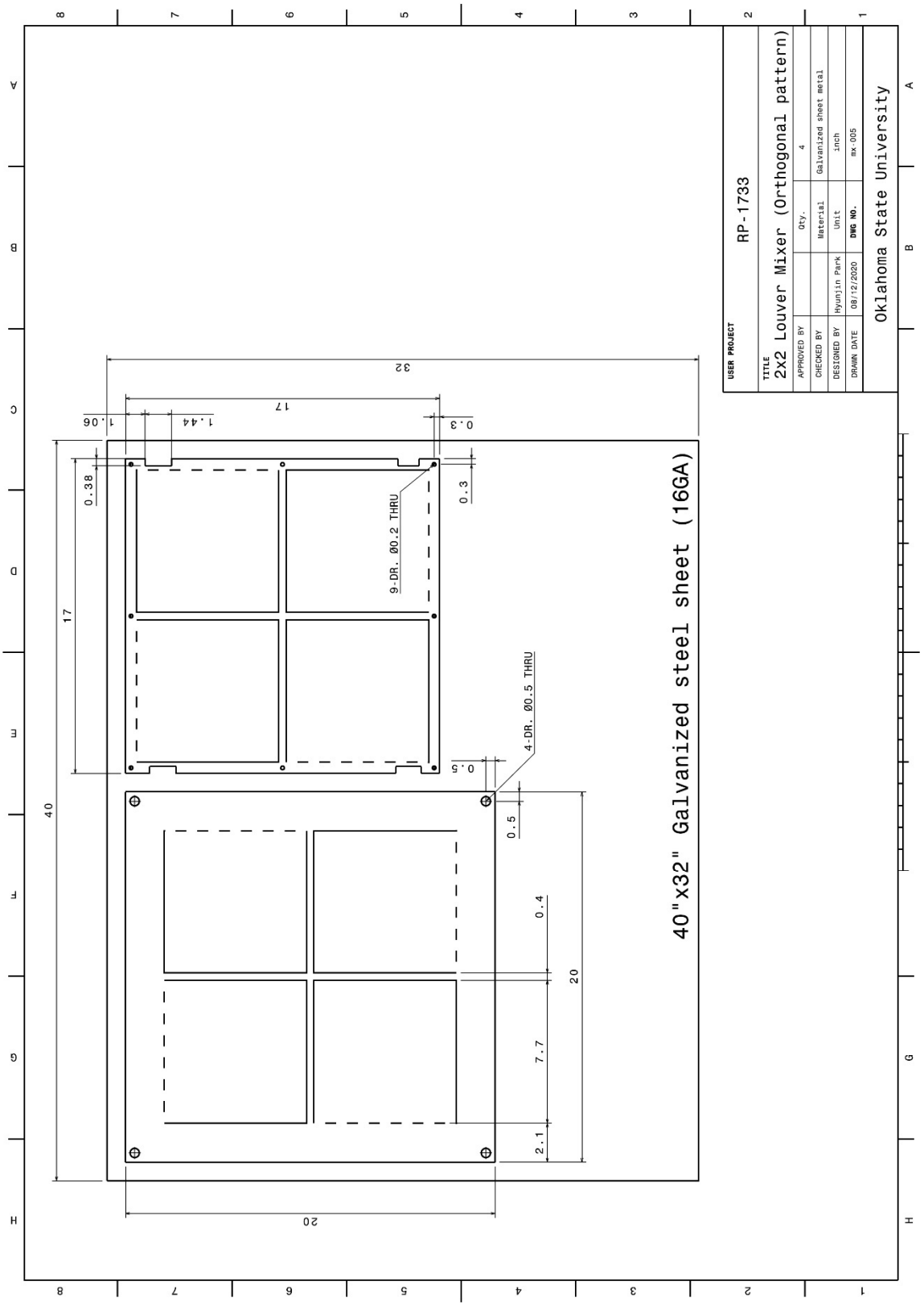
40"x32" Galvanized steel sheet (16GA)
9-DR. Ø0.2 THRU
4-DR. Ø0.5 THRU
32
17
1.06
1.44
0.3
0.38
0.5
0.4
7.7
2.1
20
40
USER PROJECT
RP-1733
TITLE
2x2 Louver Mixer (Orthogonal pattern)
APPROVED BY
CHECKED BY
DESIGNED BY
Hyunjin Park
DRAWN DATE
08/12/2020
Qty.
4
Material
Galvanized sheet metal
Unit
inch
DWG NO.
mx-005
Oklahoma State University

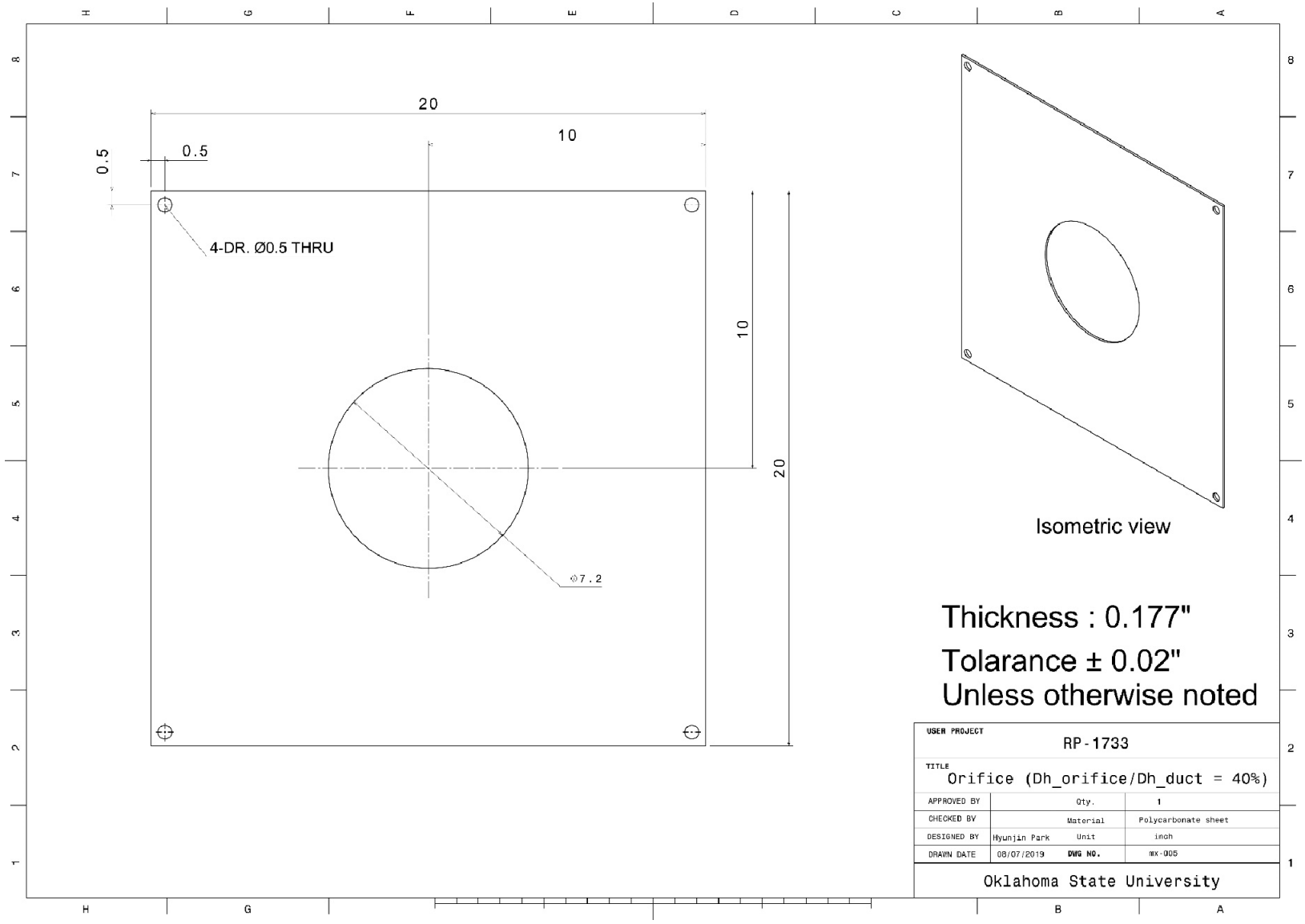
20
10
0.5
0.5
4-DR. Ø0.5 THRU
10
20
Ø7.2
Isometric view
Thickness : 0.177"
Tolarance ± 0.02"
Unless otherwise noted
USER PROJECT
RP-1733
TITLE
Orifice (Dh_orifice/Dh_duct = 40%)
APPROVED BY
CHECKED BY
DESIGNED BY
Hyunjin Park
DRAWN DATE
08/07/2019
Qty.
1
Material
Polycarbonate sheet
Unit
inch
DWG NO.
mx-005
Oklahoma State University

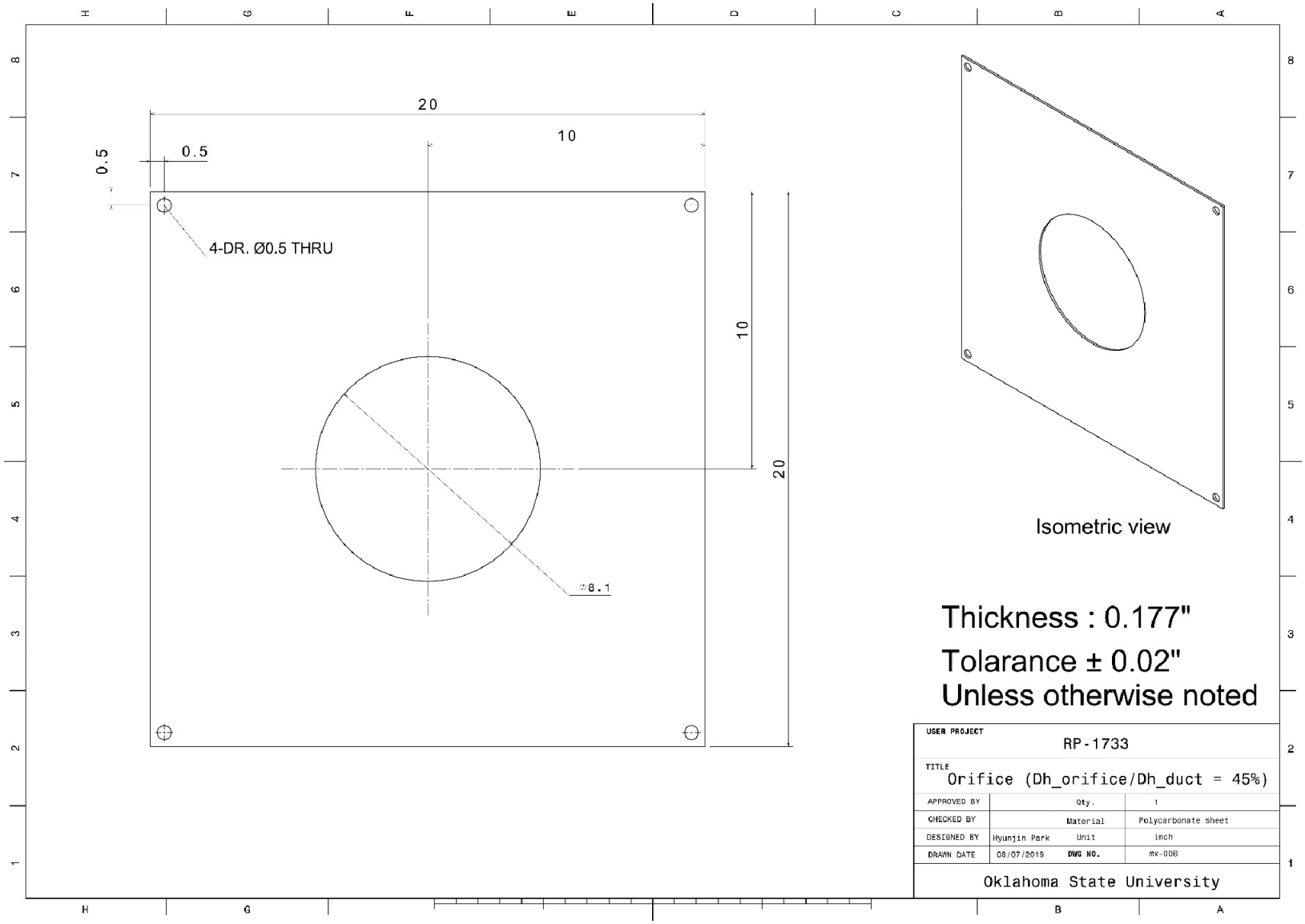
20
10
0.5
0.5
4-DR. Ø0.5 THRU
10
20
Ø8.1
Isometric view
Thickness : 0.177"
Tolarance ± 0.02"
Unless otherwise noted
USER PROJECT
RP-1733
TITLE
Orifice (Dh_orifice/Dh_duct = 45%)
APPROVED BY
CHECKED BY
DESIGNED BY
Hyunjin Park
DRAWN DATE
08/07/2019
Qty.
1
Material
Polycarbonate sheet
Unit
inch
DWG NO.
mx-008
Oklahoma State University

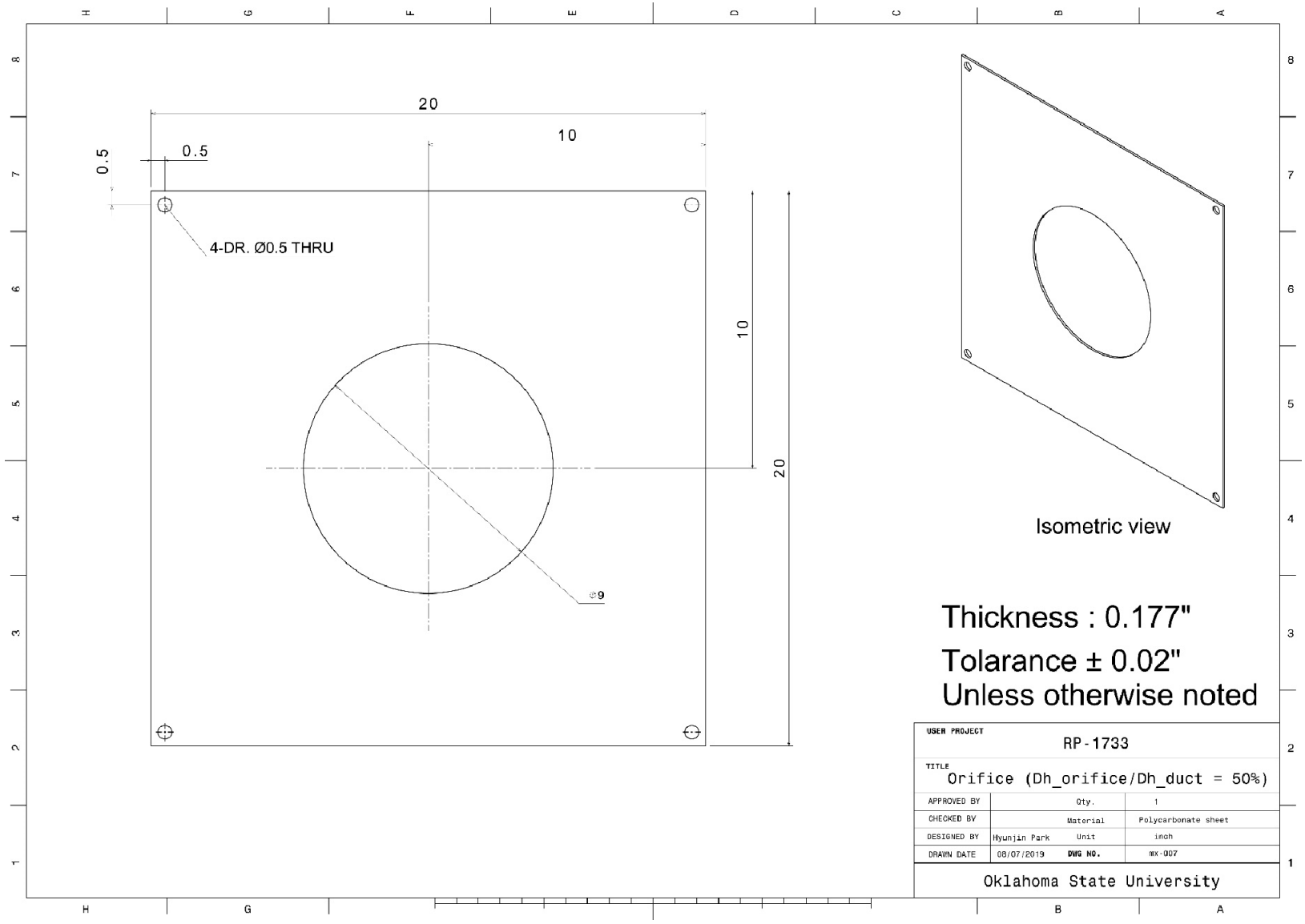
20
10
0.5
0.5
4-DR. Ø0.5 THRU
10
20
Ø9
Isometric view
Thickness : 0.177"
Tolarance ± 0.02"
Unless otherwise noted
USER PROJECT
RP-1733
TITLE
Orifice (Dh_orifice/Dh_duct = 50%)
APPROVED BY
CHECKED BY
DESIGNED BY
Hyunjin Park
DRAWN DATE
08/07/2019
Qty.
1
Material
Polycarbonate sheet
Unit
inch
DWG NO.
mx-007
Oklahoma State University

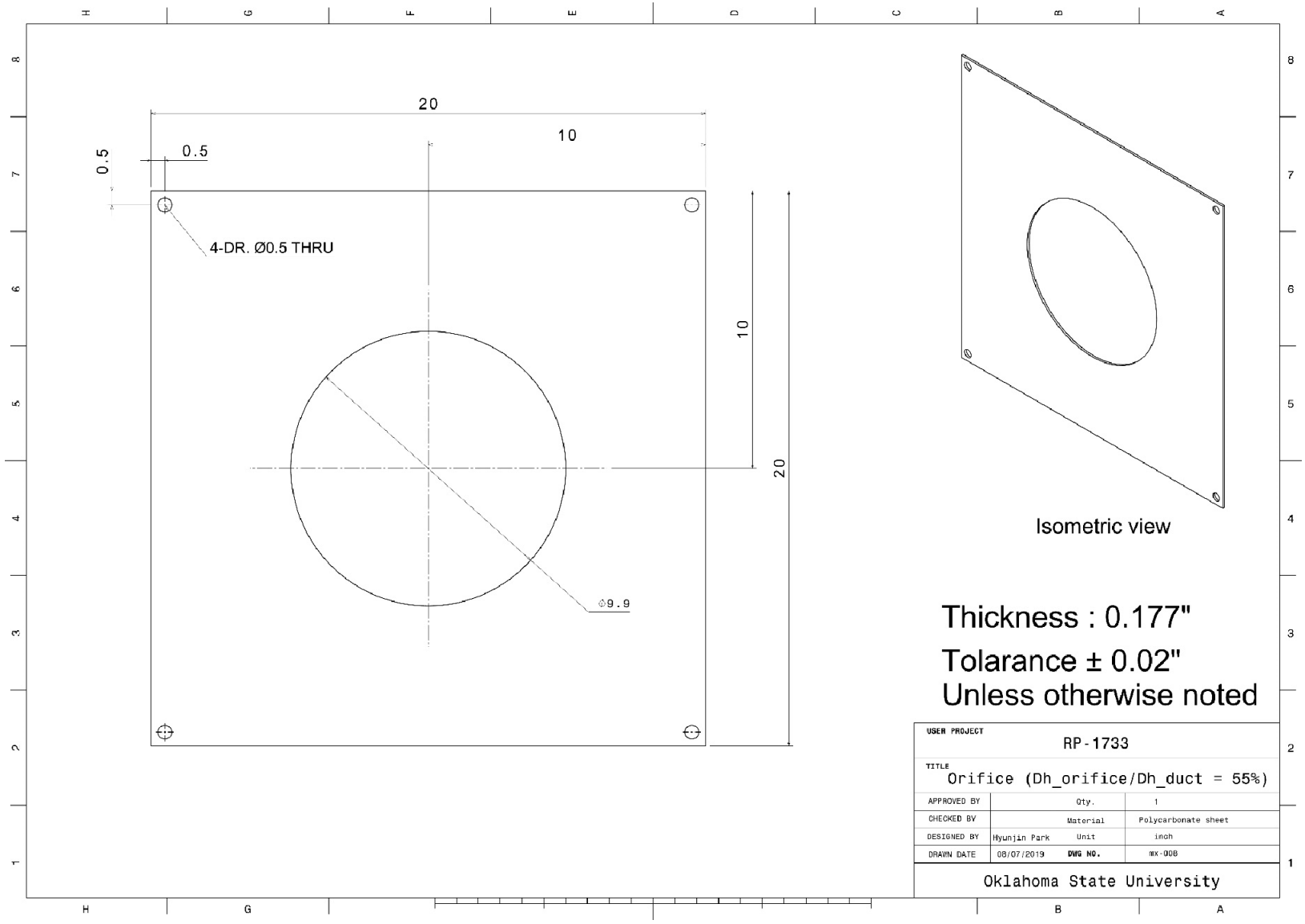
20
10
0.5
0.5
4-DR. Ø0.5 THRU
10
20
⌀9.9
Isometric view
Thickness : 0.177"
Tolarance ± 0.02"
Unless otherwise noted
USER PROJECT
RP-1733
TITLE
Orifice (Dh_orifice/Dh_duct = 55%)
APPROVED BY
CHECKED BY
DESIGNED BY
Hyunjin Park
DRAWN DATE
08/07/2019
Qty.
1
Material
Polycarbonate sheet
Unit
inch
DWG NO.
mx-008
Oklahoma State University

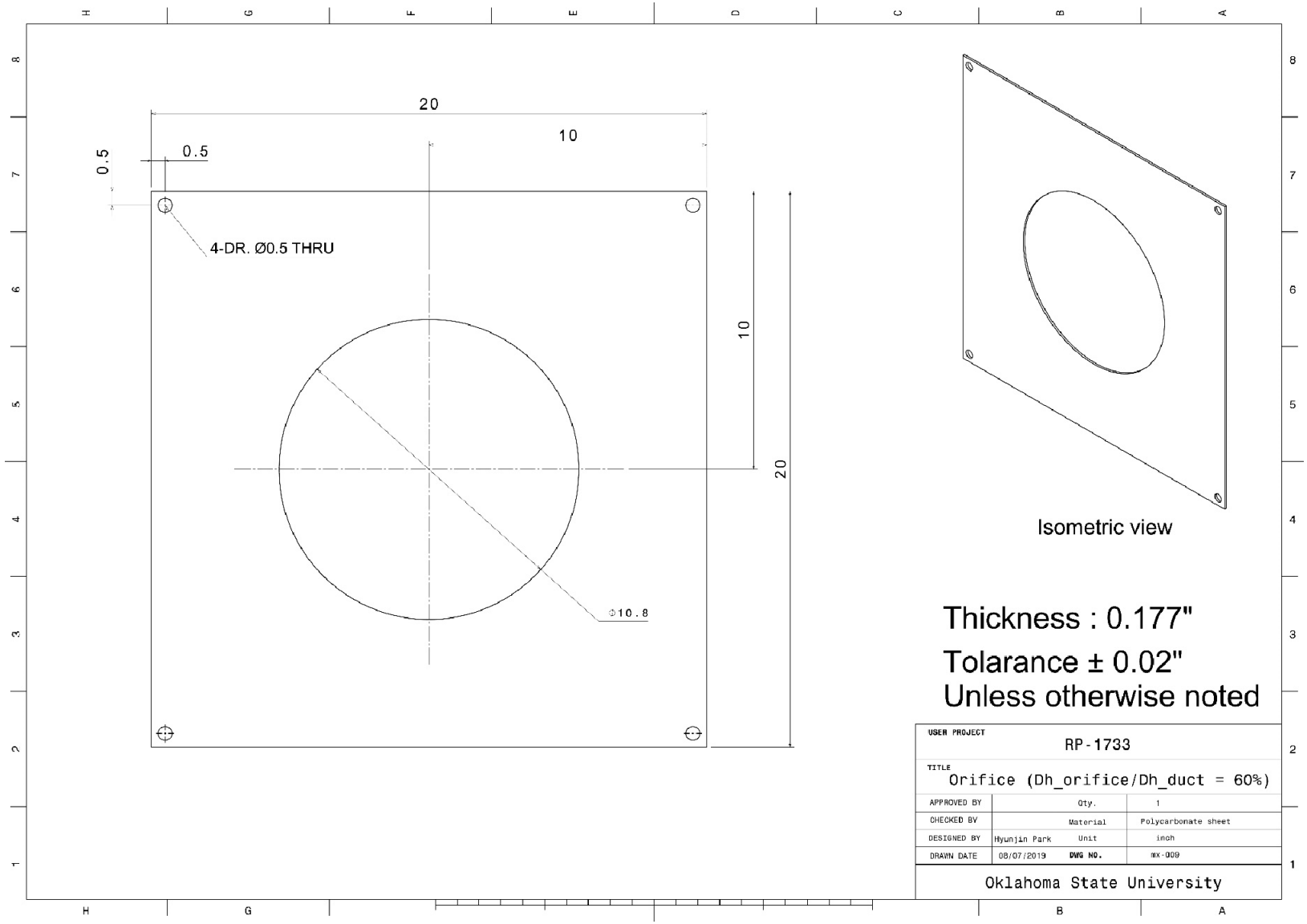
20
10
0.5
0.5
4-DR. Ø0.5 THRU
10
20
Ø10.8
Isometric view
Thickness : 0.177"
Tolarance ± 0.02"
Unless otherwise noted
USER PROJECT
RP-1733
TITLE
Orifice (Dh_orifice/Dh_duct = 60%)
APPROVED BY
CHECKED BY
DESIGNED BY
Hyunjin Park
DRAWN DATE
08/07/2019
Qty.
1
Material
Polycarbonate sheet
Unit
inch
DWG NO.
mx-009
Oklahoma State University

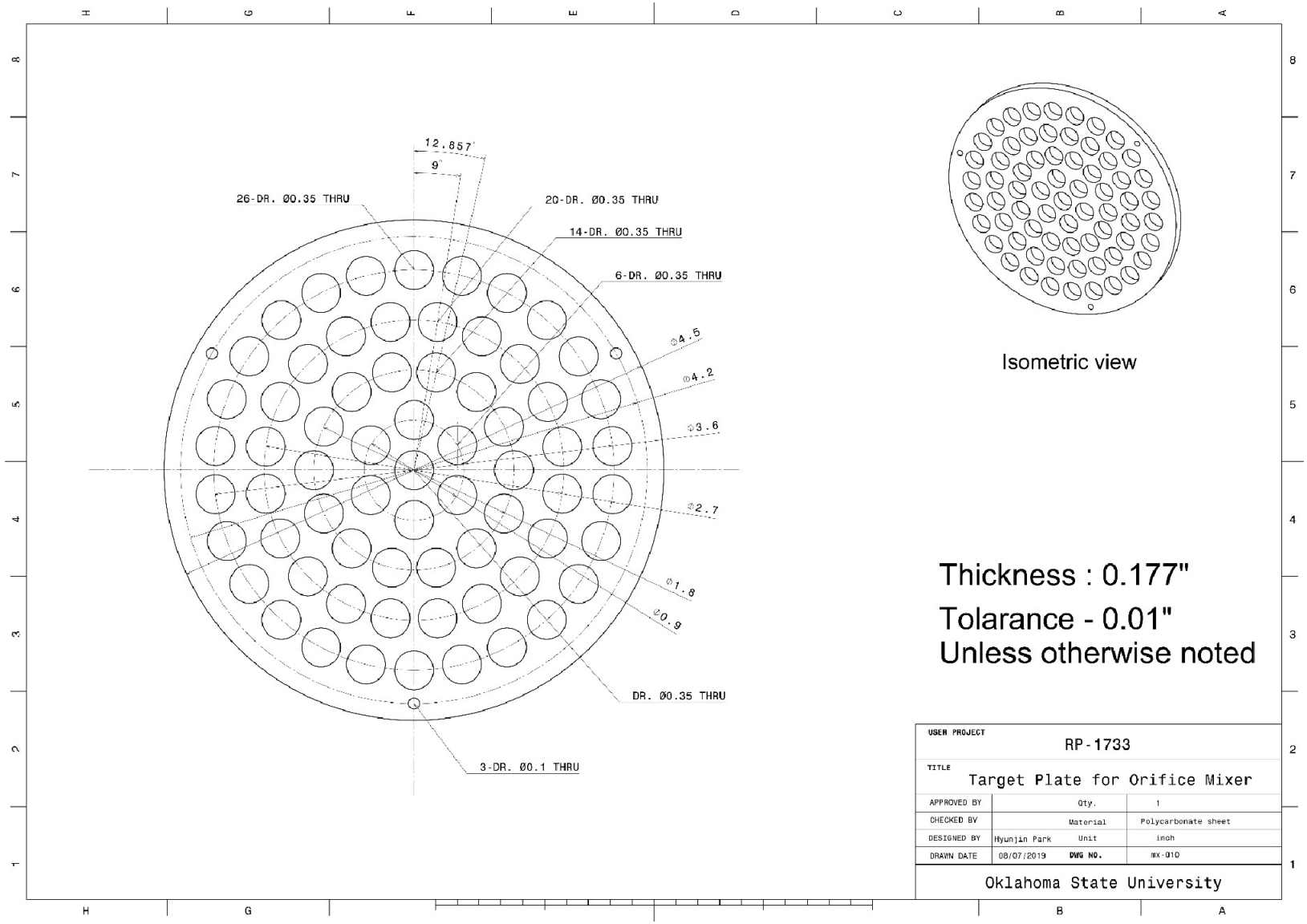
12.857°
9°
26-DR. Ø0.35 THRU
20-DR. Ø0.35 THRU
14-DR. Ø0.35 THRU
6-DR. Ø0.35 THRU
Ø4.5
Ø4.2
Ø3.6
Ø2.7
Ø1.8
Ø0.9
DR. Ø0.35 THRU
3-DR. Ø0.1 THRU
Isometric view
Thickness : 0.177"
Tolarance - 0.01"
Unless otherwise noted
USER PROJECT
RP-1733
TITLE
Target Plate for Orifice Mixer
APPROVED BY
CHECKED BY
DESIGNED BY
Hyunjin Park
DRAWN DATE
08/07/2019
Qty.
1
Material
Polycarbonate sheet
Unit
inch
DWG NO.
mx-010
Oklahoma State University

Appendix D: Data for Air Mixer, Sampler, and In-situ Testing

1. Experimental Data for Air Mixer Testing

1.1. Inherent mixing

No mixer applied

Mixing length (D_h)	Air temp. @ upper inlet (°F)	Air flowrate @ upper inlet (CFM)	Air temp. @ lower inlet (°F)	Air flowrate @ lower inlet (CFM)	Total flowrate (CFM)	Mixing effectiveness (%)	ΔP (inWC)
1.0	70	250	90	250	501.9	17.5	0.0101
1.5					499.6	22.6	0.0094
2.0					500.8	26.8	0.0096
2.5					500.2	30.9	0.0099
3.0					499.1	35.3	0.0108
3.3					501.8	37.8	0.0116
2.0	70	50	90	50	102.6	80.9	0.0032
		125		125	249.0	40.7	0.0062
		250		250	500.0	26.9	0.0102
		375		375	749.6	21.5	0.0217
		500		500	996.0	17.4	0.0280
2.0	70	50	90	450	498.0	68.8	0.0063
		150		350	497.6	34.8	0.0102
		250		250	500.8	26.5	0.0098
		350		150	498.3	43.5	0.0117
		450		50	499.9	80.8	0.0076

1.2. Baseline louver mixer

Dual baseline louver mixer

Mixer spacing (D_h)	Mixing length (D_h)	Air temp. @ upper inlet (°F)	Air flowrate @ upper inlet (CFM)	Air temp. @ lower inlet (°F)	Air flowrate @ lower inlet (CFM)	Total flowrate (CFM)	Mixing effectiveness (%) based on SD method	Mixing effectiveness (%) based on Range method	ΔP (inWC)
0.6	1.0	70	250	90	250	501.0	43.7	21.6	0.0136
	1.5					498.1	49.2	27.1	0.0155
	2.0					498.6	55.3	32.9	0.0170
	2.5					500.4	60.9	39.3	0.0176
	3.0					502.2	64.9	44.2	0.0178
	3.3					501.7	67.1	47.4	0.0186
1.0	1.5					501.0	58.2	40.1	0.0128
	2.0					500.4	61.3	45.8	0.0163
	2.5					499.0	66.2	51.7	0.0173
	3.0					498.7	70.8	57.4	0.0180
	3.3					500.6	73.2	60.8	0.0185
1.5	2.0					500.3	71.8	53.8	0.0125
	2.5					497.8	72.5	58.9	0.0159
	3.0					500.1	75.1	64.0	0.0171
	3.3					500.0	78.7	69.9	0.0181
2.0	2.5					499.3	78.6	68.3	0.0125
	3.0					500.6	77.6	64.5	0.0161
	3.3					500.6	79.8	68.2	0.0174
1.5	2.0	70	50	90	50	102.9	89.5	85.6	0.0010
			125		125	249.2	76.9	61.0	0.0061
			250		250	501.4	71.7	53.6	0.0134
			375		375	751.6	75.5	51.6	0.0314
			500		500	999.4	76.5	54.7	0.0398
1.5	2.0	70	50	90	450	500.3	86.4	76.1	0.0107
			150		350	500.0	75.4	54.0	0.0111
			250		250	500.0	73.7	51.1	0.0149
			350		150	500.1	77.8	63.0	0.0125
			450		50	498.9	87.7	83.7	0.0088

Single baseline louver mixer: Vertical deflection louver orientation

Mixing length (D_h)	Air temp. @ upper inlet (°F)	Air flowrate @ upper inlet (CFM)	Air temp. @ lower inlet (°F)	Air flowrate @ lower inlet (CFM)	Total flowrate (CFM)	Mixing effectiveness (%)	ΔP (inWC)
1.0	70	250	90	250	498.8	44.0	0.0117
1.5					497.9	64.1	0.0110
2.0					503.2	76.3	0.0123
2.5					501.8	80.6	0.0133
3.0					499.1	82.8	0.0139
3.3					500.7	83.5	0.0145
2.0	70	50	90	50	99.7	91.1	0.0026
		125		125	249.1	78.6	0.0073
		250		250	500.5	76.2	0.0144
		375		375	753.5	80.6	0.0326
		500		500	997.5	80.9	0.0417
2.0	70	50	90	450	502.4	87.9	0.0100
		150		350	500.4	79.8	0.0115
		250		250	499.3	80.8	0.0110
		350		150	500.1	84.5	0.0102
		450		50	500.7	91.9	0.0079

Single baseline louver mixer: Horizontal deflection louver orientation

Mixing length (D_h)	Air temp. @ upper inlet (°F)	Air flowrate @ upper inlet (CFM)	Air temp. @ lower inlet (°F)	Air flowrate @ lower inlet (CFM)	Total flowrate (CFM)	Mixing effectiveness (%)	ΔP (inWC)
1.0	70	250	90	250	501.1	23.1	0.0141
1.5					500.3	29.6	0.0138
2.0					501.6	38.1	0.0149
2.5					500.0	46.0	0.0151
3.0					501.3	52.6	0.0157
3.3					501.3	56.8	0.0161
2.0	70	50	90	50	99.9	71.0	0.0016
		125		125	247.8	46.5	0.0076
		250		250	501.4	37.9	0.0145
		375		375	750.9	32.9	0.0317
		500		500	994.8	31.1	0.0406
2.0	70	50	90	450	501.4	65.6	0.0104
		150		350	502.8	40.9	0.0101
		250		250	500.2	33.5	0.0138
		350		150	498.0	44.2	0.0120
		450		50	500.6	75.9	0.0091

1.3. Orifice mixer

Orifice mixer: Orifice hole dia. = 0.4 D_h

Mixing length (D_h)	Air temp. @ upper inlet (°F)	Air flowrate @ upper inlet (CFM)	Air temp. @ lower inlet (°F)	Air flowrate @ lower inlet (CFM)	Total flowrate (CFM)	Mixing effectiveness (%)	ΔP (inWC)
1.0	70	250	90	250	499.1	73.8	0.6616
1.5					500.9	73.3	0.6629
2.0					500.7	75.1	0.6541
2.5					500.2	80.0	0.6348
3.0					496.7	86.2	0.6116
3.3					499.9	89.7	0.5999
2.0	70	50	90	50	101.5	89.9	0.0463
		125		125	249.5	80.5	0.2283
		250		250	500.8	75.0	0.6676
		350		350	696.0	73.8	0.7676
2.0	70	50	90	450	492.4	92.2	0.4554
		150		350	500.5	82.0	0.4480
		250		250	500.0	74.2	0.5499
		350		150	501.5	86.7	0.5080
		450		50	497.0	97.7	0.4827

Orifice mixer: Orifice hole dia. = 0.5 D_h

Mixing length (D_h)	Air temp. @ upper inlet (°F)	Air flowrate @ upper inlet (CFM)	Air temp. @ lower inlet (°F)	Air flowrate @ lower inlet (CFM)	Total flowrate (CFM)	Mixing effectiveness (%)	ΔP (inWC)
1.0	70	250	90	250	499.1	65.1	0.2657
1.5					500.8	65.3	0.2605
2.0					500.9	69.6	0.2480
2.5					500.1	75.9	0.2363
3.0					498.8	83.2	0.2279
3.3					499.3	87.0	0.2241
2.0	70	50	90	50	98.3	91.7	0.0188
		125		125	248.6	80.7	0.1010
		250		250	500.8	70.1	0.2510
		375		375	750.2	64.6	0.4327
		400		400	800.1	64.1	0.4459
2.0	70	50	90	450	498.0	86.7	0.1954
		150		350	497.0	74.7	0.2573
		250		250	499.2	70.1	0.2492
		350		150	499.5	81.5	0.2792
		450		50	499.7	96.2	0.2481

Orifice mixer: Orifice hole dia. = 0.6 D_h

Mixing length (D_h)	Air temp. @ upper inlet (°F)	Air flowrate @ upper inlet (CFM)	Air temp. @ lower inlet (°F)	Air flowrate @ lower inlet (CFM)	Total flowrate (CFM)	Mixing effectiveness (%)	ΔP (inWC)
1.0	70	250	90	250	498.8	50.5	0.1255
1.5					500.5	53.1	0.1183
2.0					501.0	58.6	0.1115
2.5					499.9	64.9	0.1054
3.0					499.6	73.3	0.1011
3.3					499.9	78.1	0.1011
2.0	70	50	90	50	100.5	80.8	0.0104
		125		125	247.8	71.4	0.0469
		250		250	503.9	58.7	0.1148
		375		375	750.6	51.9	0.2060
		435		435	872.8	51.1	0.2357
2.0	70	50	90	450	500.5	84.5	0.0868
		150		350	499.7	66.6	0.1137
		250		250	496.8	59.1	0.1099
		350		150	498.7	71.9	0.1197
		450		50	500.1	93.2	0.1049

1.4. Orifice-target mixer

Orifice-target mixer: Orifice hole dia. = 0.4 D_h

Orifice-target spacing (D_h)	Mixing length (D_h)	Air temp. @ upper inlet (°F)	Air flowrate @ upper inlet (CFM)	Air temp. @ lower inlet (°F)	Air flowrate @ lower inlet (CFM)	Total flowrate (CFM)	Mixing effectiveness (%)	ΔP (inWC)
0.6	1.0	70	250	90	250	499.0	60.5	0.6030
	1.5					499.5	63.5	0.5989
	2.0					499.8	69.5	0.5831
	2.5					499.8	77.6	0.5670
	3.0					499.9	85.5	0.5570
	3.3					499.5	89.7	0.5534
1.0	1.5					500.8	63.7	0.5977
	2.0					499.8	68.2	0.5811
	2.5					501.1	76.2	0.5659
	3.0					499.3	84.3	0.5550
	3.3					499.5	88.8	0.5520
1.5	2.0					501.1	69.9	0.5796
	2.5					498.7	76.8	0.5606
	3.0					501.0	85.4	0.5483
	3.3					500.5	89.4	0.5469
2.0	2.5					499.7	76.3	0.5650
	3.0					499.3	84.5	0.5478
	3.3					500.1	88.9	0.5414

Orifice-target mixer: Orifice hole dia. = 0.5 D_h

Orifice-target spacing (D_h)	Mixing length (D_h)	Air temp. @ upper inlet (°F)	Air flowrate @ upper inlet (CFM)	Air temp. @ lower inlet (°F)	Air flowrate @ lower inlet (CFM)	Total flowrate (CFM)	Mixing effectiveness (%)	ΔP (inWC)
0.6	1.0	70	250	90	250	502.1	54.8	0.2668
	1.5					500.5	58.0	0.2600
	2.0					499.3	64.4	0.2477
	2.5					499.4	72.7	0.2384
	3.0					500.9	81.2	0.2332
	3.3					500.2	85.0	0.2338
1.0	1.5					499.8	59.0	0.2590
	2.0					500.5	63.9	0.2475
	2.5					499.5	71.3	0.2372
	3.0					501.5	80.6	0.2317
	3.3					497.9	85.2	0.2320
1.5	2.0					501.5	63.7	0.2463
	2.5					498.8	70.1	0.2366
	3.0					501.2	79.3	0.2306
	3.3					500.5	84.1	0.2280
2.0	2.5					499.4	70.9	0.2366
	3.0					501.4	79.4	0.2296
	3.3					501.5	84.0	0.2289

Orifice-target mixer: Orifice hole dia. = 0.6 D_h

Orifice-target spacing (D_h)	Mixing length (D_h)	Air temp. @ upper inlet (°F)	Air flowrate @ upper inlet (CFM)	Air temp. @ lower inlet (°F)	Air flowrate @ lower inlet (CFM)	Total flowrate (CFM)	Mixing effectiveness (%)	ΔP (inWC)
0.6	1.0	70	250	90	250	500.6	45.8	0.1206
	1.5					499.2	49.4	0.1137
	2.0					501.0	57.1	0.1063
	2.5					500.5	66.2	0.1024
	3.0					500.9	74.7	0.1012
	3.3					498.0	79.0	0.1020
1.0	1.5					499.6	49.5	0.1135
	2.0					500.5	56.5	0.1058
	2.5					499.3	65.3	0.1014
	3.0					500.3	73.7	0.1006
	3.3					502.9	77.7	0.1007
1.5	2.0					501.0	57.4	0.1067
	2.5					500.2	65.8	0.1010
	3.0					500.5	74.0	0.1006
	3.3					500.2	78.3	0.1010
2.0	2.5					500.1	65.2	0.1038
	3.0					498.7	74.5	0.1014
	3.3					500.6	78.4	0.1021

1.5. Orthogonal pattern louver mixer

1.5.1. Louver size: 6 by 6 array

Dual orthogonal pattern louver mixer: CCW-CCW orientation, and louver angle of 30°

Mixer spacing (D_h)	Mixing length (D_h)	Air temp. @ upper inlet (°F)	Air flowrate @ upper inlet (CFM)	Air temp. @ lower inlet (°F)	Air flowrate @ lower inlet (CFM)	Total flowrate (CFM)	Mixing effectiveness (%)	ΔP (inWC)
0.8	1.0	70	250	90	250	500.8	37.5	0.0327
	1.5					498.1	48.8	0.0318
	2.0					500.5	55.5	0.0319
	2.5					499.7	59.6	0.0313
	3.0					499.3	62.6	0.0318
	3.3					501.4	64.1	0.0320
1.0	1.5					499.5	49.4	0.0313
	2.0					502.8	55.9	0.0320
	2.5					500.8	60.2	0.0318
	3.0					499.3	63.2	0.0318
	3.3					500.5	64.6	0.0322
1.5	2.0					500.8	54.4	0.0311
	2.5					499.6	59.2	0.0323
	3.0					498.9	62.1	0.0325
	3.3					501.0	63.2	0.0321
2.0	2.5					499.8	57.1	0.0313
	3.0					499.4	62.2	0.0329
	3.3					499.5	64.2	0.0329
1.5	2.0	70	50	90	50	100.3	78.2	0.0018
			125		125	248.8	55.2	0.0069
			250		250	500.5	55.5	0.0256
			375		375	751.5	50.0	0.0622
			500		500	998.5	47.9	0.0850
1.5	2.0	70	50	90	450	501.6	76.8	0.0229
			150		350	499.5	59.0	0.0227
			250		250	500.9	51.8	0.0298
			350		150	500.5	61.6	0.0266
			450		50	500.5	81.8	0.0212

Dual orthogonal pattern louver mixer: CCW-CCW orientation, and louver angle of 40°

Mixer spacing (D_h)	Mixing length (D_h)	Air temp. @ upper inlet (°F)	Air flowrate @ upper inlet (CFM)	Air temp. @ lower inlet (°F)	Air flowrate @ lower inlet (CFM)	Total flowrate (CFM)	Mixing effectiveness (%)	ΔP (inWC)
0.8	1.0	70	250	90	250	498.9	48.4	0.0472
	1.5					499.2	58.0	0.0471
	2.0					500.5	65.1	0.0466
	2.5					500.3	69.1	0.0450
	3.0					499.8	71.5	0.0453
	3.3					499.7	72.6	0.0456
1.0	1.5					500.9	55.6	0.0467
	2.0					500.6	63.5	0.0468
	2.5					499.3	67.7	0.0459
	3.0					501.1	70.4	0.0453
	3.3					499.9	71.5	0.0459
1.5	2.0					498.6	59.6	0.0455
	2.5					499.7	66.4	0.0466
	3.0					499.2	69.7	0.0456
	3.3					499.8	71.0	0.0463
2.0	2.5					498.5	61.9	0.0451
	3.0					499.1	68.1	0.0466
	3.3					500.3	69.9	0.0467
1.5	2.0	70	50	90	50	99.5	83.3	0.0019
			125		125	248.1	61.8	0.0097
			250		250	499.6	60.3	0.0405
			375		375	749.1	55.4	0.0907
			500		500	1000.8	53.8	0.1265
1.5	2.0	70	50	90	450	501.4	79.5	0.0345
			150		350	501.8	63.6	0.0369
			250		250	498.8	56.7	0.0476
			350		150	498.7	68.0	0.0399
			450		50	500.4	83.9	0.0353

Dual orthogonal pattern louver mixer: CCW-CCW orientation, and louver angle of 50°

Mixer spacing (D_h)	Mixing length (D_h)	Air temp. @ upper inlet (°F)	Air flowrate @ upper inlet (CFM)	Air temp. @ lower inlet (°F)	Air flowrate @ lower inlet (CFM)	Total flowrate (CFM)	Mixing effectiveness (%)	ΔP (inWC)
0.8	1.0	70	250	90	250	500.8	54.0	0.0786
	1.5					501.6	68.6	0.0782
	2.0					500.4	75.4	0.0761
	2.5					498.5	78.1	0.0749
	3.0					500.3	79.9	0.0758
	3.3					499.3	80.7	0.0762
1.0	1.5					501.3	64.5	0.0768
	2.0					500.5	74.7	0.0768
	2.5					499.8	77.5	0.0759
	3.0					499.8	78.6	0.0753
	3.3					499.3	79.1	0.0760
1.5	2.0					501.4	70.2	0.0751
	2.5					500.8	76.4	0.0767
	3.0					501.3	77.6	0.0754
	3.3					500.2	78.8	0.0753
2.0	2.5					500.7	71.4	0.0755
	3.0					500.6	75.1	0.0760
	3.3					500.1	75.8	0.0753
1.5	2.0	70	50	90	50	99.5	79.0	0.0041
			125		125	249.7	72.2	0.0183
			250		250	500.5	70.5	0.0770
			375		375	750.4	68.0	0.1294
			460		460	920.5	67.1	0.1649
1.5	2.0	70	50	90	450	499.9	85.1	0.0517
			150		350	498.9	74.7	0.0614
			250		250	499.3	69.6	0.0578
			350		150	497.5	73.5	0.0556
			450		50	500.6	87.0	0.0489

Dual orthogonal pattern louver mixer: CW-CCW orientation, and louver angle of 30°

Mixer spacing (D_h)	Mixing length (D_h)	Air temp. @ upper inlet (°F)	Air flowrate @ upper inlet (CFM)	Air temp. @ lower inlet (°F)	Air flowrate @ lower inlet (CFM)	Total flowrate (CFM)	Mixing effectiveness (%)	ΔP (inWC)
0.8	1.0	70	250	90	250	498.7	49.6	0.0758
	1.5					498.9	57.8	0.0745
	2.0					497.7	61.1	0.0748
	2.5					500.3	63.7	0.0740
	3.0					499.4	65.1	0.0740
	3.3					499.9	65.9	0.0751
1.0	1.5					499.8	58.4	0.0723
	2.0					500.7	62.2	0.0735
	2.5					499.3	64.7	0.0737
	3.0					499.3	66.2	0.0734
	3.3					501.0	67.1	0.0735
1.5	2.0					498.7	62.6	0.0704
	2.5					500.1	66.0	0.0715
	3.0					498.9	67.8	0.0718
	3.3					499.9	68.8	0.0725
2.0	2.5					498.3	67.1	0.0692
	3.0					501.3	70.2	0.0711
	3.3					499.2	71.7	0.0719
1.5	2.0	70	50	90	50	99.5	79.9	0.0035
			125		125	249.1	65.0	0.0295
			250		250	498.9	63.4	0.0832
			375		375	750.0	61.7	0.1367
			460		460	917.7	61.1	0.1733
1.5	2.0	70	50	90	450	503.1	79.7	0.0562
			150		350	500.5	66.1	0.0580
			250		250	499.2	62.7	0.0634
			350		150	498.2	67.5	0.0608
			450		50	499.5	85.7	0.0523

Dual orthogonal pattern louver mixer: CCW-CCW orientation, and louver angle of 60°

Mixer spacing (D_h)	Mixing length (D_h)	Air temp. @ upper inlet (°F)	Air flowrate @ upper inlet (CFM)	Air temp. @ lower inlet (°F)	Air flowrate @ lower inlet (CFM)	Total flowrate (CFM)	Mixing effectiveness (%)	ΔP (inWC)
0.8	1.0	70	250	90	250	501.6	66.1	0.1203
	1.5					500.7	80.0	0.1204
	2.0					500.2	83.5	0.1195
	2.5					500.5	85.4	0.1180
	3.0					500.0	86.7	0.1182
	3.3					499.8	87.4	0.1181
1.0	1.5					499.1	76.3	0.1212
	2.0					501.0	82.2	0.1212
	2.5					498.3	84.2	0.1195
	3.0					500.0	84.7	0.1200
	3.3					500.5	85.0	0.1198
1.5	2.0					500.2	77.1	0.1197
	2.5					501.1	82.2	0.1205
	3.0					500.6	84.2	0.1190
	3.3					499.4	84.9	0.1191
2.0	2.5					498.8	79.5	0.1196
	3.0					499.1	81.8	0.1195
	3.3					497.8	83.6	0.1191
1.5	2.0	70	50	90	50	100.4	87.4	0.0046
			125		125	250.2	79.2	0.0311
			250		250	501.3	76.2	0.1054
			375		375	751.0	74.4	0.2201
			430		430	960.1	73.6	0.2723
1.5	2.0	70	50	90	450	499.5	87.5	0.0962
			150		350	500.2	78.4	0.1193
			250		250	500.0	76.4	0.1186
			350		150	499.0	81.7	0.1230
			450		50	497.7	90.0	0.1142

Single orthogonal pattern louver mixer: CCW orientation, and louver angle of 30°

Mixing length (D_h)	Air temp. @ upper inlet (°F)	Air flowrate @ upper inlet (CFM)	Air temp. @ lower inlet (°F)	Air flowrate @ lower inlet (CFM)	Total flowrate (CFM)	Mixing effectiveness (%)	ΔP (inWC)
1.0	70	250	90	250	499.3	35.3	0.0203
1.5					499.6	44.0	0.0222
2.0					500.2	49.7	0.0221
2.5					501.4	53.7	0.0224
3.0					499.8	56.9	0.0232
3.3					499.9	58.2	0.0244
2.0	70	50	90	50	99.0	79.7	0.0006
		125		125	250.2	53.6	0.0043
		250		250	501.2	52.7	0.0177
		375		375	749.1	47.8	0.0408
		500		500	1000.1	45.0	0.0579
2.0	70	50	90	450	499.2	75.0	0.0135
		150		350	498.3	57.8	0.0191
		250		250	498.5	49.6	0.0214
		350		150	498.2	63.1	0.0179
		450		50	500.9	82.4	0.0138

Single orthogonal pattern louver mixer: CCW orientation, and louver angle of 40°

Mixing length (D_h)	Air temp. @ upper inlet (°F)	Air flowrate @ upper inlet (CFM)	Air temp. @ lower inlet (°F)	Air flowrate @ lower inlet (CFM)	Total flowrate (CFM)	Mixing effectiveness (%)	ΔP (inWC)
1.0	70	250	90	250	500.4	44.4	0.0270
1.5					500.3	51.5	0.0278
2.0					499.2	57.3	0.0280
2.5					499.6	60.6	0.0284
3.0					500.7	63.2	0.0290
3.3					499.3	64.3	0.0301
2.0	70	50	90	50	102.7	83.9	0.0006
		125		125	246.7	59.5	0.0060
		250		250	498.3	58.9	0.0245
		375		375	750.0	52.7	0.0579
		500		500	1001.2	50.7	0.0824
2.0	70	50	90	450	497.8	77.1	0.0196
		150		350	497.0	61.8	0.0266
		250		250	501.6	57.2	0.0271
		350		150	499.1	65.8	0.0281
		450		50	498.6	82.2	0.0240

Single orthogonal pattern louver mixer: CCW orientation, and louver angle of 50°

Mixing length (D_h)	Air temp. @ upper inlet (°F)	Air flowrate @ upper inlet (CFM)	Air temp. @ lower inlet (°F)	Air flowrate @ lower inlet (CFM)	Total flowrate (CFM)	Mixing effectiveness (%)	ΔP (inWC)
1.0	70	250	90	250	499.5	51.9	0.0418
1.5					498.1	58.0	0.0422
2.0					499.8	64.3	0.0422
2.5					498.9	68.9	0.0433
3.0					501.1	72.4	0.0442
3.3					499.4	72.6	0.0456
2.0	70	50	90	50	103.2	79.1	0.0021
		125		125	248.8	66.9	0.0110
		250		250	501.2	63.9	0.0472
		375		375	750.3	61.3	0.0797
		420		420	940.0	60.8	0.1067
2.0	70	50	90	450	497.9	83.6	0.0291
		150		350	497.6	69.6	0.0383
		250		250	498.8	63.3	0.0470
		350		150	498.8	70.7	0.0406
		450		50	500.7	85.0	0.0353

Single orthogonal pattern louver mixer: CCW orientation, and louver angle of 60°

Mixing length (D_h)	Air temp. @ upper inlet (°F)	Air flowrate @ upper inlet (CFM)	Air temp. @ lower inlet (°F)	Air flowrate @ lower inlet (CFM)	Total flowrate (CFM)	Mixing effectiveness (%)	ΔP (inWC)
1.0	70	250	90	250	499.1	62.4	0.0749
1.5					500.1	69.9	0.0760
2.0					500.7	74.7	0.0762
2.5					497.5	78.2	0.0763
3.0					498.5	80.6	0.0777
3.3					499.9	81.5	0.0784
2.0	70	50	90	50	100.1	88.0	0.0032
		125		125	251.0	78.5	0.0162
		250		250	497.7	75.0	0.0686
		375		375	750.3	71.7	0.1446
		445		445	991.5	71.3	0.1915
2.0	70	50	90	450	498.4	87.6	0.0579
		150		350	496.5	77.1	0.0727
		250		250	499.2	74.7	0.0731
		350		150	499.7	80.0	0.0758
		450		50	500.5	89.2	0.0699

Single orthogonal pattern louver mixer: CCW orientation, and louver angle of 70°

Mixing length (D_h)	Air temp. @ upper inlet (°F)	Air flowrate @ upper inlet (CFM)	Air temp. @ lower inlet (°F)	Air flowrate @ lower inlet (CFM)	Total flowrate (CFM)	Mixing effectiveness (%)	ΔP (inWC)
1.0	70	250	90	250	500.2	66.1	0.1423
1.5					500.0	72.6	0.1439
2.0					499.2	77.9	0.1439
2.5					499.1	81.7	0.1439
3.0					499.7	84.2	0.1452
3.3					501.6	85.0	0.1453
2.0	70	50	90	50	101.9	89.4	0.0071
		125		125	250.0	81.8	0.0324
		250		250	500.5	80.0	0.1222
		375		375	750.2	74.8	0.2624
		500		420	921.0	75.2	0.3058
2.0	70	50	90	450	502.2	89.0	0.1169
		150		350	498.2	79.0	0.1452
		250		250	500.8	78.2	0.1442
		350		150	500.2	83.7	0.1499
		450		50	500.4	90.9	0.1413

1.5.2. Louver size: 4 by 4 array

Dual orthogonal pattern louver mixer: CCW-CCW orientation, and louver angle of 50°

Mixer spacing (D_h)	Mixing length (D_h)	Air temp. @ upper inlet (°F)	Air flowrate @ upper inlet (CFM)	Air temp. @ lower inlet (°F)	Air flowrate @ lower inlet (CFM)	Total flowrate (CFM)	Mixing effectiveness (%)	ΔP (inWC)
0.8	1.0	70	250	90	250	498.7	58.0	0.0759
	1.5					501.0	73.6	0.0698
	2.0					499.6	82.3	0.0702
	2.5					499.3	85.3	0.0687
	3.0					499.5	87.3	0.0692
	3.3					499.9	88.2	0.0695
1.0	1.5					500.1	68.4	0.0720
	2.0					500.7	81.9	0.0705
	2.5					499.6	85.2	0.0699
	3.0					500.8	86.3	0.0693
	3.3					500.3	87.7	0.0697
1.5	2.0					500.5	72.1	0.0705
	2.5					500.2	80.7	0.0709
	3.0					501.0	83.3	0.0706
	3.3					500.6	83.6	0.0703
2.0	2.5					501.7	74.8	0.0723
	3.0					499.6	81.7	0.0710
	3.3					500.2	83.7	0.0723
1.5	2.0	70	50	90	50	99.5	85.3	0.0019
			125		125	250.4	73.7	0.0149
			250		250	501.5	72.5	0.0622
			375		375	749.7	69.9	0.1395
			500		500	1002.9	68.5	0.1866
1.5	2.0	70	50	90	450	498.3	84.8	0.0565
			150		350	498.8	73.4	0.0707
			250		250	500.2	71.6	0.0703
			350		150	499.3	77.0	0.0735
			450		50	500.1	88.0	0.0676

Dual orthogonal pattern louver mixer: CCW-CCW orientation, and louver angle of 60°

Mixer spacing (D_h)	Mixing length (D_h)	Air temp. @ upper inlet (°F)	Air flowrate @ upper inlet (CFM)	Air temp. @ lower inlet (°F)	Air flowrate @ lower inlet (CFM)	Total flowrate (CFM)	Mixing effectiveness (%)	ΔP (inWC)
0.8	1.0	70	250	90	250	500.6	70.1	0.1264
	1.5					500.7	85.5	0.1219
	2.0					499.9	88.0	0.1220
	2.5					499.5	88.6	0.1198
	3.0					499.8	89.8	0.1204
	3.3					501.1	90.2	0.1205
1.0	1.5					499.1	82.5	0.1214
	2.0					500.2	87.4	0.1220
	2.5					501.5	88.4	0.1213
	3.0					500.2	89.0	0.1200
	3.3					498.8	89.6	0.1205
1.5	2.0					500.3	82.8	0.1197
	2.5					499.2	87.1	0.1207
	3.0					499.7	88.7	0.1184
	3.3					498.7	88.9	0.1188
2.0	2.5					500.2	83.6	0.1230
	3.0					500.1	87.6	0.1213
	3.3					500.2	88.4	0.1211
1.5	2.0	70	50	90	50	100.1	91.7	0.0041
			125		125	249.4	85.3	0.0296
			250		250	499.3	84.3	0.1045
			375		375	749.7	82.5	0.2241
			425		425	950.9	81.8	0.2710
1.5	2.0	70	50	90	450	500.9	89.5	0.0979
			150		350	497.0	84.0	0.1230
			250		250	499.3	83.6	0.1206
			350		150	498.8	87.2	0.1255
			450		50	500.9	93.0	0.1172

Single orthogonal pattern louver mixer: CCW orientation, and louver angle of 60°

Mixing length (D_h)	Air temp. @ upper inlet (°F)	Air flowrate @ upper inlet (CFM)	Air temp. @ lower inlet (°F)	Air flowrate @ lower inlet (CFM)	Total flowrate (CFM)	Mixing effectiveness (%)	ΔP (inWC)
1.0	70	250	90	250	499.8	71.0	0.0804
1.5					500.8	75.5	0.0798
2.0					498.3	79.6	0.0816
2.5					499.3	81.6	0.0819
3.0					500.9	82.8	0.0820
3.3					498.8	83.6	0.0821
2.0	70	50	90	50	101.7	90.6	0.0031
		125		125	248.8	82.3	0.0170
		250		250	499.4	80.3	0.0699
		375		375	750.9	77.7	0.1576
		500		500	1004.0	76.9	0.2056
2.0	70	50	90	450	498.9	88.9	0.0638
		150		350	499.1	80.7	0.0815
		250		250	500.6	79.5	0.0806
		350		150	500.8	83.4	0.0842
		450		50	499.8	90.7	0.0778

Single orthogonal pattern louver mixer: CCW orientation, and louver angle of 70°

Mixing length (D_h)	Air temp. @ upper inlet (°F)	Air flowrate @ upper inlet (CFM)	Air temp. @ lower inlet (°F)	Air flowrate @ lower inlet (CFM)	Total flowrate (CFM)	Mixing effectiveness (%)	ΔP (inWC)
1.0	70	250	90	250	500.4	79.0	0.1428
1.5					500.3	83.8	0.1441
2.0					497.2	87.2	0.1438
2.5					500.1	88.8	0.1440
3.0					500.8	89.5	0.1442
3.3					500.7	89.7	0.1435
2.0	70	50	90	50	100.7	92.6	0.0054
		125		125	252.1	88.2	0.0374
		250		250	500.8	87.5	0.1286
		375		375	750.6	85.8	0.2622
		450		450	901.9	85.5	0.3026
2.0	70	50	90	450	500.3	91.9	0.1170
		150		350	499.1	87.2	0.1461
		250		250	499.6	87.0	0.1447
		350		150	498.2	89.6	0.1492
		450		50	498.0	94.2	0.1403

Single orthogonal pattern louver mixer: CCW orientation, louver angle of 70°, and swapped inlet temperature configuration

Mixing length (D_h)	Air temp. @ upper inlet (°F)	Air flowrate @ upper inlet (CFM)	Air temp. @ lower inlet (°F)	Air flowrate @ lower inlet (CFM)	Total flowrate (CFM)	Mixing effectiveness (%)	ΔP (inWC)
1.0	90	250	70	250	500.4	79.2	0.1408
1.5					500.7	83.5	0.1418
2.0					499.4	86.8	0.1416
2.5					498.2	88.7	0.1422
3.0					499.3	89.5	0.1450
3.3					500.0	89.9	0.1436
2.0	90	50	70	50	99.4	88.4	0.0075
		125		125	249.1	86.3	0.0364
		250		250	499.4	86.8	0.1416

1.5.3. Louver size: 2 by 2 array

Dual orthogonal pattern louver mixer: CCW-CCW orientation, and louver angle of 50°

Mixer spacing (D_h)	Mixing length (D_h)	Air temp. @ upper inlet (°F)	Air flowrate @ upper inlet (CFM)	Air temp. @ lower inlet (°F)	Air flowrate @ lower inlet (CFM)	Total flowrate (CFM)	Mixing effectiveness (%)	ΔP (inWC)
0.8	1.0	70	250	90	250	500.6	45.9	0.0717
	1.5					500.2	69.5	0.0760
	2.0					499.1	80.0	0.0717
	2.5					500.4	86.0	0.0712
	3.0					500.8	89.6	0.0707
	3.3					497.6	90.8	0.0711
1.0	1.5					499.0	58.8	0.0722
	2.0					499.5	76.5	0.0691
	2.5					500.5	86.6	0.0688
	3.0					500.5	90.9	0.0675
	3.3					500.3	91.8	0.0685
1.5	2.0					499.8	72.6	0.0700
	2.5					501.2	82.7	0.0687
	3.0					498.5	89.3	0.0679
	3.3					500.2	90.8	0.0671
2.0	2.5					500.3	75.9	0.0682
	3.0					501.0	85.3	0.0697
	3.3					499.0	88.9	0.0697
1.5	2.0	70	50	90	50	99.2	86.6	0.0032
			125		125	249.5	72.6	0.0187
			250		250	502.2	71.4	0.0633
			375		375	750.9	69.4	0.1363
			500		500	1000.4	69.8	0.1788
1.5	2.0	70	50	90	450	498.0	86.3	0.0549
			150		350	499.3	73.2	0.0701
			250		250	500.6	71.1	0.0703
			350		150	499.4	78.7	0.0714
			450		50	500.7	90.6	0.0646

Dual orthogonal pattern louver mixer: CCW-CCW orientation, and louver angle of 70°

Mixer spacing (D_h)	Mixing length (D_h)	Air temp. @ upper inlet (°F)	Air flowrate @ upper inlet (CFM)	Air temp. @ lower inlet (°F)	Air flowrate @ lower inlet (CFM)	Total flowrate (CFM)	Mixing effectiveness (%)	ΔP (inWC)
0.8	1.0	70	250	90	250	500.8	74.4	0.2645
	1.5					499.9	89.5	0.2607
	2.0					500.0	94.0	0.2570
	2.5					501.0	94.7	0.2528
	3.0					499.4	96.2	0.2527
	3.3					499.3	96.8	0.2520
1.0	1.5					498.1	89.6	0.2630
	2.0					500.4	95.2	0.2586
	2.5					500.6	96.1	0.2541
	3.0					499.6	96.7	0.2528
	3.3					500.2	97.3	0.2514
1.5	2.0					500.9	93.7	0.2601
	2.5					500.2	97.4	0.2554
	3.0					500.6	97.4	0.2508
	3.3					500.2	97.7	0.2491
2.0	2.5					500.9	95.8	0.2538
	3.0					500.3	97.7	0.2515
	3.3					500.5	98.1	0.2486

Single orthogonal pattern louver mixer: CCW orientation, and louver angle of 70°

Mixing length (D_h)	Air temp. @ upper inlet (°F)	Air flowrate @ upper inlet (CFM)	Air temp. @ lower inlet (°F)	Air flowrate @ lower inlet (CFM)	Total flowrate (CFM)	Mixing effectiveness (%)	ΔP (inWC)
1.0	70	250	90	250	499.9	70.4	0.1859
1.5					500.7	79.3	0.1844
2.0					500.0	85.4	0.1856
2.5					499.9	88.4	0.1836
3.0					500.5	89.6	0.1852
3.3					499.9	90.9	0.1853

2. CFD Simulation Data for Air Sampler Testing

2.1. Testing conditions

Case #	Sampling hole type	Hole size (in)	Hole pitch (in)	Material	Duct size (in^2)	Inlet vel. profile	Inlet temp. profile	Branch outlet BC	Emissivity	Hole facing angle (°)
1	DOE_D	0.375	3.5	PVC	18x18	linear	linear	Pressure out (P=0 Pa)	N/A	0
2	DOE_D	0.375	3.5	PVC	21x18	inverse linear	linear	Pressure out (P=0 Pa)	N/A	0
3	DOE_D	0.375	3.5	PVC	21x18	constant	linear	Pressure out (P=0 Pa)	N/A	0
4	DOE_D	0.375	3.5	PVC	18x18	parabolic	linear	Pressure out (P=0 Pa)	N/A	0
5	DOE_D	0.375	3.5	PVC	21x18	inverse parabolic	linear	Pressure out (P=0 Pa)	N/A	0
6	DOE_D	0.375	3.5	PVC	18x18	random	linear	Pressure out (P=0 Pa)	N/A	0
7	Large_D	0.5	3.5	PVC	18x18	linear	linear	Pressure out (P=0 Pa)	N/A	0
8	Large_D	0.5	3.5	PVC	18x18	inverse linear	linear	Pressure out (P=0 Pa)	N/A	0
9	Large_D	0.5	3.5	PVC	18x18	constant	linear	Pressure out (P=0 Pa)	N/A	0
10	Large_D	0.5	3.5	PVC	18x18	parabolic	linear	Pressure out (P=0 Pa)	N/A	0
11	Large_D	0.5	3.5	PVC	18x18	inverse parabolic	linear	Pressure out (P=0 Pa)	N/A	0
12	Large_D	0.5	3.5	PVC	18x18	random	linear	Pressure out (P=0 Pa)	N/A	0
13	Small_D	0.25	3.5	PVC	18x18	linear	linear	Pressure out (P=0 Pa)	N/A	0
14	Small_D	0.25	3.5	PVC	18x18	inverse linear	linear	Pressure out (P=0 Pa)	N/A	0
15	Small_D	0.25	3.5	PVC	18x18	constant	linear	Pressure out (P=0 Pa)	N/A	0
16	Small_D	0.25	3.5	PVC	18x18	parabolic	linear	Pressure out (P=0 Pa)	N/A	0
17	Small_D	0.25	3.5	PVC	18x18	inverse parabolic	linear	Pressure out (P=0 Pa)	N/A	0
18	Small_D	0.25	3.5	PVC	18x18	random	linear	Pressure out (P=0 Pa)	N/A	0
19	Variable_D	0.25-0.5	3.5	PVC	18x18	linear	linear	Pressure out (P=0 Pa)	N/A	0
20	Variable_D	0.25-0.5	3.5	PVC	18x18	inverse linear	linear	Pressure out (P=0 Pa)	N/A	0
21	Variable_D	0.25-0.5	3.5	PVC	18x18	constant	linear	Pressure out (P=0 Pa)	N/A	0
22	Variable_D	0.25-0.5	3.5	PVC	18x18	parabolic	linear	Pressure out (P=0 Pa)	N/A	0
23	Variable_D	0.25-0.5	3.5	PVC	18x18	inverse parabolic	linear	Pressure out (P=0 Pa)	N/A	0
24	Variable_D	0.25-0.5	3.5	PVC	18x18	random	linear	Pressure out (P=0 Pa)	N/A	0
25	DOE_D	0.375	3.5	PVC	18x18	constant	inverse linear	Pressure out (P=0 Pa)	N/A	0
26	DOE_D	0.375	3.5	PVC	18x18	constant	parabolic	Pressure out (P=0 Pa)	N/A	0
27	Large_D	0.5	3.5	PVC	18x18	constant	inverse linear	Pressure out (P=0 Pa)	N/A	0

(continued)

Case #	Sampling hole type	Hole size (in)	Hole pitch (in)	Material	Duct size (in^2)	Inlet vel. profile	Inlet temp. profile	Branch outlet BC	Emissivity	Hole facing angle (°)
27	Large_D	0.5	3.5	PVC	18x18	constant	inverse linear	Pressure out (P=0 Pa)	N/A	0
28	Large_D	0.5	3.5	PVC	18x18	constant	parabolic	Pressure out (P=0 Pa)	N/A	0
29	Small_D	0.25	3.5	PVC	18x18	constant	inverse linear	Pressure out (P=0 Pa)	N/A	0
30	Small_D	0.25	3.5	PVC	18x18	constant	parabolic	Pressure out (P=0 Pa)	N/A	0
31	Variable_D	0.25-0.5	3.5	PVC	18x18	constant	inverse linear	Pressure out (P=0 Pa)	N/A	0
32	Variable_D	0.25-0.5	3.5	PVC	18x18	constant	parabolic	Pressure out (P=0 Pa)	N/A	0
33	DOE_D	0.375	variable	PVC	18x18	linear	linear	Pressure out (P=0 Pa)	N/A	0
34	DOE_D	0.375	variable	PVC	18x18	inverse linear	linear	Pressure out (P=0 Pa)	N/A	0
35	DOE_D	0.375	variable	PVC	18x18	constant	linear	Pressure out (P=0 Pa)	N/A	0
36	DOE_D	0.375	variable	PVC	18x18	parabolic	linear	Pressure out (P=0 Pa)	N/A	0
37	DOE_D	0.375	variable	PVC	18x18	inverse parabolic	linear	Pressure out (P=0 Pa)	N/A	0
38	DOE_D	0.375	variable	PVC	18x18	random	linear	Pressure out (P=0 Pa)	N/A	0
39	Small_D	0.25	variable	PVC	18x18	linear	linear	Pressure out (P=0 Pa)	N/A	0
40	Small_D	0.25	variable	PVC	18x18	inverse linear	linear	Pressure out (P=0 Pa)	N/A	0
41	Small_D	0.25	variable	PVC	18x18	constant	linear	Pressure out (P=0 Pa)	N/A	0
42	Small_D	0.25	variable	PVC	18x18	parabolic	linear	Pressure out (P=0 Pa)	N/A	0
43	Small_D	0.25	variable	PVC	18x18	inverse parabolic	linear	Pressure out (P=0 Pa)	N/A	0
44	Small_D	0.25	variable	PVC	18x18	random	linear	Pressure out (P=0 Pa)	N/A	0
45	Small_D	0.25	3.5	AL	18x18	constant	linear	Pressure out (P=0 Pa)	N/A	0
46	Small_D	0.25	3.5	SS	18x18	constant	linear	Pressure out (P=0 Pa)	N/A	0
47	Small_D	0.25	3.5	Adiabatic	18x18	constant	linear	Pressure out (P=0 Pa)	N/A	0
48	Small_D	0.25	variable	AL	18x18	constant	linear	Pressure out (P=0 Pa)	N/A	0
49	Small_D	0.25	variable	SS	18x18	constant	linear	Pressure out (P=0 Pa)	N/A	0
50	Small_D	0.25	variable	Adiabatic	18x18	constant	linear	Pressure out (P=0 Pa)	N/A	0
51	Variable_D	0.25-0.5	3.5	AL	18x18	constant	linear	Pressure out (P=0 Pa)	N/A	0
52	Variable_D	0.25-0.5	3.5	SS	18x18	constant	linear	Pressure out (P=0 Pa)	N/A	0
53	Variable_D	0.25-0.5	3.5	Adiabatic	18x18	constant	linear	Pressure out (P=0 Pa)	N/A	0
54	DOE_D	0.375	variable	AL	18x18	constant	linear	Pressure out (P=0 Pa)	N/A	0
55	DOE_D	0.375	variable	SS	18x18	constant	linear	Pressure out (P=0 Pa)	N/A	0
56	DOE_D	0.375	variable	Adiabatic	18x18	constant	linear	Pressure out (P=0 Pa)	N/A	0

(continued)

Case #	Sampling hole type	Hole size (in)	Hole pitch (in)	Material	Duct size (in^2)	Inlet vel. profile	Inlet temp. profile	Branch outlet BC	Emissivity	Hole facing angle (°)
56	DOE_D	0.375	variable	Adiabatic	18x18	constant	linear	Pressure out (P=0 Pa)	N/A	0
57	Variable_D	0.25-0.5	3.5	AL	18x18	linear	linear	Pressure out (P=0 Pa)	N/A	0
58	Variable_D	0.25-0.5	3.5	SS	18x18	linear	linear	Pressure out (P=0 Pa)	N/A	0
59	Variable_D	0.25-0.5	3.5	Adiabatic	18x18	linear	linear	Pressure out (P=0 Pa)	N/A	0
60	Variable_D	0.25-0.5	3.5	AL	18x18	parabolic	linear	Pressure out (P=0 Pa)	N/A	0
61	Variable_D	0.25-0.5	3.5	SS	18x18	parabolic	linear	Pressure out (P=0 Pa)	N/A	0
62	Variable_D	0.25-0.5	3.5	Adiabatic	18x18	parabolic	linear	Pressure out (P=0 Pa)	N/A	0
63	DOE_D	0.375	variable	AL	18x18	constant	linear	Pressure out (P=0 Pa)	0.1	0
64	DOE_D	0.375	variable	AL	18x18	constant	linear	Pressure out (P=0 Pa)	0.5	0
65	DOE_D	0.375	variable	AL	18x18	constant	linear	Pressure out (P=0 Pa)	0.95	0
66	DOE_D	0.375	variable	AL	18x18	constant	linear	Pressure out (P=0 Pa)	0.1	0
67	DOE_D	0.375	variable	AL	18x18	constant	linear	Pressure out (P=0 Pa)	0.5	0
68	DOE_D	0.375	variable	AL	18x18	constant	linear	Pressure out (P=0 Pa)	0.95	0
69	DOE_D	0.375	variable	AL	18x18	constant	parabolic	Pressure out (P=0 Pa)	0.1	0
70	DOE_D	0.375	variable	AL	18x18	constant	parabolic	Pressure out (P=0 Pa)	0.5	0
71	DOE_D	0.375	variable	AL	18x18	constant	parabolic	Pressure out (P=0 Pa)	0.95	0
72	DOE_D	0.375	3.5	PVC	18x18	linear	linear	Pressure out (P=0 Pa)	N/A	90
73	DOE_D	0.375	3.5	PVC	18x18	inverse linear	linear	Pressure out (P=0 Pa)	N/A	90
74	DOE_D	0.375	3.5	PVC	18x18	constant	linear	Pressure out (P=0 Pa)	N/A	90
75	DOE_D	0.375	3.5	PVC	18x18	parabolic	linear	Pressure out (P=0 Pa)	N/A	90
76	DOE_D	0.375	3.5	PVC	18x18	linear	linear	Pressure out (P=0 Pa)	N/A	180
77	DOE_D	0.375	3.5	PVC	18x18	inverse linear	linear	Pressure out (P=0 Pa)	N/A	180
78	DOE_D	0.375	3.5	PVC	18x18	constant	linear	Pressure out (P=0 Pa)	N/A	180
79	DOE_D	0.375	3.5	PVC	18x18	parabolic	linear	Pressure out (P=0 Pa)	N/A	180
80	DOE_D	0.375	3.5	PVC	18x18	linear	linear	Pressure out (P=0 Pa)	N/A	0
81	DOE_D	0.375	3.5	PVC	18x18	inverse linear	linear	Pressure out (P=0 Pa)	N/A	0
82	DOE_D	0.375	3.5	PVC	18x18	constant	linear	Pressure out (P=0 Pa)	N/A	0
83	DOE_D	0.375	3.5	PVC	18x18	parabolic	linear	Pressure out (P=0 Pa)	N/A	0
84	DOE_D	0.375	3.5	PVC	18x18	constant	linear	Mass flow out (0.0004 kg/s)	N/A	0
85	DOE_D	0.375	3.5	PVC	18x18	constant	linear	Mass flow out (0.0004 kg/s)	N/A	0

(continued)

Case #	Sampling hole type	Hole size (in)	Hole pitch (in)	Material	Duct size (in^2)	Inlet vel. profile	Inlet temp. profile	Branch outlet BC	Emissivity	Hole facing angle (°)
86	DOE_D	0.375	3.5	PVC	18x18	constant	linear	Mass flow out (0.0004 kg/s)	N/A	0
87	DOE_D	0.375	3.5	PVC	18x18	constant	linear	Mass flow out (0.0004 kg/s)	N/A	0
88	DOE_D	0.375	3.5	PVC	18x18	constant	linear	Mass flow out (0.0004 kg/s)	N/A	0
89	DOE_D	0.375	3.5	PVC	18x18	constant	linear	Mass flow out (25 cfm)	N/A	0
90	Variable_D	0.375	3.5	PVC	18x18	constant	linear	Mass flow out (0.0004 kg/s)	N/A	0
91	Variable_D	0.375	3.5	PVC	18x18	constant	linear	Mass flow out (0.0004 kg/s)	N/A	0
92	Variable_D	0.375	3.5	PVC	18x18	constant	linear	Mass flow out (0.0004 kg/s)	N/A	0
93	Variable_D	0.375	3.5	PVC	18x18	constant	linear	Mass flow out (25 cfm)	N/A	0
94	Variable_D	0.375	3.5	PVC	18x18	constant	linear	Mass flow out (25 cfm)	N/A	0
95	DOE_D	0.375	3.5	PVC	18x18	constant	linear	high-high	N/A	0
96	DOE_D	0.375	3.5	PVC	18x18	constant	linear	high-low	N/A	0
97	DOE_D	0.375	3.5	PVC	18x18	constant	linear	low-high	N/A	0
98	DOE_D	0.375	3.5	PVC	18x18	constant	linear	low-low	N/A	0
99	DOE_D	0.375	3.5	PVC	18x18	linear	linear	high-high(7fps)	N/A	0
100	DOE_D	0.375	3.5	PVC	18x18	linear	linear	high-low(2.5fps)	N/A	0
101	DOE_D	0.375	3.5	PVC	18x18	linear	linear	low-high	N/A	0
102	DOE_D	0.375	3.5	PVC	18x18	linear	linear	low-low	N/A	0
103	DOE_D	0.375	3.5	PVC	18x18	inverse linear	linear	high-high	N/A	0
104	DOE_D	0.375	3.5	PVC	18x18	inverse linear	linear	high-low	N/A	0
105	DOE_D	0.375	3.5	PVC	18x18	inverse linear	linear	low-high	N/A	0
106	DOE_D	0.375	3.5	PVC	18x18	inverse linear	linear	low-low	N/A	0
107	DOE_D	0.375	3.5	PVC	18x18	constant	linear	high-25fps	N/A	0
108	DOE_D	0.375	3.5	PVC	18x18	constant	linear	high-50fps	N/A	0
109	DOE_D	0.375	3.5	PVC	18x18	constant	linear	high-75fps	N/A	0
110	Small_D_2	0.125	3.5	PVC	18x18	constant	linear	high-2.5fps	N/A	0
111	Small_D_2	0.125	3.5	PVC	18x18	constant	linear	high-7fps	N/A	0
112	Small_D_2	0.125	3.5	PVC	18x18	constant	linear	high-25fps	N/A	0
113	Small_D_2	0.125	3.5	PVC	18x18	constant	linear	high-109fps	N/A	0
114	Large_D_2	0.625	3.5	PVC	18x18	constant	linear	high-2.5fps	N/A	0
115	Large_D_2	0.625	3.5	PVC	18x18	constant	linear	high-7fps	N/A	0

(continued)

Case #	Sampling hole type	Hole size (in)	Hole pitch (in)	Material	Duct size (in^2)	Inlet vel. profile	Inlet temp. profile	Branch outlet BC	Emissivity	Hole facing angle (°)
116	Large_D_2	0.625	3.5	PVC	18x18	constant	linear	high-25fps	N/A	0
117	Large_D_2	0.625	3.5	PVC	18x18	constant	linear	high-109fps	N/A	0
118	Small_D	0.25	3.5	PVC	18x18	constant	linear	high-2.5fps	N/A	0
119	Small_D	0.25	3.5	PVC	18x18	constant	linear	high-7fps	N/A	0
120	Small_D	0.25	3.5	PVC	18x18	constant	linear	high-25fps	N/A	0
121	Small_D	0.25	3.5	PVC	18x18	constant	linear	high-109fps	N/A	0
122	Large_D	0.5	3.5	PVC	18x18	constant	linear	high-2.5fps	N/A	0
123	Large_D	0.5	3.5	PVC	18x18	constant	linear	high-7fps	N/A	0
124	Large_D	0.5	3.5	PVC	18x18	constant	linear	high-25fps	N/A	0
125	Large_D	0.5	3.5	PVC	18x18	constant	linear	high-109fps	N/A	0
126	Large_D	0.5	3.5	PVC	18x18	constant	linear	high-50fps	N/A	0
127	Large_D	0.5	3.5	PVC	18x18	constant	linear	high-75fps	N/A	0
128	Small_D_2	0.125	3.5	PVC	18x18	constant	linear	high-50fps	N/A	0
129	Small_D_2	0.125	3.5	PVC	18x18	constant	linear	high-75fps	N/A	0
130	Large_D_2	0.625	3.5	PVC	18x18	constant	linear	high-50fps	N/A	0
131	Large_D_2	0.625	3.5	PVC	18x18	constant	linear	high-75fps	N/A	0
132	Small_D	0.25	3.5	PVC	18x18	constant	linear	high-50fps	N/A	0
133	Small_D	0.25	3.5	PVC	18x18	constant	linear	high-75fps	N/A	0
134	Small_D_2	0.125	3.5	PVC	18x18	constant	linear	100cfm-2.5fps	N/A	0
135	Small_D_2	0.125	3.5	PVC	18x18	constant	linear	100cfm-7fps	N/A	0
136	Small_D_2	0.125	3.5	PVC	18x18	constant	linear	100cfm-25fps	N/A	0
137	Small_D_2	0.125	3.5	PVC	18x18	constant	linear	100cfm-50fps	N/A	0
138	Small_D_2	0.125	3.5	PVC	18x18	constant	linear	100cfm-75fps	N/A	0
139	Small_D	0.25	3.5	PVC	18x18	constant	linear	100cfm-2.5fps	N/A	0
140	Small_D	0.25	3.5	PVC	18x18	constant	linear	100cfm-7fps	N/A	0
141	Small_D	0.25	3.5	PVC	18x18	constant	linear	100cfm-25fps	N/A	0
142	Small_D	0.25	3.5	PVC	18x18	constant	linear	100cfm-50fps	N/A	0
143	Small_D	0.25	3.5	PVC	18x18	constant	linear	100cfm-75fps	N/A	0
144	DOE_D	0.375	3.5	PVC	18x18	constant	linear	100cfm-25fps	N/A	0
145	DOE_D	0.375	3.5	PVC	18x18	constant	linear	100cfm-50fps	N/A	0

(continued)

Case #	Sampling hole type	Hole size (in)	Hole pitch (in)	Material	Duct size (in^2)	Inlet vel. profile	Inlet temp. profile	Branch outlet BC	Emissivity	Hole facing angle (°)
146	DOE_D	0.375	3.5	PVC	18x18	constant	linear	100cfm-75fps	N/A	0
147	Large_D	0.5	3.5	PVC	18x18	constant	linear	100cfm-2.5fps	N/A	0
148	Large_D	0.5	3.5	PVC	18x18	constant	linear	100cfm-7fps	N/A	0
149	Large_D	0.5	3.5	PVC	18x18	constant	linear	100cfm-25fps	N/A	0
150	Large_D	0.5	3.5	PVC	18x18	constant	linear	100cfm-50fps	N/A	0
151	Large_D	0.5	3.5	PVC	18x18	constant	linear	100cfm-75fps	N/A	0
152	DOE_D*	0.1875	1.75	PVC	9x9	constant	linear	high-5fps	N/A	0
153	DOE_D*	0.1875	1.75	PVC	9x9	constant	linear	high-14fps	N/A	0
154	DOE_D*	0.1875	1.75	PVC	9x9	constant	linear	high-50fps	N/A	0
155	DOE_D*	0.1875	1.75	PVC	9x9	constant	linear	high-100fps	N/A	0
156	DOE_D*	0.1875	1.75	PVC	9x9	constant	linear	high-150fps	N/A	0
157	DOE_D*	0.1875	1.75	PVC	9x9	constant	linear	high-218fps	N/A	0
158	Small_D*	0.125	1.75	PVC	9x9	constant	linear	high-5fps	N/A	0
159	Small_D*	0.125	1.75	PVC	9x9	constant	linear	high-14fps	N/A	0
160	Small_D*	0.125	1.75	PVC	9x9	constant	linear	high-50fps	N/A	0
161	Small_D*	0.125	1.75	PVC	9x9	constant	linear	high-100fps	N/A	0
162	Small_D*	0.125	1.75	PVC	9x9	constant	linear	high-150fps	N/A	0
163	Small_D*	0.125	1.75	PVC	9x9	constant	linear	high-218fps	N/A	0
164	Large_D*	0.25	1.75	PVC	9x9	constant	linear	high-5fps	N/A	0
165	Large_D*	0.25	1.75	PVC	9x9	constant	linear	high-14fps	N/A	0
166	Large_D*	0.25	1.75	PVC	9x9	constant	linear	high-50fps	N/A	0
167	Large_D*	0.25	1.75	PVC	9x9	constant	linear	high-100fps	N/A	0
168	Large_D*	0.25	1.75	PVC	9x9	constant	linear	high-150fps	N/A	0
169	Large_D*	0.25	1.75	PVC	9x9	constant	linear	high-218fps	N/A	0
170	Small_D2*	0.125	1.75	PVC	9x9	constant	linear	high-5fps	N/A	0
171	Small_D2*	0.125	1.75	PVC	9x9	constant	linear	high-14fps	N/A	0
172	Small_D2*	0.125	1.75	PVC	9x9	constant	linear	high-50fps	N/A	0
173	Small_D2*	0.125	1.75	PVC	9x9	constant	linear	high-100fps	N/A	0
174	Small_D2*	0.125	1.75	PVC	9x9	constant	linear	high-150fps	N/A	0
175	Small_D2*	0.125	1.75	PVC	9x9	constant	linear	high-218fps	N/A	0

(continued)

Case #	Sampling hole type	Hole size (in)	Hole pitch (in)	Material	Duct size (in^2)	Inlet vel. profile	Inlet temp. profile	Branch outlet BC	Emissivity	Hole facing angle (°)
176	DOE_D	0.375"	3.5"	PVC	18x18	constant_1000CFM	70, 90F	hole vel_2.5 fps	N/A	0
177	DOE_D	0.375"	3.5"	PVC	18x18	constant_500CFM	70, 90F	hole vel_2.5 fps	N/A	0
178	DOE_D	0.375"	3.5"	PVC	18x18	constant_1000CFM	70, 90F	hole vel_7 fps	N/A	0
179	DOE_D	0.375"	3.5"	PVC	18x18	constant_1000CFM	70, 90F	hole vel_25 fps	N/A	0
180	DOE_D	0.375"	3.5"	PVC	18x18	constant_100CFM	70, 90F	1.5cfm sampling	N/A	0
181	DOE_D	0.375"	3.5"	PVC	18x18	constant_500CFM	70, 90F	1.5cfm sampling	N/A	0
182	DOE_D	0.375"	3.5"	PVC	18x18	constant_1000CFM	70, 90F	1.5cfm sampling	N/A	0
183	variable_D	0.25-0.5	3.5"	PVC	18x18	constant_100CFM	70, 90F	1.5cfm sampling	N/A	0
184	variable_D	0.25-0.5	3.5"	PVC	18x18	constant_500CFM	70, 90F	1.5cfm sampling	N/A	0
185	variable_D	0.25-0.5	3.5"	PVC	18x18	constant_1000CFM	70, 90F	1.5cfm sampling	N/A	0
186	variable_D	0.25-0.5	3.5"	AL	18x18	constant_1000CFM	70, 90F	1.5cfm sampling	N/A	0
187	variable_D	0.25-0.5	3.5"	SS	18x18	constant_1000CFM	70, 90F	1.5cfm sampling	N/A	0
188	variable_D	0.25-0.5	3.5"	Adiabatic	18x18	constant_1000CFM	70, 90F	1.5cfm sampling	N/A	0
189	variable_D	0.25-0.5	3.5"	PVC	18x18	300:700 cfm(L:H)	70, 90F	1.5cfm sampling	N/A	0
190	variable_D	0.25-0.5	3.5"	PVC	18x18	700:300 cfm(L:H)	70, 90F	1.5cfm sampling	N/A	0
191	DOE_D (8 holes)	0.375	2"	PVC	18x18	constant_1000CFM	70, 90F	1.5cfm sampling	N/A	0
192	DOE_D (7 holes)	0.375	2.3333"	PVC	18x18	constant_1000CFM	70, 90F	1.5cfm sampling	N/A	0
193	DOE_D (6 holes)	0.375	2.8"	PVC	18x18	constant_1000CFM	70, 90F	1.5cfm sampling	N/A	0
194	DOE_D (4 holes)	0.375	4.66667"	PVC	18x18	constant_1000CFM	70, 90F	1.5cfm sampling	N/A	0
195	DOE_D (3 holes)	0.375	7"	PVC	18x18	constant_1000CFM	70, 90F	1.5cfm sampling	N/A	0
196	Variable_D (8 holes)	0.25-0.5	2"	PVC	18x18	constant_1000CFM	70, 90F	1.5cfm sampling	N/A	0
197	Variable_D (7 holes)	0.25-0.5	2.3333"	PVC	18x18	constant_1000CFM	70, 90F	1.5cfm sampling	N/A	0
198	Variable_D (6 holes)	0.25-0.5	2.8"	PVC	18x18	constant_1000CFM	70, 90F	1.5cfm sampling	N/A	0
199	Variable_D (4 holes)	0.25-0.5	4.66667"	PVC	18x18	constant_1000CFM	70, 90F	1.5cfm sampling	N/A	0
200	Variable_D (3 holes)	0.25-0.5	7"	PVC	18x18	constant_1000CFM	70, 90F	1.5cfm sampling	N/A	0
201	DOE_D (8 holes)	0.375	2"	PVC	18x18	300:700 cfm(L:H)	70, 90F	1.5cfm sampling	N/A	0
202	DOE_D (7 holes)	0.375	2.3333"	PVC	18x18	300:700 cfm(L:H)	70, 90F	1.5cfm sampling	N/A	0
203	DOE_D (6 holes)	0.375	2.8"	PVC	18x18	300:700 cfm(L:H)	70, 90F	1.5cfm sampling	N/A	0
204	DOE_D (5 holes)	0.375	2.8"	PVC	18x18	300:700 cfm(L:H)	70, 90F	1.5cfm sampling	N/A	0

(continued)

Case #	Sampling hole type	Hole size (in)	Hole pitch (in)	Material	Duct size (in^2)	Inlet vel. profile	Inlet temp. profile	Branch outlet BC	Emissivity	Hole facing angle (°)
205	DOE_D (4 holes)	0.375	4.66667"	PVC	18x18	300:700 cfm(L:H)	70, 90F	1.5cfm sampling	N/A	0
206	DOE_D (3 holes)	0.375	7"	PVC	18x18	300:700 cfm(L:H)	70, 90F	1.5cfm sampling	N/A	0
207	DOE_D (8 holes)	0.375	2"	PVC	18x18	700:300 cfm(L:H)	70, 90F	1.5cfm sampling	N/A	0
208	DOE_D (7 holes)	0.375	2.3333"	PVC	18x18	700:300 cfm(L:H)	70, 90F	1.5cfm sampling	N/A	0
209	DOE_D (6 holes)	0.375	2.8"	PVC	18x18	700:300 cfm(L:H)	70, 90F	1.5cfm sampling	N/A	0
210	DOE_D (5 holes)	0.375	3.5"	PVC	18x18	700:300 cfm(L:H)	70, 90F	1.5cfm sampling	N/A	0
211	DOE_D (4 holes)	0.375	4.66667"	PVC	18x18	700:300 cfm(L:H)	70, 90F	1.5cfm sampling	N/A	0
212	DOE_D (3 holes)	0.375	7"	PVC	18x18	700:300 cfm(L:H)	70, 90F	1.5cfm sampling	N/A	0
213	Variable_D (8 holes)	0.25-0.5	2"	PVC	18x18	300:700 cfm(L:H)	70, 90F	1.5cfm sampling	N/A	0
214	Variable_D (7 holes)	0.25-0.5	2.3333"	PVC	18x18	300:700 cfm(L:H)	70, 90F	1.5cfm sampling	N/A	0
215	Variable_D (6 holes)	0.25-0.5	2.8"	PVC	18x18	300:700 cfm(L:H)	70, 90F	1.5cfm sampling	N/A	0
216	Variable_D (4 holes)	0.25-0.5	4.66667"	PVC	18x18	300:700 cfm(L:H)	70, 90F	1.5cfm sampling	N/A	0
217	Variable_D (3 holes)	0.25-0.5	7"	PVC	18x18	300:700 cfm(L:H)	70, 90F	1.5cfm sampling	N/A	0
218	Variable_D (8 holes)	0.25-0.5	2"	PVC	18x18	700:300 cfm(L:H)	70, 90F	1.5cfm sampling	N/A	0
219	Variable_D (7 holes)	0.25-0.5	2.3333"	PVC	18x18	700:300 cfm(L:H)	70, 90F	1.5cfm sampling	N/A	0
220	Variable_D (6 holes)	0.25-0.5	2.8"	PVC	18x18	700:300 cfm(L:H)	70, 90F	1.5cfm sampling	N/A	0
221	Variable_D (4 holes)	0.25-0.5	4.66667"	PVC	18x18	700:300 cfm(L:H)	70, 90F	1.5cfm sampling	N/A	0
222	Variable_D (3 holes)	0.25-0.5	7"	PVC	18x18	700:300 cfm(L:H)	70, 90F	1.5cfm sampling	N/A	0
223	Variable_D (8 holes)	0.25-0.5	2"	PVC	18x18	constant_1000CFM	70, 90F	3cfm sampling	N/A	0
224	Variable_D (8 holes)	0.25-0.5	2"	PVC	18x18	constant_1000CFM	70, 90F	3.5cfm sampling	N/A	0
225	Variable_D (8 holes)	0.25-0.5	2"	PVC	18x18	constant_1000CFM	70, 90F	4cfm sampling	N/A	0

2.2. Testing results

Case #	P @in [inWC]	Q @inlet [cfm]	Q @sample [cfm]	T_mean @inlet [F]	T_mean @duct out [F]	T_mean @sampler out [F]	T_max @ inlet [F]	T_min @inlet [F]	ΔT_max @inlet [F]	Sampler bias [%]
1	0.000875	999.0	-0.590	82.67	82.67	87.14	90	70	12.67	-35.3
2	0.000732	1165.5	-0.762	77.33	77.33	78.26	90	70	12.67	-7.4
3	0.001047	1166.7	-0.733	80.00	80.00	83.71	90	70	10.00	-37.1
4	-0.000259	1000.0	-0.696	80.00	80.00	82.74	90	70	10.00	-27.4
5	0.000487	1166.6	-0.526	80.00	80.00	85.49	90	70	10.00	-54.9
6	-0.005629	1000.0	-0.337	80.12	80.12	85.46	90	70	10.12	-52.7
7	0.000861	999.0	-0.772	82.67	82.67	87.56	90	70	12.67	-38.6
8	0.000895	999.0	-0.969	77.33	77.33	77.06	90	70	12.67	2.1
9	0.001324	1000.0	-0.801	80.00	80.00	84.30	90	70	10.00	-43.0
10	-0.000106	1000.1	-0.860	80.00	80.00	82.82	90	70	10.00	-28.2
11	0.000757	999.9	-0.589	80.00	80.00	88.02	90	70	10.00	-80.2
12	-0.005655	1000.0	-0.420	80.12	80.12	85.86	90	70	10.12	-56.7
13	0.000866	999.0	-0.395	82.67	82.67	86.02	90	70	12.67	-26.4
14	0.000861	999.0	-0.438	77.33	77.33	80.76	90	70	12.67	-27.1
15	0.001373	1000.0	-0.468	80.00	80.00	83.62	90	70	10.00	-36.2
16	-0.000011	1000.1	-0.437	80.00	80.00	83.06	90	70	10.00	-30.6
17	0.000749	999.9	-0.363	80.00	80.00	84.79	90	70	10.00	-47.9
18	-0.005682	1000.0	-0.191	80.12	80.12	85.65	90	70	10.12	-54.7
19	0.000902	999.0	-0.448	82.67	82.67	85.71	90	70	12.67	-24.0
20	0.000873	999.0	-0.975	77.33	77.33	76.97	90	70	12.67	2.8
21	0.001342	1000.0	-0.701	80.00	80.00	81.97	90	70	10.00	-19.7
22	-0.000037	1000.1	-0.640	80.00	80.00	82.50	90	70	10.00	-25.0
23	0.000757	999.9	-0.643	80.00	80.00	80.13	90	70	10.00	-1.3
24	-0.005543	1000.0	-0.298	80.12	80.12	84.69	90	70	10.12	-45.1
25	0.001332	1000.0	-0.715	80.00	80.00	76.16	90	70	10.00	38.4
26	0.001340	1000.0	-0.716	83.33	83.33	83.03	90	70	13.33	2.3
27	0.001313	1000.0	-0.802	80.00	80.00	75.66	90	70	10.00	43.4
28	0.001344	1000.0	-0.801	83.33	83.34	82.21	90	70	13.33	8.4
29	0.001370	1000.0	-0.468	80.00	80.00	76.29	90	70	10.00	37.1
30	0.001343	1000.0	-0.468	83.33	83.33	82.88	90	70	13.33	3.4
31	0.001368	1000.0	-0.701	80.00	80.00	78.01	90	70	10.00	19.9
32	0.001327	1000.0	-0.701	83.33	83.33	84.01	90	70	13.33	-5.1
33	0.000862	999.0	-0.522	82.67	82.67	86.61	90	70	12.67	-31.1
34	0.000890	999.0	-0.840	77.33	77.33	77.61	90	70	12.67	-2.2
35	0.001381	1000.0	-0.710	80.00	80.00	82.98	90	70	10.00	-29.8
36	-0.000018	1000.1	-0.669	80.00	80.00	82.73	90	70	10.00	-27.3
37	0.000762	999.9	-0.555	80.00	80.00	83.79	90	70	10.00	-37.9
38	-0.005458	1000.0	-0.189	80.12	80.12	85.24	90	70	10.12	-50.6
39	0.000862	999.0	-0.384	82.67	82.67	85.76	90	70	12.67	-24.4

(continued)

Case #	P @in [inWC]	Q @inlet [cfm]	Q @sample [cfm]	T_mean @inlet [F]	T_mean @duct out [F]	T_mean @sampler out [F]	T_max @ inlet [F]	T_min @inlet [F]	ΔT_max @inlet [F]	Sampler bias [%]
40	0.000854	999.0	-0.454	77.33	77.33	80.48	90	70	12.67	-24.9
41	0.001350	1000.0	-0.470	80.00	80.00	83.50	90	70	10.00	-35.0
42	-0.000063	1000.1	-0.426	80.00	80.00	83.13	90	70	10.00	-31.3
43	0.000751	999.9	-0.370	80.00	80.00	84.39	90	70	10.00	-43.9
44	-0.005715	1000.0	-0.175	80.12	80.12	85.56	90	70	10.12	-53.8
45	0.001359	1000.0	-0.468	80.00	80.00	83.43	90	70	10.00	-34.3
46	0.001373	1000.0	-0.468	80.00	80.00	84.16	90	70	10.00	-41.6
47	0.001359	1000.0	-0.468	80.00	80.00	80.43	90	70	10.00	-4.3
48	0.001350	1000.0	-0.470	80.00	80.00	83.29	90	70	10.00	-32.9
49	0.001350	1000.0	-0.470	80.00	80.00	84.07	90	70	10.00	-40.7
50	0.001362	1000.0	-0.470	80.00	80.00	80.06	90	70	10.00	-0.6
51	0.001368	1000.0	-0.701	80.00	80.00	82.22	90	70	10.00	-22.2
52	0.001368	1000.0	-0.701	80.00	80.00	82.57	90	70	10.00	-25.7
53	0.001334	1000.0	-0.701	80.00	80.00	78.98	90	70	10.00	10.2
54	0.001345	1000.0	-0.710	80.00	80.00	82.91	90	70	10.00	-29.1
55	0.001355	1000.0	-0.710	80.00	80.00	83.44	90	70	10.00	-34.4
56	0.001341	1000.0	-0.710	80.00	80.00	80.16	90	70	10.00	-1.6
57	0.000849	999.0	-0.447	82.67	82.67	85.06	90	70	12.67	-18.9
58	0.000856	999.0	-0.448	82.67	82.67	86.06	90	70	12.67	-26.8
59	0.000896	999.0	-0.450	82.67	82.67	85.25	90	70	12.67	-20.4
60	-0.000049	1000.1	-0.643	80.00	80.00	82.32	90	70	10.00	-23.2
61	-0.000049	1000.1	-0.643	80.00	80.00	82.84	90	70	10.00	-28.4
62	-0.000049	1000.1	-0.643	80.00	80.00	80.74	90	70	10.00	-7.4
63	0.001345	1000.0	-0.710	80.00	80.00	83.11	90	70	10.00	-31.1
64	0.001378	1000.0	-0.710	80.00	80.00	82.56	90	70	10.00	-25.6
65	0.001322	1000.0	-0.709	80.00	80.00	82.40	90	70	10.00	-24.0
66	0.001340	1000.0	-0.710	80.00	79.98	82.92	90	70	10.00	-29.2
67	0.001360	1000.0	-0.710	80.00	79.98	82.90	90	70	10.00	-29.0
68	0.001355	1000.0	-0.710	80.00	79.98	82.87	90	70	10.00	-28.7
69	0.001348	1000.0	-0.710	83.33	83.33	82.60	90	70	13.33	5.5
70	0.001378	1000.0	-0.710	83.33	83.33	82.62	90	70	13.33	5.4
71	0.001366	1000.0	-0.711	83.33	83.33	82.62	90	70	13.33	5.3
72	0.000916	999.0	-0.692	82.67	82.67	80.06	90	70	12.67	20.6
73	0.000913	999.0	-0.692	77.33	77.32	84.93	90	70	12.67	-60.0
74	0.001340	1000.0	-0.692	80.00	80.00	82.69	90	70	10.00	-26.9
75	-0.000020	1000.1	-0.692	80.00	80.00	82.85	90	70	10.00	-28.5
76	0.000862	999.0	-0.699	82.67	82.67	79.57	90	70	12.67	24.5
77	0.000850	999.0	-0.702	77.33	77.32	86.25	90	70	12.67	-70.4
78	0.001343	1000.0	-0.701	80.00	80.00	83.68	90	70	10.00	-36.8
79	-0.000025	1000.1	-0.705	80.00	80.00	84.24	90	70	10.00	-42.4
80	0.000867	999.0	-0.709	82.67	82.67	86.67	90	70	12.67	-31.6

(continued)

Case #	P @in [inWC]	Q @inlet [cfm]	Q @sample [cfm]	T_mean @inlet [F]	T_mean @duct out [F]	T_mean @sampler out [F]	T_max @ inlet [F]	T_min @inlet [F]	ΔT_max @inlet [F]	Sampler bias [%]
81	0.000853	999.0	-0.709	77.33	77.33	78.10	90	70	12.67	-6.1
82	0.001356	1000.0	-0.704	80.00	80.00	83.90	90	70	10.00	-39.0
83	-0.000007	1000.1	-0.692	80.00	80.00	82.76	90	70	10.00	-27.6
84	0.000035	100.0	-0.756	80.00	79.98	83.00	90	70	10.00	-30.0
85	0.000156	250.0	-0.706	80.00	79.99	83.35	90	70	10.00	-33.5
86	0.000463	500.0	-0.705	80.00	79.99	83.58	90	70	10.00	-35.8
87	0.000841	750.0	-0.698	80.00	80.00	83.78	90	70	10.00	-37.8
88	0.001364	1000.0	-0.711	80.00	80.00	83.89	90	70	10.00	-38.9
89	0.000634	1000.0	-25.435	80.00	79.97	81.21	90	70	10.00	-12.1
90	0.000036	100.0	-0.705	80.00	79.99	80.89	90	70	10.00	-8.9
91	0.000452	500.0	-0.698	80.00	80.00	81.63	90	70	10.00	-16.3
92	0.001352	1000.0	-0.703	80.00	80.00	81.96	90	70	10.00	-19.6
93	0.000670	1000.0	-25.367	80.00	80.02	79.13	90	70	10.00	8.7
94	0.000660	1000.0	-25.000	80.00	80.03	78.99	90	70	10.00	10.1
95	0.001317	1000.0	-1.617	80.00	80.00	82.60	90	70	10.00	-26.0
96	0.001334	1000.0	-0.575	80.00	80.00	84.21	90	70	10.00	-42.1
97	0.000032	100.0	-1.711	80.00	79.97	82.14	90	70	10.00	-21.4
98	0.000037	100.0	-0.583	80.00	79.98	83.26	90	70	10.00	-32.6
99	0.000835	999.0	-1.651	82.67	82.67	84.20	90	70	12.67	-12.0
100	0.000861	999.0	-0.582	82.67	82.67	87.00	90	70	12.67	-34.1
101	0.000022	99.9	-1.648	82.67	82.68	82.45	90	70	12.67	1.7
102	0.000024	99.9	-0.577	82.67	82.67	83.63	90	70	12.67	-7.6
103	0.000845	999.0	-1.643	77.33	77.32	81.06	90	70	12.67	-29.5
104	0.000888	999.0	-0.582	77.33	77.33	77.81	90	70	12.67	-3.8
105	0.000022	99.9	-1.669	77.33	77.25	81.73	90	70	12.67	-34.7
106	0.000024	99.9	-0.588	77.33	77.30	82.74	90	70	12.67	-42.7
107	0.001171	1000.0	-5.819	80.00	79.99	81.81	90	70	10.00	-18.1
108	0.001029	1000.0	-11.699	80.00	79.98	81.57	90	70	10.00	-15.7
109	0.000925	1000.0	-17.363	80.00	79.98	81.41	90	70	10.00	-14.1
110	0.001367	1000.0	-0.064	80.00	80.00	86.78	90	70	10.00	-67.8
111	0.001384	1000.0	-0.179	80.00	80.00	85.24	90	70	10.00	-52.4
112	0.001311	1000.0	-0.655	80.00	80.00	83.08	90	70	10.00	-30.8
113	0.001285	1000.0	-2.837	80.00	80.00	81.31	90	70	10.00	-13.1
114	0.001332	1000.0	-1.602	80.00	79.99	84.88	90	70	10.00	-48.8
115	0.001257	1000.0	-4.509	80.00	79.98	84.30	90	70	10.00	-43.0
116	0.000927	1000.0	-16.127	80.00	79.94	83.40	90	70	10.00	-34.0
117	-0.000552	1000.0	-70.527	80.00	79.76	83.10	90	70	10.00	-31.0
118	0.001355	1000.0	-0.256	80.00	80.00	84.76	90	70	10.00	-47.6
119	0.001340	1000.0	-0.738	80.00	80.00	82.98	90	70	10.00	-29.8
120	0.001282	1000.0	-2.616	80.00	80.00	81.57	90	70	10.00	-15.7
121	0.001024	1000.0	-11.356	80.00	79.99	80.84	90	70	10.00	-8.4

(continued)

Case #	P @in [inWC]	Q @inlet [cfm]	Q @sample [cfm]	T_mean @inlet [F]	T_mean @duct out [F]	T_mean @sampler out [F]	T_max @ inlet [F]	T_min @inlet [F]	ΔT_max @inlet [F]	Sampler bias [%]
122	0.001338	1000.0	-1.035	80.00	80.00	84.23	90	70	10.00	-42.3
123	0.001263	1000.0	-2.863	80.00	79.99	83.26	90	70	10.00	-32.6
124	0.001078	1000.0	-10.332	80.00	79.98	82.35	90	70	10.00	-23.5
125	0.000162	1000.0	-45.326	80.00	79.91	82.00	90	70	10.00	-20.0
126	0.000818	1000.0	-20.717	80.00	79.95	82.24	90	70	10.00	-22.4
127	0.000492	1000.0	-31.053	80.00	79.93	82.16	90	70	10.00	-21.6
128	0.001319	1000.0	-1.300	80.00	80.00	82.15	90	70	10.00	-21.5
129	0.001301	1000.0	-1.953	80.00	80.00	81.67	90	70	10.00	-16.7
130	0.000478	1000.0	-32.243	80.00	79.89	83.35	90	70	10.00	-33.5
131	0.000055	1000.0	-48.283	80.00	79.84	83.16	90	70	10.00	-31.6
132	0.001235	1000.0	-5.292	80.00	79.99	81.13	90	70	10.00	-11.3
133	0.001138	1000.0	-7.811	80.00	79.99	80.94	90	70	10.00	-9.4
134	0.000038	100.0	-0.064	80.00	80.00	86.29	90	70	10.00	-62.9
135	0.000037	100.0	-0.179	80.00	79.99	84.28	90	70	10.00	-42.8
136	0.000036	100.0	-0.647	80.00	79.99	81.99	90	70	10.00	-19.9
137	0.000034	100.0	-1.292	80.00	79.98	81.22	90	70	10.00	-12.2
138	0.000032	100.0	-1.942	80.00	79.98	80.90	90	70	10.00	-9.0
139	0.000037	100.0	-0.256	80.00	79.99	83.78	90	70	10.00	-37.8
140	0.000036	100.0	-0.724	80.00	79.98	82.13	90	70	10.00	-21.3
141	0.000029	100.0	-2.623	80.00	79.97	81.06	90	70	10.00	-10.6
142	0.000021	100.0	-5.226	80.00	79.96	80.76	90	70	10.00	-7.6
143	0.000013	100.0	-7.864	80.00	79.95	80.64	90	70	10.00	-6.4
144	0.000016	100.0	-5.792	80.00	79.91	81.52	90	70	10.00	-15.2
145	0.000004	100.0	-11.812	80.00	79.83	81.28	90	70	10.00	-12.8
146	-0.000012	100.0	-17.494	80.00	79.74	81.23	90	70	10.00	-12.3
147	0.000035	100.0	-1.036	80.00	79.96	83.73	90	70	10.00	-37.3
148	0.000029	100.0	-2.897	80.00	79.92	82.73	90	70	10.00	-27.3
149	0.000005	100.0	-10.365	80.00	79.74	82.24	90	70	10.00	-22.4
150	-0.000019	100.0	-20.776	80.00	79.47	82.01	90	70	10.00	-20.1
151	-0.000041	100.0	-30.901	80.00	79.21	81.82	90	70	10.00	-18.2
152	0.005309	500.0	-0.288	80.00	80.00	84.20	90	70	10.00	-42.0
153	0.005131	500.0	-0.805	80.00	80.00	82.63	90	70	10.00	-26.3
154	0.004509	500.0	-2.904	80.00	79.99	81.62	90	70	10.00	-16.2
155	0.003879	500.0	-5.888	80.00	79.98	81.36	90	70	10.00	-13.6
156	0.003670	500.0	-8.733	80.00	79.98	81.22	90	70	10.00	-12.2
157	0.002697	500.0	-12.706	80.00	79.97	81.12	90	70	10.00	-11.2
158	0.005254	500.0	-0.128	80.00	80.00	84.84	90	70	10.00	-48.4
159	0.005112	500.0	-0.368	80.00	80.00	83.00	90	70	10.00	-30.0
160	0.004959	500.0	-1.341	80.00	80.00	81.51	90	70	10.00	-15.1
161	0.004834	500.0	-2.627	80.00	79.99	81.06	90	70	10.00	-10.6
162	0.004356	500.0	-3.917	80.00	79.99	80.88	90	70	10.00	-8.8

(continued)

Case #	P @in [inWC]	Q @inlet [cfm]	Q @sample [cfm]	T_mean @inlet [F]	T_mean @duct out [F]	T_mean @sampler out [F]	T_max @ inlet [F]	T_min @inlet [F]	ΔT_max @inlet [F]	Sampler bias [%]
163	0.003979	500.0	-5.714	80.00	79.99	80.75	90	70	10.00	-7.5
164	0.005161	500.0	-0.516	80.00	80.00	84.24	90	70	10.00	-42.4
165	0.004999	500.0	-1.442	80.00	79.99	83.28	90	70	10.00	-32.8
166	0.004244	500.0	-5.170	80.00	79.98	82.32	90	70	10.00	-23.2
167	0.003264	500.0	-10.313	80.00	79.96	82.12	90	70	10.00	-21.2
168	0.001944	500.0	-15.449	80.00	79.93	82.06	90	70	10.00	-20.6
169	0.000324	500.0	-22.508	80.00	79.91	81.96	90	70	10.00	-19.6
170	0.005312	500.0	-0.032	80.00	80.00	86.95	90	70	10.00	-69.5
171	0.005401	500.0	-0.089	80.00	80.00	85.27	90	70	10.00	-52.7
172	0.005185	500.0	-0.330	80.00	80.00	82.97	90	70	10.00	-29.7
173	0.005210	500.0	-0.650	80.00	80.00	82.12	90	70	10.00	-21.2
174	0.005163	500.0	-0.966	80.00	80.00	81.60	90	70	10.00	-16.0
175	0.004953	500.0	-1.409	80.00	80.00	81.21	90	70	10.00	-12.1
176	0.001324	1000.0	-0.577	79.99	79.99	86.31	90	70	10.01	-63.1
177	0.000464	500.0	-0.575	79.99	79.99	86.02	90	70	10.01	-60.2
178	0.001320	1000.0	-1.627	79.99	79.99	83.97	90	70	10.01	-39.8
179	0.001174	1000.0	-5.793	79.99	79.98	82.79	90	70	10.01	-27.9
180	0.000033	100.0	-1.635	79.99	79.94	83.28	90	70	10.01	-32.8
181	0.000455	500.0	-1.521	79.99	79.98	83.79	90	70	10.01	-38.0
182	0.001319	1000.0	-1.512	79.99	79.99	84.14	90	70	10.01	-41.4
183	0.000033	100.0	-1.516	79.99	79.99	79.87	90	70	10.01	1.3
184	0.000455	500.0	-1.528	79.99	79.99	80.44	90	70	10.01	-4.5
185	0.001352	1000.0	-1.521	79.99	79.99	80.76	90	70	10.01	-7.7
186	0.001327	1000.0	-1.519	79.99	79.99	81.38	90	70	10.01	-13.9
187	0.001352	1000.0	-1.521	79.99	79.99	81.55	90	70	10.01	-15.5
188	0.001619	1000.0	-1.524	79.99	80.00	77.80	90	70	10.01	21.9
189	0.000684	1000.3	-1.511	75.99	75.99	77.44	90	70	14.01	-10.3
190	0.000723	999.7	-1.511	83.99	83.99	84.04	90	70	13.99	-0.3
191	0.001331	1000.0	-1.500	79.99	79.99	85.63	90	70	10.01	-56.4
192	0.001300	1000.0	-1.521	79.99	79.99	85.12	90	70	10.01	-51.2
193	0.001331	1000.0	-1.525	79.99	79.99	84.64	90	70	10.01	-46.5
194	0.001291	1000.0	-1.500	79.99	79.99	83.82	90	70	10.01	-38.3
195	0.001335	1000.0	-1.553	79.99	79.99	83.08	90	70	10.01	-30.9
196	0.001334	1000.0	-1.500	79.99	79.99	82.75	90	70	10.01	-27.5
197	0.001329	1000.0	-1.524	79.99	79.99	82.05	90	70	10.01	-20.6
198	0.001319	1000.0	-1.507	79.99	79.99	81.41	90	70	10.01	-14.2
199	0.001297	1000.0	-1.500	79.99	79.99	80.09	90	70	10.01	-1.0
200	0.001307	1000.0	-1.517	79.99	79.99	79.55	90	70	10.01	4.4
201	0.000732	1000.3	-1.500	75.99	75.99	79.23	90	70	14.01	-23.1
202	0.000699	1000.3	-1.509	75.99	75.99	79.82	90	70	14.01	-27.3
203	0.000704	1000.3	-1.525	75.99	75.99	80.48	90	70	14.01	-32.0

(continued)

Case #	P @in [inWC]	Q @inlet [cfm]	Q @sample [cfm]	T_mean @inlet [F]	T_mean @duct out [F]	T_mean @sampler out [F]	T_max @ inlet [F]	T_min @inlet [F]	ΔT_max @inlet [F]	Sampler bias [%]
204	0.000715	1000.3	-1.516	75.99	75.99	80.94	90	70	14.01	-35.3
205	0.000734	1000.3	-1.519	75.99	75.99	81.77	90	70	14.01	-41.2
206	0.000712	1000.3	-1.517	75.99	75.99	80.69	90	70	14.01	-33.5
207	0.000705	999.7	-1.512	83.99	83.99	89.73	90	70	13.99	-41.0
208	0.000755	999.7	-1.532	83.99	83.99	89.40	90	70	13.99	-38.6
209	0.000709	999.7	-1.535	83.99	83.99	88.28	90	70	13.99	-30.6
210	0.000737	999.7	-1.512	83.99	83.99	87.22	90	70	13.99	-23.0
211	0.000720	999.7	-1.523	83.99	83.99	85.50	90	70	13.99	-10.7
212	0.000709	999.7	-1.528	83.99	83.99	85.35	90	70	13.99	-9.7
213	0.000717	1000.3	-1.516	75.99	75.99	76.96	90	70	14.01	-6.9
214	0.000725	1000.3	-1.543	75.99	75.99	77.17	90	70	14.01	-8.4
215	0.000733	1000.3	-1.528	75.99	75.99	77.28	90	70	14.01	-9.1
216	0.000721	1000.3	-1.500	75.99	75.99	77.98	90	70	14.01	-14.2
217	0.000712	1000.3	-1.511	75.99	75.99	76.89	90	70	14.01	-6.4
218	0.000718	999.7	-1.500	83.99	83.99	87.40	90	70	13.99	-24.3
219	0.000716	999.7	-1.530	83.99	83.99	86.38	90	70	13.99	-17.0
220	0.000728	999.7	-1.521	83.99	83.99	84.78	90	70	13.99	-5.6
221	0.000736	999.7	-1.500	83.99	84.00	81.86	90	70	13.99	15.2
222	0.000744	999.7	-1.500	83.99	84.00	82.13	90	70	13.99	13.3
223	0.001286	1000.0	-2.957	79.99	79.99	81.26	90	70	10.01	-12.7
224	0.001238	1000.0	-3.533	79.99	79.99	81.01	90	70	10.01	-10.2
225	0.001277	1000.0	-4.029	79.99	79.99	80.81	90	70	10.01	-8.1

3. Experimental Data for Air Sampler Testing

Case #	Test	Hole Dia.	Spacing	Material	Flowrate ratio (L:H)	Total flowrate (CFM)	Inlet temp (H:L)	Hole facing angle (°)	Sampling flowrate per tube (CFM)	Sampler bias (%)
1	Material effect	Variable	Equal (3.5″)	PVC	5:5	1000	70:90	0	1.5	-1.7
2				AL	5:5					-13.7
3					6.5:3.5					-9.8
4					3.5:6.5					-8.0
5				SS	5:5					-13.3
6					6.5:3.5					-9.3
7					3.5:6.5					-8.7
8				adiabatic	5.5					-7.3
9					6.5:3.5					-3.9
10					3.5:6.5					-7.8
11	Hole size effect	DOE_D: 0.375"	Equal	PVC	3.5:6.5	1000	70:90	0	1.5	-19.5
12		Large_D: 0.5"								-22.4
13		Small_D: 0.25"								-17.3
14		Variable_D								-2.7
15		DOE_D: 0.375"			5:5					-26.5
16		Large_D: 0.5"								-44.8
17		Small_D: 0.25"								-15.5
18		Variable_D								-1.7
19		DOE_D: 0.375"			6.5:3.5					-14.1
20		Large_D: 0.5"								-27.0
21		Small_D: 0.25"								-3.4
22		Variable_D								0.4
23	Hole spacing effect	DOE_D	Equal (3.5″)	PVC	3.5:6.5	1000	70:90	0	1.5	-19.5
24					5:5					-26.5
25					6.5:3.5					-14.1
26			Variable		3.5:6.5					-20.2
27					5:5					-31.5
28					6.5:3.5					-17.3

(continued)

Case #	Test	Hole Dia.	Spacing	Material	Flowrate ratio (L:H)	Total flowrate (CFM)	Inlet temp (H:L)	Hole facing angle (°)	Sampling flowrate per tube (CFM)	Sampler bias (%)
29	Hole facing direction	DOE_D	Equal (3.5″)	PVC	3.5:6.5	1000	70:90	0	1.5	-19.5
30					5:5					-26.5
31					6.5:3.5					-14.1
32					3.5:6.5			90		-24.3
33					5:5					-19.5
34					6.5:3.5					-0.6
35					3.5:6.5			180		-33.1
36					5:5					-23.1
37					6.5:3.5					-2.0
38	Total flowrate effect	DOE_D	Equal (3.5″)	PVC	5:5	100	70:90	0	1.5	47.4
39		Variable_D								44.3
40		DOE_D				500				-19.0
41		Variable_D								4.5
42		DOE_D				1000				-26.5
43		Variable_D								-1.7
44	Ave. vel@sampling hole	0.125"	Equal (3.5″)	PVC	5:5	1000	70:90	0	0.064 (for V_hole_av=2.5 fps)	69.4
45									0.179 (for V_hole_av=7 fps)	22.6
46									0.639 (for V_hole_av=25 fps)	-19.8
47		0.25"							0.256 (for V_hole_av=2.5 fps)	11.2
48									0.716 (for V_hole_av=7 fps)	-17.7
49									2.557 (for V_hole_av=25 fps)	-15.0
50		0.375"							0.575 (for V_hole_av=2.5 fps)	-27.7
51									1.611 (for V_hole_av=7 fps)	-26.1
52									5.752 (for V_hole_av=25 fps)	-25.4
53		0.5"							1.023 (for V_hole_av=2.5 fps)	-42.9
54									2.863 (for V_hole_av=7 fps)	-43.3

4. Experimental Data for In-situ Testing

4.1. Testing conditions

#	Air condition at upper inlet	Flowrate at upper inlet	Air condition at lower inlet	Total flowrate	Heating pattern	Nominal capacity of heating source	Mixer type	Overall mixing length
1	70°F DB, 50% RH	315 CFM	70°F DB, 50% RH	900 CFM	Diagonal 1	1 ton	Single Orth. 4x4, 60deg	2.0 D_h
2		450 CFM						
3		585 CFM						
4		450 CFM			Diagonal 2			
5		450 CFM			Low			
6		450 CFM			Diagonal 1			1.25 D_h
7								1.0 D_h
8								0.75 D_h
9								0.5 D_h
10	70°F DB, 50% RH	175 CFM	70°F DB, 50% RH	500 CFM	Diagonal 1	1 ton	Single Orth. 4x4, 60deg	2.0 D_h
11		250 CFM						
12		325 CFM						
13		250 CFM			Diagonal 2			
14		250 CFM			Low			
15	70°F DB, 50% RH	125 CFM	70°F DB, 50% RH	250 CFM	Diagonal 1	1 ton	Single Orth. 4x4, 60deg	2.0 D_h
16		250 CFM		500 CFM				
17		375 CFM		750 CFM				
18		450 CFM		900 CFM				
19	70°F DB, 50% RH	125 CFM	70°F DB, 50% RH	250 CFM	Diagonal 1	1 ton	No mixer	-
20		250 CFM		500 CFM				
21		375 CFM		750 CFM				
22		450 CFM		900 CFM				
23	70°F DB, 50% RH	250 CFM	70°F DB,	500 CFM	Diagonal 2	1 ton	No mixer	-
24			50% RH		Low			

4.2. Testing results

#	Air enthalpy @ up inlet(W)	Air enthalpy @ low inlet(W)	Air enthalpy @ inlet(W)	Air enthalpy @ test section(W)	Change in air enthalpy(W)	Heater power (W)	Difference in energy (W)	Sampler-based capacity measurement accuracy (%)	TC grid-based capacity measurement accuracy (%)	Mass balance (%)
1	6926.9	12025.2	18952.1	22154.4	3202.3	3242.7	-40.5	-1.2	1.3	-0.2
2	8908.4	8895.0	17803.4	21048.9	3245.5	3280.2	-34.7	-1.1	1.5	0.1
3	11765.0	7065.1	18830.1	22136.0	3305.9	3251.0	55.0	1.7	5.2	1.7
4	8901.5	8905.8	17807.3	21132.7	3325.3	3306.5	18.8	0.6	-0.7	0.1
5	8888.2	8918.3	17806.5	20995.3	3188.8	3278.7	-89.9	-2.7	2.9	0.0
6	9174.8	9182.4	18357.2	21589.3	3232.2	3220.6	11.5	0.4	2.5	0.7
7	9025.0	9130.0	18155.0	21256.2	3101.2	3225.3	-124.1	-3.8	-1.3	-0.8
8	8970.8	9079.6	18050.3	21234.5	3184.2	3214.4	-30.3	-0.9	4.8	-0.5
9	8947.1	9041.8	17988.9	21267.3	3278.3	3216.6	61.8	1.9	2.5	-0.4
10	3848.9	7080.9	10929.8	13638.5	2708.7	3088.5	-379.8	-12.3	-10.1	-3.5
11	5045.7	5060.3	10106.0	12936.2	2830.2	3095.6	-265.3	-8.6	-6.1	-2.4
12	7192.5	3967.0	11159.5	14080.7	2921.3	3081.8	-160.5	-5.2	-3.5	0.1
13	5065.6	5094.6	10160.1	13023.2	2863.1	3098.2	-235.1	-7.6	-9.7	-2.8
14	5090.7	5131.6	10222.3	12884.6	2662.3	3067.0	-404.7	-13.2	-7.5	-3.1
15	2752.5	2795.1	5547.6	7288.0	1740.4	3016.6	-1276.3	-42.3	-41.4	-4.6
16	5045.7	5060.3	10106.0	12936.2	2830.2	3095.6	-265.3	-8.6	-6.1	-2.4
17	7493.3	7625.0	15118.2	18159.9	3041.7	3225.7	-183.9	-5.7	-3.2	-0.5
18	8908.4	8895.0	17803.4	21048.9	3245.5	3280.2	-34.7	-1.1	1.5	0.1
19	2547.8	2547.4	5095.2	6845.3	1750.1	3013.5	-1263.4	-41.9	-42.0	-3.4
20	5044.6	5072.0	10116.6	13239.6	3123.0	3060.7	62.3	2.0	-0.6	-2.0
21	7567.9	7627.7	15195.6	18655.1	3459.5	3168.9	290.6	9.2	12.3	-0.4
22	9040.6	9110.3	18150.9	21790.2	3639.3	3240.8	398.5	12.3	18.8	1.9
23	9062.9	9147.4	18210.3	21782.8	3572.4	3272.7	299.7	9.2	1.1	2.6
24	9089.4	9167.3	18256.7	22150.1	3893.4	3211.5	681.9	21.2	17.0	2.3

VITA

HYUNJIN PARK

Candidate for the Degree of

Doctor of Philosophy

Thesis: DEVELOPMENT OF RECOMMENDATIONS FOR AIR MIXER AND SAMLER DESIGN AND COMBINATIONS THEREOF FOR PERFORMANCE TESTING OF HVAC EQUIPMENT

Major Field: Mechanical and Aerospace Engineering

Biographical:

Education:

Completed the requirements for the Doctor of Philosophy in Mechanical and Aerospace Engineering at Oklahoma State University, Stillwater, Oklahoma in May, 2023.

Received the Master of Science in Mechanical Engineering at Inje University, Republic of Korea in 2011, and the Bachelor of Science in Mechanical Engineering at Inje University in Republic of Korea in 2009.

Experience:

Worked as a Researcher at Inje university, Republic of Korea (Oct. 2011-Jul. 2018)
Worked as a Machine Design Engineer at Halder-Roemheld Korea Ltd., Republic of Korea (Jul. 2014-Dec.2015)
Worked as a Lecturer at Youngsan University, Republic of Korea (Sep. 2013-Jul. 2018)
Worked as a Lecturer at Inje University, Republic of Korea (Sep. 2011-Dec. 2015)

Professional Memberships:
Student member ASHRAE